Effect of Blood Flow on High Intensity Focused Ultrasound Therapy in an Isolated, Perfused Liver Model



David J. Holroyd

MB ChB BMedSci MSc (Res) MRCS (Eng)

Nuffield Department of Surgical Sciences

University of Oxford

A thesis submitted for the degree of

Doctor of Philosophy

Trinity Term, 2015

I declare that the work presented in this thesis is my own.

David Holroyd

20th May 2015

ACKNOWLEDGEMENTS

I am indebted to my supervisors, Professor Constantin Coussios and Professor Peter Friend, without whom I would not have been able to undertake and complete this research. I am extremely grateful for their mentorship and unwavering support over the last four years.

It has been a pleasure to work in the Biomedical Ultrasonics, Biotherapy and Biopharmaceuticals Laboratory (BUBBL). I was privileged to work with three postdoctoral researchers in biomedical engineering; Elenonora Mylonopoulou, Carl Jensen and James Choi, with whom this research was performed in collaboration with and who assisted with all of the HIFU experiments, undertook all of the Matlab programming and endured many a frustrating night trying to place and locate thermocouples akin to finding a needle in a haystack. Dr. Daniel Chung, a radiologist, was also a pivotal member of the "perfused liver team", providing expertise in liver ultrasonography and in targeting/locating thermocouples. I am extremely grateful to Eleonora, Daniel, Carl and James as none of the work would have been possible without their considerable support, expertise, skill, hard work and patience. They also made the 36-hour experiments bearable (even fun, dare I say) and provided many an entertaining moment over a perfused pig's liver.

Reena Ravikumar, a surgical trainee also undertaking a DPhil within the NDS, was an invaluable source of support and surgical knowledge, assisting with the *in vivo* surgical procedures and with the normothermic liver perfusion set up.

Nearly every member of the BUBBL group has helped me in some way or another. Whilst I cannot mention them all individually, I would particularly like to thank Dr. Jamie Collin and Dr. Olga Boubriak for their expert advice and insightful discussions regarding HIFU and histology, respectfully. The diverse academic backgrounds of the members of the BUBBL group

The research undertaken in this thesis was part of a collaborative, multi-centre project under the "Transcostal High Intensity Focused Ultrasound (THIFU) for the Treatment of Cancer" programme of work, which was led by Professor Nader Saffari. I am grateful to all members of the THIFU consortium for their advice, discussions and feedback. However, I would particularly like to thank Professor Gail ter Haar and Dr. Ian Rivens and their team of researchers from the Institute of Cancer Research for their substantial help, discussions and advice relating to the project.

The animal work could not have taken place without the expertise and assistance of the staff at the Northwick Park Institute of Medical Research (NPIMR) and in the Biomedical Sciences (BMS) Division at the University of Oxford. In particular, I would like to thank Cathy Gray and Lindsey Fletcher at the NPIMR and Dr. Caroline Bergmann, Emma Bartlett and Maria Martinez (BMS), who helped massively in arranging the *in vivo* work, undertook the animal husbandry and performed the general anaesthesia. I am thankful to a

number of people from BUBBL and the NDS, namely Murali Somasundaram, Marie-Albane de Saint Victor, Srikanth Reddy and Calum Crake, who assisted with the *in vivo* organ donation procedures.

I am also extremely grateful to OrganOx Ltd., in particular Dr Les Russell, for their support in providing the normothermic liver perfusion device and for many useful discussions regarding perfusion preservation. Several of the pieces of equipment used for the research were custom manufactured by Jim Fisk and David Salisbury in the IBME workshop. I would also like to thank Tracey King and Carol Bradford, who provided invaluable administrative and organisational support.

Final mention must go to my wife, Ailsa, who has been a constant source of support throughout, singlehandedly looking after our newborn twins whilst I spent 48 hours at a time looking after a perfused pig's liver.

The funding for the research undertaken in this work was generously provided by the Engineering and Physical Sciences Research Council (EP/F02617X/1) as part of the Transcostal High Intensity Focused Ultrasound for the Treatment of Cancer programme grant.

ABSTRACT

High intensity focused ultrasound (HIFU) is an emerging non-invasive thermal ablative modality that can be utilised for the treatment of solid organ tumours, including liver cancer. Acoustic cavitation is a phenomenon that can occur during HIFU and its presence can enhance heating rates. One major limitation of thermal ablative techniques in general, such as radiofrequency and microwave ablation, is the heat sink effect imparted by large vasculature. Thermal advection from blood flow in vessels ≥ 3 – 4 mm in diameter has been shown to significantly reduce heating rates and peak temperatures in the target tissue, potentially leading to treatment failure.

With regards to HIFU therapy, a clearer understanding is required of the effects of blood flow on heating, cavitation and thermal tissue necrosis, which is the treatment endpoint in clinical thermal ablation. Therefore, the overall aim of this thesis project was to elucidate the effects of blood flow on HIFU-induced heating, cavitation and histological assessment of thermal ablation.

An isolated, perfused porcine liver model was used in order to provide a relevant test bed, with physiological and anatomical characteristics similar to the *in vivo* human liver. The normothermic liver perfusion device used in all studies presented in this work can keep an organ alive in a functional state *ex vivo* for in excess of 72 hours. A therapeutic HIFU system was used in order to deliver HIFU therapy to regions of hepatic parenchyma

adjacent (≤ 3 mm) to large (≥ 5 mm) blood vessels or away from vasculature (≥ 1 cm) at either 1.06 MHz or at 3.18 MHz. Cavitation events during HIFU therapy were spatio-temporally monitored using a previously developed passive acoustic mapping (PAM) technique. The cavitation threshold at each frequency was determined through assessment of acoustic emissions acquired through PAM during HIFU exposure at a range of acoustic pressures. Real time thermal data during HIFU therapy were obtained using an implantable 400 μm thermocouple, aligned with the HIFU focus, in order to assess the effect of large vessel blood flow on peak tissue temperatures. Thermal data were obtained at 1.06 MHz, in the presence of acoustic cavitation and at 3.18 MHz, in the absence of cavitation, both in the presence and complete absence of blood flow. Finally, histological assessment of cell viability and cell death was performed in order to determine whether any heat sink effect could be overcome, with the achievement of complete tissue necrosis in treatment regions directly adjacent to large vasculature.

This work demonstrated that in perfused, functional liver tissue, the presence of large vasculature and physiological blood flow does not significantly affect ablative HIFU therapy, both in terms of peak focal tissue temperatures attained and histological evidence of complete tissue necrosis. Therefore, HIFU may be superior to other ablative modalities in treating tumours in tissue regions adjacent to major vascular structures, but further work needs to be performed to correlate the experimental findings with clinical outcomes.

CONTENTS

i - List of Figures

ii - List of Tables

iii – Abbreviations and Symbols

Chapter 1 - Introduction

1.1 – Thesis Aim

1.2 – Liver Cancer Epidemiology

1.2.1 – Primary liver cancer

1.2.2 – Liver metastases

1.3 – Liver Anatomy and Physiology

1.4 – The Treatment of Liver Cancer

1.4.1 – Surgical resection and transplantation

1.4.2 – Chemotherapy and Radiotherapy

1.4.2.1 – Biological therapies

1.4.2.2 – Locoregional therapies

1.4.3– Ablative therapies

1.4.3.1 – Mechanism of thermal ablation

1.4.3.2 – Radiofrequency ablation

1.4.3.3 – Microwave ablation

1.4.3.4 – Cryoablation

1.5 – High Intensity Focused Ultrasound

1.5.1 – The basis of HIFU

1.5.2 – HIFU-induced heating

1.5.3 – HIFU-induced cavitation

1.5.4 – Clinical applications of HIFU

1.5.4.1 – Thermal ablation

1.5.4.2 – Drug delivery

1.5.4.3 – Sonothrombolysis

1.6 – Limitations of Current Thermal Ablative Therapies

1.6.1 – The “heat sink” effect

1.6.1.1 – Modeling heat transfer

1.6.1.2 – Perfusion effects in radiofrequency ablation

1.6.1.3 – Perfusion effects in microwave ablation

1.6.1.4 – Perfusion effects in HIFU therapy

1.6.2 – Monitoring thermal ablation

1.6.2.1 – Radiological monitoring of RFA and MWA

1.6.2.2 – Monitoring during HIFU therapy

1.7 – Summary

Chapter 2 - Methods

2.1 - Introduction

2.2 – Porcine liver model

2.3 – Isolated normothermic liver perfusion

2.3.1 – Organ donation procedure

2.3.2 – Isolated normothermic perfusion

2.3.3 – Organ function

2.4 – HIFU setup

2.4.1 – Alignment protocol

2.5 – Experimental protocol

2.5.1 – Location selection

2.5.2 – Exposure protocol

2.5.3 – Passive acoustic mapping (PAM)

2.5.4 – Thermometry

2.5.5 – Perfusion Vs. no perfusion

Chapter 3 – Liver Perfusion Preservation

3.1 – Introduction

3.2 – Methods

3.3 – Results

3.4 – Discussion

Chapter 4 – The Effect of Perfusion on HIFU-Induced Cavitation

4.1 – Introduction

4.2 – Study aims

4.3 – Materials and methods

4.3.1 – Perfused liver model

4.3.2 – HIFU set up

4.3.3 – Passive acoustic mapping

4.3.4 – HIFU protocol

4.4 – Results

4.4.1 – Passive acoustic mapping of cavitation activity

4.4.2 – Cavitation threshold at 1.06 MHz

4.4.3 – Cavitation energy at 1.06 MHz

4.4.4 – Cavitation threshold at 3.18 MHz

4.5 – Discussion

4.5.1 – Cavitation threshold

4.5.2 – The effects of blood flow on cavitation

4.5.3 – Source of cavitation nuclei

4.6 - Conclusions

Chapter 5 – The Effect of Perfusion on HIFU-Induced Heating

5.1 – Introduction

5.2 – Study aims

5.3 – Methods

5.3.1 – Perfused liver model

5.3.2 – HIFU set up

5.3.3 – Exposure protocol

5.4 – Results

5.4.1 – Preliminary experiments to determine optimum exposure protocol

5.4.2 – Effects of perfusion on heating at 1.06 MHz

5.4.3 – The relationship between cavitation and heating at 1.06 MHz

5.4.4 – Effects of perfusion on heating at 3.18 MHz

5.5 – Discussion

5.5.1 – The effects of perfusion on HIFU-induced heating

5.5.2 – Comparison with perfusion effects in RFA and MWA

5.5.3 – The relationship between cavitation and heating

5.5.4 – Further work

5.6 - Conclusions

Chapter 6 – The Effect of Perfusion on Histological Assessment of Tissue Ablation in HIFU Therapy

6.1 – Introduction

6.2 – Study aims

6.3 – Methods

6.3.1 – Perfused liver model set up

6.3.2 – HIFU set up

6.3.3 – Lesion threshold studies

6.3.4 – Volume ablation studies

6.3.5 – Gross histopathology

6.3.6 – Frozen sectioning technique

6.3.7 – Histological assessment of tissue viability following ablation

6.3.8 – NADH staining

6.3.9 – Ethidium homodimer-1 staining

6.3.10 – Immunofluorochemistry

6.3.11 – Assessment of apoptotic activity

6.4 – Results

6.4.1 – Preliminary lesion threshold studies

6.4.2 – Volume ablation studies

6.4.3 – Assessment of cell viability

6.4.4 – Assessment of cell death

6.4.5 – Assessment of apoptotic activity

6.5 – Discussion

6.5.1 – Assessment of cell death

6.5.2 – Limitations

6.6 – Conclusions

Chapter 7 – Discussion and Conclusions

7.1 – Summary of achievements

7.2 – Suggestions for future work

7.2.1 – Validation of the isolated, perfused porcine liver model

7.2.2 – Real time treatment monitoring during HIFU ablation

7.2.3 – Clinical trials

7.2.4 – Applicability of the current work to other uses of HIFU

vi - References

vii - Appendices

LIST OF FIGURES

Figure 1.1 Commonest causes of death in the UK and number of deaths for 2011

Figure 1.2 *Age-standardised incidence rates for primary liver cancer worldwide in 2008*

Figure 1.3 *Age-standardised incidence rates for colorectal cancer worldwide in 2008*

Figure 1.4 *Major vascular and biliary anatomy of the liver as described by Couinard*

Figure 1.5 *Structure of the hepatic lobule, acinus and sinusoid*

Figure 1.6 *Treatment algorithm for primary HCC*

Figure 1.7 *Management algorithm for colorectal liver metastases*

Figure 1.8 *Mechanisms of tissue ablation in RF and MW therapy*

Figure 1.9 *Heating profile in RFA therapy*

Figure 1.10 *3 year local recurrence rates following microwave ablation therapy for liver cancer in relation to tumour size and underlying*

histopathological subtype

Figure 1.11 *3-year survival following microwave ablation therapy for colorectal liver metastases and other disease pathology*

Figure 1.12 *Schematic diagram showing HIFU ablation of a liver tumour*

Figure 1.13 *Heating in porcine adipose tissue in the absence of inertial cavitation and in the presence of cavitation*

Figure 1.14 *Mechanisms of heat transfer during ablative therapy*

Figure 1.15 *Effect of vessel number and hepatic inflow tract clamping on RFA lesion volume*

Figure 1.16 *Regression plots showing inverse correlation between RFA lesion diameter / RFA lesion volume and hepatic blood flow*

Figure 1.17 *Gross appearance of an RFA lesion adjacent to a 4 mm hepatic vein*

Figure 1.18 *Gross appearance and NADH staining of a MWA lesion adjacent to a 6 mm hepatic vein*

Figure 1.19 *Gross appearance and NADH staining of a MWA lesion adjacent to a 6 mm hepatic vein*

Figure 1.20 *Lesion diameter as a function of exposure time for HIFU lesions made in rat liver in the presence and absence of perfusion*

Figure 1.21 *Passive acoustic and hyperecho maps formed during a 5 s HIFU*

exposure at 8.0 MPa $_{pk-}$ in bovine liver

Figure 2.1 *Portal venous and hepatic venous arrangement of the pig liver (From Court et al. 2003)*

Figure 2.2 *Haematoxylin and eosin stain of sectioned porcine liver (100 x) showing the hexagaonal hepatic lobule surrounded by a fibrous layer*

Figure 2.3a *IVC, portal venous and hepatic arterial pressure and flow rates as a function of time during 72 hour extracorporeal porcine normothermic liver perfusion (From Butler et al. 2002)*

Figure 2.3b *pH and base excess as a function of time during 72 hour extracorporeal porcine normothermic liver perfusion (From Butler et al. 2002)*

Figure 2.3c *ALT/ALP, bile output and oxygen consumption during 72 hour extracorporeal porcine normothermic liver perfusion (From Butler et al. 2002)*

Figure 2.4 *Diagram of the Extracorporeal Liver Perfusion Device (ECLPD)*

Figure 2.5 *Photograph of the ECLPD*

Figure 2.6 *Photograph of a normothermically perfused porcine liver 1 hour following reperfusion on the ECLPD*

Figure 2.7 *Schematic diagram of the HIFU experimental set up*

Figure 2.8 *Static arrangement of the 1.06 MHz HIFU transducer and L10-5 linear array, mounted within custom-made Mylar holders and bolted together*

Figure 2.9 *Photograph of the HIFU experimental setup showing the perfused liver immersed in colloid solution, suspended in a impermeable bag / silicone sling above a water bath filled with degassed, deionised water at 37 ˚C.*

Figure 2.10 *Schematic diagram showing alignment protocol.*

Figure 2.11 *Schematic diagram showing method of passive acoustic mapping*

Figure 3.1 *Mean portal venous (a), hepatic arterial (b) and IVC (c) flow rates during NMP*

Figure 3.2 *Mean arterial PO_2 and PCO_2 during NMP*

Figure 3.3 ***Mean** pH during NMP*

Figure 3.4 *Mean blood temperature during NMP*

Figure 3.5 *Bile production during NMP in the cannulated CBD and total bile production at the end of NMP*

Figure 3.6 *Appearance of the perfused porcine liver following approximately 60*

minutes of NMP, prior to placing in a water bath and commencing HIFU experiments

Figure 3.7 *Gross appearance following 17 to 26 hours of NMP, after completion of HIFU studies*

Figure 4.1 *Schematic diagram of the HIFU experimental set up used for cavitation studies*

Figure 4.2 *Schematic diagram showing method of passive acoustic mapping*

Figure 4.3 *Passive acoustic maps displaying levels and spatial distribution of broadband emissions, representing inertial cavitation, in two single locations a) A microvascular-perfused area, away from a large vessel and b) A region of liver parenchyma directly adjacent to a large (≥ 5 mm) blood vessel.*

Figure 4.4 *PAMs showing focal cavitation activity and off-focus cavitation*

Figure 4.5 *Peak focal broadband energy, representing inertial cavitation, and harmonic energy in microvascular areas and regions adjacent to a large (≥ 5 mm) blood vessel plotted as a function of peak rarefaction pressure (MPa) for 1 s CW HIFU exposures at 1.06 MHz*

Figure 4.6 *Sum of the broadband energy at the HIFU focus (logarithmic scale) over 1 s 1.06 MHz HIFU exposures as a function of peak*

rarefaction pressure in microvascular areas and tissue regions adjacent to a large (≥ 5 mm) blood vessel, in the presence and absence of blood flow

Figure 4.7 *Peak focal broadband energy and harmonic energy in microvascular areas and regions adjacent to a large (≥ 5 mm) blood vessel, plotted as a function of peak rarefaction pressure (MPa) for 1 s CW HIFU exposures at 3.18 MHz.*

Figure 4.8 *Probability of cavitation plotted as a function of peak rarefaction pressure for studies conducted in 3 normothermically-perfused livers, static ex vivo blood at 4 ˚C and 37 ˚C and 0.9% sodium chloride solution warmed to 37 ˚C (From Labouret et al. – unpublished).*

Figure 4.9 *Diagram displaying cavitation events determined by observation of broadband activity as detected by a PCD during short pulse (25 cycle) 1.067 MHz HIFU exposures in a perfused porcine liver model under normal physiological blood flow conditions and with brief cessation of perfusion (From Labouret et al. – unpublished).*

Figure 4.10 *Probability of cavitation during 1s CW HIFU exposures plotted as a function of peak rarefaction pressure for studies performed under normoxic, normocapnic , hyperoxic, hypoxic, hypocapnic and hypercapnic conditions (From Labouret et al. – unpublished).*

Figure 5.1 *Schematic diagram of the HIFU experimental set up used for thermal studies*

Figure 5.2 *B-mode ultrasonography showing a microvascular area (L) and with colour Doppler (R), demonstrating a large (5 mm) portal venous branch, which was subsequently targeted for large vessel thermometry studies*

Figure 5.3 *Representative thermometry curves in a microvascular region and in tissue adjacent to a large (> 5 mm) blood vessel showing temperature changes during 6 s HIFU exposures at acoustic pressures ranging from 3.7 to 14.7 MPa $_{PPk}$.*

Figure 5.4 *Representative temperature curves for 1 s 1.06 MHz HIFU exposures at range of peak rarefactional pressures (1.88 MPa $_{pk-}$ to 5.58 MPa $_{pk-}$)*

Figure 5.5 *Mean peak temperature rise measured by direct real time thermometry as a function of peak rarefactional pressure in microperfused tissue regions (Figure 4.5 a, n = 4) and in tissue regions adjacent to a large (≥ 5 mm) blood vessel (Figure 4.5 b, n = 4).*

Figure 5.6 *Mean peak temperature rises during 1 s 1.06 MHz HIFU exposures in both microperfused areas (blue markers) and regions adjacent to a large (≥ 5 mm) blood vessel in both the presence of blood flow and*

in the absence of perfusion.

Figure 5.7 *Paired mean differences in peak temperature rise during 1 s 1.06 MHz HIFU exposures in microperfused tissue (n = 4) and areas immediately adjacent to a large (≥ 5 mm) blood vessel (n = 4).*

Figure 5.8 *Maximum broadband energy at the HIFU focus for each of the 1 s 1.06 MHz exposures, calculated from PAMs, as a function of peak rarefactional pressure.*

Figure 5.9 *PAMs mapping both summative broadband emissions and harmonic emissions during 1 s, 1.06 MHz exposures at 4.65 MPa $_{Pk-}$ (top) and 5.58 MPa $_{Pk-}$ (bottom) in a single microvascular-perfused area in the presence of blood flow (left) and in the absence of perfusion (right).*

Figure 5.10 *PAMs mapping both summative broadband emissions and harmonic emissions during 1 s, 1.06 MHz exposures at 4.65 MPa $_{Pk-}$ (top) and 5.58 MPa $_{Pk-}$ (bottom) in a single tissue region adjacent to a large (≥ 5 mm) vessel in the presence of blood flow (left) and in the absence of perfusion (right).*

Figure 5.11 *Peak temperature rise as a function of broadband energy for 1s 1.06 MHz HIFU exposures at 5 peak rarefactional pressures ranging from 1.88 – 5.58 MPa in microvascular areas and regions adjacent to a large (≥ 5 mm) vessel, both in the presence of blood flow and*

the absence of perfusion.

Figure 5.12 *Representative temperature curves for 1 s 3.18 MHz HIFU exposures at a range of peak rarefactional pressures (0.90 MPa $_{pk-}$ to 5.16 MPa $_{pk-}$).*

Figure 5.13 *Mean peak temperature rise as a function of peak rarefactional pressure (MPa) during 1 s continuous wave 3.18 MHz HIFU exposures in microvascular tissue regions (Figure 5.13 a, n = 3) and areas adjacent to a large (≥ 5 mm) blood vessel (Figure 5.13 b, n = 3).*

Figure 5.14 *Mean difference in peak temperature rise during 1 s 3.18 MHz HIFU exposures in microperfused tissue (n = 3) and areas immediately adjacent to a large (≥ 5 mm) blood vessel (n = 3) between values obtained at a given acoustic pressure in the presence and in the absence of blood flow, with the perfusion device turned off*

Figure 6.1 *Schematic diagram showing protocol for lesion threshold studies*

Figure 6.2 *Diagram showing 5 x 3 Raster scan ablation of a perivascular volume of hepatic parenchyma.*

Figure 6.3 *NADH staining following HIFU ablation (from Luo et al. 2009)*

Figure 6.4 *Indirect immunofluorescence using a primary IgG antibody to the specific antigen target e.g. mouse anti-Caspase-3, and a fluorophore-conjugated secondary antibody to the species of the primary antibody, e.g. FITC-conjugated donkey anti-mouse (from Odell and Cook, 2013)*

Figure 6.5 *Apoptotic cell signaling pathways (from Xu and Shi, 2007)*

Figure 6.6 *Gross histology following lesion threshold studies*

Figure 6.7 *Measurement of vessel diameter using B-mode ultrasound and subsequent quantification of flow velocity using colour Doppler*

Figure 6.8 *B-mode images of 4 individual large vessels locations with colour Doppler, assessing vessel flow rates*

Figure 6.9 *Hyperecho formation during HIFU exposure*

Figure 6.10 *Macroscopic appearance of 4 perivascular HIFU lesions*

Figure 6.11 *Close up appearance of a perivascular HIFU lesion*

Figure 6.12 *Positive NADH stain controls*

Figure 6.13 *NADH staining of control liver parenchyma*

Figure 6.14 *Negative NADH stain controls*

Figure 6.15 *Micrographs (10 x magnification) showing NADH staining at the HIFU lesion periphery*

Figure 6.16 *Image of a NADH stained frozen section of a HIFU lesion adjacent to a large blood vessel*

Figure 6.17 *NADH staining of tissue adjacent to the vessel wall at the edge of the HIFU lesion.*

Figure 6.18 *NADH staining of vessel wall (VW) and perivascular tissue away from the HIFU lesion (a and c) and within 2 separate HIFU lesions (b and d).*

Figure 6.19 *NADH staining of tissue at the vessel wall interface at the periphery of 4 HIFU lesions.*

Figure 6.20 *NADH staining of tissue within the HIFU ablation volume from 2 different lesions, adjacent to a large vessel.*

Figure 6.21 *NADH staining and ethidium homodimer-1 fluorescent staining of negative control liver parenchyma from untreated normothermically perfused porcine livers and positive control tissue from liver samples heated to 60 °C for 10 minutes in a water bath.*

Figure 6.22 *NADH staining and ethidium homodimer-1 staining of the edge of a HIFU lesion positioned at the vessel wall– vessel interface.*

Figure 6.23 *NADH staining and corresponding ethidium homodimer-1 staining of the same tissue from the edge of two HIFU lesions adjacent to large vessels.*

Figure 6.24 *NADH staining and ethidium homodimer-1 staining of the edge of a HIFU lesion.*

Figure 6.25 *Cleaved caspase-3 expression within ablated areas of liver parenchyma and untreated tissue*

Figure 6.26 *Cleaved caspase-3 immunofluorescence at the HIFU lesion periphery*

LIST OF TABLES

Table 1.1 *Summary of cavitation thresholds at 1 MHz for different ex vivo and in vivo tissues*

Table 1.2 *Summary of clinical studies investigating HIFU as an ablative therapy*

Table 2.1 *Hepatic venous and portal venous pressures, hepatic arterial, PV and total hepatic blood flow rates, together with relative proportions in pigs and humans*

Table 2.2 *Vascular pressure and gas partial pressure ranges during normothermic perfusion preservation*

Table 4.1 *HIFU parameters for cavitation studies*

Table 5.1 *HIFU exposure parameters for preliminary thermal experiments*

Table 5.2 *HIFU exposure parameters for thermal experiments performed at 1.06 MHz*

Table 5.3 *HIFU exposure parameters for experiments performed at 3.18 MHz*

Table 6.1 *HIFU parameters for volume ablation studies*

Abbreviations and Symbols

˚C	Degrees Celsius
ALT	Alanine aminotransferase
AST	Aspartate aminotransferase
CBD	Common bile duct
CEM_{43}	Cumulative equivalent minutes at 43 ˚C
CO_2	Carbon dioxide
CRLM	Colorectal liver metastases
CT	Computerised tomography
CW	Continuous wave
DAQ	Data acquisition
DC	Duty cycle
ECLPD	Extracorporeal liver perfusion device
ECMO	Extra-corporeal membrane oxygenator
Ethd-1	Ethidium homodimer-1
H&E	Haematoxylin and eosin
H^+	Hydrogen ions
H_2O	Water
HA	Hepatic artery
Hb	Haemoglobin
HBV	Hepatitis B virus
HCC	Hepatocellular carcinoma
HCO_3	Bicarbonate
HCV	Hepatitis C virus
HIFU	High intensity focused ultrasound
IVC	Inferior vena cava

kPa	Kilopascals
L	Litre
LV	Large vessel
MHz	Megahertz
Mins	Minutes
mm	Millimeters
MP	Microperfused
MPa	Megapascals
MRI	Magnetic resonance imaging
MV	Microvasculature
MWA	Microwave ablation
NADH	Nicotinamide adenine dinucleotide
nm	Nanometers
NMP	Normothermic machine perfusion
O_2	Oxygen
OLT	Orthotopic liver transplantation
P_aCO_2	Arterial partial pressure of carbon dioxide
PAM	Passive acoustic mapping
P_aO_2	Arterial partial pressure of oxygen
PC	Personal computer
PCD	Passive cavitation detector
PCO_2	Partial pressure of carbon dioxide
PEI	Percutaneous ethanol
Pk-	Peak negative
PO_2	Partial pressure of oxygen
PPK	Peak-to-peak
PPV	Proportional pinch valve
PRFP	Peak focal rarefactional pressure
PV	Portal vein
RFA	Radiofrequency ablation
s	Seconds

SD	Standard deviation
SEM	Standard error of the mean
T	Temperature
TPN	Total parenteral nutrition
US	Ultrasound
Δ	Change
λ	Wavelength
μm	Micrometers
Ω	Ohms

CHAPTER 1

INTRODUCTION

1.1 Thesis Aim

The overall aim of the current work was to elucidate the effects of perfusion on high intensity focused ultrasound (HIFU) therapy, in particular on cavitation, heating and histological tissue damage during thermal ablation by HIFU. The clinical motivation behind this work is that current minimally invasive thermal ablative strategies used in the treatment of liver cancer, namely radiofrequency (RFA) and microwave ablation (MWA) are limited by large vessel perfusion. Clinical data suggest that both RFA and MWA are less effective in the treatment of primary liver cancer and liver metastases compared to conventional surgical resection. Although studies describing mathematical models of the effects of capillary and large vessel perfusion on HIFU-induced heating are available, there has been little work investigating perfusion effects *in vivo*. Therefore, developing a thermal ablation technique with fewer perfusion effects than current ablative therapies may improve oncological outcomes in the treatment of liver cancer.

The aim was addressed by performing a number of HIFU studies in an *ex vivo*, normothermically perfused porcine liver model, with similar physiological and anatomical characteristics to a human liver. During HIFU therapy, cavitation events were recorded, quantified and mapped using a passive acoustic mapping technique and

direct temperature changes were measured in real time. Histological studies were performed to provide evidence of tissue necrosis throughout the intended HIFU focus in order to correlate thermometry and cavitation data with evidence of tissue damage at a microscopic level.

The novelty of this work includes the use of a unique extracorporeal, normothermic liver perfusion device to provide a functional, relevant porcine liver model, with similar perfusion and anatomical characteristics to that of a human liver. Studies have demonstrated that the perfusion device can keep a liver alive *ex vivo* for in excess of 72 hours. Real time temperature measurements during HIFU therapy, acquired through an implanted needle thermocouple, could be studied, which have not been reported in previous *in vivo* studies. A novel technique, in which acoustic emission data were captured passively during HIFU therapy by a diagnostic linear array and then subjected to a beam-forming algorithm to map and quantify cavitation in time and space, was performed to assess the effects of perfusion on HIFU-induced cavitation in real time. Whilst limited histological data are available describing the effects of perfusion on lesion formation in HIFU therapy, no studies have been published detailing the histological effects of large vessel blood flow, which is one of the major factors limiting efficacy in current clinical ablative therapies.

1.2 Liver Cancer Epidemiology

The overall incidence of cancer has increased over the last thirty years, both within the UK and worldwide, with the age-standardised incidence increasing by 14 % in males and 32 % in females over this period, although rates have remained relatively static over the last 10 years (Ferlay et al., 2010, Jemal et al., 2011). In 2007, the age-standardised incidence in the UK for all cancers excluding non-melanoma skin cancer was 409 per 100,000 in males and 357 per 100,000 in females (Olsen et al., 2008). Overall, cancer is the leading cause of mortality within the UK, roughly equating to around the number of deaths per annum contributable to respiratory and cardiac diseases combined (*Figure 1.1*). In 2012, around 162,000 people died from cancer within the UK, with most of these deaths due to metastatic spread.

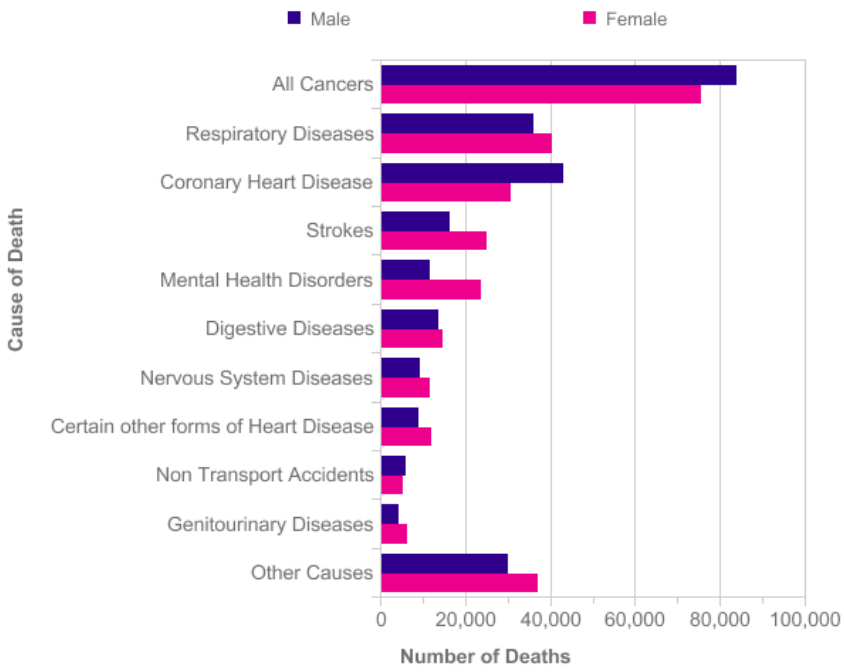


Figure 1.1 *– Commonest causes of death in the UK and number of deaths for 2011, per sex (Cancer Research UK).*

Cancer is also a leading cause of morbidity, affecting patients' quality-of-life and leading to significant socioeconomic costs in terms of community and hospital care.

1.2.1 Primary Liver Cancer

Although primary hepatic cancer, typically hepatocellular carcinoma (HCC), is uncommon in the UK, ranking 18th on the list of the commonest cancers, with an incidence of 5.1 per 100,000 population per annum (Office for National Statistics Data, 2013), the incidence is much greater within areas of Asia and Africa due to the high prevalence of Hepatitis B and C and is increasing in the Western world. In Eastern Asia, it is estimated that the incidence of HCC is around 45 per 100,000 population per annum (*Figure 1.2*), which is similar to the incidence of colorectal cancer in Western Europe (Nordenstedt et al., 2010, Jemal et al., 2011). Hepatocellular carcinoma has an estimated annual incidence of around 1 million patients worldwide and is an increasing problem in both the developed and developing world. In 2011, just fewer than 4500 people were diagnosed with hepatocellular carcinoma in the UK.

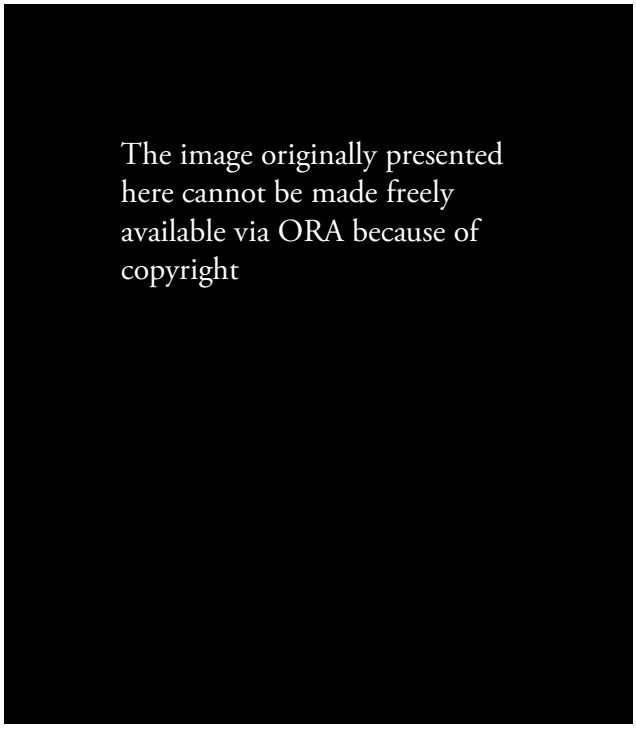


Figure 1.2 *– Age-standardised incidence rates for primary liver cancer worldwide in 2008. From Jemal et al. (2011)*

1.2.2 Liver Metastases

In Western countries, the majority of liver cancer is due to metastatic spread from primary malignancies of other organs. The liver is the second most common site for malignant spread, only exceeded by metastasis to lymph nodes and, in an autopsy study, 50 % of patients with cancer had evidence of hepatic metastasis at the time of death (Viadana and Au, 1975, Hess et al., 2006). Colorectal cancer is the most frequent cause of hepatic metastases due to portal seeding from haematogenous spread via the portal venous system. As a result of this mechanism, colorectal liver metastases are often isolated with no evidence of disseminated, extrahepatic spread, unlike other gastrointestinal tract cancers, such as gastric or pancreatic adenocarcinoma (Weiss et al., 1980, Baker and Pelley, 1995, Weiss et al., 1986).

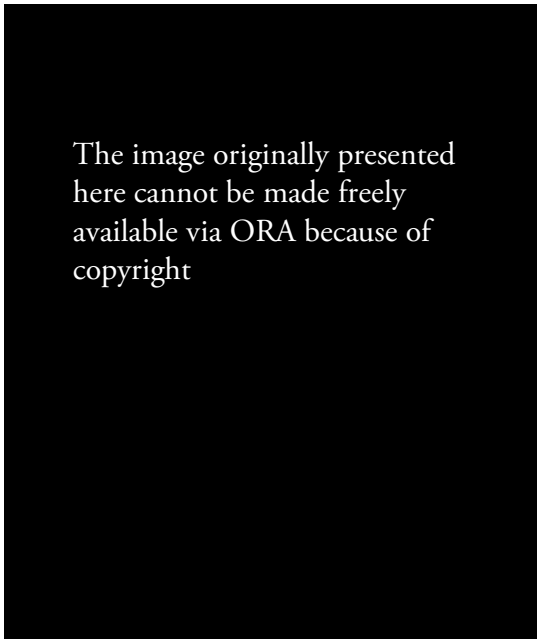


Figure 1.3 *– Age-standardised incidence rates for colorectal cancer worldwide in 2008. From Jemal et al. (2011)*

The incidence of colorectal cancer in the UK in 2009 was 66.6 per 100,000, making it the third most common malignancy after breast and lung cancer, accounting for 13 % of all new cancer cases. In 2011, 41,581 people were diagnosed with colorectal cancer in the UK (Office for National Statistics Data, 2013). Approximately 14-30 % of patients with colorectal cancer will have evidence of synchronous hepatic metastasis at presentation and a further 20 % will develop metachronous liver disease during the clinical course of the disease (Manfredi et al., 2006, Jones et al., 2012, Gatta et al., 2000). Therefore, the incidence of colorectal liver metastasis is in the order of 30 per 100,000 population, or around 20,000 people, in the UK per annum. In addition, a number of patients with primary neoplasms that frequently metastasize to the liver, including breast, gastric, oesophageal and lung cancer, will have liver disease at the time of presentation or will develop hepatic metastases during their disease course.

Therefore, patients with primary or secondary liver cancer are a common clinical entity and effective radical therapies and palliative strategies are required in order to provide curative potential where possible, or prolong survival and reduce morbidity.

1.3 Liver Anatomy and Physiology

The liver is a highly perfused organ, receiving approximately 30% of resting cardiac output, depending on the splanchnic flow. Uniquely, the liver receives a dual blood supply from the hepatic artery, supplying approximately 25% of the total hepatic blood flow, and the portal vein, supplying approximately 75%. Total blood flow to the liver is approximately 14.3-19.7 mL/min/kg, equating to 1.0-1.4 L/min for a 70 kg adult, roughly 25 – 30 % of the total body blood flow (Carlisle et al., 1992, Jakab et al., 1995, Dobson et al., 1953). The common hepatic artery, a branch of the coeliac axis arising from the abdominal aorta, has a mean arterial pressure of ≈ 90 - 100 mmHg and a mean flow rate of around 250 – 400 ml/min. The portal vein receives venous blood from the large and small bowel, pancreas, spleen and stomach, with a mean pressure of around 7 - 10 mmHg and a total flow rate of ≈ 750 – 1000 ml/min (*Figure 1.4*).

Given that the mass of an adult human liver is generally between 800 and 2200 g, the perfusion rate per unit volume of hepatic tissue is therefore around 60 – 100 ml/g/min. Differences exist in perfusion rates according to the splanchnic circulation, which is increased after eating, between different hepatic segments and also between healthy and cirrhotic liver (Taniguchi et al., 1993).

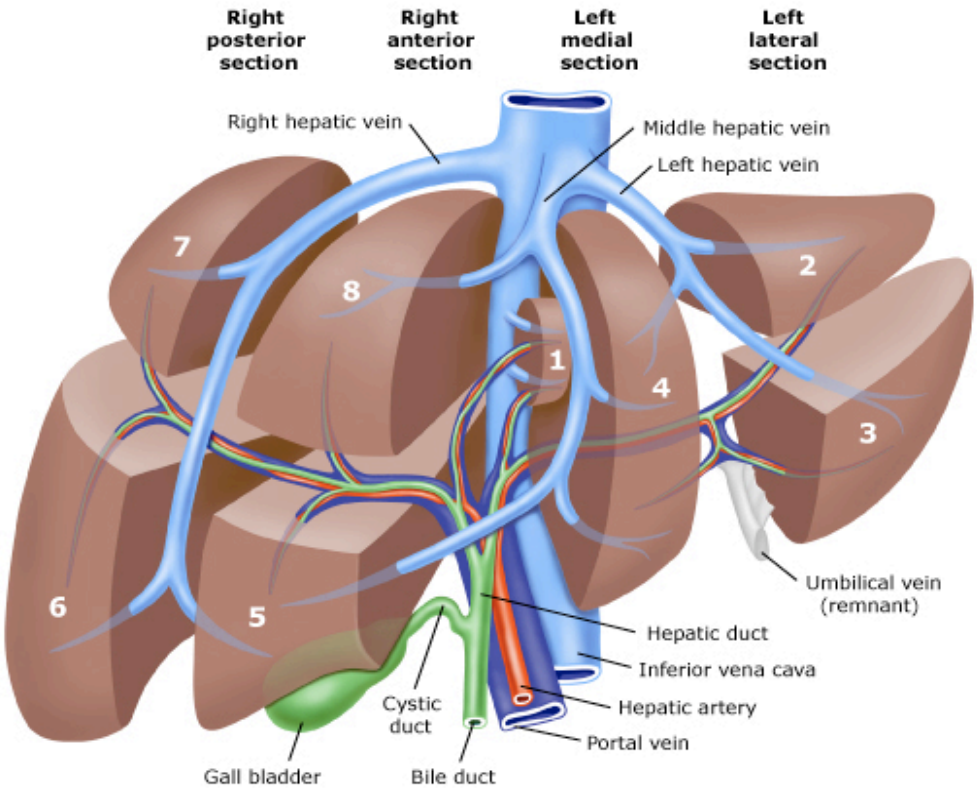


Figure 1.4 – *Major vascular and biliary anatomy of the liver as described by Couinard. The blood supply is via the common hepatic artery, a branch of the coeliac axis, although aberrant arteries exist in a small number of patients, and the portal vein. Drainage is via the hepatic veins into the inferior vena cava. The liver is divided into eight segments, each of which has is its own segmental artery, portal vein, hepatic vein and bile duct (Siriwardena et al., 2014).*

Hepatic tissue is highly heterogeneous, with a number of large vessels and biliary structures running within the parenchyma. The areas of tissues next to the largest vessels, with the most significant heat sink potential, lie at and near the porta hepatis and posteriorly, at the confluence of the hepatic veins and adjacent to the IVC. Flow rates in the hepatic IVC can be as high as 4 l/min, whilst flow rates in the left and right main portal veins are generally around 300 – 500 ml/min. The tissue regions towards the peripheries, where the hepatic parenchyma is more homogenous as vascular and biliary

structures gradually decrease in diameter are generally less susceptible to perfusion-related effects.

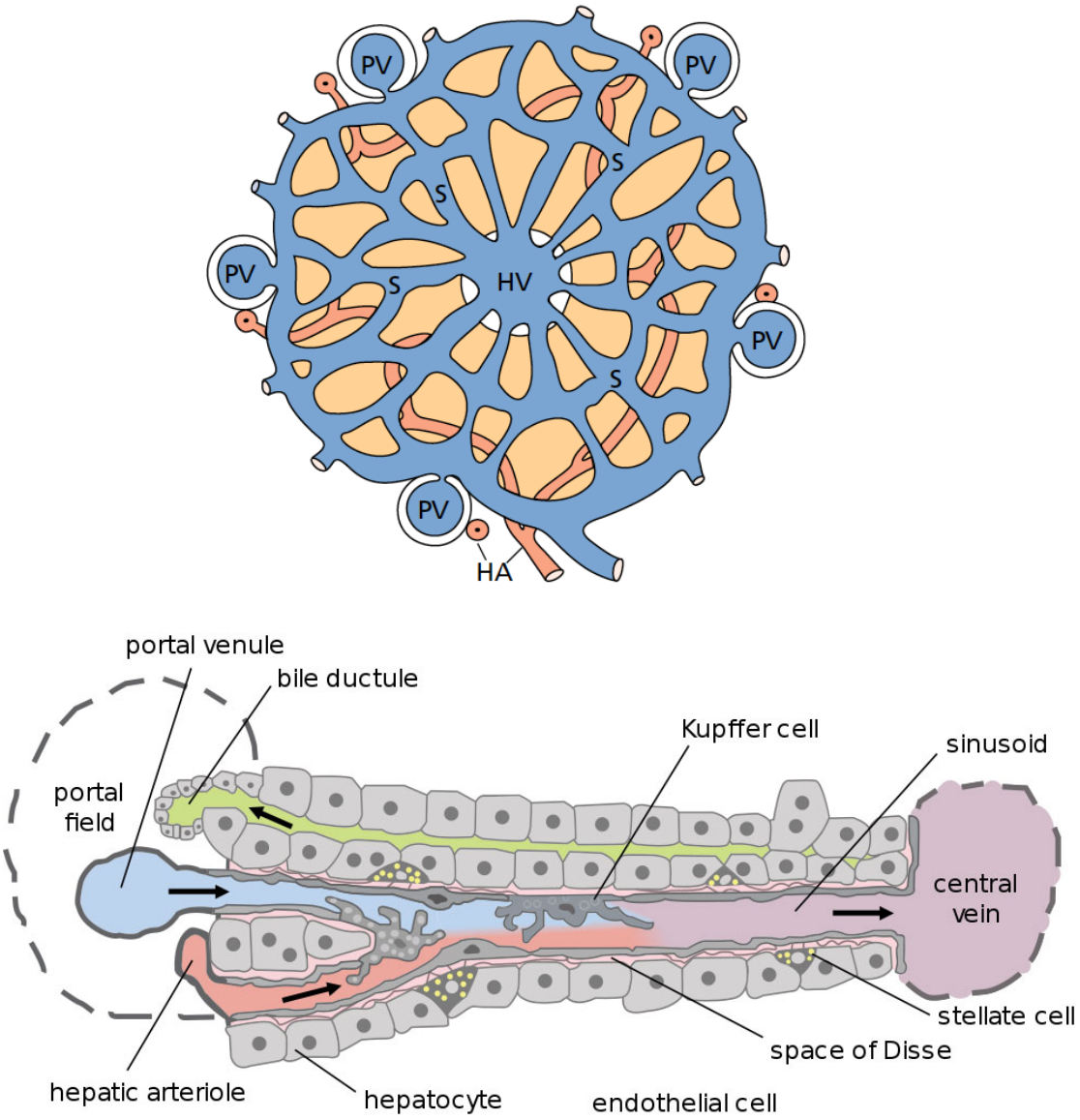


Figure 1.5 *– Structure of the hepatic lobule and acinus (top) and sinusoid (bottom). The lobule is hexagonal in geometry whilst each acinus, representing a single functional unit of the liver, is diamond shaped. Each acinus has a portal venule (PV) and terminal hepatic arteriole (HA), which mix in the hepatic sinusoids (S), draining into a central hepatic venule (HV). Hepatocytes, separated from the sinusoids by fenestrated epithelium, are the main functional cells within the liver. Bile ductules are arranged between layers of hepatocytes and transport bile, produced by the hepatocytes, into the major bile ducts (Frevert et al., 2005).*

Hepatic therapies are, therefore, potentially subject to significant perfusion effects, which may be more pronounced than in other, less well-perfused organs. Within a given treatment volume, there may be significant perfusion differences due to the presence of large vasculature, potentially causing a significant heat sink effect on a small part of the focal volume. Patient-specific factors, such as the presence of cirrhosis, may need to be taken into consideration when accounting for hepatic perfusion as these may affect global and local blood flow characteristics.

1.4 The Treatment of Liver Cancer

A number of factors affect the choice of treatment for liver cancer, including the primary histological type, performance status and wishes of the patient, the number, anatomical location and size of hepatic lesions and whether there is any evidence of extra-hepatic metastasis. In general terms, there are 4 broad categories of liver cancer, which all have different treatment algorithms depending on patient and disease characteristics. Therapeutic indications and options for hepatocellular carcinoma, colorectal liver metastases (CRLM), non-colorectal liver metastases (NCRLM) and neuroendocrine tumours all differ, due to the reasons detailed above. Typical management strategies for HCC and CRLM are shown below in *Figures 1.6* and *1.7*.



Figure 1.6 - Treatment algorithm for primary HCC. Curative treatments include resection, liver transplantation and ablation. PS = Performance status, CTP = Child-Turcotte-Pugh Score, OLT = orthotopic liver transplantatiom, PEI = percutaneous ethanol injection, RFA = Radiofrequency ablation (Forner et al., 2012).

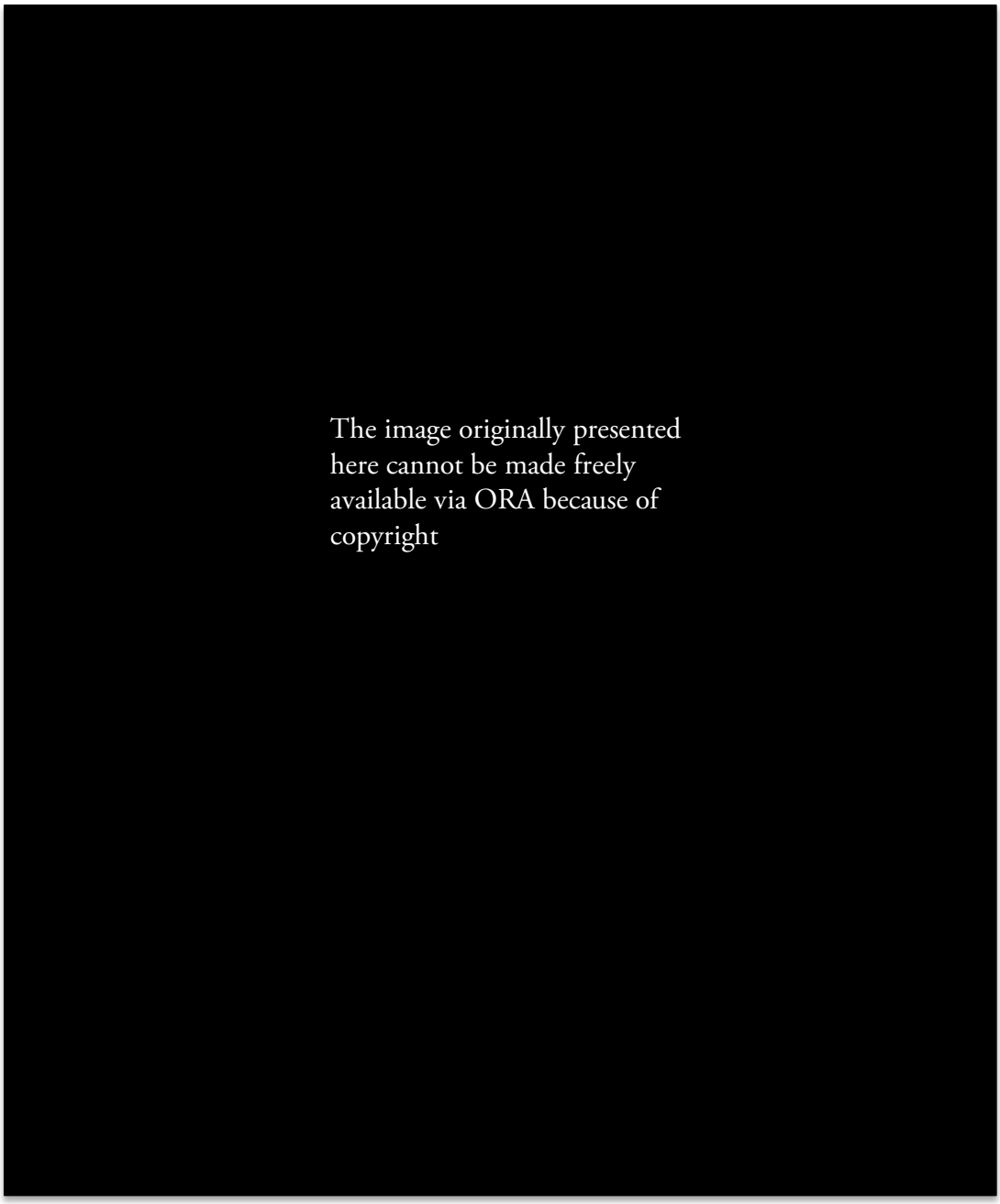


Figure 1.7 - *Management algorithm for colorectal liver metastases. Surgical resection with neoadjuvant / adjuvant chemotherapy is the gold standard curative strategy for potentially resectable disease. From (Haddad et al., 2011)*

1.4.1 Surgical Resection and Liver Transplantation

Surgical resection, or liver transplantation for primary HCC meeting specific criteria (see *Figure 1.6*), remain the gold-standard curative option for suitable liver cancer in patients whose performance status is sufficiently good enough to undergo major surgery (Clavien et al., 2012, Forner et al., 2012, Ryder, 2003, Al-Asfoor et al., 2008, Fong et al., 1997). Although, only around 15 – 20 % of patients with colorectal liver metastases will have hepatic disease amenable to surgical resection, given that around 42,000 people are diagnosed with colorectal cancer in the UK per annum with approximately 15 - 30 % having liver metastases at the time of presentation, a patient presenting with isolated, potentially treatable colorectal liver metastases is still a relatively common clinical entity. Non-colorectal liver metastases are rarely amenable to resection due to the presence of extra-hepatic macro- or micro-metastatic disease and outcomes are poor following resection, even when feasible. In addition, around 80 – 85 % of patients with either HCC or colorectal liver metastases will be unsuitable for either surgical resection or liver transplantation, in the case of HCC, at the time of presentation, either because of disseminated disease, cirrhosis, anatomical irresectibility or poor performance status (Fong et al., 1997, Steele and Ravikumar, 1989, Abdalla et al., 2004, Abdalla et al., 2006).

For the minority of patients with solitary or confined colorectal liver metastases amenable to resection, surgical resection provides the best chance of long-term survival, with reported actuarial survival rates of 30 – 40 % (Nordlinger et al., 2008). However, approximately 60 – 70 % of patients who have undergone radical surgical treatment for hepatic metastases will suffer a relapse of their disease, usually within the liver. One

recent meta-analysis of nineteen studies and 2247 patients reported a mean 5-year survival rate of 38.4 % (range 17 – 61 %) following hepatic resection of colorectal metastases (Jones et al., 2012). A separate meta-analysis reported 10-year survival rates, representing an effective cure rate, of 17-33 % (Memon and Beckingham, 2001).

1.4.2 Chemotherapy and Radiotherapy

Chemotherapy remains the mainstay palliative treatment for both primary and secondary liver cancer, but is also frequently used as a neo-adjuvant or adjuvant therapy for radical surgical or ablative therapies in order to downstage disease prior to treatment, or to improve post-treatment outcomes (Van Cutsem et al., 2010). Neoadjuvant chemotherapy with the FOLFOX regime prior to hepatic resection has been reported to improve the 5-year progression-free survival by around 7 % in a randomized controlled trial (Nordlinger et al., 2008).

One of the main factors limiting conventional chemotherapy is the systemic toxicity and unwanted side effects, which are often the dose-limiting factors, restricting the concentration of chemotherapy that can be delivered to the tumour site, which in turn limits treatment efficacy. A number of strategies have been developed in order to improve efficacy, whilst reducing systemic side effects.

1.4.2.1 Biological therapies

Personalised medicine is increasingly being utilized in clinical practice in order to define an individual patient's disease characteristics at the molecular level and to target these biomarkers accordingly. A number of monoclonal antibodies have been introduced into

the clinical arena, which specifically target malignant colorectal adenocarcinoma cells through cancer-specific receptors and aim to improve treatment efficacy when used in conjunction with conventional chemotherapy (Maughan et al., 2014). A number of Phase II randomized trials investigating the efficacy of Cetuximab, a monoclonal antibody that inhibits epidermal growth factor in patients with wild-type *k-ras* disease, have shown an improved progression-free survival compared to chemotherapy alone (Bokemeyer et al., 2011, Van Cutsem et al., 2011), although other randomized trials have failed to demonstrate this benefit (Maughan et al., 2011). However, the development of targeted biological therapeutic agents remains an attractive research area as there is a strong clinical need to improve treatment efficacy by specifically targeting malignant cells, whilst sparing healthy tissue from the adverse effects of cytotoxic chemotherapeutic agents and / or radiotherapy.

1.4.2.2 Loco-regional Therapies

A number of loco-regional therapies such as transarterial chemoembolization (TACE) and selective internal radiotherapy treatment (SIRT) are increasingly being used, which have been developed as another strategy in order to improve treatment efficacy, whilst minimising systemic toxicity and side effects. Given that systemic toxicity is usually the dose-limiting factor, selective delivery of chemotherapy allows a much higher dose to be delivered direct to the tumour and a higher intra-tumoural concentration to be achieved.

A branch, or branches, of the proper hepatic artery typically supplies most hepatocellular carcinomas. In TACE, mesenteric angiography and selective injection of drug-eluting particles, such as gelatin or polymer microspheres loaded with doxorubicin or cisplatin,

directly into the feeding artery supplying the HCC allows delivery of high concentrations of chemotherapeutic agents direct to the tumour tissue, whilst minimising exposure of normal hepatic tissue and other organs to cytotoxic agents. Embolisation of the feeding artery by injection of embolic particles is also performed in combination with selective chemotherapy delivery, which reduces the tumour's blood supply, reducing the tumour growth rate until neovascularization occurs, whilst also reducing washout of the chemotherapeutic agent since tumoural blood flow is reduced following embolisation. Therefore, a higher dose of the chemotherapeutic agent remains within the tumour for a longer period of time than conventional systemic chemotherapy. The concentration within the tumour can be up to 40 times that of the adjacent tissue, and thus the normal hepatic tissue is relatively spared.

SIRT is used in the palliative treatment of both primary and metastatic liver cancers. Similar to TACE, the feeding artery arising from the proper hepatic artery is selectively catheterized following mesenteric angiography. Glass or resin microspheres containing radioactive yttrium-90 are infused directly into the feeding artery.

1.4.3 Thermal Ablative Therapies

First introduced into clinical practice in the early 1990's, thermal ablative therapies are increasingly being used as either an alternative or adjunct to surgery in the radical treatment of both primary and secondary liver cancer, or occasionally as a palliative therapy (see *Figures 1.6* and *1.7*). In the treatment of HCC, established liver cirrhosis often precludes resection of early stage disease and ablative therapies provide a potentially curative management strategy if liver transplantation is contraindicated, or not a viable

option. For colorectal liver metastases, thermal ablation may be used to treat disease present in the minor lobe combined with surgical resection of the major lobe, or as part of a two-stage procedure. Additionally, thermal ablation may be used in patients with relatively low-volume, potentially curable disease, who are not fit for major hepatic resection.

Radiofrequency (RFA) and microwave (MWA) are the two thermal ablative modalities most commonly used in current clinical practice, although techniques such as cryoablation are also used less frequently. High intensity focused ultrasound is a novel thermal therapy, which uses high energy, focused sound waves to heat tissue. One of the main benefits of thermal ablative techniques is that they are minimally invasive, requiring less physiological reserve and therefore are available to a higher number of patients than conventional surgical interventions. For ablative therapies to replace surgical resection as the gold standard curative treatment for liver cancer, equivalence would need to be demonstrated in terms of short and long term oncological and survival outcomes. However, whilst there are some data available that suggest that thermal ablation may be equivalent to surgical resection in the treatment of small (< 3 cm) tumours, this is not the case for larger tumours. The reasons for this are discussed later in this chapter, in Section 1.6.

1.4.3.1 Mechanism of Thermal Ablation

The goal of primary goal of ablation is to eradicate all viable malignant cells within a specified target tissue volume, usually including a margin of 0.5 – 1 cm of apparently normal surrounding tissue. One attractive advantage of focal ablation is that the

functional liver volume is preserved, whilst malignant tissue is destroyed through a number of mechanisms including heating, freezing and exposure to cytotoxic agents.

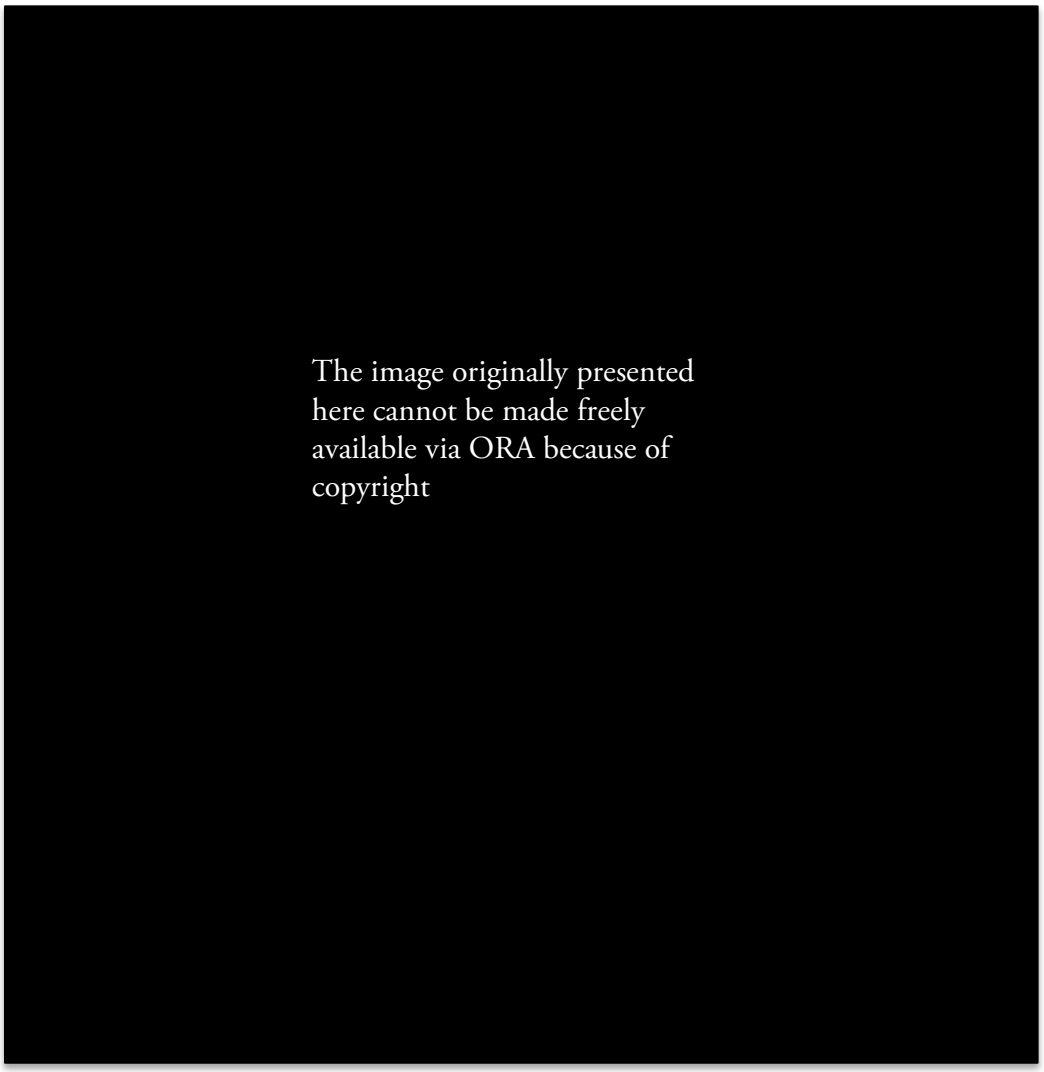


Figure 1.8 – *Mechanisms of tissue ablation in RF and MW therapy. From (Chu and Dupuy, 2014)*

The most widely implemented ablative methods in clinical practice are those that use heating to coagulate and destroy tissue. In order to induce coagulative necrosis within a given tissue volume, a minimum temperature of 55 ˚C needs to be reached and maintained for time intervals in excess of 1 s, although longer endpoints of 4 – 6 minutes are commonly in current clinical practice to ensure irreversible injury has been induced

(Wu et al., 2001). Above this temperature, near instantaneous coagulation of proteins and irreversible damage to critical mitochondrial and cytosolic enzyme complexes occurs, inducing cell death. Although the primary importance is that of complete ablation of all viable tumour tissue, it is also important to minimise collateral damage to surrounding structures, such as blood vessels and bile ducts.

Given than heat-induced cytotoxicity is dependent on both temperature and time, the thermal dose delivered by a number of therapies, including ablative modalities, has been proposed as a metric of thermal cell and tissue damage. Sarapeto and Dewey (1984) proposed the concept of cumulative equivalent minutes at 43 ˚C (CEM_{43}) as a method of integrating time and temperature variables as a single measurement. 43 ˚C was chosen as a normalisation temperature as, above this threshold, for every 1 ˚C temperature increment, the equivalent thermal effects are achieved in half the time than at 1 ˚C lower (Sapareto and Dewey, 1984). It is also known that different tissues and cells require differing thermal doses to achieve the same effect, which means that tumours are highly likely to have varying ablative thresholds according to histological subtype (Yarmolenko et al., 2011).

1.4.3.2 Radiofrequency Ablation

In radiofrequency ablation (RFA), a high-frequency alternating electrical current, generally in the range 200 – 1200 kHz, is delivered to target tissue through a needle electrode, which is converted to heat energy at the electrode tip. The needle electrode is inserted into the target tissue under CT, ultrasound or MRI guidance. An RF generator supplies RF power to the electrode, creating a voltage between the electrode and the

grounding pad, which acts as large, dispersive electrode. As the current alternates, ions within the tissue are agitated and, due to the naturally high resistance of tissue, this process causes frictional heating in the immediate vicinity of the electrode, known as the Joule effect. Heating occurs most rapidly in the tissue with the highest current density, i.e. the tissue surrounding the electrode, whilst more peripheral tissue is heated through thermal conduction.



Figure 1.9 – *Heating profile in RFA therapy. Heating rates and tissue temperatures are highest in the immediate vicinity of the electrode, whilst these decrease significantly as a function of distance from the electrode. (Ahmed et al., 2011).*

Since RFA was introduced into clinical practice in the early 1990s, a number of randomized controlled trials (RCT) and case series have assessed the efficacy of RFA in the treatment of both primary and metastatic liver cancer. In a recent Cochrane meta-analysis by Weis *et al.* of 3 RCTs comparing RFA to surgical resection in the treatment of hepatocellular carcinoma, whilst no significant differences were evident in between the two treatments in terms of the hazard ratio for 2 year and overall survival, there was a

significant difference in terms of event-free survival and local progression in favour of conventional surgical resection (Weis et al., 2013, Chen et al., 2006, Feng et al., 2012, Huang et al., 2010). On removing the trial with a high risk of bias from the analysis, surgical resection was found to provide an increased 2-year and overall survival benefit compared to RFA. Similarly, three systematic reviews and meta-analyses of trials comparing percutaneous ablation to surgical resection in the treatment of early stage HCC found that, whilst 1-year survival rates were similar in the two groups, the 3 and 5 year survival and 1, 3 and 5 year disease-free survival rates were significantly higher in the surgical resection group than the percutaneous RFA group, although patients undergoing hepatic resection had a significantly longer hospital stay and risk of postoperative complications (Duan et al., 2013, Ni et al., 2013, Qi et al., 2014).

There are fewer data available concerning the efficacy of RFA in the management of resectable colorectal liver metastases, with no RCTs currently available and only a relatively small number of clinical controlled trials and observational studies (Aloia et al., 2006, Mulier et al., 2008a, Mulier et al., 2008b, Oshowo et al., 2003, Park et al., 2008, Abdalla et al., 2004, Kim et al., 2011). However, these data suggest that RFA is not equivalent to surgical resection in the treatment of potentially resectable CRLM, although high quality RCTs need to be performed to assess this further. Cirocchi *et al.* (2012) undertook a systematic review and meta-analysis of 13 non-randomised studies and, although there was an inherently high degree of bias due to the trial designs, most studies reported a significantly reduced survival at either 3 or 5 years in the RFA group compared to the surgical resection group and an overall lower disease-free survival. In a retrospective comparative analysis of RFA Vs. surgical resection, Kim *et al.* (2011) and

Mulier *et al.* (2008b) suggested that RFA of solitary CRLM of < 3 cm in diameter achieved similar oncological outcomes to surgical resection. RFA has a role in the management of patients with small, irresectable CLRM, due to either disease factors, or due to patient fitness / wishes. Solbiati *et al*. reported 1, 3 and 5-year survival rates of 98 %, 69 % and 25 % and local tumour progression of 12 % following RFA of small (< 3.3 cm) CRLM in the above patient groups. In terms of the approach for RFA, percutaneous RFA appears to be associated with poorer disease-free survival compared to intraoperative surgical RFA, due to metastatic seeding along the RFA antenna track (Mulier et al., 2008b).

A number of factors affect the efficacy of RFA in successfully treating both primary and secondary malignant hepatic tumours, including head advection from large blood vessels, tumour size and accurate treatment monitoring. These limitations are discussed later in this chapter in Section 1.6.

1.4.3.3 Microwave Ablation

Microwave ablation uses electromagnetic waves within the microwave frequency spectrum in order to heat tissue. Two clinical generator systems are in widespread clinical use; one that operates at 2.4 GHz and one that operates at 915 MHz. Tissues high in water content are particularly responsive to heating through microwave energy as polar molecules, usually water molecules, are made to realign with the oscillating electrical field at rates of over several million times per second. Some of the kinetic energy from the rotating water molecules is converted into thermal energy, thus increasing the temperature of the tissue in which this process is occurring. In MWA, an

antenna is inserted into the target tissue and is used to deliver the electromagnetic energy in a targeted manner. Unlike RFA, in which an electrically conductive path is required, microwaves propagate through tissues with low electrical / thermal conductivity, high impedance and can penetrate charred or desiccated tissue, increasing the efficacy of heating. As distance from the electrode increases, the power decreases at a much lower rate than that seen in RFA.

As MWA has been used clinically for a shorter period of time than RFA, there are fewer long-term outcome data available. Additionally, only one small randomized controlled trial has been performed comparing MWA to surgical resection (Shibata et al., 2000, Bala et al., 2013). Shibata *et al.* (2000) randomized 30 patients with multiple colorectal liver metastases to either MWA or partial hepatectomy. The authors reported a mean survival of 27 months in the MWA group versus 25 months in the hepatectomy group, with disease-free intervals of 11 and 13 months respectively, with neither of these differences being statistically significant. However, as noted in a recent systematic review a significant degree of bias was present in the study by Shibata *et al.* and further larger, high quality randomized controlled trials need to be performed to assess the efficacy of MWA further compared to conventional resectional surgery (Bala et al., 2013).

Several non-randomised, retrospective studies have demonstrated that the factors influencing outcomes following MWA are similar to those affecting RFA outcomes, with tumour sizes > 3 cm, proximity to a large vessel and multiple tumour foci all associated with poorer recurrence rates and survival. Leung *et al.* (2014) conducted a retrospective single-centre analysis of MWA of 416 primary and secondary liver tumours in 176

patients. They reported local recurrence in 8% of tumours and 18 % of patients. Similar to RFA, factors associated with significantly higher rates of recurrence included proximity to a major blood vessel (< 10 mm from the IVC, major branch of the hepatic vein or segmental pedicle), tumour diameter > 3 cm and greater than 3 tumours in total. Three-year local recurrence rates were 1 % for tumours < 1 cm compared to 33 % for tumours > 3 cm in diameter (*Figure 1.10 – left*). As expected, tumour histopathology also affected local recurrence, with HCC and CRLM pathological subtypes displaying significantly lower recurrence rates at l and 3 years compared to non-CRLM and biliary carcinomas (*Figure 1.8 – right*).



Figure 1.10 – *3 year local recurrence rates following microwave ablation therapy for liver cancer in relation to tumour size (L) and underlying histopathological subtype (R). (Leung et al., 2014b)*

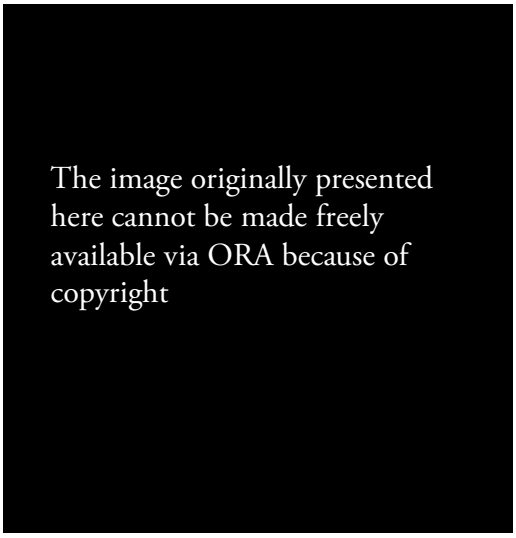


Figure 1.11 *– 3-year survival following microwave ablation therapy for colorectal liver metastases and other disease pathology. (Leung et al., 2014b)*

Median survival was reported to be 57 months, whilst three-year survival for patients with CRLM was 70 % compared to 80 % for other pathologies (*Figure 1.11*). Recurrence and mortality data from their study were comparable to published outcomes following surgical resection.

1.4.3.4 Cryoablation

In addition to thermal ablation by heating, cryoablation, where the focal tissue temperature is rapidly reduced to around - 75 °C, is used clinically. Small, hollow needles are introduced into the target tissue and cooled fluids are instilled, reducing the temperature in the surrounding tissue through thermal conduction. Rapid freezing disrupts cell membranes through the formation of ice crystals, induces apoptosis and causes coagulation of the local blood supply, leading to cell ischaemia and cellular necrosis.

Non-randomised clinical studies investigating cryoablation as an ablative method for the treatment of colorectal liver metastases have demonstrated varying results, with reported 1-, 3- and 5-year survival rates of between 46 % and 90 %, 8 % and 60 % and 0 % and 44 % respectively, with a median survival of 23 – 94 months (Bageacu et al., 2007, Pathak et al., 2011, Yan et al., 2003, Joosten et al., 2005, Niu et al., 2007, Seifert et al., 2005). However, safety concerns have led to other ablative techniques being adopted over cryotherapy. In the reported studies, procedure-associated morbidity was high, with major complication rates varying from 7 % to 66 %. One of the main concerns regarding cryoablation is cryoshock, whereby a systemic inflammatory response can occur following ablation, with studies reporting cryoshock as being responsible for approximately 15 – 20 % of peri-procedural deaths.

1.5 High Intensity Focused Ultrasound (HIFU)

1.5.1 The Basis of High Intensity Focused Ultrasound

High intensity focused ultrasound (HIFU) is a type of medical ultrasound and works on similar principles to diagnostic ultrasound. Ultrasound waves are created by applying an alternating electrical current across a piezoelectric material, such as quartz crystal. The piezoelectric crystal expands and shrinks proportionally in response to the voltage applied across it and the alternating current causes the crystal to vibrate at ultrasonic frequencies, emitting an ultrasound wave. However, the energy levels used in HIFU therapy are several orders of magnitude greater than those used in diagnostic medical ultrasound. Additionally, clinical applications of HIFU typically use frequencies between 0.5 and 3.5 MHz, compared to a frequency range of 1 – 20 MHz for diagnostic ultrasound.

In HIFU therapy, high-amplitude sound waves are focused deep within tissue, which can cause bio-effects through mechanical processes, or through conversion to thermal energy, thus heating tissue within the focal volume. The size of the HIFU volume is dependent on the geometry and frequency of the HIFU transducer, or transducers if a multi-element array is used, but is much smaller than the treatment volume encountered in RFA or MWA, is typically ellipsoidal in geometry, around 2 - 3 mm in diameter and 12 - 15 mm in length at 1 MHz. The size of the focus is a limitation in clinical HIFU treatment in that the volume ablated with each exposure is small compared to the volume of each tumour. Therefore, multiple exposures are required in order to completely ablate each tumour, often equating to a treatment time in excess of 2 hours and up to 6 hours in total (*Figure 1.12*).

1.5.2 HIFU-Induced Heating

HIFU-induced heating relies on viscous absorption of high amplitude sound waves that can be focused deep within tissue. As a result, heating occurs at the focus and, above a certain thermal threshold, this results in coagulative necrosis and ablation of the heated tissue volume (Wu et al., 2002). Unlike RFA and MWA, which require percutaneous insertion of an electrode into the target tissue, HIFU is completely non-invasive.

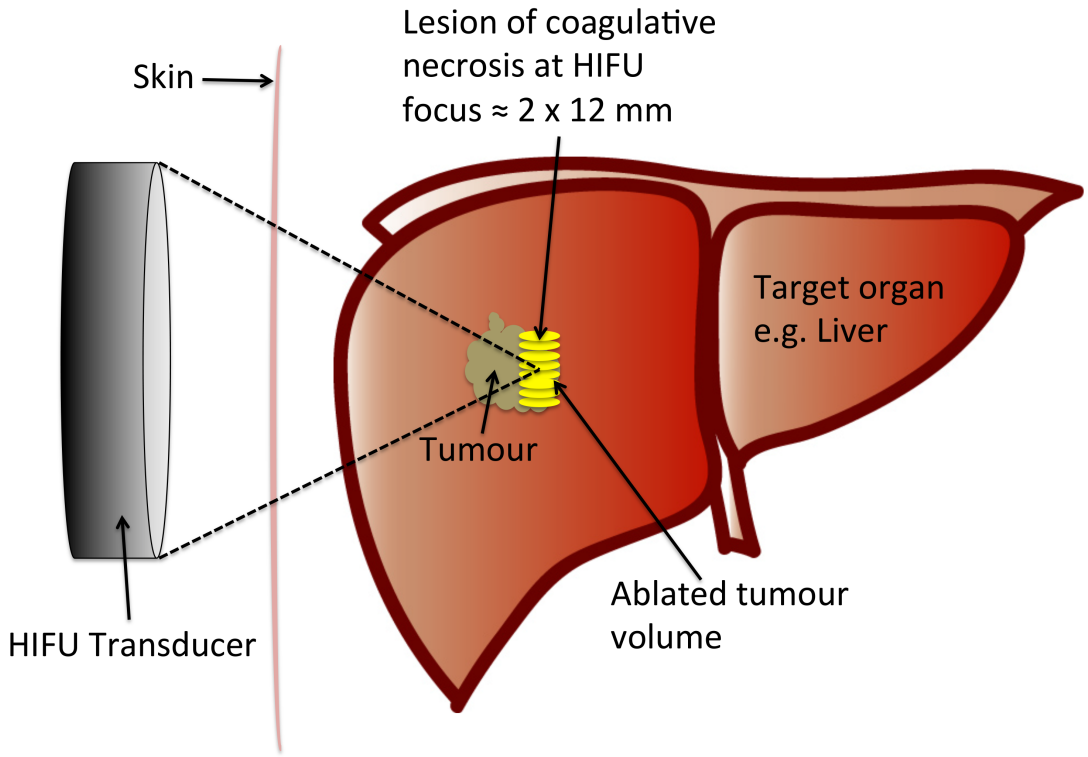


Figure 1.12 – *Schematic diagram showing HIFU ablation of a liver tumour. The treatment is completely non-invasive, with the HIFU focus positioned within the liver several centimetres in front of the transducer. The acoustic energy is focused at this point, leading to tissue heating and ablation through the process of coagulative necrosis, if the tissue temperature reaches*

beyond the threshold required. The HIFU focal volume is small and multiple exposures are needed to "paint" an entire tumour.

Lynn *et al.* first showed that focused ultrasound waves could be used to heat and destroy areas of *ex vivo* tissue (Lynn et al., 1942). The first *in vivo* studies were performed by Wall *et al.* in 1951, who demonstrated that central nervous tissue could be irreversibly damaged through exposure to a focused ultrasound beam, whilst not causing damage to the tissue interpositioned between the transducer and the focus (Fry et al., 1954, Wall et al., 1951).

1.5.3 HIFU-Induced Cavitation

When a tissue or liquid is placed under a sufficiently high enough acoustic pressure amplitude during HIFU therapy, small cavities can form under the rarefactional part of the pressure cycle. These microscopic bubbles initially start to oscillate linearly when the acoustic pressure of the HIFU field is low: a process known as stable cavitation, but the oscillation increases in non-linearity as the acoustic pressure field increases in amplitude. Oscillating bubbles emit their own acoustic pressure waves, which can be detected and monitored. With linear oscillation, bubbles emit acoustic pressure waves at the HIFU drive frequency and then subsequently at harmonic and subharmonics of the fundamental frequency as the HIFU pressure field is increased. Beyond a certain pressure amplitude, termed the inertial cavitation threshold, the oscillating bubbles start to expand unstably over the rarefactional half-cycle and collapse violently under the compressional half-cycle. This process, known as inertial cavitation, can be detected through broadband emissions, which are and has been demonstrated to enhance HIFU-

induced heating (Coussios et al., 2007, Holt and Roy, 2001, Hynynen, 1991, Kyriakou et al., 2011), whilst also providing a mechanism for novel treatment monitoring strategies (Coussios et al., 2007, Gyongy and Coussios, 2010, Jensen et al., 2012).

Cavitation in ex vivo and in vivo tissues

Whilst a number of studies have investigated the cavitation threshold, defined as the lowest peak rarefaction pressure at which the probability of a cavitation event occurring is either > 50 % or 100 % depending on the study, in various *ex vivo* tissues, few studies have reported results concerning cavitation *in vivo*. It is thought that cavitation thresholds and cavitation events throughout a HIFU exposure may differ significantly between *ex vivo* and *in vivo* tissues due to perfusion factors, potentially providing and replenishing cavitation nuclei and also due to the introduction of gas into air-exposed *ex vivo* tissue, combined with the effects of tissue decomposition. A summary of studies reporting cavitation thresholds in various tissues is shown below in *Table 1.1*.

Tissue	Cavitation Threshold at 1 MHz (PRFP)	*Ex / In vivo*	Reference
Adipose tissue	2.1 MPa	*Ex vivo* – porcine	(Kyriakou et al., 2011)
	3 – 4 MPa	*Ex vivo* – porcine	(Li et al., 2014)
Liver	8 – 9 MPa	*Ex vivo* – bovine	(Li et al., 2014)
	2 MPa	*Ex vivo* – bovine	(McLaughlan et al., 2010)
Kidney	7 – 8 MPa	*Ex vivo* – porcine	(Li et al., 2014)
Muscle	5 – 6 MPa	*Ex vivo* – canine	(Hynynen, 1991)
Tongue	2 – 3 MPa	*Ex vivo* – bovine	(Li et al., 2014)
Pancreas	2 – 3 MPa	*Ex vivo* – murine	(Li et al., 2014)
	< 5 MPa	*In vivo* – murine	(Li et al., 2014)
Brain	> 12.7 MPa	*In vivo* – sheep	(Gateau et al., 2011)

Table 1.1 *– Summary of cavitation thresholds at 1 MHz for different ex vivo and in vivo tissues*

Li *et al.* determined that the cavitation threshold, which they defined as a probability of cavitation of > 50 %, was highly variable in a variety of *ex* vivo tissue media and an *in vivo* murine pancreatic tumour model, ranging between 2.5 and 10 MPa $_{Pk}$ during 1.1 MHz HIFU exposures (Li et al., 2014). The cavitation threshold appeared to vary according to the various proportions of tissue water and lipid, with homogenous tissues high in lipid content, such as adipose tissue, having a lower cavitation threshold than heterogeneous tissues with a high water content, such as kidney and liver. They also determined that the cavitation threshold of *in vivo* murine pancreatic tumours lay below the lowest peak rarefaction pressure of 5 MPa and between 2 and 3 MPa in *ex vivo* pancreatic tissue. Bovine liver and porcine kidneys were found to have a significantly higher cavitation threshold of 9 and 8 MPa $_{Pk-}$ respectively. However, there are no studies reporting the cavitation threshold of liver *in vivo.*

Cavitation-Enhanced Heating

Whilst initial work investigating ultrasound-induced cavitation was primarily as a result safety concerns regarding diagnostic ultrasound, a number of more recent studies have explored the potential benefits of cavitation in therapeutic ultrasound therapy. Inertial cavitation can be used to augment heating rates during HIFU therapy, with several studies demonstrating that heating rates in the presence of inertial cavitation exceed those measured in the absence of cavitation at a given acoustic power, as shown in *Figure 1.13* (Hynynen, 1991, Miller and Gies, 1998, Coussios et al., 2007, Kyriakou et al., 2011).

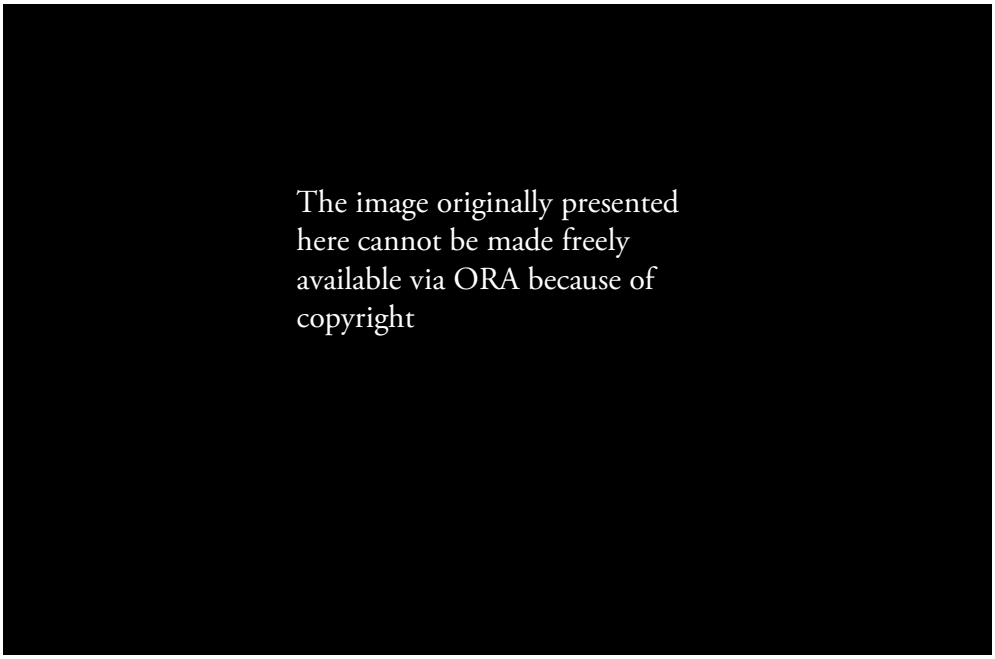


Figure 1.13 *- Heating in porcine adipose tissue in the absence of inertial cavitation (top right) and presence of cavitation (bottom right) during 2 s HIFU exposures at 0.5 MHz and 0.82 MPa* $_{Pk-}$*. Broadband (•) and harmonic emissions for each HIFU exposure (Δ) are plotted on the left-hand graphs. There is a significant enhancement of heating rates in the presence of inertial cavitation, with peak focal temperature over twice that achieved in the absence of cavitation. (Kyriakou et al., 2011)*

Given that there is significant variation in cavitation between tissues and also through the duration of a HIFU exposure *in vivo*, due to depletion and replenishment of cavitation nuclei, a number of recent studies have investigated the use of exogenous artificial cavitation nucleation agents in order to promote more predictable, consistent cavitation activity and exploit cavitation-enhanced heating further (Tung et al., 2006, Zhang and Porter, 2010).

1.5.4 Clinical Applications of HIFU

1.5.4.1 Thermal Ablation

High intensity focused ultrasound (HIFU) is a highly promising thermal ablative therapy, which is completely non-invasive and has been demonstrated to be effective against a range of solid organ tumours, including renal (Illing et al., 2005, Ritchie et al., 2010), liver (Illing et al., 2005, Kennedy et al., 2004, Ng et al., 2011, Cheung et al., 2011, Zhang et al., 2009, Fukuda et al., 2011, Jin et al., 2010, Wu et al., 2005), prostate (Crouzet et al., 2010, Lukka et al., 2011, Crouzet et al., 2014, Ganzer et al., 2013, Thuroff et al., 2003), breast (Wu et al., 2003) and pancreatic (Sung et al., 2011, Gao et al., 2013, Li et al., 2012) neoplasms, with a mixture of curative and palliative intents. Additionally, HIFU ablation is used in the treatment of symptomatic uterine fibroids, with good success (Leung et al., 2014a, Park et al., 2014).

Organ / Target	Reference	Trial Type	N	Outcomes
Kidney	(Illing et al., 2005)	Case series	6	4/6 successful radiological / histological ablation at 12 days
	(Ritchie et al., 2010)	Case series	17	10/17 successful ablation at 14-55 months
Liver	(Illing et al., 2005)	Case series	20	100% successful radiological / histological ablation at 12 days
Liver – irresectable HCC	(Ng et al., 2011)	Case series	49	Complete ablation 80% at 1month. Survival – 88 % (1 yr), 62 (3 yr)
Liver – irresectable HCC	(Zhang et al., 2009)	Case series	39	50% complete ablation. Survival – 76 % (1 yr), 50 (3 yr)
Liver – irresectable HCC	(Wu et al., 2005)	Non-randomised trial of HIFU + TACE Vs. TACE alone	26 / 24	Median survival 11.3 months / 1 yr survival 43 % (HIFU+TACE) Vs median survival 4 months / 1 yr survival 0 % (TACE alone).
Liver – small HCC (< 2cm)	(Fukuda et al., 2011)	Case series	12	92% complete ablation, 100 % survival at 10 months
	(Li et al., 2007)			

Prostate – localized prostate cancer	(Crouzet et al., 2010)	Multicentre case series	803	8 years - Overall survival 89 %, cancer-specific survival 99 %. Similar rates to radiotherapy
Prostatic adenocarinoma	(Ganzer et al., 2013)	Case series	538	Biochemical disease-free survival of 81 % / 61 % at 5 and 10 years
Prostate – localized prostate cancer	(Thuroff et al., 2003)	Case series	402	Negative biopsy rate of 87 % > 6 wks after HIFU therapy
Breast cancer	(Wu et al., 2003)	RCT – surgical excision study	23 / 25	Complete coagulative necrosis in all 23 tumours treated with HIFU prior to surgical excision
Pancreatic adenocarcinoma – advanced (palliative)	(Sung et al., 2011)	Case series	46	30 % and 22 % survival rates at 12 and 18 months. Good symptom control
Pancreatic adenocarcinoma – advanced (palliative)	(Gao et al., 2013)	Case series	39	Median time-to-progression 5 months, 6 month / 1 yr survival 82 / 31 %
Pancreatic adenocarcinoma - unresectable	(Li et al., 2012)	Case series	25	Improved pain in 23/25 patients, 1 year survival 42 %

Table 1.2 – *Summary of clinical studies investigating HIFU as an ablative therapy.*

Whilst the studies listed above are almost exclusively non-randomised, uncontrolled studies, involving relatively small study cohort sizes (evidence level III), early results are generally encouraging and comparable to other thermal ablative modalities. However, data from randomized controlled trials are required in order to assess efficacy further, in a statistically rigorous manner.

1.5.4.2 Drug Delivery

One major clinical problem is ensuring that agents, such as chemotherapy, are delivered in therapeutic concentrations to the organ, or part of an organ such as a tumour, whilst minimising systemic side effects on other body systems. As such, developing strategies for targeted drug delivery, which aim to maximize drug bioavailability within a defined volume of tissue, whilst minimising drug doses in untargeted tissue, is a current clinical priority. HIFU may be used to enhance drug delivery through a number of mechanisms, including hyperthermic release of chemotherapeutic agents from temperature-sensitive liposomes (Dromi et al., 2007, Frenkel et al., 2006, de Smet et al., 2010), use of cavitation to enhance drug delivery to tumour sites (Bazan-Peregrino et al., 2013, Graham et al., 2014), temporary disruption of the blood-brain or skin barrier (Hynynen et al., 2005, Hynynen et al., 2001, Oberli et al., 2014, Park et al., 2012) and by increasing the porosity of the cell membrane, known as sonoporation (Iwanaga et al., 2007, Marmottant and Hilgenfeldt, 2003, Sun et al., 2014).

1.5.4.3 Sonothrombolysis

Strategies aimed at improving recanalisation and outcomes following ischaemic stroke have been developed, in which ultrasound is combined with tissue plasminogen activator (tPA) in order to improve drug efficacy. Maximal delivery of tPA to a thromboembolic clot, causing partial or complete arterial occlusion of a cerebral artery, is required in order to initiate clot lysis within the shortest time possible thus minimizing cerebral ischaemia and the neurological consequences of this. The presence of ultrasound waves within blood vessels can create fluid streaming, promoting tPA circulation and increasing the surface area of the clot to the enzyme, whilst also improving penetration of the thrombolytic agent deep into the clot. The presence of acoustic cavitation during

sonothrombolysis may disrupt the clot surface, leading to mechanical thrombolysis, whilst also increasing tPA penetration into the clot. Several randomized controlled trial have demonstrated enhanced recanalization rates following sonothrombolysis with ultrasound plus tPA, compared to tPA alone (Ricci et al., 2012). The addition of microbubbles to sonothrombolytic therapy, which act as exogenous cavitation nuclei, may enhance drug delivery and improve outcomes further. Microbubbles also reduce the cavitation threshold, meaning the ultrasound intensity required to achieve this phenomenon is lower, potentially improving clinical safety (Molina et al., 2006).

1.6 Limitations of Current Clinical Ablative Therapies

Current ablative therapies are affected by a number of factors limiting their usage and efficacy in the clinical treatment, especially potentially curative treatment, of liver cancer.

1.6.1 Perfusion Effects – The "Heat Sink" Effect

One of the major limitations affecting the efficacy of thermal ablative therapies, particularly radiofrequency ablation (RFA) and microwave ablation to a lesser extent, is the "heat sink" effect caused the presence of large peritumoural blood vessels, leading to heat advection away from the ablative focus (Lu et al., 2002, Lu et al., 2010, Patterson et al., 1998, Yu et al., 2008). This effect can reduce heating rates during ablative therapy, increasing treatment time and the total amount of energy required in order to achieve ablation, whilst decreasing lesion size and leading to variability in treatment response. The most critical scenario is one where a sufficient temperature to induce coagulative necrosis cannot be attained within a region of the tumour, potentially leading to incomplete tumour ablation and treatment failure (Lu et al., 2003, Mulier et al., 2005).

1.6.1.1 Modeling Heat Transfer

Heat Transfer Mechanisms

Several heat transfer mechanisms exist that affect both heating and cooling rates of a treatment volume during thermal ablation, including conduction, advection and radiation. A number of factors relating to the anatomical location of the target volume and type of thermal ablative therapy used will determine the relative importance of each

of these heat transfer mechanisms to each specific treatment volume. In simplified terms, the factors affecting thermal necrosis of a tissue volume can be described as follows:

Coagulation Necrosis = Energy Deposited x Local Tissue Interactions – Heat Loss

The amount and rate of energy deposition depends on the method of heating used and the input power. Local tissue interactions include the type of tissue undergoing ablation, as different tissues will heat at different rates depending on their density and specific heat capacities. There are a number of routes through which thermal energy can be lost from the tissue volume being heated during ablation. The blood acts as a vehicle, transporting thermal energy from high temperature areas, including a focal tissue volume during thermal ablative therapy, to low temperature areas, a process known as thermal advection. Conduction of thermal energy from the heat source to surrounding tissue and radiation of heat also occurs (*Figure 1.14*).

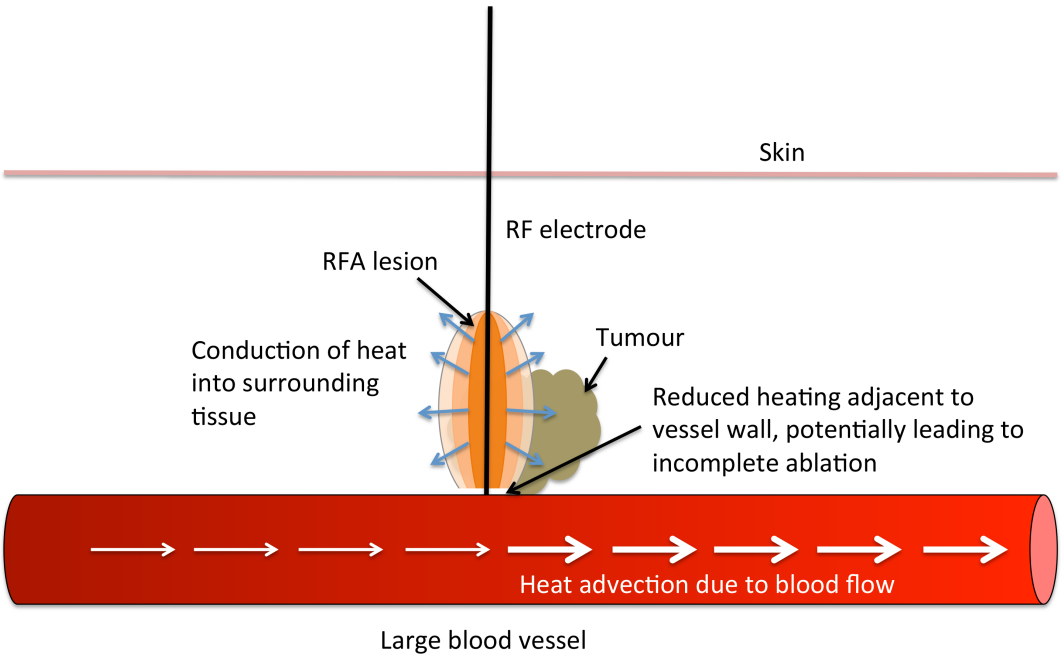


Figure 1.14 – *Mechanisms of heat transfer during ablative therapy. Conduction of thermal energy away from the focal zone increases occurs, increasing the surrounding tissue temperature, whilst heat advection due to large vessel blood flow cools the vessel wall and immediate perivascular tissue. Similarly, heat advection also occurs as a result of local capillary perfusion within the focal tissue volume.*

Theoretical modeling of the effects of heat transfer on the ablation volume *in vivo* is difficult due to tissue inhomogeneity, especially with respect to blood perfusion, which is the dominant route of heat transfer away from the treatment focus. Numerous models have been proposed, including the Pennes' Bioheat Transfer Equation (PBTE), which models the effect of blood flow in tissue by adding a perfusion term to the traditional heat conduction equation (Payne et al., 2010, Pennes, 1948). Pennes suggested that the rate of heat transfer between a specific tissue volume and the blood flowing through it is proportional to the product of the overall vascular perfusion rate of the tissue volume and the difference between the tissue temperature and the arterial blood temperature.

If metabolic heat source and conductivity (Fourier's law) terms are also included, then Pennes' bioheat equation is as follows:

$$\rho c \frac{\partial T}{\partial t} = \nabla \bullet \left(k \nabla T\right) + \dot{q}''' m + \omega \rho_b c_b \left(T_a - T\right)$$

Tissue conductivity and temperature gradient

Metabolic heat source rate

Perfusion term

Where *is* ω is the overall vascular perfusion rate per unit volume of tissue, C_b is the specific heat of blood, ρ_b is the blood density, k is the thermal conductivity of the tissue, T is the tissue temperature and T_a is the arterial blood temperature. The PBTE provides a model for one-dimensional, steady state heat transfer and includes a perfusion term, which accounts for the overall tissue perfusion rate, and a term which account for convective cooling, whilst assuming that the temperatures of capillary blood entering and leaving a tissue volume are the same. Pennes believed that the majority of heat transfer occurred in the capillary bed due to the high surface area available for heat exchange. The effects of individual blood vessels are not accounted for in the equation and thus the point-by-point temperature variation due to the presence of large blood vessels cannot be modeled by the PBTE. Therefore, the PBTE does not accurately model the cooling effect of a single large blood vessel on heating an adjacent tissue volume during ablative therapy as the model assumes tissue homogeneity in terms of perfusion.

Whilst HIFU-induced heating and cooling at low intensities is reasonably well-predicted by the PBTE, mathematical modeling of HIFU therapy is complicated further by the

presence of inertial cavitation, which can enhance heating rates significantly, highly non-linear propagation and the presence of boiling within tissue. Several studies have published more complex models attempting to account for the effects of cavitational and non-linear heating, neither of which are accounted for in the PBTE (Solovchuk et al., 2013, Damianou and Hynynen, 1993, Hariharan et al., 2007).

1.6.1.2 Perfusion Effects in Radiofrequency Ablation

The effects of large vessel perfusion on heating are one of the major limitations in clinical radiofrequency ablation. There are substantial clinical and experimental data demonstrating the impact of heat advection from blood vessels greater than 4 mm in diameter on heating rates and peak temperatures attained over a treatment volume, treatment times, lesion size and total energy input required in RFA therapy (Lu et al., 2002, Patterson et al., 1998, Tamaki et al., 2004, Dodd et al., 2013, Bitsch et al., 2006, Chang et al., 2002, Chinn et al., 2001, Frich et al., 2006, Goldberg et al., 1998, Wu et al., 2009, Welp et al., 2006, Thanos et al., 2008, Shen et al., 2003, Scott et al., 2002, Metcalfe et al., 2007, Mulier et al., 2005).

A number of experimental studies in both perfused *ex vivo* and *in vivo* porcine models have demonstrated that minimum lesion size and volume are inversely proportional to hepatic blood flow, and the number of blood vessels flowing through an RFA treatment volume, as demonstrated in *Figures 1.15* and *1.16* (Chang et al., 2002, Huang et al., 2012, Lehmann et al., 2009, Lu et al., 2002, Patterson et al., 1998, Washburn et al., 2003, Welp et al., 2006, Metcalfe et al., 2007, Bangard et al., 2006).



Figure 1.15 *– Effect of vessel number and hepatic inflow tract clamping on RFA lesion volume. a) Linear regression analysis of RFA lesion volume as a function of number of central vessels running through an RFA lesion. The lesion volume is indirectly proportional to the number of vessels present (β = -0.56, p = 0.0004). b) Lesion volume with and without Pringle's maneuver, demonstrating significantly higher volumes in the absence of hepatic arterial and portal venous flow (p < 0.001). From Patterson et al., 1998.*

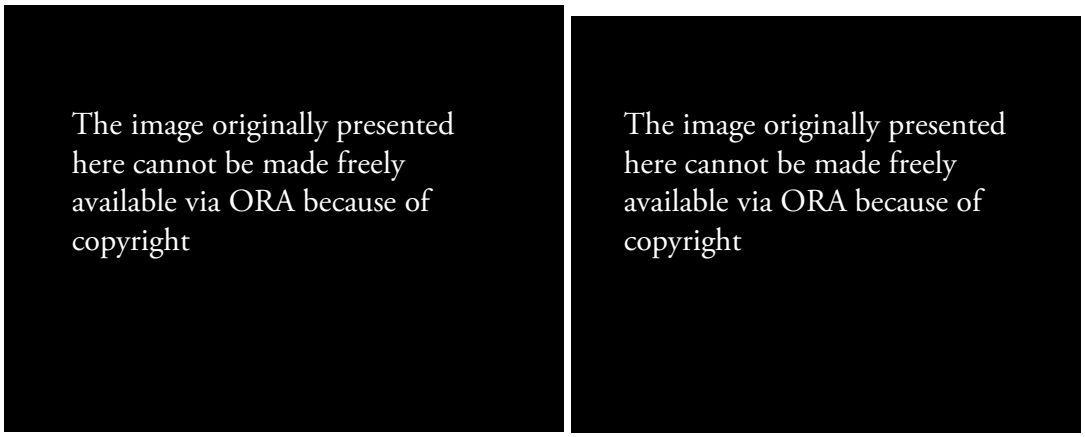


Figure 1.16 *– Regression plots showing inverse correlation between RFA lesion diameter and hepatic blood flow (L) and RFA lesion volume and hepatic blood flow (R). From Huang et al. (2012).*

Studies have also demonstrated that blood vessels of 3 - 4 mm in diameter and greater impart a clinically significant heat sink effect on RFA therapy (Lu et al., 2002, Lu et al., 2003). If a vessel larger than 4 mm exists within the RFA treatment volume, then viable

tissue may remain directly adjacent to the vessel wall as heat advection due to blood flow limits the peak temperature rise in this tissue to a temperature beneath the threshold for ablation (*Figure 1.17*).

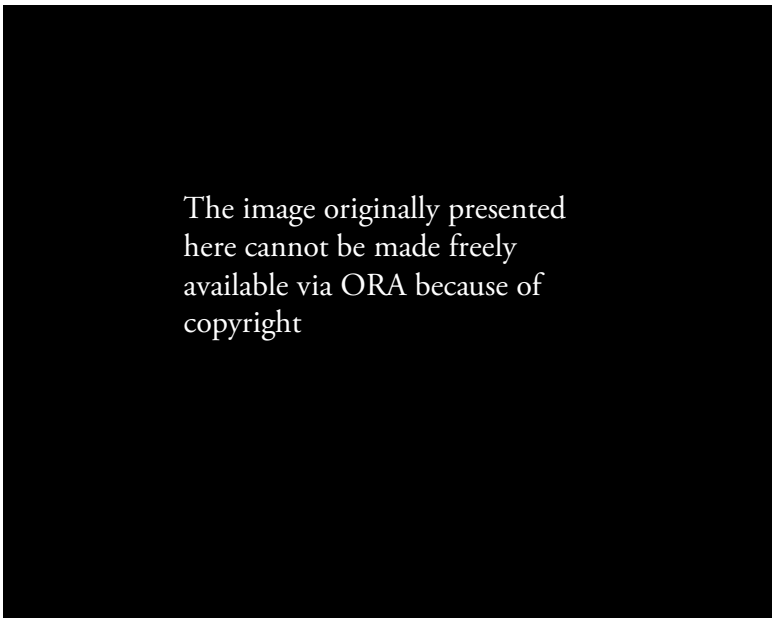


Figure 1.17 – *Gross appearance of an RFA lesion (R) adjacent to a 4 mm hepatic vein. Viable liver tissue, shown by the white arrows, remains between the RFA lesion and the vessel wall, indicative of the heat sink effect. From Lu et al. (2002).*

A number of preclinical studies have investigated the effects of performing Pringle's maneuver on RFA, in which the portal inflow tract (hepatic artery and portal vein), is temporarily occluded, thus greatly reducing or even stopping hepatic blood flow (Chang et al., 2002, Chinn et al., 2001, Frich et al., 2006, Kim et al., 2004, Patterson et al., 1998, Scott et al., 2002). These studies demonstrated that the sizes of RFA lesions, created under vascular occlusion were greater than those made in the presence of normal hepatic blood flow, whilst lesion geometry was also more consistent.

Clinical data generally support the findings of experiment studies, with several studies demonstrating increased rates of recurrence for tumours adjacent to major blood vessels treated by RFA (Ng et al., 2006, Lu et al., 2003, Mulier et al., 2005, Teratani et al., 2006, Kim et al., 2006). Lu *et al.* determined that a perivascular tumour location, adjacent to a blood vessel of ≥ 3 mm in diameter, was the single most important independent risk factor impacting local disease recurrence or residual disease (Lu et al., 2003). A meta-analysis of 5224 tumours ablated by RFA demonstrated an increased risk of local recurrence in those patients with tumours adjacent to a large blood vessel. However, 2 fairly large recent studies did not reveal a significant association between perivascular tumour location and risk of local recurrence or 2-year survival, achieving broadly equivalent results (Ng et al., 2006, Teratani et al., 2006).

Mullier *et al.* (2005) conducted a multivariate meta-analysis of factors influencing local tumour recurrence after RFA of 5224 primary and metastatic liver cancers. Similar to other comparative retrospective studies, the authors found an increased risk of recurrence when a tumour was situated near a large vessel (< 5 mm from a vessel > 3 mm in diameter), with a recurrence rate of 37 % compared to 6 % (Lu et al., 2003, Bowles et al., 2001, Machi et al., 2001). A greater recurrence risk was also associated with increasing tumour size, with rates of 14 % in tumours under 3 cm, 25 % in tumours between 3 and 5 cm and 58 % in treated tumours over 5 cm. Whilst hepatic vascular inflow occlusion during RFA improves efficacy over ablations performed under normal perfusion conditions, with recurrence rates of 9 % compared to 12 %, Pringle's maneuver may be associated with an increased risk of portal vein thrombosis, so should be used cautiously (Mulier et al., 2002).

1.6.1.3 Perfusion Effects in Microwave Ablation

The perfusion effects of large vessels lying adjacent to a target hepatic treatment volume are significantly reduced in microwave ablative (MWA) therapy compared to RFA (Dodd et al., 2013, Garrean et al., 2009, Schramm et al., 2007, Bhardwaj et al., 2011), although Yu *et al.* demonstrated that, in an experimental *in* vivo porcine model, vessels of > 3 mm, particularly those > 6 mm can still impart a clinically significant heat sink effect (Yu et al., 2008). Histologically, viable tissue may remain between the ablated tissue region and the vessel wall in approximately 25 % of ablations adjacent to a > 6 mm blood vessel and 12 % of ablations next to a 3 – 6 mm blood vessel (*Figures 1.18* and *1.19*). However, Garrean *et al.* (2009) demonstrated complete ablation of tissue next to large hepatic and portal veins following experimental MWA in a porcine model, with no sparing of hepatic tissue due to the heat sink effect. Also, it was observed that MWA during a period of cessation of hepatic blood flow (Pringle's maneuver) resulted in a 70% increase in ablation zone diameter, compared with ablations performed during periods of normal hepatic perfusion.



Figure 1.18 – *Gross appearance (L) and NADH staining (R) of a MWA lesion adjacent to a 6 mm hepatic vein. Viable cells stain purple, whilst ablated tissues appear as non-staining areas on NADH staining. No heat sink effect is evident, with complete ablation (A) up to the vessel wall (V). From Yu et al. 2008.*

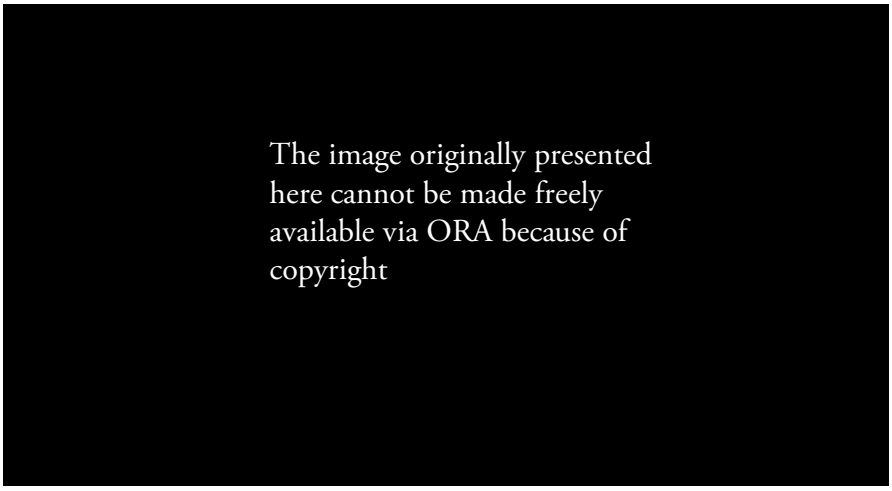


Figure 1.19 – *Gross appearance (L) and NADH staining (R) of a MWA lesion adjacent to a 6 mm hepatic vein. A moderate heat sink effect is present, with a rim of viable hepatic tissue between the vessel wall and the MWA lesion, marked by the double black arrows. (Yu et al., 2008)*

RFA and MWA heat tissue within the ablation volume through inherently different mechanisms, which may explain the reduced heat sink effect seen in MWA. RFA relies on conduction of high-frequency alternating current through water in the target tissue. Most of the heating occurs within a few millimetres of the RF electrode, with the majority of heating occurring due to conduction of thermal energy away from the actively heated tissue. As the temperature of the tissue increases with RF therapy, water evaporates and conduction decreases as a result of increasing resistance. Close to the

electrode, the tissue temperature increases rapidly as a result and charring frequently occurs, reducing peripheral distribution of thermal energy further still. Since MWA does not rely on conduction in order to induce heating rather, instead, microwave energy is delivered directly to the tissue; MWA is less affected by tissue desiccation and changes in tissue resistance than RFA. Conduction is an inefficient mechanism for tissue heating as power decreases exponentially with distance from the heat source. In RFA, power decreases proportionally to $1/r^2$, where r is the radial distance from the RF applicator electrode. In MWA therapy, the power fall-off is proportional to $1/r$. Therefore, there is improved tissue penetration in MWA over RFA and MWA should achieve more even heating throughout the treatment volume, shorter treatment times, larger ablation volumes and higher temperatures in the target tissue. Additionally, conductive heating, which is less applicable to MWA than RFA, is particularly susceptible to the heat sink effect from sources of thermal advection, such as local blood flow (Wright et al., 2005).

1.6.1.4 Perfusion Effects in HIFU Therapy

Similar to microwave ablation, HIFU therapy delivers energy to the target tissue directly, leading to active heating and does not rely on conduction of thermal energy in order to achieve ablation. However, the HIFU-mediated thermal and cavitation mechanisms that induce coagulative necrosis during HIFU ablative treatment have been studied little *in vivo* to date and the effects of perfusion on HIFU therapy remain unclear.

Mathematical and Ex-Vivo Experimental Modeling

Mathematical modeling of heating during HIFU therapy is complicated by the presence and effects of cavitation, non-linear propagation of ultrasound and boiling, all of which

differ between different types of tissue and also within the same organ, due to tissue heterogeneity (Khokhlova et al., 2006, Holt and Roy, 2001). The varying cavitation thresholds and levels of cavitation during HIFU exposures of different tissues, potentially leads to highly variable rates of heating due to cavitation enhancement. Hariharan *et al.* modeled the effects of large vessel perfusion on HIFU-induced heating at moderate exposure intensities (Hariharan et al., 2007). They reported that at most treatment locations, large vessel blood flow has a minimal clinically significant effect on heating during HIFU therapy. However, when the treatment volume is placed at a location within one beam width (≈ 2 – 3 mm) of a large vessel, then lesion volume may be reduced by up to 40 %. The effect is more pronounced when the longitudinal (long) axis of the HIFU beam is parallel to the blood vessel, compared with when the transverse (short) axis is parallel to the vessel as the area for heat diffusion is greater. Using both a numerical and an *in vitro* gel phantom model, Huang *et al*. determined that convective cooling by large vessel perfusion can significantly affect HIFU-induced heating, demonstrating that blood vessels with a flow rate of 2 cm s^{-1} (6.4 ml/min) through a 2.3 mm vessel can reduce the peak temperature rise in the vessel wall by approximately 25 % (Huang et al., 2004a). Solovchuk *et al.* (2013) proposed a mathematical model, accounting for the effects of both large vessel and microvascular blood flow and also convective cooling from vascular acoustic streaming resulting from HIFU therapy. They demonstrated that velocities due to acoustic streaming could be up to a magnitude higher than physiological blood flow velocities and have a significant effect on HIFU-induced heating, although ablative temperatures could still be attained (Solovchuk et al., 2013).

Animal Studies

Given that mathematical and *in* vitro models may not accurately represent the human tissue, cavitation and perfusion characteristics found *in vivo*, studies investigating the effects of blood flow on HIFU therapy in animal models are likely to more realistically simulate the *in vivo* clinical scenario. Using an experimental rabbit model, Zhou *et al.* performed HIFU ablation of hepatic VX2 tumours following assessment and quantification of tumoural blood supply using contrast-enhanced ultrasound. Real-time temperature changes during HIFU therapy were recorded via an implantable thermocouple. They reported that, whilst peak temperatures and the temperature-increase phase were not affected by the level of tumoural blood supply, temperature-decrease rates were significantly higher in treated tumours with a greater degree of perfusion compared to more mature tumours with a relatively lower blood supply (Zhou et al., 2012). In another study, Jiang *et al.* reported that, in a goat *in vivo* study, ablation of liver tissue directly adjacent to and 5 mm away from a portal vein required 21 % and 10 % more energy than ablations performed 10 mm from a portal vessel (Jiang et al., 2013). Chen *et al.* studied the effect of Pringle's maneuver on HIFU ablation of liver parenchyma in a rat model (Chen et al., 1993). They demonstrated that lesion diameters were significant smaller in the presence of normal hepatic perfusion compared to lesions made during periods of hepatic inflow cessation due to Pringle's maneuver, at a number of HIFU intensities and exposure durations (*Figure 1.20*).



Figure 1.20 – *Lesion diameter as a function of exposure time for HIFU lesions made in rat liver in the presence and absence of perfusion at a spatial intensity of 106 W cm^{-2} (Chen et al., 1993).*

Parmentier and Melodelima conducted a number of studies investigating the use of a novel multi-element toroidal HIFU transducer in the ablation of hepatic tissue (Melodelima et al., 2009, Parmentier et al., 2009). Although the focal volume of the 256-element HIFU transducer was much larger than those used in other animal and *ex vivo* studies, and HIFU transducers commonly used in clinical practice, they reported that complete ablation of tissue right up to a 5 mm blood vessel wall could be achieved.

Clinical Studies

Clinical data regarding the influence of blood flow on HIFU ablation is limited and, of the studies available, all involve a small study size and are of evidence Level 3 or below. Wiart *et al.* undertook a study investigating the effects of regional prostatic blood flow as

measured by MRI on HIFU ablation for localized prostatic cancer (Wiart et al., 2007). Out of 48 patients treated in the study, 31 patients responded to HIFU ablation, defined as having a PSA nadir < 0.2 ng/ml, whilst 17 patients did not respond. The authors demonstrated a statistically higher pre-treatment regional prostatic blood flow in the non-responder group compared to the responder group, suggesting higher blood flow rates reduce the efficacy HIFU ablation, possibly due to a heat sink effect.

There are also limited clinical data suggesting that the ablation of liver tumours adjacent to major vasculature by HIFU is both safe and effective (Zhang et al., 2009). In a clinical study investigating HIFU ablation of 47 irresectable hepatocellular carcinomas adjacent to major vasculature in 39 patients, Zhang *et al.* reported that complete tumour necrosis, as assessed by interval CT/MRI scanning, was achieved in 50 % of cases, with little or no effect on vascular integrity. Mean tumour size was 7.4 cm, above the usual threshold for thermal ablation in HCC, and tumours were located adjacent to the IVC, right / middle / left hepatic veins, main portal vein or 1st order branches of the portal vein. Of the tumours where incomplete necrosis occurred, ablation of 50 % of the total lesion volume was achieved in all cases. Local tumour progression only occurred in 1/21 lesions in which complete ablation was achieved and the overall survival rates at 1, 2, 3 and 5 years were 75.8 %, 63.6 %, 49.8 % and 31.8 % respectively. Accounting for the fact that the survival rate for irresectable, untreated HCC is generally less than 6 months, these early data are promising (Bruix et al., 1998, Pelletier et al., 1998). The authors also hypothesised that, given that the temperature-increase phase during HIFU is rapid and that the primary heating mechanism is due to direct delivery of energy to the target tissue, with minimal reliance on thermal conduction, the heating rate and peak

temperature during HIFU therapy should be minimally affected by large vessel proximity, tissue perfusion and the "heat sink" effect.

1.6.2 Monitoring Thermal Ablation

Monitoring ablative therapies in real time is a considerable challenge. In clinical practice, the ability to assess in real time whether a targeted volume of tissue has been sufficiently treated, but not over-treated, during ablative therapy is highly desirable. If tissue is undertreated or the intended target has been incompletely covered, part or all of the focal tissue volume may be exposed to sublethal temperatures and treatment failure may ensue. In contrast, overtreatment may lead to unwanted collateral thermal damage to adjacent structures, such as major bile ducts or hepatic vasculature. Tissue heterogeneity, such as the presence of vascular structures, may lead to inconsistent rates of heating due to the heat sink effect, leading to variable treatment within the focal tissue volume and incomplete ablation. Therefore, the optimal monitoring technique should be able to accurately map and quantify heating and tissue damage in real time during ablative therapy, whilst also being economically cost-effective.

1.6.2.1 Radiological Monitoring of RFA and MWA

Both RFA and MWA are hindered by suboptimal real-time monitoring techniques. Development of the ablative lesion can be visualised on CT, MRI and ultrasound. However, since most imaging is performed post-ablation, although under treatment may be detected using standard imaging techniques, they cannot be used to prevent overtreatment during therapy and excessive treatment will have occurred already.

Although MR or ultrasound thermal mapping techniques are available, these are not used routinely in clinical practice (de Senneville et al., 2007).

1.6.2.2 Monitoring During HIFU Therapy

Although a large number of strategies for monitoring HIFU treatment have been suggested, only two methods, magnetic resonance (MR) thermometry and detection of hyperecho by B-mode imaging, are in used in current clinical practice. However, several problems exist with these methods. Firstly, although MR thermometry provides accurate three-dimensional temperature measurements, there is a time delay in producing the temperature maps, meaning there is a limitation in the potential speed of reaction to any temperature rise, particularly when rates of heating are high, potentially due to cavitational activity, which may lead to over-treatment. Therefore, treatment parameters must be estimated before treatment commences, based on the HIFU transducer specifications and patient / tumour characteristics. MR thermometry is also limited in both temporal and spatial resolution, requires accurate models for each type of tissue in order to correlate MR temperature maps with tissue necrosis and financial costs remain extremely high as a dedicated MRI scanner is usually required. Similarly, monitoring HIFU ablation with hyperecho formation on B-mode imaging has several limitations. Since there is interference from the HIFU pulse, B-mode feedback can only take place following delivery of the treatment, or interwoven with non-continuous HIFU exposure, meaning true real-time monitoring is not possible. In addition, the presence of hyperecho on B-mode imaging is associated with tissue boiling, at a temperature well in excess of that required to achieve necrosis, and over-treatment. There is an increased risk

of prefocal tissue damage in the presence of boiling due to bubble reflection of the incident HIFU beam (Bailey et al., 2001, Coussios et al., 2007).

Passive Acoustic Mapping (PAM)

To address the limitations of MRI thermometry and B-mode ultrasound monitoring, using passive cavitation detection as a method to quantify heat deposition indirectly during HIFU therapy has been proposed (Farny et al., 2009). As discussed in Section 1.5.3, inertial cavitation may be detected through the presence of broadband emissions during HIFU therapy. Gyongy *et al.* (2010) developed a technique, termed passive acoustic mapping (PAM), to map and quantify broadband and harmonic emissions in real time, thereby allowing spatiotemporal quantification of inertial cavitation during HIFU therapy. Passive acoustic emissions were detected during HIFU therapy using a 64-element diagnostic linear array. Radiofrequency data from individual channels were then subjected to a beam-forming algorithm, allowing spatiotemporal maps of acoustic emissions to be created (*Figure 1.21*).



Figure 1.21 *– Passive acoustic maps showing broadband (cavitation) emissions (far left), harmonic emissioms (centre right) and hyperecho (far right) maps formed during a 5 s HIFU exposure at 8.0 MPa pk- in bovine liver. Broadband emissions up to 1.1 mJ are detected over an axial distance of approximately 10 mm and transverse distance of 2 mm. Hyperecho, indicative of tissue boiling, appears bright white on B-mode imaging. Both the hyperecho and passive acoustic maps predict and map the formed ablative lesion (centre left) well, which appears slightly in front of the intended HIFU focus. The HIFU array is positioned at top of the diagrams. The intended HIFU focus is centred at an axial and transverse distance of 0 mm, yet the peak broadband activity is mapped to a tissue region 3 mm in front of this. The gross histology (centre right) suggests that the lesion appears approximately, which correlates with the PAM and B-mode images (Jensen et al., 2012).*

A study by Jensen *et al.* (2012) demonstrated that passive acoustic mapping had a higher sensitivity, specificity, positive and negative predictive value for HIFU lesion formation compared to hyperecho monitoring using B-mode ultrasound in an *ex vivo* study in bovine liver. However, this novel ablative monitoring technique has not been assessed *in vivo* to date.

1.7 Summary

At present, surgical resection or transplantation remain the gold standard curative therapies for patients with primary and secondary liver cancer. However, only a small number of patients will have disease amenable to these interventions, or will have a performance status suitable for major surgery to be considered. Minimally invasive thermal ablative therapies, such as radiofrequency and microwave ablation are promising alternatives, but current published data fails to demonstrate clear equivalent oncological outcomes compared to conventional resectional surgery, particularly for tumours > 3 cm in diameter. Therefore, thermal ablation is generally reserved for patients who are unsuitable or unfit for surgical resection, or as an adjuvant therapy. One of the main limiting factors affecting the efficacy of thermal ablative therapies is the heat sink effect of large blood vessels, which have cooling effect on perivascular tissue through heat advection, potentially leading to incomplete ablation and treatment failure. Thermal ablative therapies are also limited by a lack of monitoring techniques to ensure therapeutic temperatures are attained throughout the intended treatment volume in real time.

Thus, development of novel ablative therapies that are minimally affected by vascular heat sink and which can be monitored in real time may help to improve outcomes following thermal ablation. High intensity focused ultrasound is a novel thermal ablative technique that may be subject to smaller perfusion effects that other ablative therapies, although there are few *in vivo* data to quantify and support this hypothesis. As a completely non-invasive therapy, morbidity associated with percutaneous or surgical

ablative techniques, particularly seeding along the RFA / MWA antenna track, may also be avoided with HIFU. Additionally, novel monitoring techniques unique to HIFU therapy may allow real time mapping quantification of ablation and, thus, improve treatment efficacy.

CHAPTER 2

MATERIALS AND METHODS

For all the studies described in this work, a novel extracorporeal, normothermically perfused porcine liver model was used. Livers were surgically explanted from 45-60 kg Landrace pigs and attached to a unique extracorporeal liver perfusion device, designed for clinical organ preservation for liver transplantation, which can maintain a liver in a physiological, functional state *ex vivo* for in excess of 72 hours. Organs were perfused with oxygenated whole blood and placed in a water bath for subsequent HIFU studies. Methods pertaining to the individual cavitation, thermometry and histological studies are detailed in Chapters 3, 4 and 5.

2.1 Introduction

The optimal preclinical model provides anatomical, physiological and pathological features as close to the *in vivo* human characteristics as possible. Numerous small and large animal models are available, all of which have advantages and limitations. In order to assess the effects of physiological blood flow on HIFU-induced heating and cavitation, a model that provided tissue structure, vascular anatomy, vessel diameters, vascular pressures and blood flow rates as near to that of the human was of primary importance. Therefore, a large animal model, with hepatic anatomical and physiological characteristics similar to that of a human liver was preferred.

2.2 The Pig as a Liver Model

The porcine liver is widely considered to be the gold-standard preclinical model for liver transplantation studies as it provides comparable anatomy and physiology to that of the human liver, whilst being ethically acceptable (Court et al., 2003, Fondevila et al., 2011, Gravante et al., 2011, Swanson et al., 2004). One major limitation of using a porcine liver model for preclinical cancer studies is that, unlike rodent models, no porcine liver tumour model, be it a spontaneous, syngeneic, genetically engineered or xenograft model, is currently available. Therefore, the pathophysiology of human liver cancer is difficult to model, whilst also accurately representing the anatomical scale and perfusion characteristics of the human liver.

Similar to the human liver, the pig liver is divided into a number of segments, each of which has its own portal venous, hepatic arterial and venous branch, together with a hepatic bile duct (*Figure 2.1*). Court *et al.* (2003) delineated the anatomy of the pig liver using post mortem acrylic casting techniques, demonstrating that the segmental vascular and biliary anatomy of the pig liver is highly similar to the human liver, making it a suitable comparable model. However, whilst the intraparenchymal venous and biliary anatomy are similar, the segmental structure of the porcine liver is much more defined externally than the human liver, with a series of deep intralobular fissures dividing the 3 main lobes.



Figure 2.1 – *Portal venous (L) and hepatic venous (R) arrangement of the pig liver. There are 8 major hepatic segments (I – VIII), similar to the human liver. (Court et al., 2003)*

In terms of perfusion parameters, porcine hepatic blood flows and pressures are also similar to the human liver, with reported values measured in 3 - 4 month old pigs weighing approximately 85 – 130 lbs (38 – 59 kg) shown below in *Table 2.1* (Drougas et al., 1996).

Parameter	Mean Value – Pig	Mean – 70 kg Human
Hepatic venous pressure (mmHg)	4.3 ± 0.4	1 - 4
Portal venous pressure (mmHg)	7.8 ± 0.5	7 - 12
Hepatic arterial blood flow (ml/min)	116 ± 24	245 ± 112
Portal venous blood flow (ml/min)	880 ± 130	945 ± 204
Total hepatic blood flow (ml/min)	1132 ± 187	1190 ± 190
Hepatic arterial blood flow (%)	15.5 ± 2.7	20.6
Portal venous blood flow (%)	84.5 ± 2.7	79.4

Table 2.1 – *Hepatic venous (HV) and portal venous (PV) pressures, hepatic arterial (HA), PV and total hepatic blood flow rates, together with relative proportions in pigs and humans. (Carlisle et al., 1992, Drougas et al., 1996)*

The mean hepatic blood flow of a 3 – 4 month old pig is roughly equivalent to that found in a 70 kg adult human, with an approximate rate of 1 – 1.4 L/min.

At a histological level, the structures of the porcine and human liver are also highly similar. Microscopically, the liver is arranged into a series of hepatic lobules that are hexagonal in shape. The liver acinus represents the functional liver unit, with each acinus receiving an end hepatic portal venule and hepatic arteriole, which drain into a hepatic venule that is located in the centre of the lobule (*Figure 2.2*).

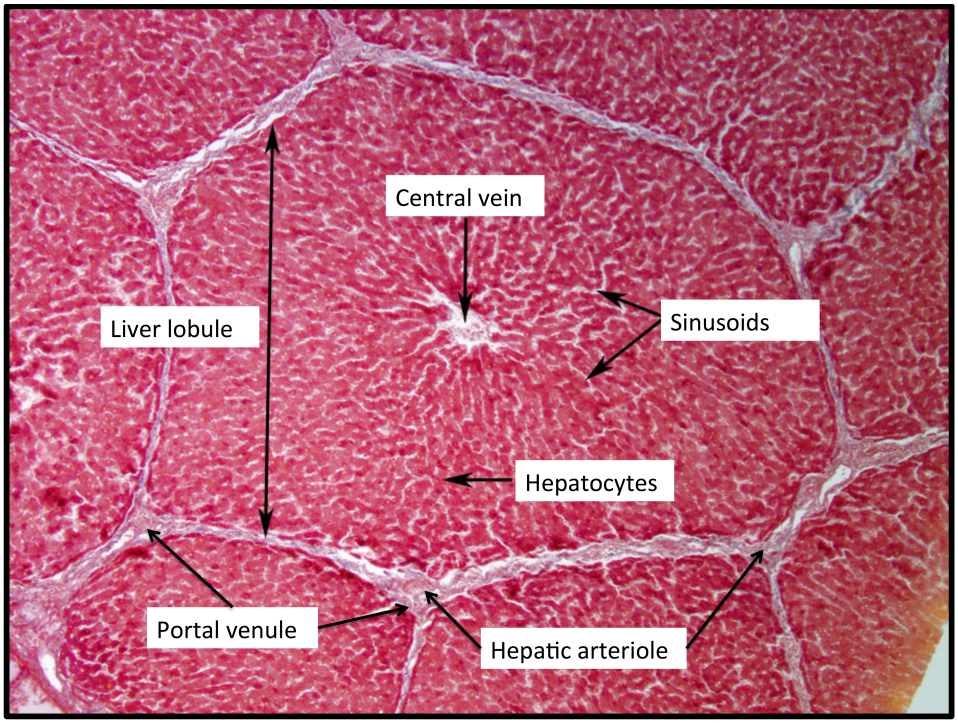


Figure 2.2 *– Haematoxylin and eosin stain of sectioned porcine liver (100 x) showing the hexagaonal hepatic lobule surrounded by a fibrous layer. There is an end hepatic portal venule and hepatic arteriole at each angle, with blood draining in to the hepatic sinuosoids and then into a central hepatic venule.*

2.3 Isolated, Normothermic Liver Perfusion

A unique, novel extracorporeal normothermic liver perfusion device, which can maintain a liver in a functional state at body temperature for in excess of 72 hours ex vivo, was used to provide a haemodynamically, physiologically relevant model of hepatic tissue perfusion (Brockmann et al., 2009, Butler et al., 2002, Reddy et al., 2004, St Peter et al., 2002a). The normothermic liver perfusion device perfuses an organ with blood, heated to 37 ˚C and oxygenated to maintain partial pressures of oxygen and carbon dioxide within a normal *in vivo* range, at physiological vascular pressures. The technology was primarily developed to improve organ preservation prior to transplantation. Over the past decade or so, a number of porcine studies have been conducted using the same technology as used in this work, which have demonstrated that physiological flow rates, biochemistry, acid-base balance, hepatic synthetic function and tissue structure at a histological level are all maintained during liver preservation by normothermic perfusion.

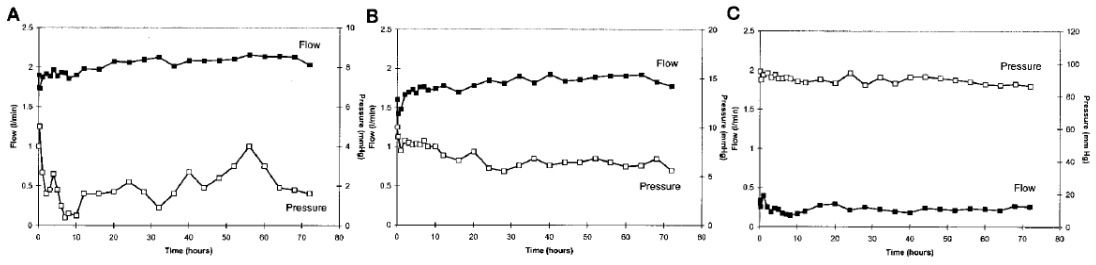


Figure 2.3a – *A) IVC pressure and flow B) Portal venous pressure and flow and C) Hepatic arterial pressure and flow, all plotted as a function of time during 72 hour extracorporeal porcine normothermic liver perfusion. These data demonstrate that physiological vascular pressures and flow rates are maintained for at least 72 hours. From Butler et al., 2002.*

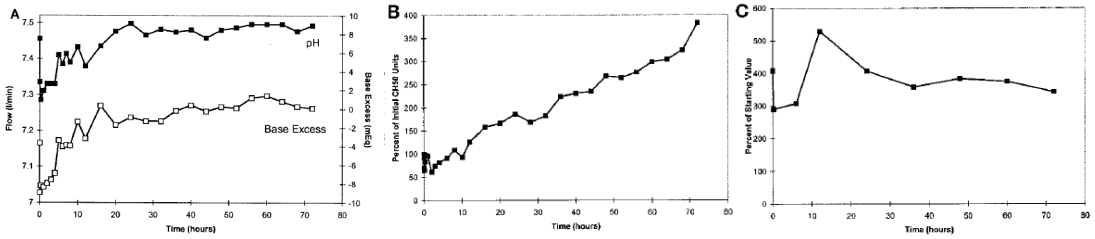


Figure 2.3b – *pH and base excess and plotted as a function of time. The normal human reference range for pH is 7.35 to 7.45, whilst the normal reference range for base excess is -2.5 to 2.5 mEq. From Butler et al., 2002.*

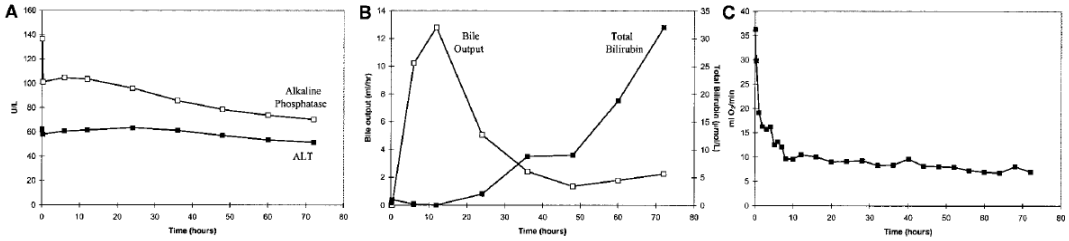


Figure 2.3c – *A) Alanine transferase (ALT) and alkaline phosphatase (ALP), B) Bile output (ml/hr) and total bilirubin and C) Oxygen consumption as determined by the Fick equation. From Butler et al., 2002 (Butler et al., 2002).*

Figures 2.3 a to *c* show vascular flow rates / pressures, acid-base balance, transaminase levels, bile production and oxygen consumption over the duration of 72 hour normothermic liver perfusions, with haemodynamic, biochemical and functional parameters remaining within normal physiological limits. These data demonstrate that a liver can be maintained in a stable, viable condition for at least 72 hours using the normothermic liver perfusion preservation technique adopted for this work.

2.3.1 *Ex* Vivo Perfused Liver as a Heat Sink Model

Although the perfusion device used in the studies described above and for this current work has not been used previously to investigate perfusion effects in thermal therapies, a number of published studies have demonstrated a heat sink effect from large vasculature on RFA and MWA using similar *ex vivo* perfused liver models (Bitsch et al., 2006, Dodd et al., 2013, Huang et al., 2012). Dodd *et al.* (2013) investigated the effects of perfusion on both RFA and MWA in *ex vivo* bovine liver perfused with oxygenated autologous blood at 37 ˚C, demonstrating a significant inverse relationship between portal venous blood flow and RFA, but not MWA, lesion volume and diameter. Therefore, these studies suggest that heat sink can be successfully modeled using an *ex vivo* perfused liver.

2.3.2 Organ Donation Procedure

All animal work was performed at either Northwick Park Institute for Medical Research (NPIMR) or at the Department of Biomedical Sciences (BMS), University of Oxford. White Landrace pigs weighing 45-60 kg were used for organ donation and were treated in accordance with the United Kingdom Animals (Scientific Procedures) Act 1986 under Project Licenses 30/2873 and 30/2750. Ethical approval from the University of Oxford local ethics committee had been previously obtained as part of the project license application process.

All pigs were received into the animal facility > 24 hours in advance of the planned procedure to allow time for acclimatization. A normal diet was supplied up until 12 hours before the intended anaesthetic time, after which animals were fasted but were allowed access to water. Preoperative husbandry was carried out by the animal technicians at the NPIMR and BMS under the supervision of the Named Animal Care and Welfare Officers (Mrs. Cathy Gray and Ms. Maria Martinez).

Pigs were sedated using intramuscular midazolam (0.2 mg/kg) prior to isofluorane induction of general anaesthesia (Mrs. Cathy Gray (Northwick Park Institute for Medical Research)), Dr. Caroline Bergmann (University of Oxford) and Ms. Emma Bartlett (University of Oxford). Vascular access was obtained by peripheral cannulation of an ear vein, after which endotracheal intubation or surgical tracheostomy was performed and animals were ventilated by intermittent positive pressure ventilation. Throughout the

procedure, pulse oximetry, pulse, blood pressure and core temperature were continuously monitored and recorded.

Following sterile preparation of the surgical field with Betadine, the external carotid artery was cannulated with a 20G Angiocath (BD, UK) and connected to a pressure tranducer to facilitate intraoperative invasive arterial blood pressure monitoring. The internal jugular vein was cannulated with a cut 5 mm Heidelberger extension set (Braun, UK) for central venous access.

Livers were surgically explanted using a standard technique for heart-beating donation, as described previously (Brockmann et al., 2009, Jamieson et al., 2011). A midline laparotomy was performed, self-retaining retractors placed and small bowel packed into a sterile isolation bag (ViDrape, Medical Concepts Development, UK) to permit easy caudal retraction. The liver was retracted cranially to expose the porta hepatis and lesser omentum. The visceral peritoneum overlying the lesser omentum was divided using sharp dissection and the common bile duct (CBD) was identified and dissected from surrounding structures. The CBD was ligated in continuity and then divided at its distal end, leaving sufficient length for subsequent cannulation. Following division of the common bile duct, the common hepatic artery was skeletalised down to a level close to its origin at the coeliac trunk using blunt and sharp dissection and the hepatic arterial bifurcation, left and right hepatic arteries were all positively identified. The gastroduodenal and right gastric arterial branches were ligated in continuity with 2/0 Vicryl and divided and the hepatic portal vein was also skeletalised down to the level of the confluence of the splenic vein and superior mesenteric vein, providing sufficient

length distal to the bifurcation for subsequent cannulation of the vessels. Vascular slings were placed around both the common hepatic artery and the hepatic portal vein. Attention then turned to the infrahepatic inferior vena cava (IVC). The peritoneum overlying the suprarenal IVC was divided and the IVC was mobilized completely from the retroperitoneal tissue. A vascular sling was placed around the IVC.

The liver was mobilised by dissection of the triangular and coronary ligaments. The peritoneum lateral to the retrohepatic IVC was incised and the IVC mobilized completely from the renal veins to the caval opening in the diaphragm. Following this, the infrarenal abdominal aorta was exposed by dissection of the surrounding retroperitoneal tissue and three "0" Vicryl slings were placed around it in preparation for cannulation. A heparin bolus (20 000 Units; CP Pharmaceuticals, UK) was administered intravenously 5 minutes prior to aortic cannulation and a Gelofusine (Braun, UK) infusion was commenced via the central venous line (Baxter, UK). A T-shaped arteriotomy was made in the infrarenal aorta; the vessel was cannulated with a 20 Fr venous lighthouse cannula (Sorin; Italy) and secured with 3 x 0 Vicryl. Between 3 and 4 L of autologous donor blood was collected via the aortic cannula and was stored in dextrose supplemented blood transfusion bags (CPDA Single Blood Collection Systems; Baxter, UK) at 4 ˚C for subsequent use. During venesection, rapid Gelofusine infusion was performed in order to keep the systolic blood pressure above 60 mmHg, minimise warm ischaemia and the possibility of hypovolaemic cardiac arrest.
Following venesection, the diaphragm was incised, the thoracic aorta was cross-clamped and the thoracic IVC was divided. The liver was then cold perfused with hyperosmolar citrate solution (Soltran®; Baxter, UK) at 4 ˚C via the aortic cannula, with venting via the

suprahepatic IVC. After 2L of cold perfusate had been administered, the hepatic artery, portal vein and infrahepatic IVC were divided, a cuff of diaphragm was resected along with the remaining suprahepatic IVC, the liver was removed and placed in a bowl of saline ice slush. Further cold perfusion with Soltran® solution was performed via the portal vein until the liver had been homogenously cooled.

On the back table, the diaphragmatic remnants were oversewn with 3/0 Prolene in order to ligate the phrenic veins and the suprahepatic IVC was ligated with "0" Vicryl. The infrahepatic IVC was cannulated with a 28 Fr venous lighthouse cannula (Sorin, Italy) so that the fenestrae were positioned at the level of the orifices of the hepatic veins. The portal vein and the hepatic artery were cannulated with 20 Fr and 10 Fr cannulae respectively (Sorin, Italy) so that the tips lay below the level of the bifurcations of the main portal vein and proper hepatic artery respectively. Cannulae were secured with 2/0 Vicryl ligatures. The common bile duct was also cannulated with a 5 mm Heidelberger extension set (Braun, UK) to permit collection and measurement of bile production. The liver was placed in sterile intestinal bags (Vi-Drape; MCD, UK) and was packed with ice in a cool box for transportation.

2.3.3 Isolated Normothermic Perfusion Set Up

Normothermic perfusion was performed as described previously (Brockmann et al., 2009, Butler et al., 2002, Imber et al., 2002, Reddy et al., 2004), using a perfusion circuit designed to preserve donor livers at normal body temperature under near-physiological conditions prior to transplantation (Professor C.-C. Coussios and Professor P.J. Friend; OrganOx®, Oxford, UK). The perfusion device was a closed-circuit

configuration, providing two inflow lines to the liver (hepatic artery and portal vein) and one outflow tract returning venous blood from the liver via the inferior vena cava (*Figure 2.4*).

The normothermic liver perfusion device incorporated a hollow-fibre ECMO membrane oxygenator with two outflow ports (EOS ECMO PHISIO M; Sorin, Italy), a centrifugal pump (BPX80; Medtronic, USA) and a soft-shell reservoir (Capiox 1500; Terumo, USA)(Brockmann et al., 2009). Two Peltier heat exchangers maintained the blood at 37 - 39˚C. A proportional pinch valve (PPV), situated between the oxygenator and the reservoir allowed resistance to be varied, hence controlling arterial pressure. Increasing constriction of the PPV, increased the resistance on the reservoir line, increasing pressure in the arterial line at a given pump speed. Pump speed and PPV constriction were automatically controlled by the perfusion device, in order to maintain arterial, IVC and portal pressures within pre-defined limits (*Table 2.2*). Two ultrasonic sensors, located on the portal and IVC lines, measured portal and IVC flow rates directly. Hepatic arterial flow rate was automatically calculated as the difference between the IVC flow rate and portal flow rate, given that the perfusion device was a closed circuit.

Parameter	Range
Hepatic Arterial Pressure (P_{Ha})	60 – 75 mmHg
Portal Venous Pressure (P_{PV})	10 – 20 mmHg
IVC Pressure (P_{IVC})	0 – 5 mmHg
Arterial P_aO_2	12 – 20 kPa
Arterial P_aCO_2	3.5 – 6.0 kPa

Table 2.2 *– Vascular pressure and gas partial pressure ranges during normothermic perfusion preservation*

Blood gas analysis and acid-base status were monitored continuously by a Terumo in-line sensor (CDI510H; Terumo, Japan) connected to a Terumo CDI 500 system. Arterial PO_2 and PCO_2 were controlled automatically so that they remained in the range 12-20 kPa and 3.5-6 kPa respectively, whilst pH and base excess (BE) were monitored to provide information regarding the condition of the liver.

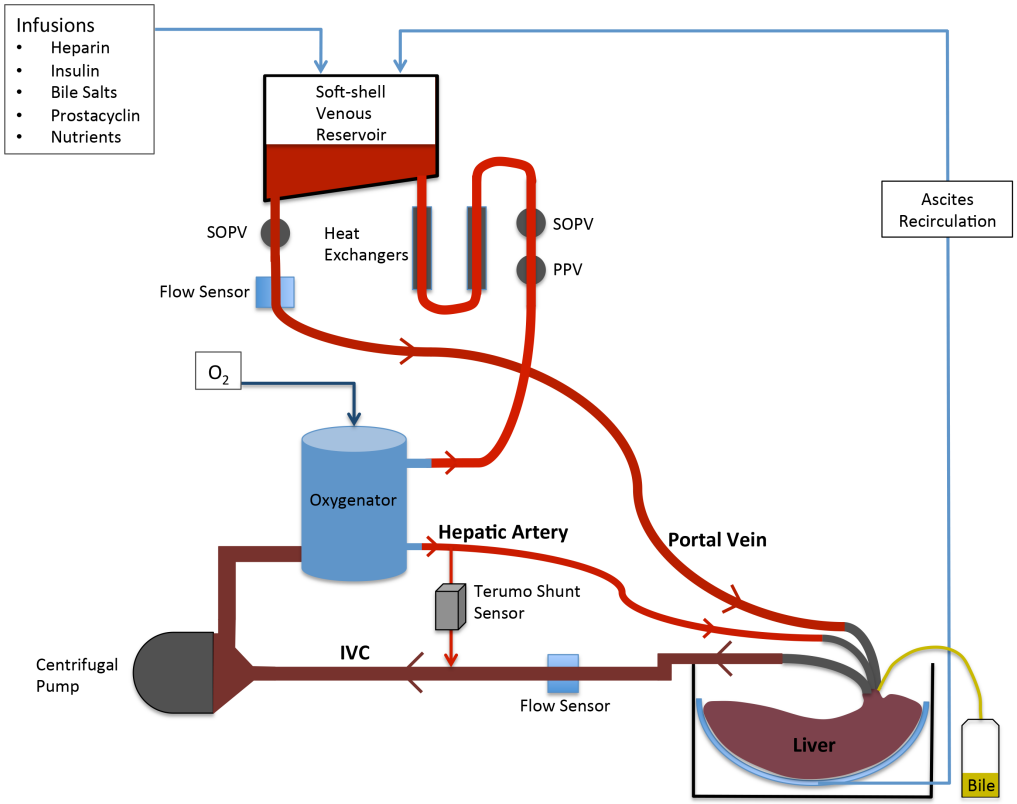


Figure 2.4 *– Extracorporeal Liver Perfusion Device (ECLPD), incorporating a centrifugal pump, hollow-fibre membrane oxygenator, soft-shell venous reservoir, in-line arterial blood gas sensor and Peltier heaters, which maintained the blood at 38 ˚C. The system provides two organ inflows (hepatic artery and portal vein) and one organ outflow (IVC) at physiological pressures and flow rates. Pump speed, portal and arterial flow were automatically controlled*

in order to maintain arterial, portal and IVC pressures within pre-defined limits of 60-75 mmHg, 10-20 mmHg and 0-5 mmHg respectively. SOPV = Shut-off Pinch Valve, PPV = Proportional Pinch Valve.

The circuit was primed with approximately 1500mL of autologous whole blood, heparin anticoagulation (10 000 Units; CP Pharmaceuticals, UK), calcium gluconate (10 mL of 10%; Braun, UK) and cefuroxime (750 mg; GlaxoSmithKline, UK). Blood was circulated through the perfusion circuit before the liver was attached so that a blood temperature of 36˚C was achieved prior to attachment of the liver. Continuous infusions of insulin (6.7 IU/hr; Novo Nordisk, Denmark), heparin (750 IU/hr), prostacyclin (epoprostenol sodium; 8 μg/hr; GlaxoSmithKline, UK) and bile acid (sodium taurocholate 2%; 140 mg/hr; NZP, New Zealand) were commenced at the start of liver perfusion. Prostacyclins increase portal flow and increase total blood flow and oxygen transport following reperfusion after warm ischaemia (Zardi et al., 2003), whilst bile acid supplementation was necessary to replace the physiological enterohepatic recirculation, whereby bile salts are reabsorbed in the terminal ileum. The liver, suspended in a silicone sling over a stainless steel bowl, was connected to the perfusion circuit and perfusion was initiated with a progressively increasing pump speed over a few minutes until an IVC pressure of 0-5mmHg was reached. Automatic constriction of the PPV along with control of the pump speed altered resistance on the reservoir line until an arterial pressure of 60 – 75 mmHg was achieved. Ascites produced by the liver was collected in the stainless steel bowl and re-circulated automatically via a peristaltic pump (Watson Marlow, Falmouth, UK).

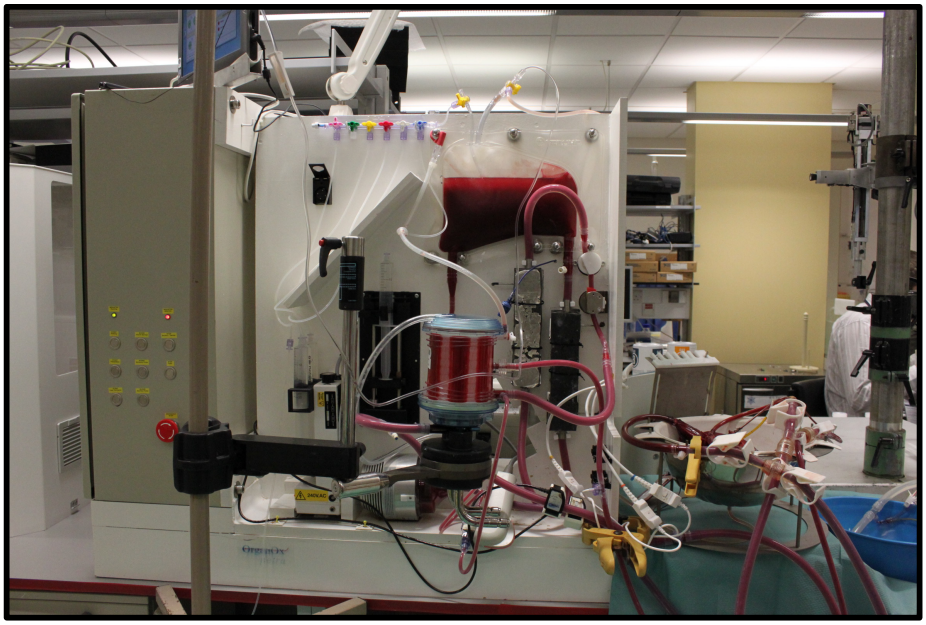


Figure 2.5 *– Photograph of the ECLPD*

Blood glucose analysis was performed hourly (Contour blood glucose test strips and Contour machine; Bayer, UK) and once blood glucose was below 12 mmol/L, a nutrient infusion (Nutriflex Plus; Braun, UK) was commenced at 15 ml/hr in order to maintain perfusate glucose levels in the range 4 to 8 mmol/L.

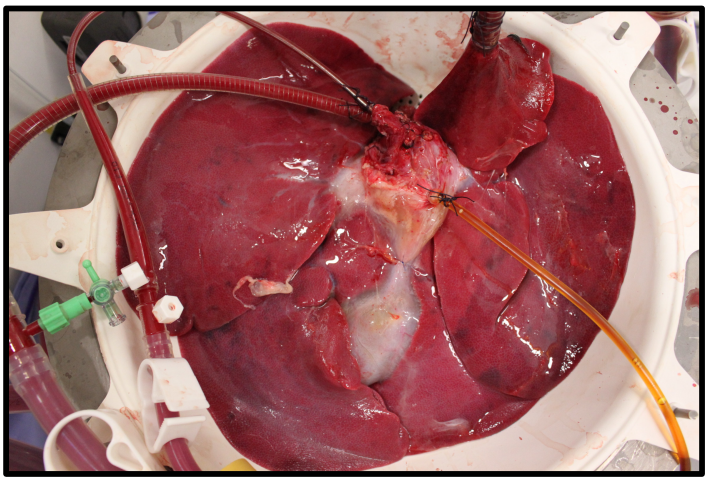


Figure 2.6 *– Photograph of a normothermically perfused porcine liver 1 hour following reperfusion on the ECLPD. The liver has started to produce bile, one marker of hepatic function, which can be seen in the clear tube to the right of the photograph.*

2.3.4 Function

Technology within the liver perfusion device permitted real time monitoring of a number of parameters during normothermic perfusion. IVC and portal venous (PV) flow rates were continuously measured via ultrasonic flow sensors, whilst hepatic arterial flow was calculated as the difference between the IVC and PV flow rate. Acid-base balance and partial pressures of O_2 and CO_2 were continuously measured via an in-line sensor attached to the oxygenator outflow and blood gas analyser (Terumo CDI510H; Terumo, Japan).

2.4 HIFU Setup

Following approximately 60 minutes of normothermic machine perfusion, the ascites recirculation was stopped, the stainless steel bowl was removed from under the liver and the liver was placed in an acoustically transparent, impermeable 50 x 50 cm sterile intestinal bag (3M, USA) filled with approximately 3 L of isotonic colloid solution (Gelofusine®, Braun, UK), which had been degassed for 2 hours using a vacuum pump and pre-heated to 37˚C. Colloid solution was used in order to provide an isotonic fluid environment with a similar oncotic pressure to that of the intravascular fluid compartment. As the colloid solution was required to provide a coupling medium to propagate the HIFU wave from the HIFU transducer to the liver tissue and also to allow any acoustic emissions from the HIFU field to propagate back, it needed to be as free of gas particles. The colloid solution was therefore degassed by placing the fluid in a vacuum flask under negative pressure for 2 hours prior to use. In previous experiments using the same normothermically perfused liver model and HIFU setup, isotonic crystalloid (0.9% sodium chloride solution) was used instead of colloid solution, but this appeared to have a detrimental effect on the liver, most likely due to the lower oncotic pressure of the crystalloid solution, leading to tissue oedema. Therefore, an approximate isotonic, iso-oncotic fluid, Gelofusine®, was used in an attempt to reduce this effect.

The bag was suspended in a silicone sling over a Perspex water bath containing an acoustic absorber in the base. The water bath was continuously degassed and heated to 37 ˚C (*Figure 2.7*) through a centrifugal pump, inline heater and membrane contactor connected to a vacuum pump (Liqui-Cel®; Membrana, USA).

A custom-manufactured, spherically focused HIFU transducer with a centre frequency of 1.06 MHz (H102D-22; Sonic Concepts Inc., WA, USA), driven at its fundamental frequency or at the third harmonic (3.18 MHz), was used to produce therapeutic ultrasound pulses. The HIFU transducer had an active diameter of 64 mm, 63 mm geometric focus and a central rectangular opening of 45 x 18 mm, permitting coaxial placement of a 128-element 5-10 MHz diagnostic linear array (model L10-5; Zonare Medical Systems, CA, USA), which was used to record acoustic emissions.

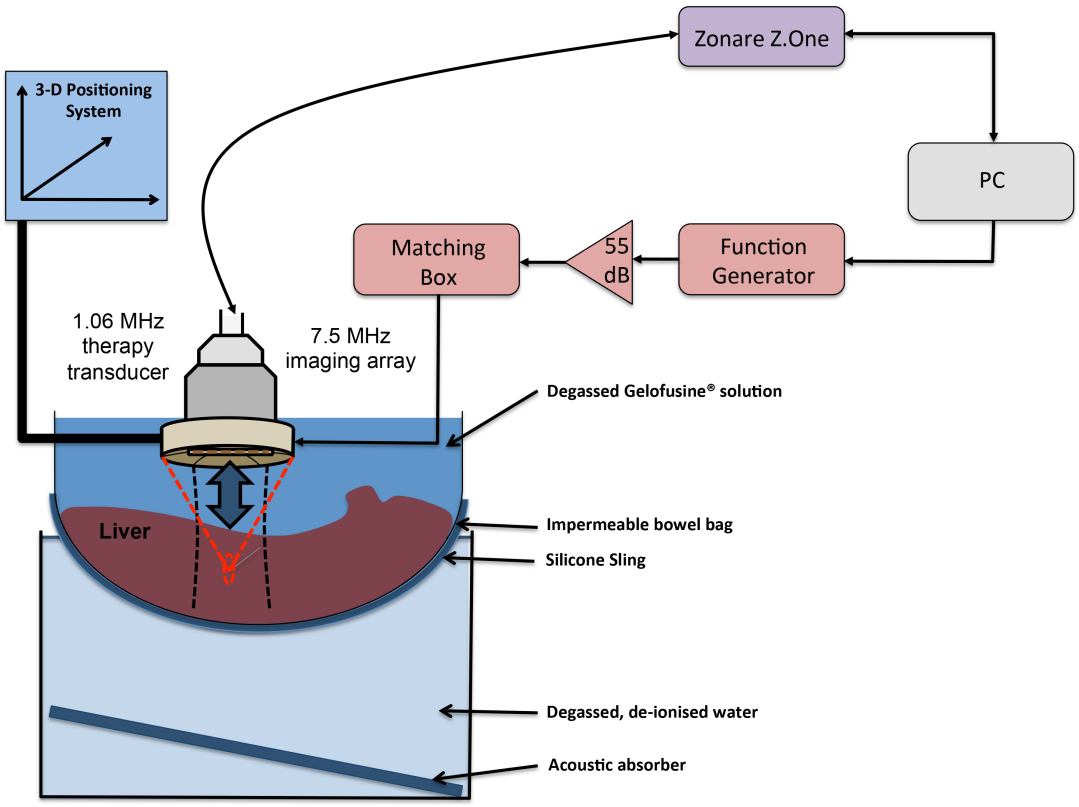


Figure 2.7 *- Schematic diagram of the HIFU experimental set up. The perfused liver, attached to the ECLPD, was immersed in an acoustically-transparent, impermeable surgical isolation bag filled with degassed colloid solution (Gelofusine®, Braun, UK), heated to 37 °C. The bag was suspended in a silicone sling over a degassed, de-ionised 37 °C water bath. The*

1.06 MHz HIFU transducer with a coaxially aligned Zonare L10-5 linear imaging array was mounted on a manual 3-D positioning system. The 1.06 MHz HIFU transducer was connected to a 50 Ω matching network. A signal generator (33250A; Agilent Technologies, CA, USA) attached to a power amplifier (model 1040L; ENI, NY, USA), was used to generate the HIFU exposures.

The HIFU transducer and 5-10 MHz diagnostic linear array were mounted within custom-made holders, which enabled stable alignment when clamped together (*Figure 2.8*). The diagnostic ultrasound engine attached to the linear array (Z.One; Zonare Medical Systems, CA, USA) could acquire conventional B-mode images or could be operated in passive mode simultaneously during HIFU exposure, allowing access to pre-beamformed in-phase and quadrature (I/Q) data from 64 individual channels (4.64 to 9.64 MHz), which could be downloaded post-exposure and post-processed to form passive acoustic maps, as described by Gyongy and Coussios (2010) and which is detailed in Section 2.5.3.

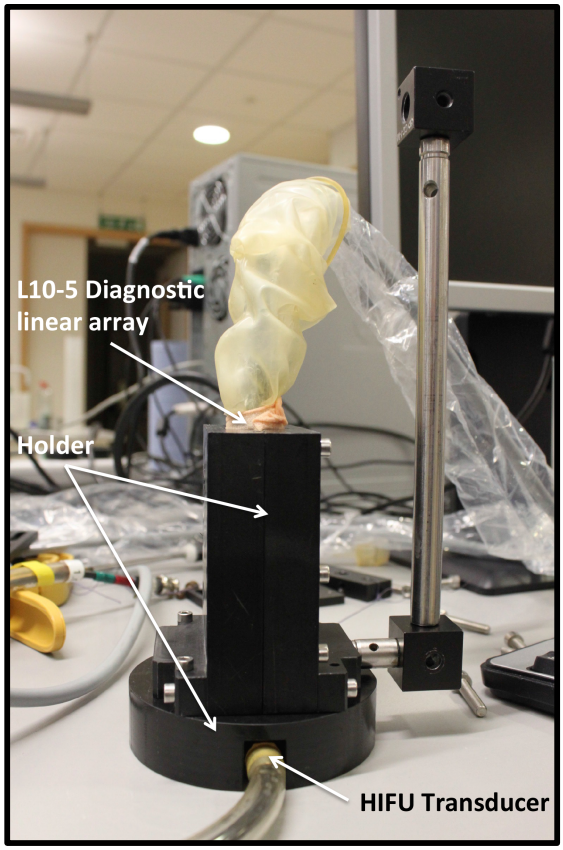


Figure 2.8 – *Static arrangement of the 1.06 MHz HIFU transducer and L10-5 linear array, mounted within custom-made Mylar holders and bolted together. The holder was designed so that the front of the linear array was mounted 10 mm back from the surface of the HIFU transducer in order to reduce thermal damage and crosstalk. The custom-made holders also permitted attachment of the transducers to a 3-D positioning system (bracket shown to right of photograph).*

The 1.06 MHz HIFU transducer was connected to a 50 Ω matching network, which was supplied with the transducer. A signal generator (33250A; Agilent Technologies, CA, USA), attached to a power amplifier (model 1040L; ENI, NY, USA), was used to generate the HIFU exposures. The 1.06 MHz HIFU transducer was calibrated in free-field conditions in water using a 400 μm needle hydrophone (SN 1056; Onda Corporation, CA, USA) at both the fundamental frequency and at the third harmonic.

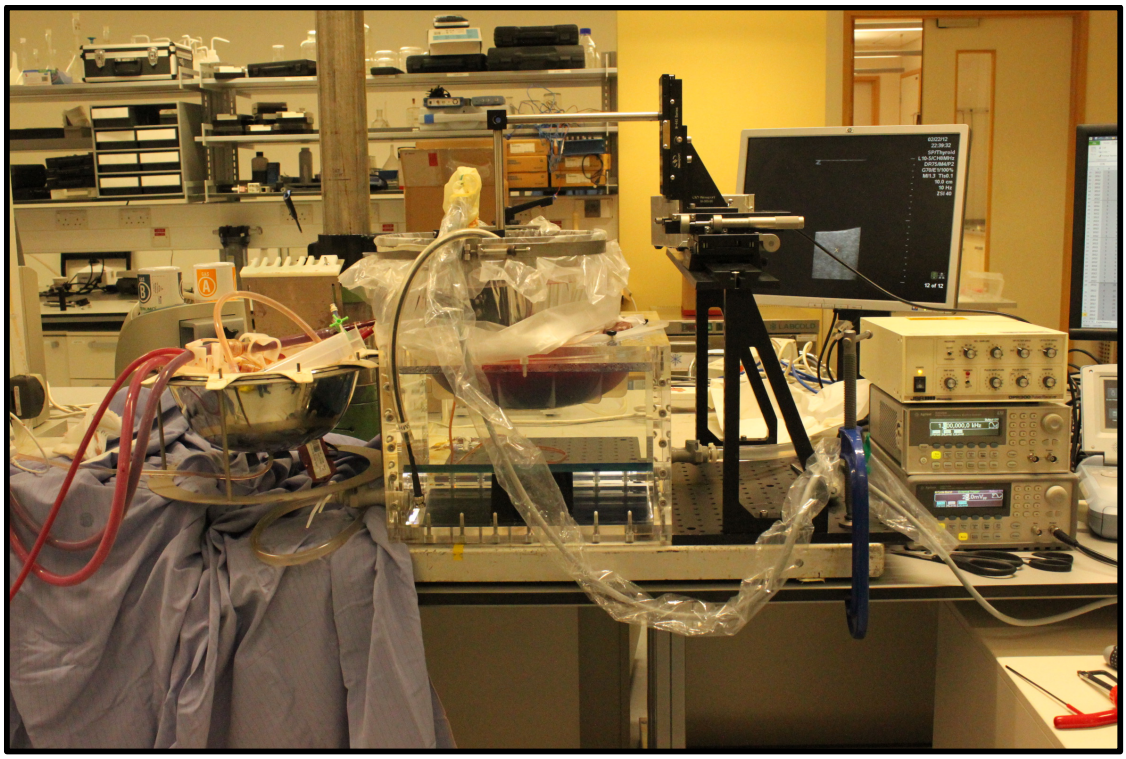


Figure 2.9 *– Photograph of the HIFU experimental setup showing the perfused liver immersed in colloid solution, suspended in a impermeable bag / silicone sling above a water bath filled with degassed, deionised water at 37 ˚C. The HIFU transducer is mounted on a 3-D positioning system and placed above the liver. Real-time B-mode imaging of the liver from the coaxially-aligned 5-10 MHz diagnostic linear array, identifying vascular and biliary structures, can be seen on the monitor.*

2.4.1 Alignment Protocol

In order to determine the position of the HIFU focus relative to the B-mode image generated by the diagnostic ultrasound system and for identification of the HIFU focus on subsequent passive acoustic maps, the following alignment protocol was undertaken (*Figure 2.10*).

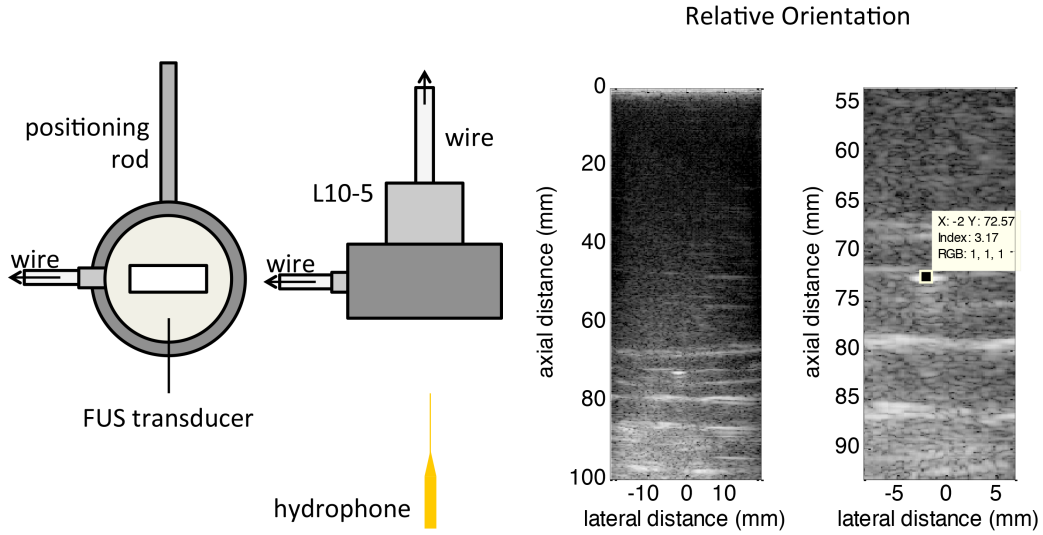


Figure 2.10 – *Schematic diagram showing alignment protocol. The HIFU transducer and 5-10 MHz linear imaging array were coaxially aligned. A needle hydrophone was used to identify and align the HIFU focus with the linear imaging array.*

2.5 Experimental Protocol

2.5.1 Location Selection

Given that one objective of the studies in this work was to determine the effects of both large vessel and capillary blood flow on cavitation, heating and ablation during HIFU therapy, two distinct types of tissue region were selected. Firstly, areas immediately adjacent (≤ 2 mm) to a large blood vessel (≥ 5 mm) and, secondly, microperfused regions of liver tissue (≥ 1 cm away from a large blood vessel) were identified using B-mode ultrasound imaging. Large vessel diameters and velocities were characterised by B-mode and Doppler ultrasound and flow rates were calculated from these measurements. Studies were performed in both large vessel (LV) and microvascular (MV) locations, comparing cavitation, heating and ablation in regions immediately adjacent to a large vessel to microperfused areas of liver parenchyma.

2.5.2 Passive Acoustic Mapping

In order to quantify and spatiotemporally map cavitation activity during HIFU therapy, passive acoustic mapping was performed. The coaxially aligned diagnostic linear array (L10-5; Zonare, USA) and diagnostic ultrasound engine (Z-One; Zonare, USA) were programmed to passively capture 64 channels of acoustic emissions data during HIFU exposures. The passively acquired I/Q channel data were downloaded, transferred to a personal computer and converted into a high-level technical computing language (Matlab R2012a; Mathworks, MA, USA) following completion of the HIFU exposure (performed by E. Mylonopoulou, C. Jensen and J. Choi). These I/Q data were first transformed to radiofrequency data and then for each of the 64 channels, a digital comb

filter was applied to the frequency domain in order to isolate the broadband signal associated with inertial cavitation from the harmonics of the 1.06 MHz or 3.18 MHz HIFU signal. The bandwith for each comb of the filter was 300 kHz around the driving frequency and around each multiple of the harmonic. Both the broadband and harmonic components of the signal were subsequently subjected to a beam-forming algorithm, as previously described by Gyongy and Coussios (*Figure 2.11*), in order to produce passive acoustic maps with individual frames that mapped spatial distribution of both broadband and harmonic emissions every 30 milliseconds (Gyongy and Coussios, 2010). The individual passive acoustic frames were integrated to produce either summative or mean acoustic energy yields across the duration of each HIFU exposure. The peak focal broadband energy was then calculated from PAMs acquired during each exposure.

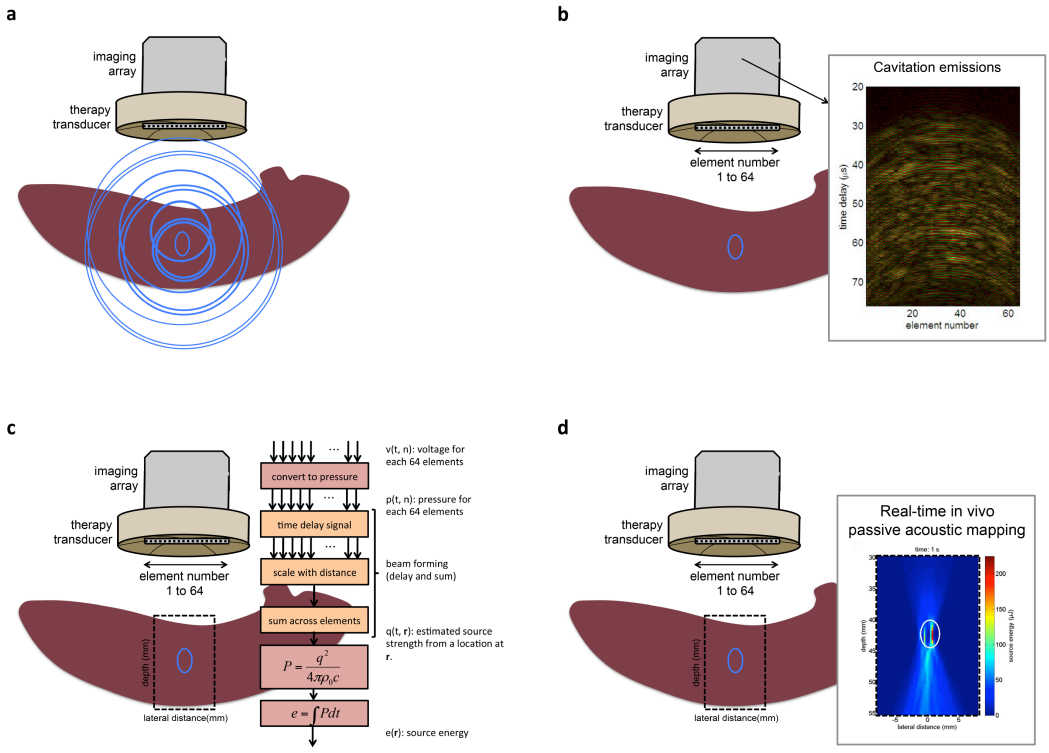


Figure 2.11 *– Schematic diagram showing method of passive acoustic mapping (PAM).*

Acoustic emissions spread spherically from the HIFU focus (a) and are captured by 64 elements of the L10-5 linear imaging array (b), giving 64 channels of in-phase and quadrature data. The inverse problem is solved from the raw I/Q data by means of a beam-forming algorithm (c), enabling acoustic emissions to be mapped quantitatively in time and space (d). As the position of the HIFU focus is known relative to the B-mode image, the HIFU focus can be plotted on the PAM (white oval).

2.5.3 Thermometry

In order to measure real time temperature changes in hepatic tissue during HIFU exposure, a 200 μm needle thermocouple (HYP-0; Omega Engineering, CT, USA) was inserted into the liver parenchyma under B-mode ultrasonographic guidance. Areas of liver parenchyma either adjacent to (≤ 2 mm) a large intrahepatic blood vessel (> 5 mm diameter) or away from large blood vessel (> 1 cm), at an approximate depth of 2 cm from the upper liver surface, were targeted. Vessel diameter and blood flow velocity were assessed by B-mode imaging and colour Doppler and recorded. Thermocouple alignment relative to the HIFU focus was performed using a previously described technique to minimize experimental error (Dasgupta et al., 2011). Following insertion of the needle thermocouple into the target tissue, the HIFU transducer was driven at 1.3 MPa_{Pk-} for 1 s every 3 s. Using the 3-D manual positioning system, the co-ordinates of the HIFU focal volume were adjusted until the location with the maximum temperature rise had been identified. These co-ordinates corresponded to alignment of the HIFU focus with the junction, which is the most temperature sensitive part, of the needle thermocouple.

The focal temperature during a 1 s HIFU exposure was measured at multiple, increasing peak rarefaction pressures at 1.06 MHz, in the presence of inertial cavitation and at 3.18 MHz, in the absence of inertial cavitation. The exposure protocol for the thermometry studies is described in detail in Chapter 4.

2.5.4 Exposure Protocol

Exposure protocols for the individual cavitation, thermometry and histological studies are detailed in Chapters 3, 4 and 5 respectively.

2.5.5 Perfusion Vs. No Perfusion

For cavitation and thermometry studies, HIFU exposures were performed at each location both in the presence and absence of perfusion, with the ECLPD turned off and with the vascular inflows and outflow tracts of the liver clamped. Following cessation of the thermocouple was retargeted before commencing thermal measurements. The same HIFU parameters used in the presence of perfusion, as described above, were used for no-flow conditions. Cessation of perfusion was kept to below 15 minutes in order to minimise warm ischaemic injury to the liver (Ishizaki et al., 2006, Torzilli et al., 2012). A period of 10 minutes of reperfusion without any intervention was undertaken prior to conducting any further measurements, in order to allow re-oxygenation of the tissue.

2.6 Summary

For the studies described in this current work, a unique normothermic liver perfusion device, designed for clinical liver transplantation and which can keep an organ alive ex vivo for in excess of 72 hours, was modified. This technique enabled HIFU studies assessing real time cavitation characteristics, thermal response and histological outcomes following ablation to be conducted within different liver regions, within an anatomically relevant, functional test bed.

CHAPTER 3

LIVER PERFUSION PRESERVATION

A unique normothermic perfusion preservation device, allowing a liver to be maintained in a functional state *ex vivo*, was used for all studies described in the current work. Porcine livers were used to provide a suitable test bed for HIFU therapies as they display similar anatomical and physiological characteristics to those of the human liver. This chapter reports the various parameters recorded by the normothermic perfusion preservation device, such as vascular flow rates and acid-base balance, assessing the function of the perfused liver.

3.1 Introduction

*Ex vivo n*ormothermic liver perfusion preservation can maintain an organ in a functional, physiological state for in excess of 72 hours (Brockmann et al., 2009, Butler et al., 2002, Reddy et al., 2004). A unique device, designed for liver preservation prior to transplantation, was used that perfuses an organ with blood, heated to 37 ˚C and oxygenated to maintain normal *in vivo* partial pressures of oxygen and carbon dioxide, at physiological vascular pressures (Metra; OrganOx®, Oxford, UK). Preclincal studies testing the normothermic liver preservation device have used a porcine model, which is anatomically and physiologically similar to the human liver. However, outside of transplantation

studies, the isolated, perfused porcine liver also provides a suitable *ex vivo* test bed for other therapies.

In the studies described in this work, the liver was placed in a bath of isotonic colloid solution and subjected to a number of HIFU exposures over a period of up to 26 hours, which was necessary to allow acoustic transmission. The normothermic perfused liver system employed in this work was designed for the preservation of organs under stable conditions, maintaining the liver in a sterile environment providing minimal stress to the tissues. The studies assessing function during and after liver perfusion preservation described above and in Chapter 2 had all been conducted under optimal conditions. Therefore, the aim of monitoring and analysis of liver perfusion parameters during the current HIFU studies was to enable assessment of the organ as a functional, near physiological test bed given the environmental conditions in which the organs were placed in and the stresses the organs were subjected to during HIFU therapy were substantially different to those conditions encountered in the previously reported studies of isolated liver perfusion.

3.2 Methods

Porcine livers were surgically explanted and connected to the normothermic liver perfusion device as detailed in Chapter 4. Technology within the liver perfusion device (Metra®; Organox, Oxford, UK) permitted real time monitoring of a number of parameters during normothermic perfusion. IVC and portal venous

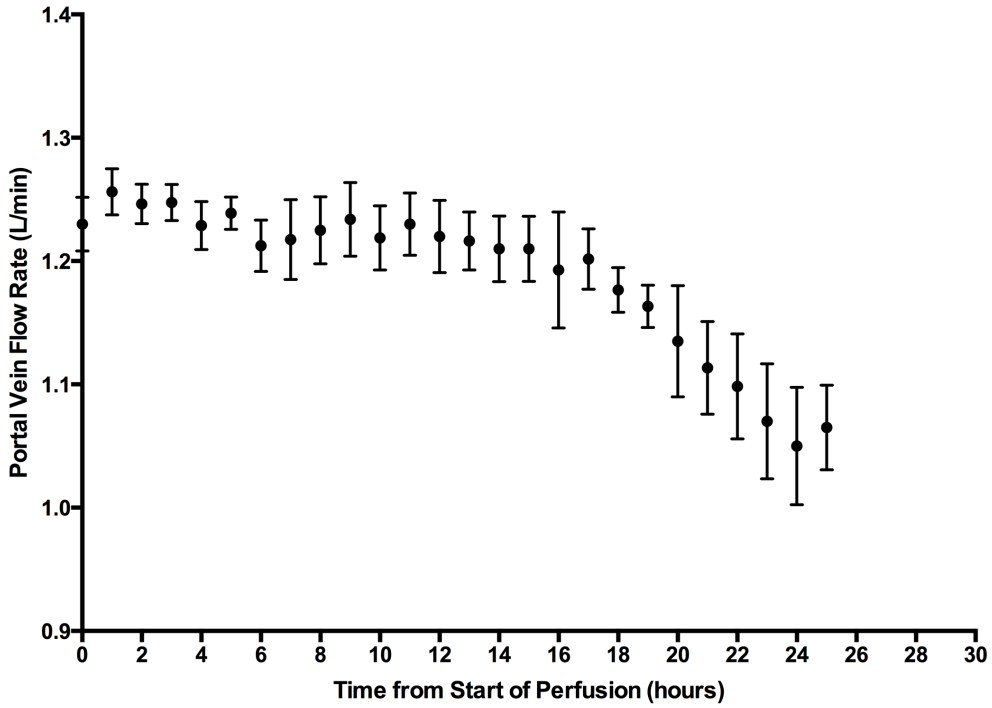
(PV) flow rates were continuously measured via ultrasonic flow sensors, whilst hepatic arterial flow was calculated as the difference between the IVC and PV flow rate. Acid-base balance and partial pressures of O_2 and CO_2 were continuously measured via an in-line sensor attached to the oxygenator outflow and blood gas analyser (Terumo CDI510H; Terumo, Japan).

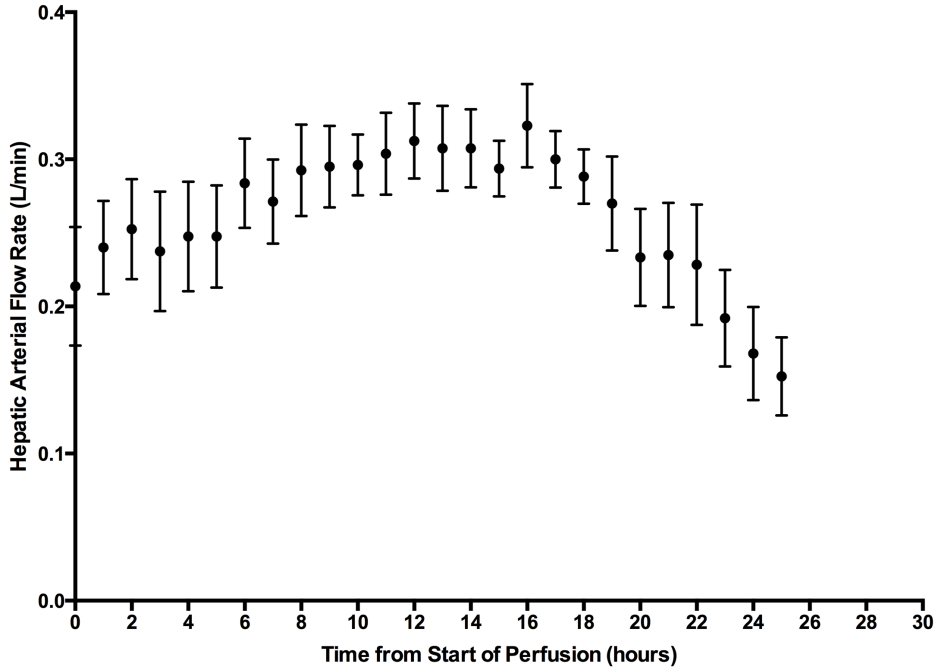
Raw data were downloaded from the liver perfusion device following each study, imported into Microsoft Excel (Microsoft, Seattle, USA) and processed using a statistical software package (Prism; Graphpad, USA). Data are expressed as a mean ± SEM.

3.3 Results

In total, 16 isolated, perfused porcine livers were used for the studies detailed in Chapters 4, 5 and 6. The median cold ischaemic time, defined as the time from the start of cold perfusion with Soltran® solution via the aortic cannula during the liver explantation procedure, to the start of reperfusion on the normothermic perfusion device, was 190 minutes (range 120 – 255 minutes). Cannulation of the hepatic vessels, transportation and priming of the normothermic perfusion device occurred during this phase.

The mean perfusion time, defined as the time from the start of normothermic machine perfusion (NMP) to the time NMP was stopped and the liver was removed from the device, was 23 hours (range 17 to 26). Mean portal flow throughout the duration of each perfusion was 1.19 L/min, with a mean arterial flow rate of 0.26 L/min, giving a mean total hepatic flow rate of 1.45 L/min. Mean portal venous (PV), hepatic arterial (HA) and inferior vena caval (IVC) flow rates are shown below in *Figure 3.1,* whilst arterial PO_2, PCO_2 and pH are shown in *Figures 3.2 and 3.3* respectively.


Portal Vein Flow Rate (L/min)
1.4
1.3
1.2
1.1
1.0
0.9
0 2 4 6 8 10 12 14 16 18 20 22 24 26 28 30
Time from Start of Perfusion (hours)


Hepatic Arterial Flow Rate (L/min)
0.4
0.3
0.2
0.1
0.0
0 2 4 6 8 10 12 14 16 18 20 22 24 26 28 30
Time from Start of Perfusion (hours)

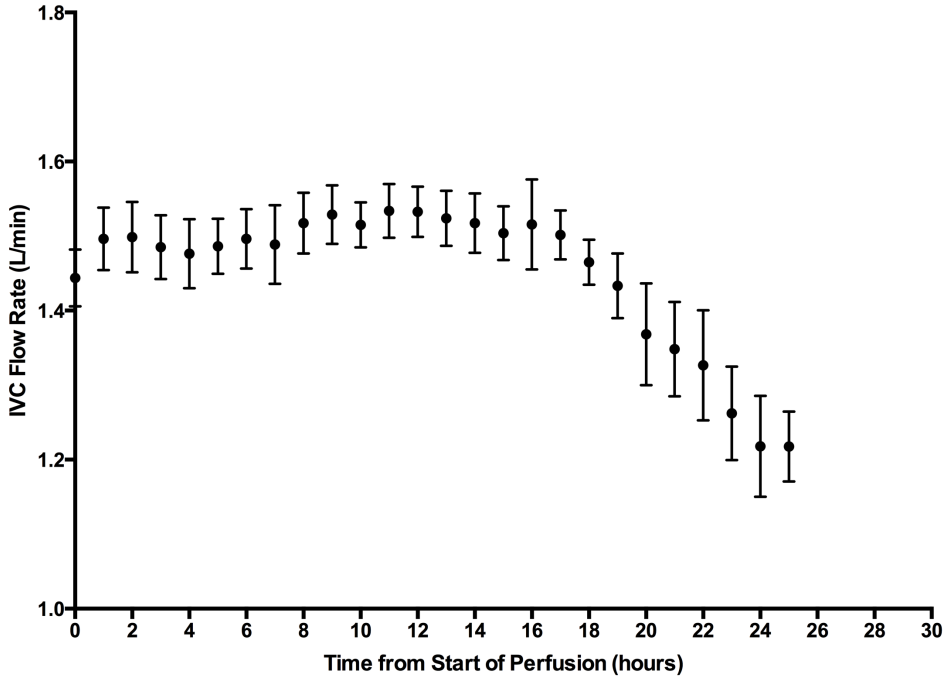


Figure 3.1 – *Mean portal venous (a), hepatic arterial (b) and IVC (c) flow rates during NMP.*

Over the final 3 – 5 hours of each perfusion, a gradual decrease in the HA, PV and total hepatic flow rates was observed.

Continuous arterial blood gas sampling via an in-line blood gas analyser allowed measurement of PO_2, PCO_2, acid-base balance and perfusate temperature. Mean PO_2 was 14.9 kPA, mean PCO_2 was 5.3 and mean pH was 7.41. The gas partial pressures were tightly controlled within a pre-specified range of 12 – 20 kPa (PO_2) and 3.5 – 6.0 kPa (PCO_2) and these remained fairly constant throughout each perfusion (*Figure 3.2*).

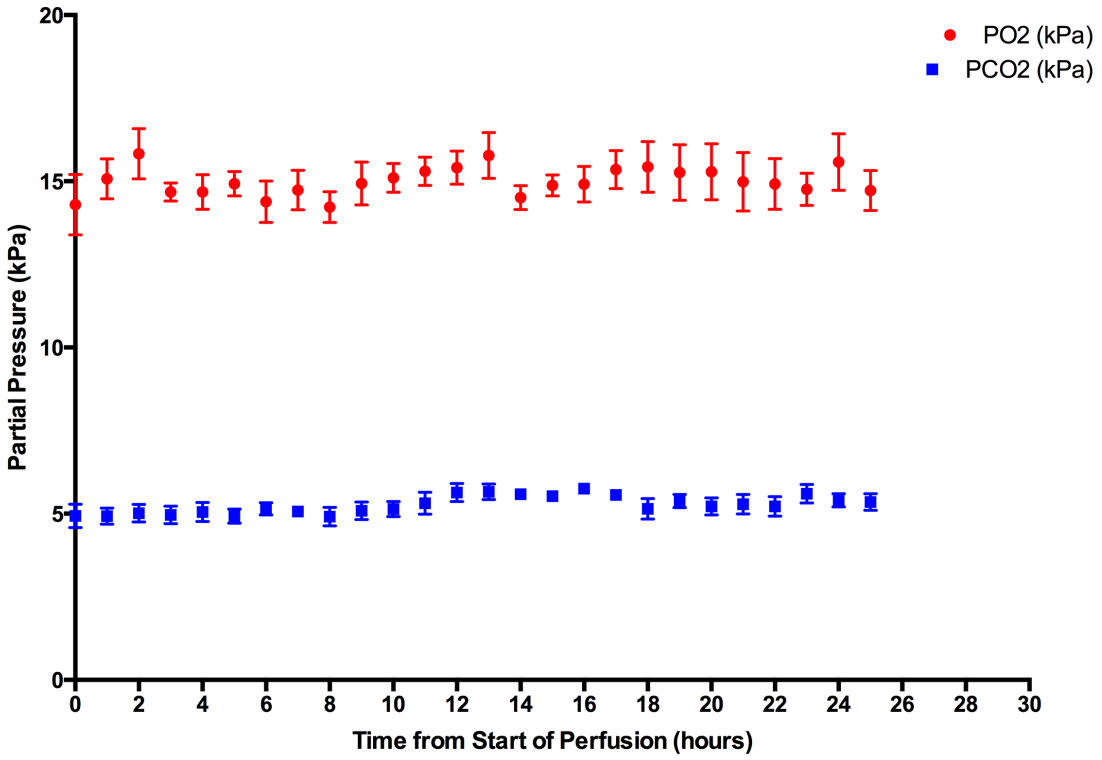


Figure 3.2 *– Mean arterial PO_2 and PCO_2 during NMP.*

Following the commencement of NMP, the perfusate was initially fairly acidotic, with a mean pH of 7.24 at T = 0 (*Figure 3.3*). Similar to previously reported studies, the isolated, perfused livers were able to gradually correct this acidosis over the subsequent 2 – 4 hours, restoring a normal pH and maintaining acid-base homeostasis. However, in each isolated, perfused liver, a gradual decrease in the pH, signifying an evolving metabolic acidosis, was observed over the final 2- 4 hours of each perfusion.

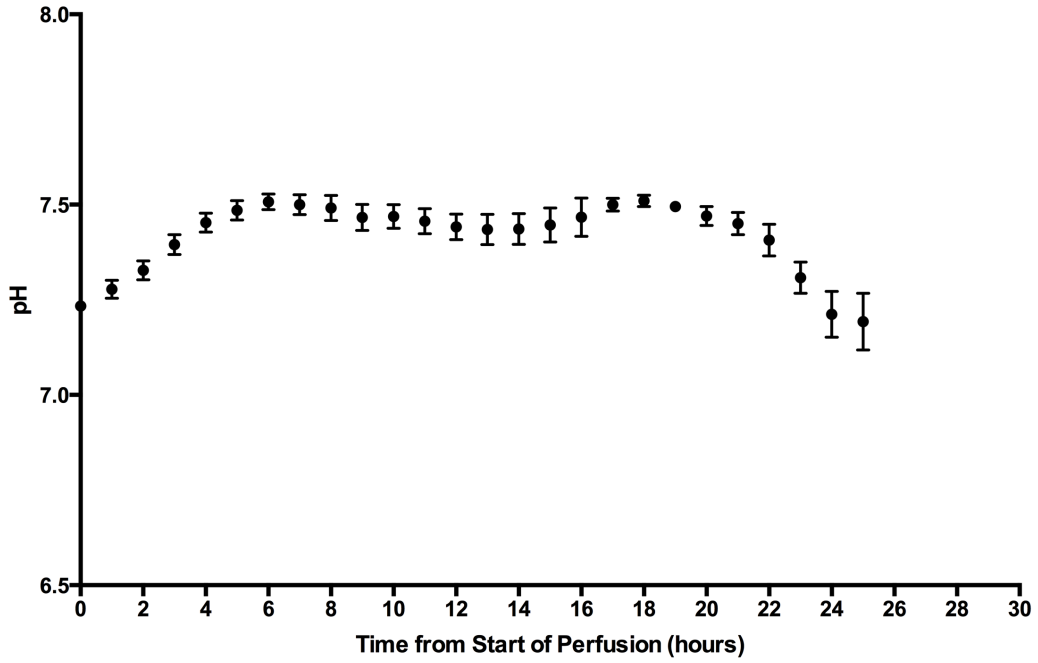


***Figure 3.3 – Mean** pH during NMP*

Continuous heating of the perfusate via in-line Peltier heaters maintained the blood at a mean temperature of 37.3 ˚C throughout each perfusion (*Figure 3.4*).

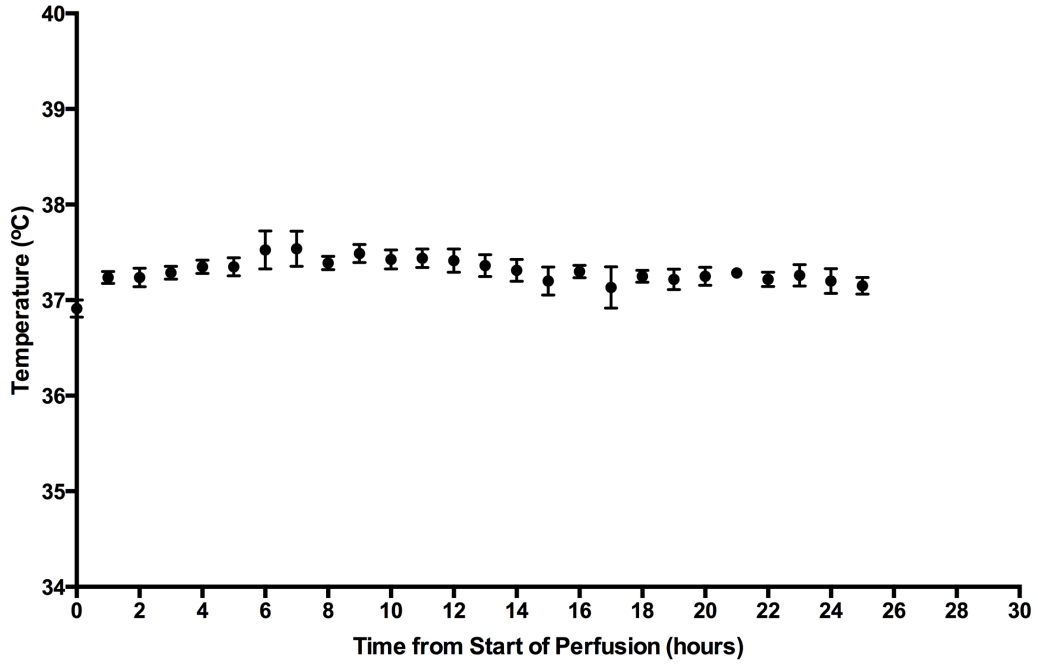


***Figure 3.4 –** Mean blood temperature during NMP*

All 16 livers produced bile, indicating functional hepatocyte activity (*Figure 3.5*). This was initially seen in the clear plastic tube used to cannulate the common bile duct (CBD) within the first 90 minutes of each perfusion, signifying early restoration of hepatic function following the period of cold static preservation.

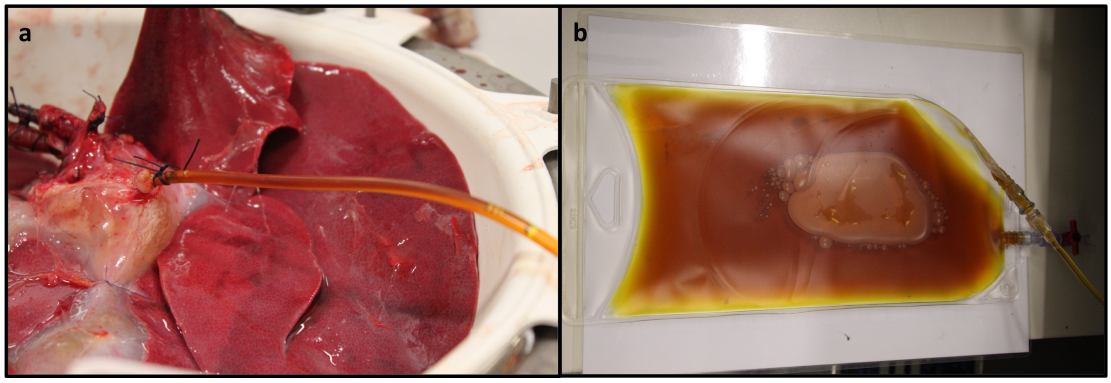


Figure 3.5 *– Bile production during NMP in the cannulated CBD (a) and total bile production at the end of NMP (b)*

The isolated, perfused livers underwent at least 60 minutes of bench top NMP prior to placing in a water bath and commencement of HIFU experiments. At the end of this resuscitation period, the organs appeared pink and well perfused in colour, with only occasional small areas of darker hepatic parenchyma, signifying regions of poorer perfusion (*Figure 3.6*).

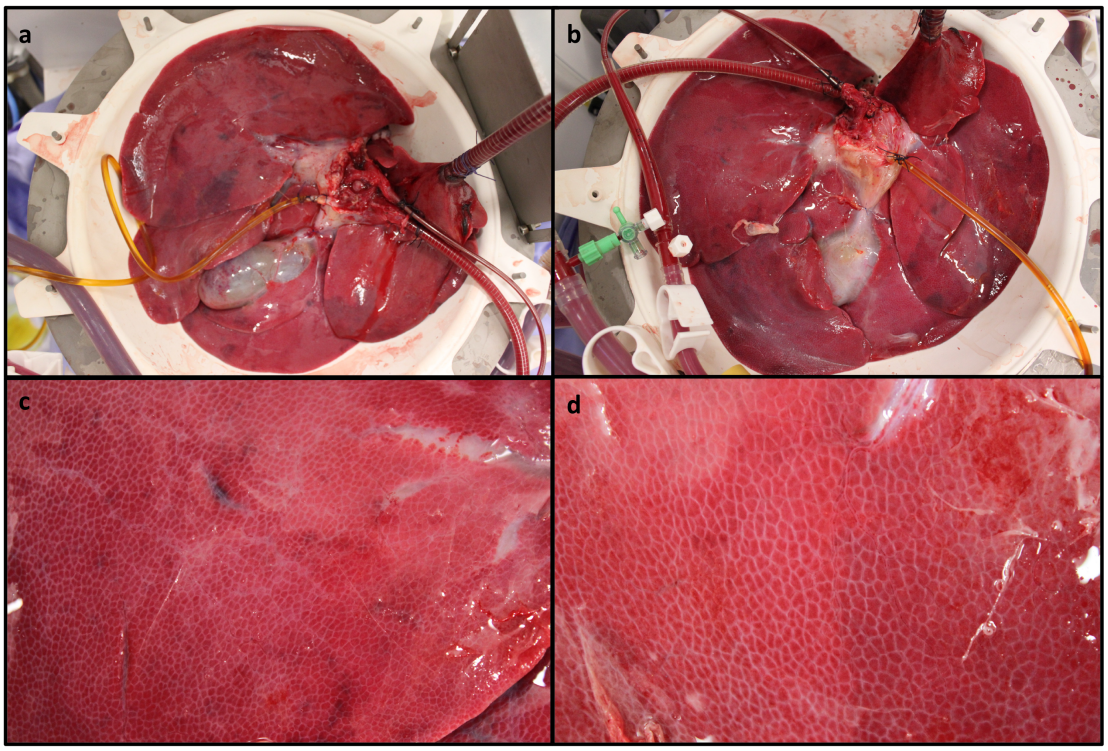


Figure 3.6 *– Appearance of the perfused porcine liver following approximately 60 minutes of NMP, prior to placing in a water bath and commencing HIFU experiments.*

At the end of NMP, 12 out of 16 livers appeared in reasonable condition, with pink parenchyma on gross examination and sectioning (*Figure 3.7*). A degree of tissue oedema was evident in all livers. In 3 of the livers used for the thermometry and cavitation studies (Chapters 4 and 5), there were patchy dark areas of parenchyma, indicating areas of ischaemia. The parenchyma appeared pink and evenly perfused in all isolated, perfused livers used for the histology studies (Chapter 6).

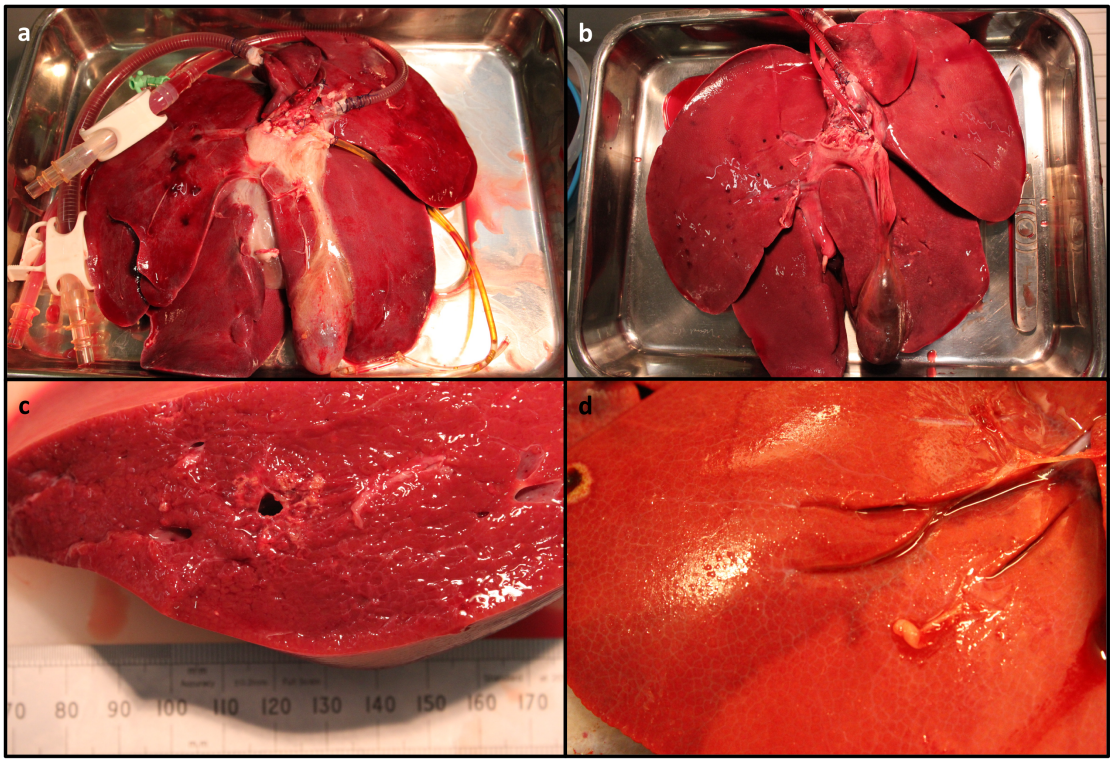


Figure 3.7 *– Gross appearance following 17 to 26 hours of NMP, after the completion of HIFU studies*

3.4 Discussion

The unique normothermic liver perfusion device, used in all of the studies in this current work, can maintain an isolated liver in a functioning state, allowing it to be utilized as *ex vivo* test bed for novel therapies. In preclinical transplantation studies, the device has been shown to maintain vascular flow rates, gas partial pressures and acid-base homeostasis within normal limits throughout normothermic machine preservation.

In this current work, unlike the preclinical NMP studies investigating this technique for organ preservation prior to transplantation, livers were placed in a water bath and subjected to HIFU therapy. A further difference from the NMP method described in the preclinical studies was that, due to the water bath, ascites and any blood loss from the organ was not collected and returned to the circulating perfusate. Placing the organ in a water bath, which was necessary in order to provide a couple for the ultrasound, caused a degree of fluid shift. To minimise this, isotonic colloid solution was used as the bathing medium, which has a similar oncotic pressure to that of the perfusate. In addition, thermometry studies were performed on several of the organs, requiring invasive thermocouple placement, which often lead to a degree of bleeding. Hence, it was anticipated that there would be a degree of deterioration in the quality and function of the organ with time, unlike the preclinical transplant studies.

From the data presented, it appears as if most livers remained functional, with near-normal flow rates and acid-base balance, comparable to previous NMP studies, until the last 2 -4 hours of perfusion (Butler et al., 2002, St Peter et al., 2003, St Peter et al.,

2002b). At this point, a trend towards an increasing metabolic acidosis, decreasing portal and arterial flow rates was seen. The most likely explanation for the deterioration in liver function and onset of metabolic acidosis is that a degree of hepatic injury evolved with time due to blood loss, intermittent ischaemia as the perfusion device was turned on and off during studies, fluid shifts and stress on the organ. Although no biochemical analysis was performed on the perfusate, it could be anticipated that transaminases would also increase significantly over this period, also suggesting increasing liver injury.

Therefore, although the isolated, perfused liver provided a functional, anatomically relevant test bed, with near normal physiological parameters, the model is not an exact replica of the *in vivo* situation. Deterioration in the quality and function of the liver tissue with time was a potential cause of artifact within the studies described in the following chapters. Repeating studies *in vivo* would aid validation of the model as a HIFU test bed.

CHAPTER 4

THE EFFECTS OF PERFUSION ON HIFU-INDUCED CAVITATION

The effects of blood flow and physiological tissue perfusion on cavitation are not known and are little described in the literature. The majority of published studies investigating ultrasound-induced cavitation in tissue have been performed using *ex-vivo*, non-perfused models. This present work aims to elucidate the effects of blood flow on HIFU-induced cavitation dynamics using a novel isolated, perfused liver model.

4.1 Introduction

During HIFU therapy, when a medium is placed under a sufficiently high enough acoustic pressure, small cavities can form under the rarefactional part of the pressure cycle. At low acoustic pressures, these cavities initially oscillate linearly but with increasing non-linearity as the acoustic pressure is increased. Beyond a certain pressure amplitude, termed the cavitation threshold, oscillating bubbles start to expand unstably under the rarefactional half-cycle and collapse violently under the compressional half-cycle. This process of inertial cavitation can be detected through broadband emissions and can potentially be used to augment HIFU-induced heating, whilst also providing a mechanism for novel treatment monitoring strategies. There are many contributing factors determining the cavitation threshold of a given medium. As well as being acoustic

pressure-dependent, the cavitation threshold increases with decreasing wavelength, hence increasing frequency. Additionally, a number of medium-based factors also affect the cavitation threshold, including the availability of particles or gas bubbles that can act as nuclei to initiate cavitation events and the temperature of the medium.

Relatively little is known about the cavitation threshold *in vivo*, particularly regarding the effects of physiological blood flow and the complex blood-tissue and tissue-tissue biological mechanisms that exist. The majority of previous work investigating ultrasound-induced cavitation at a mechanistic level has been performed in either tissue-mimicking phantoms or non-perfused, *ex vivo* tissue. However, a recent study has reported cavitation thresholds in vivo, demonstrating a threshold of < 5 MPa in murine pancreatic tumours (Li et al., 2014).

It is widely believed that the absorption of broadband energy emissions resulting from inertial cavitation activity can enhance HIFU-induced heating rates (Holt and Roy, 2001). Additionally, detection of these broadband emissions by novel techniques, such as passive acoustic mapping (PAM) may also provide a real-time method of spatially monitoring heat deposition and lesion formation during HIFU therapy (Jensen et al., 2012). The lowest acoustic pressure at which cavitation occurs: the "cavitation threshold", is frequency and tissue dependent. However, the cavitation threshold is also inherently affected by the availability of cavitation nuclei, which facilitate bubble formation under the rarefaction part of the acoustic pressure cycle, thus initiating a cavitation event. The endogenous sources of cavitation nuclei are not known and have

been little assessed, although the physiological processes that affect cavitation *in vivo* are likely to be multifactorial and complex.

4.2 Study Aims

The aim of the studies discussed in this chapter was to elucidate the effect of physiological perfusion on HIFU-induced cavitation in liver tissue. The specific objectives of the work were:

1) To determine the cavitation threshold of perfused liver tissue at 1.06 MHz and 3.18 MHz
2) To assess whether the presence of a large (≥ 5 mm) blood vessel near to a HIFU treatment focus affects the cavitation threshold or the level of cavitation energy
3) To determine whether the presence or absence of blood flow affects the level of cavitation energy, both in tissue adjacent and far away (> 1cm) from a large blood vessel.

4.3 Materials and Methods

4.3.1 Perfused Liver Model

Porcine livers were surgically explanted, transported and connected to the extracorporeal normothermic liver perfusion device (ECLPD) according to a standard technique described in Chapter 2. Following approximately 60 minutes of normothermic perfusion, the perfusion device was stopped; the stainless steel bowl was removed from under the liver and the liver was placed in an impermeable PVC bag filled with 3L of degassed isotonic colloid solution (Gelofusine®, B Braun, UK) warmed to 37 ˚C. The bag was suspended in a silicone sling over a tank of degassed water, maintained at 38 ˚C.

4.3.2 HIFU Set Up

A custom-manufactured, spherically focused HIFU transducer with a centre frequency of 1.06 MHz (H102D-22; Sonic Concepts Inc., WA, USA), driven at its fundamental frequency or at the third harmonic (3.18 MHz), was used to produce therapeutic ultrasound pulses. The HIFU transducer had an active diameter of 64 mm, 63 mm geometric focus and a central rectangular opening of 45 by 18 mm, permitting coaxial placement of a 128-element 5-10 MHz diagnostic linear array (model L10-5; Zonare Medical Systems, CA, USA), which was used both for conventional diagnostic B-mode ultrasound guidance and for passive cavitation monitoring (see Chapter 2). A typical HIFU generation loop was used. The 1.06 MHz HIFU transducer was connected to a 50 Ω matching network, which was supplied with the transducer. A signal generator

(33250A; Agilent Technologies, CA, USA) attached to a power amplifier (model 1040L; ENI, NY, USA), was used to generate the HIFU exposures (*Figure 4.1*).

The HIFU transducer was calibrated in free-field conditions in degassed, deionsed water using a 400 µm needle hydrophone (SN 1056; Onda Corporation, CA, USA) at both the fundamental frequency and at the third harmonic. The diagnostic ultrasound engine attached to the linear array (Z.One®; Zonare Medical Systems, CA, USA) could acquire conventional B-mode images or could be operated in passive mode simultaneously during HIFU exposure, allowing access to pre-beamformed in-phase and quadrature (I/Q) data from 64 individual channels (4.64 to 9.64 MHz).

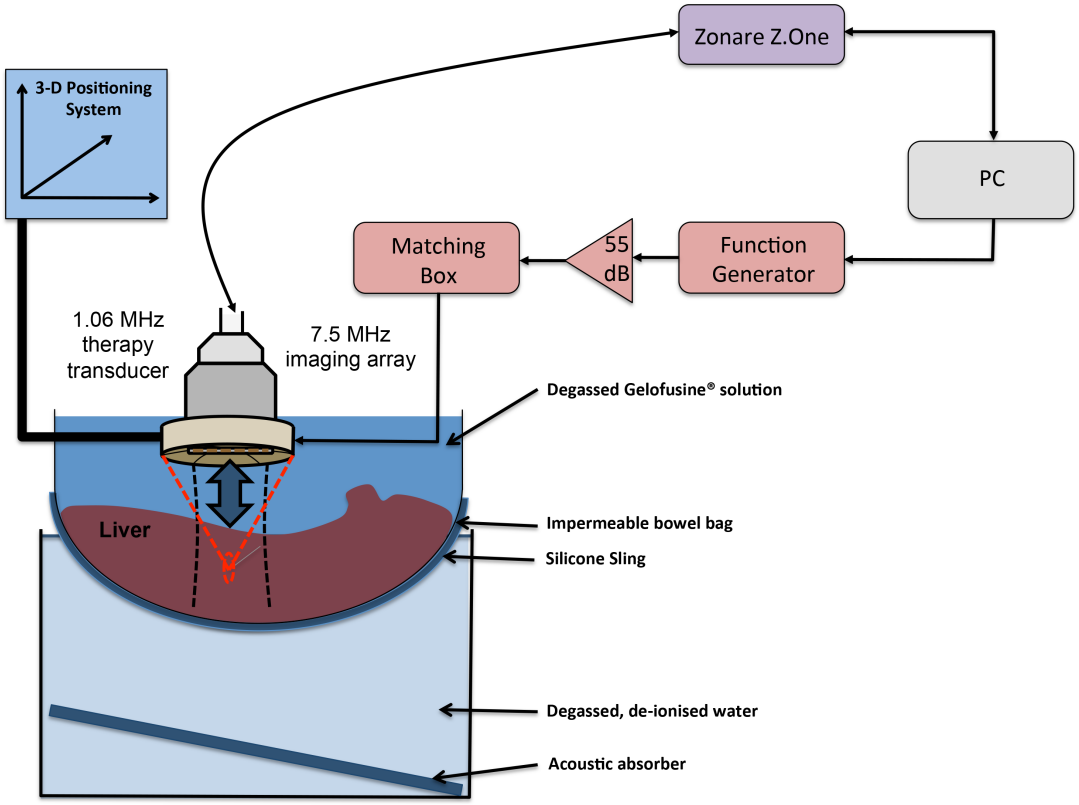


Figure 4.1 *- Schematic diagram of the HIFU experimental set up used for cavitation studies. The perfused liver, attached to the ECLPD, was immersed in an acoustically-transparent, impermeable surgical isolation bag filled with degassed colloid solution at 37 ˚C. The bag was*

suspended in a silicone sling over a degassed, de-ionised 37 ˚C water bath. The 1.06 MHz HIFU transducer with a coaxially aligned Zonare L10-5 linear imaging array was mounted on a manual 3-D positioning system. The HIFU generation loop is shown in red with a PC-controlled function generator, 55 dB amplifier and a 50 Ω matching network, driving the HIFU transducer.

Diagnostic B-mode ultrasound was used to image the liver in order to identify major arterial, portal venous, venous and biliary structures within the liver parenchyma, using both an L10-5 and an L14-5w linear array (Zonare, USA). Two distinct types of tissue region were targeted. Firstly, hepatic parenchyma directly adjacent to a large (≥ 5 mm) vessel and, secondly, areas away (> 1 cm) from a large vessel were selected using B-mode ultrasound. Flow velocities within large vessels were quantified using colour Doppler.

4.3.3 Passive Acoustic Mapping

A novel passive acoustic mapping technique, as described by Gyöngy and Coussios, was employed in order to quantify and spatiotemporally map cavitation activity during HIFU therapy (Gyongy and Coussios, 2010). The Zonare linear array could detect acoustic emissions passively and these data could be reconstructed to provide temporo-spatial maps of cavitation events in real time. It has been demonstrated that this passive acoustic mapping technique can accurately predict lesion formation in *ex vivo* bovine liver tissue and is superior to clinically used US hyperecho detection (Jensen et al., 2012).

The diagnostic linear array (L10-5; Zonare, USA) was coaxially aligned with the therapeutic 1.06 MHz HIFU transducer according to the protocol described in Section

2.4.1 so that the position of the HIFU focus was known relative to the B-mode image acquired from the diagnostic linear array. The diagnostic ultrasound engine (Z-One; Zonare, USA) was programmed to passively capture 64 channels of acoustic emissions data during HIFU exposures.

The passively acquired I/Q channel data were downloaded, transferred to a personal computer and converted into a high-level technical computing language (Matlab R2012a; Mathworks, MA, USA) following completion of the HIFU exposure (performed by E. Mylonopoulou, C. Jensen and J. Choi). These I/Q data were first transformed to radiofrequency data and then for each of the 64 channels, a digital comb filter was applied to the frequency domain in order to isolate the broadband signal associated with inertial cavitation from the harmonics of the 1.06 MHz or 3.18 MHz HIFU signal. The bandwith for each comb of the filter was 300 kHz around the driving frequency and around each multiple of the harmonic. Both the broadband and harmonic components of the signal were subsequently subjected to a beam-forming algorithm, as previously described by Gyongy and Coussios (*Figure 4.2*), in order to produce passive acoustic maps with individual frames that mapped spatial distribution of both broadband and harmonic emissions every 30 milliseconds. The individual passive acoustic frames were integrated to produce either summative or mean acoustic energy yields across the duration of each HIFU exposure.

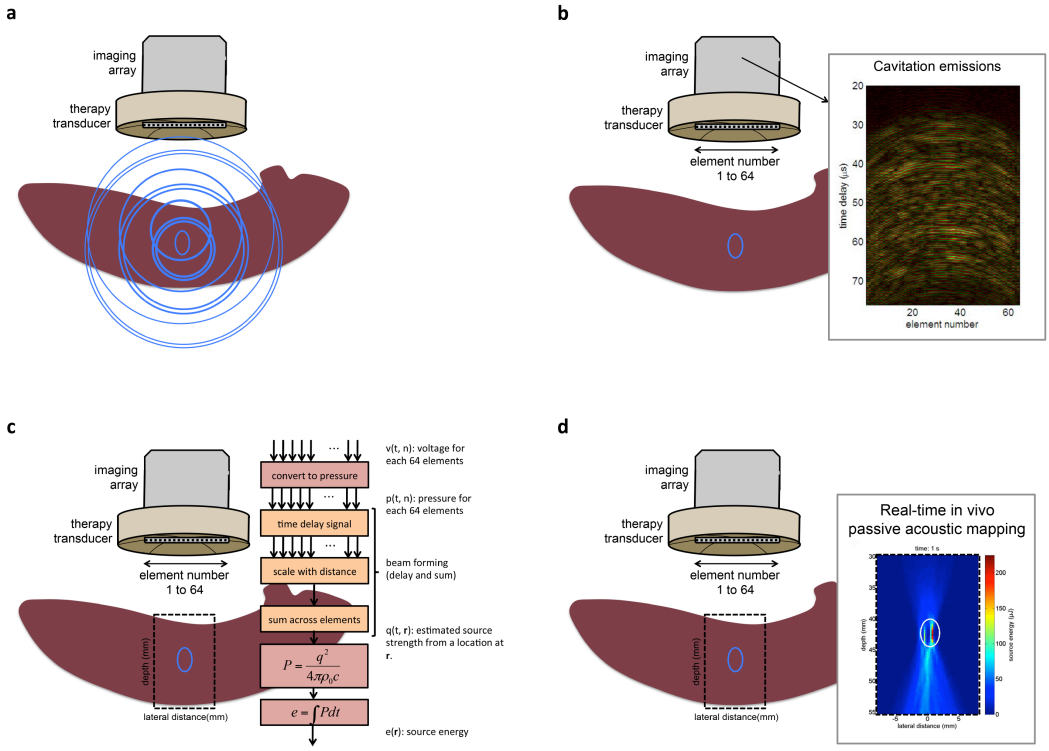


Figure 4.2 *– Schematic diagram showing method of passive acoustic mapping (PAM). Acoustic emissions spread spherically from the HIFU focus (a) and are captured by 64 elements of the L10-5 linear imaging array (b), giving 64 channels of in-phase and quadrature data. The inverse problem is solved from the raw I/Q data by means of a beam-forming algorithm (c), enabling acoustic emissions to be mapped quantitatively in time and space (d). As the position of the HIFU focus is known relative to the B-mode image, the HIFU focus can be plotted on the PAM (white oval).*

Analysis of successive frames allowed the degree and location of acoustic power sources to be monitored, whilst integration of the acoustic source power across all frames acquired provided a total acoustic energy for each location. Undesirable off-focus cavitation activity, especially pre-focal, which can lead to shielding of the intended focal region in addition to collateral tissue injury, could also be detected by examining individual

frames. The peak focal broadband energy was then calculated from PAMs acquired during each exposure.

4.3.4 HIFU Protocol

For the studies described below, the following HIFU protocols were used. At each location, seven HIFU exposures were performed at increasing peak rarefaction pressures.

Frequency	1.067 MHz
Exposure duration	1 s
Peak rarefaction pressures (MPa $_{Pk-}$)	0.99, 1.88, 2.80, 3.73, 4.65, 5.58, 7.81
Duty cycle	100%

Frequency	3.18 MHz
Exposure duration	1 s
Peak rarefaction pressures (MPa $_{Pk-}$)	0.40, 0.90, 1.75, 2.60, 3.46, 4.31, 5.16, 6.86
Duty cycle	100%

***Table 4.1** – HIFU parameters for cavitation studies*

4.4 Results

In this section, results acquired from studies performed within 8 isolated, perfused porcine livers are presented, demonstrating the effects of physiological blood flow on HIFU-induced cavitation, measured through passive acoustic mapping (PAM). As described above and in Chapters 1 and 2, PAM can quantitatively map acoustic emissions spatiotemporally in real time, providing a method to assess the level and location of acoustic cavitation during HIFU therapy. In order to assess the effects of both large vessel blood flow and microvascular perfusion on HIFU therapy, two distinct regions of tissue were targeted. Firstly areas of hepatic parenchyma directly adjacent to a large (≥ 5 mm) vessel and secondly, areas away (> 1 cm) from a large vessel were selected using B-mode diagnostic ultrasound imaging. Measurements were made at each location in the presence of perfusion and in the absence of perfusion, with the liver perfusion device stopped and the inflow/outflow tracts clamped.

4.4.1 Passive Acoustic Mapping of Cavitation Activity

At each location, acoustic emissions were monitored and recorded through passive acoustic mapping (PAM) during 1 second HIFU exposures at a number of increasing peak rarefaction pressures ranging from 0.9 to 7.8 MPa. Passive acoustic maps of the total broadband emissions and total harmonic emissions from each HIFU exposure were constructed from the 64-channel I/Q data of acoustic emission acquired in real time by the Zonare Z.One system in passive mode using the digital comb filter as described in *Section 4.3.3*. Examples of PAMs from studies performed at two single locations, one in

a microvascular-perfused tissue region and one in an area directly adjacent to a large (≥ 5 mm) blood vessel, are displayed in *Figure 4.3* below.

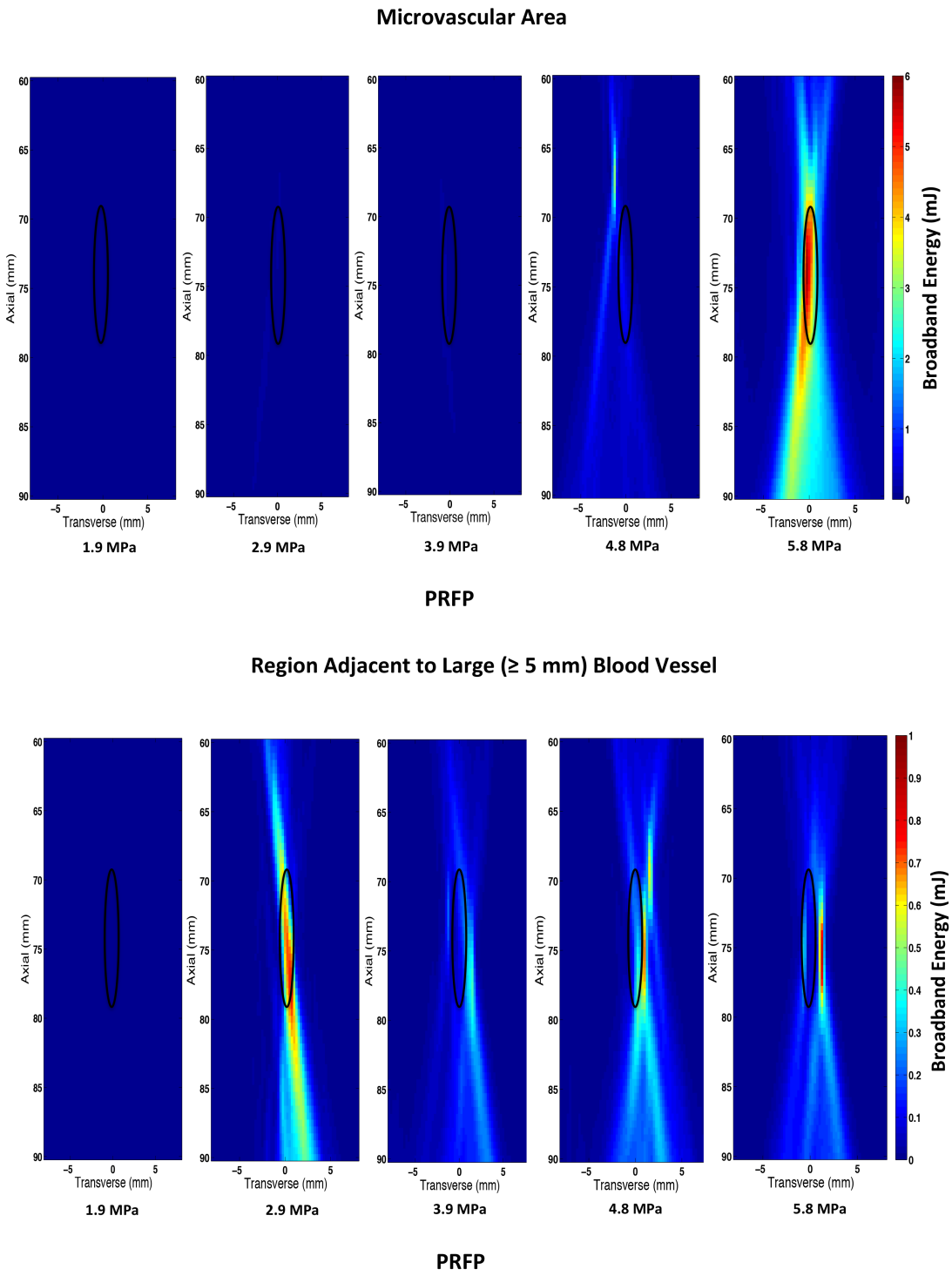


Figure 4.3 a and b – *Passive acoustic maps displaying levels and spatial distribution of broadband emissions, representing inertial cavitation, in two single locations a) A*

microvascular-perfused area, away from a large vessel and b) A region of liver parenchyma directly adjacent to a large (≥ 5 mm) blood vessel.

For the results presented in the following sections, the acoustic emissions detected at the HIFU focus were measured. Any off-focus cavitation activity, such as that shown below in *Figure 4.4*, was therefore excluded from these data.

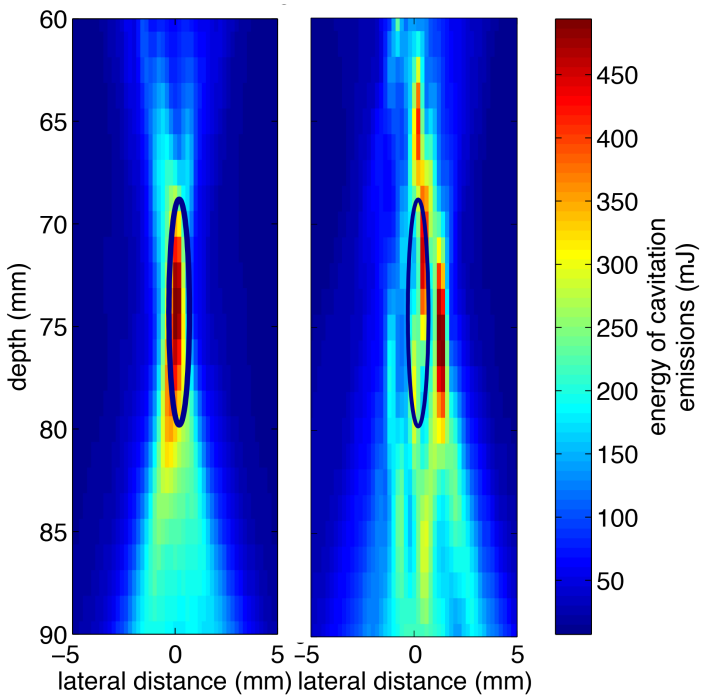


Figure 4.4 – *PAMs showing focal cavitation activity (L) and off-focus cavitation (R).*

4.4.2 Cavitation Threshold at 1.06 MHz

The cavitation threshold at 1.06 MHz, defined as the lowest peak rarefaction pressure at which broadband emissions representing acoustic cavitation could be detected was estimated for both microvascular areas (> 1 cm away from a large blood vessel) and tissue regions directly adjacent to a large (≥ 5 mm) blood vessel, in the presence of blood flow.

The peak focal broadband energy representing inertial cavitation, calculated from the PAMs of each HIFU exposure, across a range of peak rarefaction pressures is displayed in *Figures 4.5*.

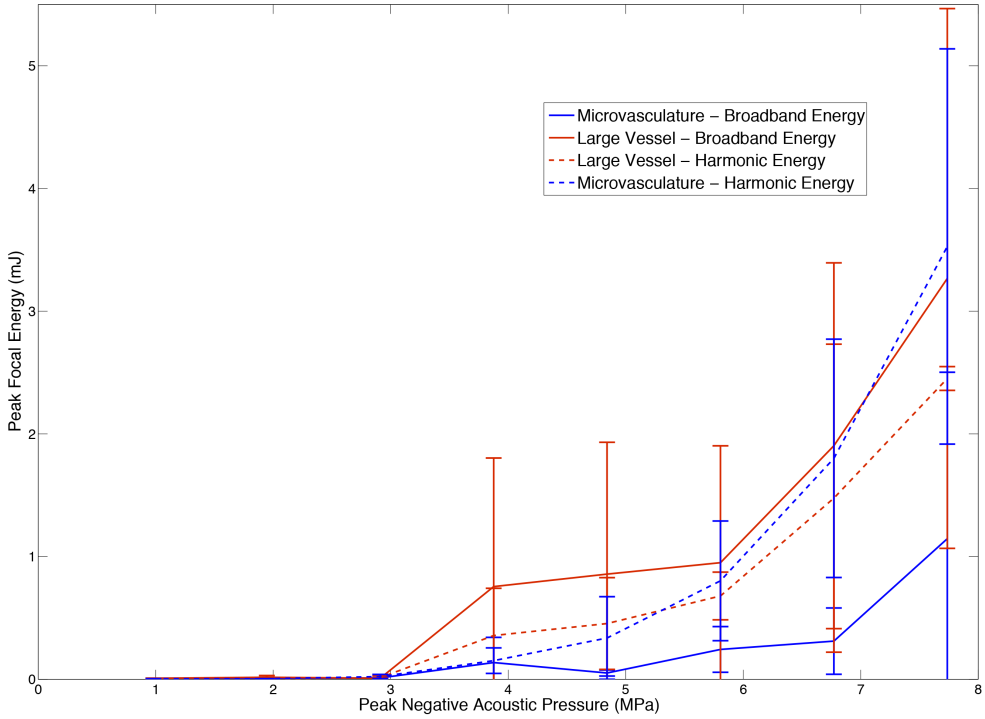


Figure 4.5 *– Peak focal broadband energy (solid lines), representing inertial cavitation, and harmonic energy (dashed lines) in microvascular areas (blue) and regions adjacent to a large (≥ 5 mm) blood vessel (red) plotted as a function of peak rarefaction pressure (MPa) for 1 s CW HIFU exposures at 1.06 MHz. The increase in broadband emissions between 3 and 4 MPa* $_{Pk-}$ *in both tissue regions is indicative of the onset of inertial cavitation activity above this acoustic pressure, thus representing the cavitation threshold.*

At each location, the cavitation threshold, defined as the lowest peak focal rarefaction pressure at which inertial cavitation was observed, was estimated from the passive

acoustic maps of emissions during HIFU therapy. At 1.06 MHz, the cavitation threshold both in areas adjacent to large blood vessels and in microperfused areas, away from major vasculature, appears to lie approximately between 3 and 4 MPa $_{Pk-}$. The rise in broadband emissions between 3 and 4 MPa $_{pk-}$, with a corresponding increase in harmonic emissions on a similar scale to the calculated broadband emissions, is suggestive of the presence of inertial cavitation. The emissions in the harmonic frequency range are likely to be an artifact of the digital comb filter, with broadband emissions within the 0.3 MHz bandwidth around the driving frequency and each multiple of the harmonic being incorrectly assigned as harmonic emissions.

4.4.3 Cavitation Energy at 1.06 MHz

In order to assess the amount of energy generated through inertial cavitation activity, the cumulative broadband energy detected during HIFU exposures within the perfused liver was calculated. This was done for exposures performed in areas directly adjacent to a large blood vessel and in microvascular regions, > 1 cm away from a large vessel, both in the presence and absence of blood flow. These data are displayed below in *Figure 4.6*.

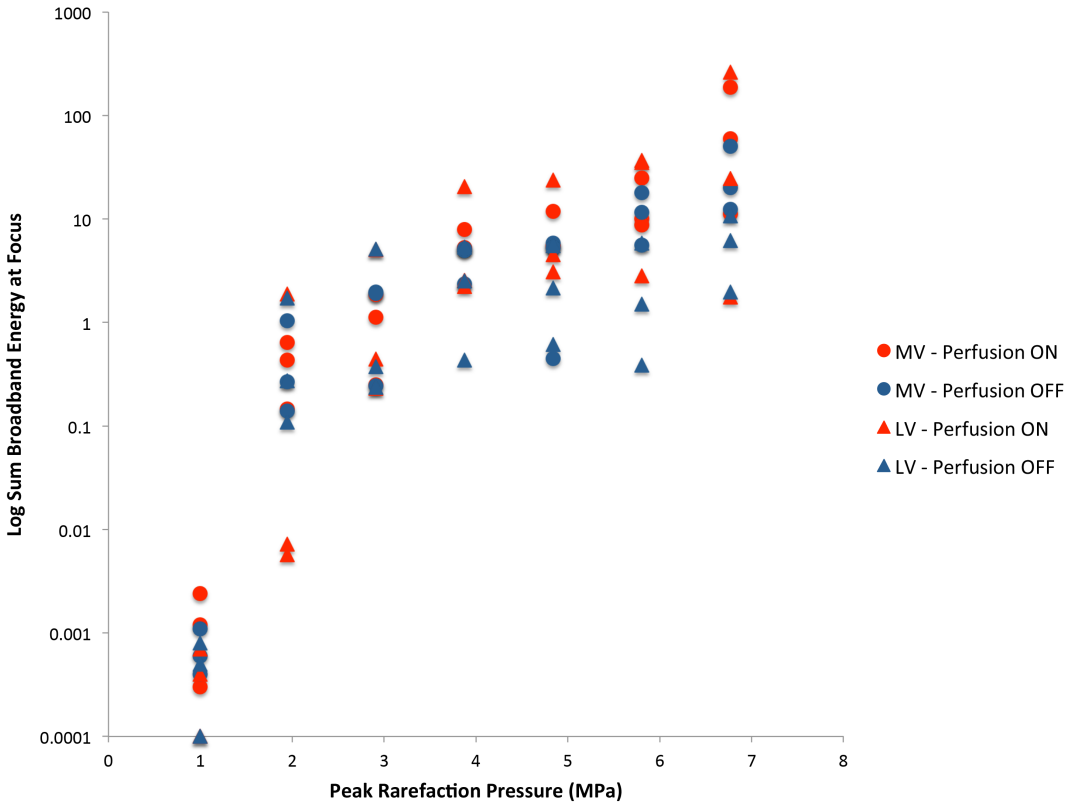


Figure 4.6 *– Sum of the broadband energy at the HIFU focus (logarithmic scale) over 1 s 1.06 MHz HIFU exposures as a function of peak rarefaction pressure in microvascular (MV) areas and tissue regions adjacent to a large (≥ 5 mm) blood vessel (LV), in the presence and absence of blood flow*

Although not statistically significant, the data displayed in *Figures 4.5* and *4.6* suggest that there could be higher levels of broadband emissions, hence greater levels of cavitation energy in areas adjacent to large vasculature compared to microvascular regions at 1.06 MHz (P = 0.12). However, the amount of cavitation occurring during each 1 s exposure at a given pressure was highly variable, indicated by the wide standard deviation displayed in the error bars at each data point in *Figure 4.5*. The presence of significant levels of inertial cavitation at peak rarefaction pressures of 3 – 4 MPa means that above this acoustic pressure threshold, tissue heating could be as a result of a combination of

non-linear heating and cavitation-enhanced heating. This is described further in Chapter 5.

4.4.4 Cavitation Threshold at 3.18 MHz

Similar to the studies performed at 1.06 MHz, the cavitation threshold at 3.18 MHz, was estimated for both microvascular areas (> 1 cm away from a large blood vessel) and tissue regions directly adjacent to a large (≥ 5 mm) blood vessel, in the presence of blood flow.

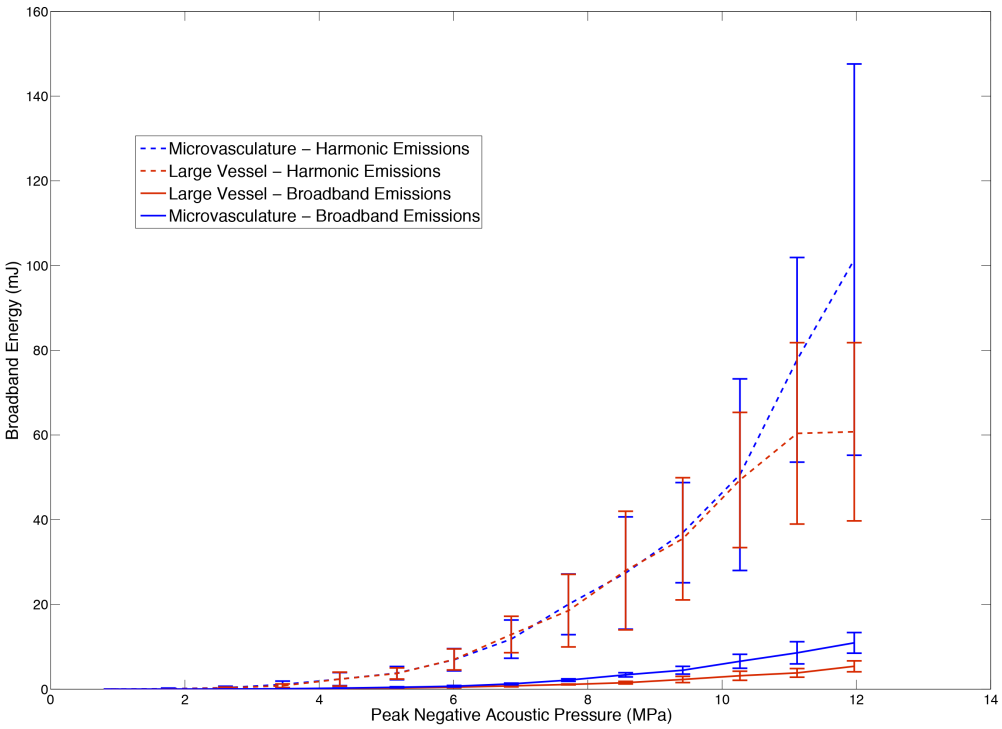


Figure 4.7 - *Peak focal broadband energy (solid lines), representing inertial cavitation, and harmonic energy (dashed lines) in microvascular areas (blue) and regions adjacent to a large (≥ 5 mm) blood vessel (red), plotted as a function of peak rarefaction pressure (MPa), for 1 s CW HIFU exposures at 3.18 MHz.*

In *Figure 4.7*, a ten-fold increase in harmonic emissions compared to broadband emissions with increasing peak rarefaction pressure was observed. The increase in harmonic emissions is due to increased tissue scattering and non-linearity. The small increase in broadband emissions with increasing peak rarefaction pressure is most likely artifact from the digital comb filter processing, with spillover of the harmonic signal outwith of the 0.3 MHz frequency range around each multiple of the harmonic. This indicates that at 3.18 MHz, no significant inertial cavitation activity occurred at the peak rarefaction focal pressures tested, demonstrating that the cavitation threshold had not been reached by the maximum peak rarefaction focal pressure used of 12 MPa $_{pk-}$. Thus, any tissue heating 3.18 MHz at peak rarefaction pressures up to 12 MPa should be as a result of non-linear heating predominantly, rather than through inertial cavitation-enhanced heating.

4.5 Discussion

The purpose of this current work was to determine the cavitation threshold within a physiologically perfused liver model and to elucidate the effects of blood flow and vascular anatomy on cavitation in order to estimate the potential contribution of cavitation on heating and thermal lesion formation in subsequent HIFU ablation studies, presented in Chapters 5 and 6. Real time observations of the effects of blood flow on HIFU-induced cavitation within a physiologically relevant, isolated, perfused porcine liver model are made for the first time. A unique aspect of this model is the ability to turn the pump on and off, thus enabling the assessment of the effect of perfusion in tissue regions proximal or distal to major blood vessels. Previous experimental models of isolated liver perfusion used to investigate HIFU therapy have typically either been hypothermic or at room temperature, using an acellular perfusion solution, limiting the physiological applicability of resulting observations in terms of cavitational tissue characteristics (Bu et al., 2013, Izamis et al., 2014). However, studies investigating RF or MW ablation using ex vivo perfused bovine or porcine liver models have previously demonstrated a heat sink effect, suggesting that the ex vivo isolated, perfused liver is a suitable model for investigating the effects of large vessel perfusion in HIFU therapy (Bitsch et al., 2006, Dodd et al., 2013, Welp et al., 2006).

Until recently, the effects of physiological tissue perfusion on HIFU-induced cavitation have been little assessed. Furthermore, the sources of endogenous cavitation nuclei and the inhibitory or up-regulating factors affecting these remain unknown. In this study, a novel passive acoustic mapping technique (Gyongy and Coussios, 2010) was used to

localise and quantify broadband emissions, providing real time, temporo-spatial information assessing acoustic cavitation.

4.5.1 Cavitation Threshold

From the studies presented in this chapter, it appears as if the inertial cavitation threshold, the lowest acoustic pressure at which broadband emissions are observed, lies between 3 and 4 MPa $_{Pk-}$ at 1.06 MHz within the perfused liver model, irrespective of whether the target tissue lies adjacent to a large (≥ 5 mm) blood vessel, or within microvascular-perfused areas of the hepatic parenchyma. At 3.18 MHz, the cavitation threshold was not reached by the maximum peak rarefactional focal pressure used of 12 MPa and it therefore lies in excess of this value. The cavitation threshold of 3 to 4 MPa $_{Pk-}$ at 1.06 MHz concurs with the findings by Labouret *et al.* from studies within the same perfused liver model (unpublished), but using a short HIFU pulses (25 cycles) and a passive cavitation detector (PCD) to observe the presence of any broadband activity, representing inertial cavitation. This cavitation threshold level is also similar to that recently reported in murine pancreatic tumours *in vivo* by Li *et al.* (2014), although different definitions of cavitation threshold were used in both the studies performed by Labouret *et al.* and Li *et al.* compared to this work. However, the cavitation threshold appears to be lower in the perfused liver model than that of non-perfused fresh cadaveric liver tissue, with Li *et al.* (2014) reporting a cavitation threshold of 8 – 9 MPa $_{Pk-}$ in *ex vivo* bovine liver.

The studies by Li *et al.* and Labouret *et al.* used a similar method of detecting and assessing the presence of broadband emissions, through a passive cavitation detector and

oscilloscope. As can be seen in *Figure 3.8* below, in the 3 perfused liver studies performed by Labouret *et al.*, a cavitation probability of close to 1, i.e. the probability of observing broadband activity during a 25 cycle HIFU exposure out of 10 repeats, was not reached until around 3 – 4 MPa $_{Pk-}$, which is an identical range to that identified in this study, by quantification of broadband emissions through passive acoustic mapping.

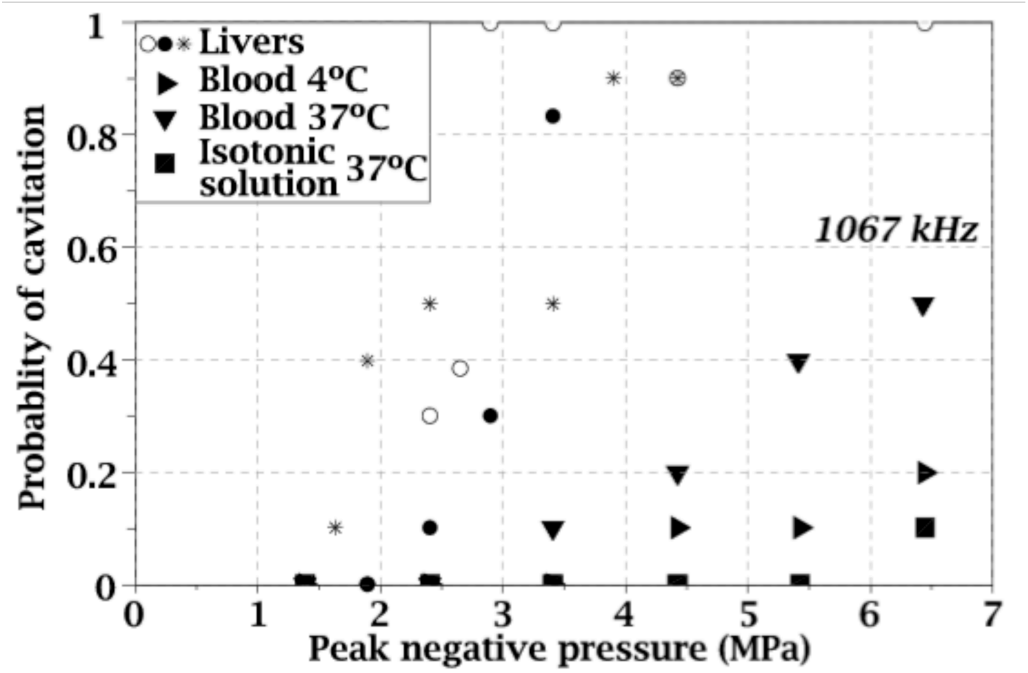


Figure 4.8 – *Probability of cavitation plotted as a function of peak rarefaction pressure for studies conducted in 3 normothermically-perfused livers, static ex vivo blood at 4 ˚C and 37 ˚C and 0.9% sodium chloride solution warmed to 37 ˚C. It is not until around 3 – 4 MPa $_{Pk-}$ until the probability of cavitation in the perfused liver model nears 1 (from Labouret et al). However, the probabilities of cavitation in static blood and 0.9% sodium chloride are significantly lower than those observed in the perfused livers, suggesting an important blood-tissue interaction.*

The peak cavitation energy released across the whole HIFU exposure duration was calculated from the PAMs. It appears that, although the cavitation threshold is the same, there may be a difference in the peak level of cavitation energy emissions observed between large vessel and microperfused regions, although not statistically significant in this study (*Figure 4.5*). If this apparent difference does exist, the reasons for it are unclear, although it could be that the vascular endothelium either provides a surface that facilitates nucleation or, alternatively may be the source of cavitation nuclei through the release of endogenous compounds such as nitric oxide.

4.5.2 The Effects of Blood Flow on Cavitation

From the work presented in this chapter, the presence of active blood flow does not appear to affect the cavitation threshold significantly, as initial broadband activity appeared within the same acoustic pressure range when the liver perfusion device was switched off and the inflow / outflow tracts clamped as when the studies were performed under full physiological blood flow conditions (*Figure 4.6*). Although not statistically significant, there appears to be a trend towards lower total levels of cavitation energy in the absence compared to the presence of perfusion, especially at the higher end of the acoustic pressure range that was tested.

No published studies have investigated cavitation activity under physiological perfusion conditions compared to no-flow conditions in a consistent tissue model. Labouret *et al.* (unpublished) conducted studies to determine whether perfusion affects cavitation within the perfused liver, or whether static blood within the organ would produce the same levels of cavitation activity. In their experiment, cavitation nuclei were destroyed with a

series of rapid short HIFU pulses until no further cavitation events were observed (no broadband activity on the oscilloscope PCD output). With continuing normal blood flow, further cavitation events were observed after another 10 seconds, suggesting replenishment of cavitation nuclei. In the absence of perfusion, no further cavitation events were witnessed during the period of no blood flow (40 seconds) and for a further 10 seconds after normal perfusion was restored (*Figure 4.9*, below).

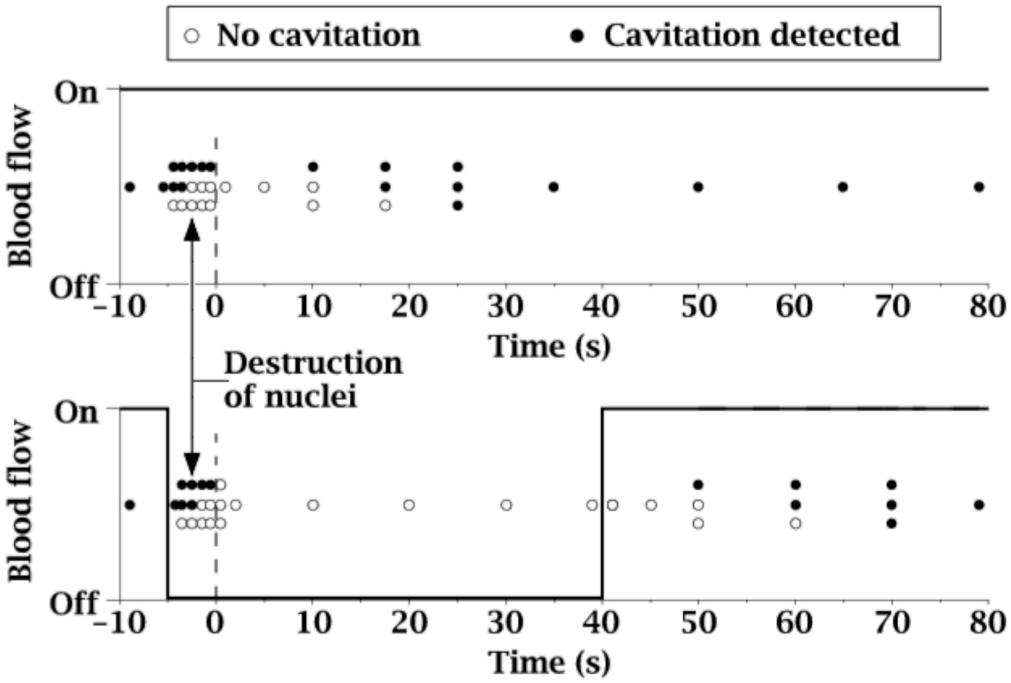


Figure 4.9 – *Diagram displaying cavitation events determined by observation of broadband activity as detected by a PCD during short pulse (25 cycle) 1.067 MHz HIFU exposures in a perfused porcine liver model under normal physiological blood flow conditions (top) and with brief cessation of perfusion (bottom). Cavitation nuclei were destroyed with a series of rapid short HIFU pulses until no further cavitation events were observed (no broadband activity on the oscilloscope PCD output). With normal blood flow, further cavitation events were observed after a further 10 seconds, suggesting replenishment of cavitation nuclei. In the*

absence of perfusion, no further cavitation events were witnessed during the period of no blood flow (40 seconds) and for a further 10 seconds after normal perfusion was restored. From Labouret et al. (unpublished).

It is therefore likely that the cavitation threshold and levels of cavitation energy within the perfused liver rely on a blood-tissue interaction and also active blood flow to continually replenish cavitation nuclei. In the context of the results presented in this chapter, our observations approximately fit with those of Labouret *et al.* In the studies performed under no flow condition, the cavitation threshold remained at 3 – 4 MPa $_{Pk-}$, which would correlate with the period of cavitation nuclei destruction in Labouret *et al.*'s studies. However, given that perfusion was not restored in between HIFU exposures in the increasing acoustic pressure ramp, it could be expected that lower levels of cavitation activity would be observed during subsequent HIFU exposures at higher acoustic pressures as cavitation nuclei were depleted, but not replenished. An emerging trend, although not statistically significant due to small numbers, can be seen in *Figure 4.6*, particularly in areas adjacent to a large vessel, whereby the initial increase in cavitation energy can be seen at around 3 MPa $_{Pk-}$, but in the absence of perfusion, the cavitation energy levels remain relatively low at higher acoustic pressures compared with the levels observed in the presence of perfusion, possibly due to a lack of replenishment of cavitation nuclei. Given that the exposure duration for the HIFU exposures used in this study were short (1 s), it would be interesting to see if this trend became more apparent and significant with longer exposure durations, allowing more time for nuclei to be depleted further and not replenished in the absence of perfusion.

4.5.3 Sources of Cavitation Nuclei

Little is known about the sources of endogenous cavitation nuclei and the effect of blood flow on cavitation. One limitation of the studies performed using the isolated, perfused liver model is that there is potential to introduce sources of cavitation nuclei during organ procurement, cold storage and connection to the ECLPD, particularly given that the exact sources of cavitation nuclei are not known. Therefore all results presented in this chapter need repeating *in vivo* for confirmation the *ex vivo* perfused liver model accurately reflects the *in vivo* situation and that the cavitation threshold and levels of cavitation activity remain the same.

One advantageous feature of the isolated, perfused liver model that was used in the studies described in this chapter was that it permitted either physiological blood flow through the liver or complete cessation of blood flow. In order to determine whether constituents of the blood alone was responsible for the cavitation threshold observed within the *ex vivo* Labouret *et al.* performed studies to determine the cavitation threshold in static, *ex vivo* blood compared to a control solution of 0.9% sodium chloride solution. They observed that the probability of cavitation of blood at 37 ˚C was significantly lower than that of 0.9% sodium chloride at 37 ˚C and blood at 4 ˚C (*Figure 4.8*). However, the probabilities of cavitation and the cavitation thresholds within all three static media were significantly less that those observed in the perfused liver model, suggesting an important tissue-blood interaction in cavitation dynamics and in the supply of cavitation nuclei.

The Effect of Varying Oxygen and Carbon Dioxide Partial Pressures on Cavitation

One additional advantageous feature of the ECLPD was that it allowed various parameters to be altered, including P_aO_2, P_aCO_2, blood temperature and hepatic arterial, portal venous and IVC pressures. In studies performed by S. Labouret *et al.*, using the identical isolated, perfused liver model set up as described in this chapter, we conducted experiments to investigate the effects of blood perfusion, temperature and varying P_aO_2 / P_aCO_2 on cavitation dynamics.

In a further series of studies, the partial pressures of oxygen and carbon dioxide in the blood perfusing the porcine livers were altered in order to investigate the effects of P_aO_2 and P_aCO_2 on cavitation dynamics (*Figure 4.10*). The ECLPD maintains a physiologically normal P_aO_2 of 12 to 16 kPa and P_aCO_2 of 3.5 to 6 kPa, however these could be adjusted by varying the ratio of oxygen to air supplying the ECMO oxygenator. Hyperoxic (P_aO_2 24.6 kPa), hypoxic (P_aO_2 4.8 kPa), hypercapnic (P_aCO_2 11.9 kPa) and hypocapnic (P_aCO_2 2.3 kPa) conditions were all induced and the probabilities of cavitation measured under these conditions, as described previously.

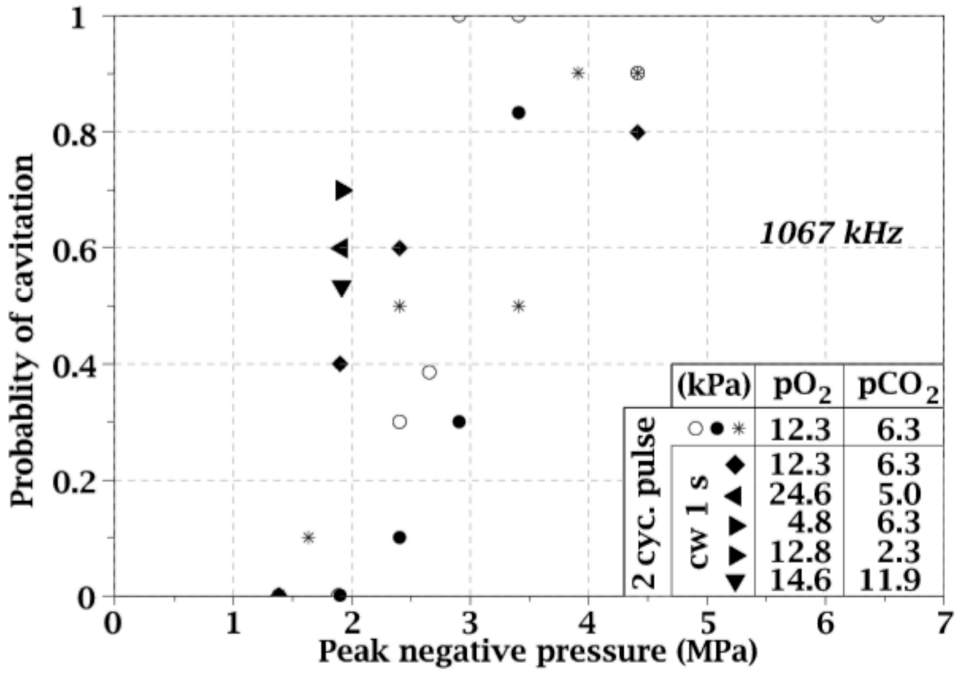


Figure 4.10 – *Probability of cavitation during 1s CW HIFU exposures plotted as a function of peak rarefaction pressure for studies performed under normoxic, normocapnic (diamonds), hyperoxic (left-pointing triangle), hypoxic (right-pointing triangle), hypocapnic (right-pointing triangle) and hypercapnic conditions (downward-pointing triangle). From Labouret et al - unpublished.*

Although only one set of measurements were performed under each condition, meaning no statistical inferences can be made, there does not appear to be a major difference in the probability of cavitation at the single acoustic pressure of 1.9 MPa $_{Pk-}$ tested, all appearing in the range of 0.4 – 0.7. Therefore, the P_aO_2 and P_aCO_2 do not seem to impart a large effect on cavitation, although further, more rigorous studies need to be performed to confirm this and whether dissolved / Hb-bound oxygen or dissolved CO_2 are significant sources of cavitation nuclei *in vivo*. It is possible that another molecule, or series of molecules are the predominant nuclei for cavitation *in vivo*. Further studies, for

example investigating the role of nitric oxide in HIFU-induced cavitation, need to be performed in order to elucidate the source of cavitation nuclei *in vivo* further.

4.6 Conclusions

The cavitation threshold in *ex* vivo functional, perfused porcine liver tissue lies between 3 – 4 MPa $_{Pk-}$ at 1.06 MHz and above 12 MPa $_{Pk-}$ at 3.18 MHz. These values are lower than the reported cavitation threshold in unperfused *ex vivo* liver tissue, but similar to the value recently reported *in vivo* by Li *et al.* (2014) in a murine pancreatic cancer model. The proximity of large vasculature does not appear to affect the cavitation threshold, with broadband emissions appearing at the same acoustic pressure range in tissue adjacent to large (≥ 5 mm) blood vessels and in microperfused regions.

CHAPTER 5

THE EFFECTS OF PERFUSION ON HIFU-INDUCED HEATING

Although HIFU is currently in clinical use for the thermal ablation of solid organ tumours, the effects of blood flow and physiological perfusion on tissue heating have been little investigated. One of the main limitations of radiofrequency ablation is the heat sink effect, whereby heat advection from large blood vessels adjacent to, or in the treatment volume can significantly reduce focal temperatures and can lead to incomplete tumour ablation and treatment failure. The aim of the work presented in this chapter is to identify the effects of large vessel and microvascular perfusion on HIFU-induced heating.

5.1 Introduction

One of the major factors limiting the efficacy of thermal ablative therapies, particularly radiofrequency ablation, is the "heat sink effect", caused by heat advection away from the thermal source by blood flowing through large vessels. This mechanism can limit the peak temperature attained within areas of the ablative focal tissue volume, potentially leading to incomplete treatment. Radiofrequency ablation is particularly susceptible to the heat sink effect and it has previously been demonstrated that viable tumour cells can potentially remain untreated when a blood vessel ≥ 4 mm in diameter lies adjacent or runs through a treatment volume.

Liver tissue is heterogeneous in nature, with a number of vascular and biliary structures running through the liver parenchyma, with a range of diameters and flow rates. Therefore, the impact of the vascular anatomy on the heating of a given treatment volume may vary significantly depending on the anatomical location of the treatment target within the liver.

A large number of studies have investigated the effects of large and small vessel perfusion on radiofrequency (RFA) and microwave ablation (MWA) of liver tumours (Lu et al., 2002, Yu et al., 2008, Patterson et al., 1998). These have demonstrated that vessels over 4 mm in diameter impart a significant heat sink effect on RFA, increasing treatment time, total energy required, whilst decreasing focal peak temperatures and this can lead to incomplete ablation and treatment failure (Lu et al., 2003, Lu et al., 2005, Mulier et al., 2005). The heat sink effect on MWA therapy is lower than RFA, but still decreases heating rates, lesion size, increasing treatment time and total energy, although MWA treatment success rates of perivascular tumours is significantly higher than RFA.

Although the effects of physiological tissue perfusion on HIFU ablation has been investigated mathematically using a number of different models, it has been studied little experimentally, particularly in tissue models. Therefore, the aims of the studies performed in this chapter were to assess the effect of large vessel blood flow and microvascular perfusion on heating during HIFU therapy in functioning hepatic tissue.

5.2 Study Aims

The aim of the studies discussed in this chapter was to elucidate the effects of physiological perfusion on HIFU-induced heating in liver tissue. The specific objectives of the work were:

1) To assess whether the presence of a large (≥ 5 mm) blood vessel near to a HIFU treatment focus significantly affects the peak temperature rise attained during HIFU therapy – the "heat sink effect"
2) To determine whether the presence or absence of blood flow affects the peak temperature rise achieved during HIFU therapy, both in tissue adjacent and far away (> 1cm) from a large blood vessel.
3) To determine the acoustic pressure required to attain clinically relevant ablative temperature rises in perfused liver tissue at 1.06 MHz and 3.18 MHz
4) To assess the impact of cavitation on heating during HIFU therapy in perfused liver tissue.

5.3 Materials and Methods

5.3.1 Perfused Liver Model

Porcine livers were surgically explanted, cold preserved, transported and connected to the extracorporeal normothermic liver perfusion device (ECLPD) according to a standard technique described in Chapter 2, Section 2.3. In total, 8 separate perfused liver studies were performed for the experiments described in this chapter.

Following reperfusion on the normothermic liver perfusion device, the liver was left for approximately 60 minutes to allow the organ to recover from the period of cold ischaemia. During this time, early evidence of resumption of hepatic function was observed, with bile appearing in the biliary cannula. At the end of this period, the stainless steel bowl was removed from under the liver and the liver was placed in an impermeable PVC bag (Vi-Drape; Medical Concepts Development, USA) filled with approximately 3L of degassed isotonic colloid solution (Gelofusine®; B Braun, UK) warmed to 37 ˚C. A vacuum pump connected to an airtight flask was used to degas the colloid solution prior to use. The PVC bag containing the liver was suspended in a silicone sling over a tank of degassed water, at 38 ˚C. The water bath was continuously degased and the temperature maintained at 38 ˚C through a centrifugal pump, inline heater and membrane contactor connected to a vacuum pump (Liqui-Cel®; Membrana, USA).

5.3.2 HIFU Setup

A custom-manufactured, spherically focused HIFU transducer with a centre frequency of 1.06 MHz (H102D-22; Sonic Concepts Inc., WA, USA), driven at its fundamental frequency or at the third harmonic (3.18 MHz), was used to produce therapeutic ultrasound pulses. The HIFU set up for the studies performed in this chapter is described in detail in Chapter 2, Section 2.4 and is displayed below in *Figure 5.1*. The 128-element 5-10 MHz diagnostic linear array (model L10-5; Zonare Medical Systems, CA, USA) was used for both conventional diagnostic B-mode ultrasound guidance and for passive cavitation monitoring. All studies were performed with the assistance of Dr. Daniel Chung (radiological assessment and thermocouple placement), Dr. Eleonora Mylonopoulou, Dr. Carl Jensen and Dr. James Choi (HIFU set up, programming, data post-processing).

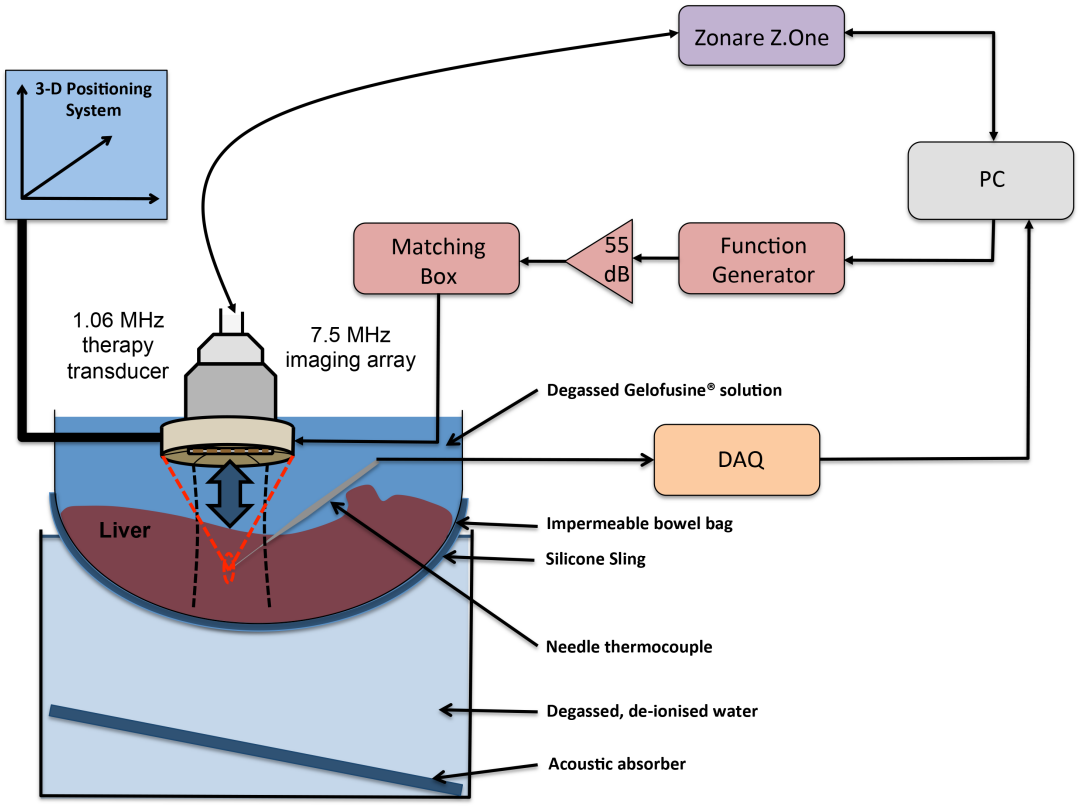


Figure 5.1 - *Schematic diagram of the HIFU experimental set up used for thermal studies. The perfused liver, attached to the ECLPD, was immersed in an acoustically-transparent, impermeable surgical isolation bag filled with degassed colloid solution at 37 ˚C. The bag was suspended in a silicone sling over a degassed, de-ionised 37 ˚C water bath. The 1.06 MHz HIFU transducer with a coaxially aligned Zonare L10-5 linear imaging array was mounted on a manual 3-D positioning system. The HIFU generation loop is shown in red with a PC-controlled function generator, 55 dB amplifier and a 50 Ω matching network, driving the HIFU transducer. The PC was also used to record thermometry data from the 200 μm thermocouple, via a data acquisition box.*

The HIFU transducer was calibrated in free-field conditions in degassed, deionsed water using a 400 μm needle hydrophone (SN 1056; Onda Corporation, CA, USA) at both the fundamental frequency and at the third harmonic. The diagnostic ultrasound engine attached to the linear array (Z.One®; Zonare Medical Systems, CA, USA) could acquire conventional B-mode images or could be operated in passive mode simultaneously during HIFU exposure, allowing access to pre-beamformed in-phase and quadrature (I/Q) data from 64 individual channels (4.64 to 9.64 MHz).

Diagnostic B-mode ultrasound was used to image the liver in order to identify major arterial, portal venous, venous and biliary structures within the liver parenchyma, using both the coaxially mounted L10-5 and a handheld L14-5w linear array (Zonare, USA). Two distinct types of tissue region were targeted (see *Figure 4.2*). Firstly, hepatic parenchyma directly adjacent to a large (≥ 5 mm) vessel and, secondly, areas away (> 1 cm) from a large vessel were selected using B-mode ultrasound. Vessel diameters were

measured using B-mode ultrasound images and flow velocities within large vessels were quantified using colour Doppler. In order to record real-time thermometry data during HIFU therapy, a 200 μm fine needle thermocouple (HYP-0; Omega Engineering, CT, USA) was subsequently inserted into these tissue regions under real-time B-mode ultrasound guidance (assistance from Dr. D. Chung). In large vessel regions, the tip of the thermocouple was placed so that it lay in tissue directly adjacent to the vascular wall, as it is known that this is the tissue most susceptible to the effects of heat advection due to large vessel blood flow. Given that the junction, the most thermosensitive part of the needle thermocouple, lies approximately 1-2 mm back from the tip, it was estimated that the thermocouple focus lay within 2 mm of the large vessels.

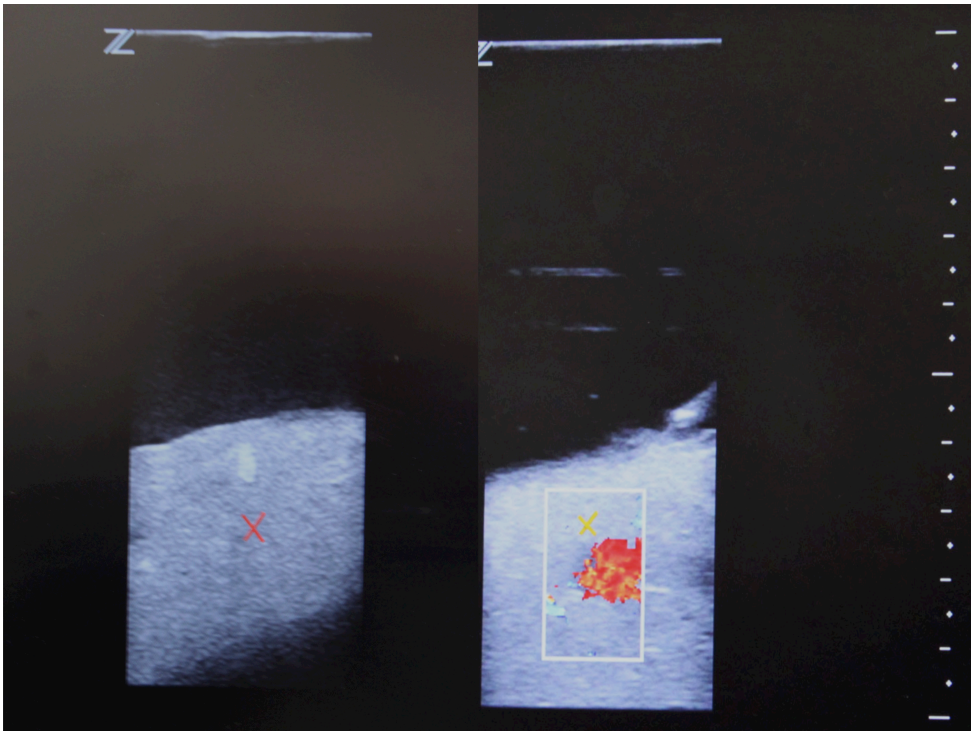


Figure 5.2 *– B-mode ultrasonography showing a microvascular area (L) and with colour Doppler (R), demonstrating a large (5 mm) portal venous branch, which was subsequently targeted for large vessel thermometry studies.*

Alignment of the HIFU focus relative to the thermocouple was performed using a previously described technique to minimize experimental error (Dasgupta et al., 2011). Following insertion of the needle thermocouple into the target tissue under B-mode ultrasonographic guidance, thermocouple alignment was achieved by driving the HIFU transducer at 1.3 MPa $_{Pk-}$ at 1.06 MHz, or at 1.5 MPa $_{Pk-}$ at 3.18 MHz, for 1 s every 5 s. These acoustic pressures were selected as they induced a temperature rise of approximately 3-5 ˚C in the target tissue, well below that required to cause tissue ablation, and were also below the cavitation threshold at both frequencies (see Chapter 4). This therefore allowed the HIFU focus to be accurately identified using thermometry readings, whilst minimising the thermal and cavitation effects of HIFU on the target tissue, affecting subsequent experiments. Using the manual positioning system, the co-ordinates of the HIFU focus were adjusted until the location with the maximum temperature rise had been identified. It was assumed that these co-ordinates represented the point where the thus HIFU focus was maximally aligned with the thermocouple junction.

Preliminary Studies

Preliminary studies were performed in order to determine the optimal set up, alignment protocol and HIFU exposure parameters for subsequent thermal response studies. Five perfused porcine livers were used for these preliminary experiments. The HIFU parameters used are shown below in *Table 5.1*.

Frequency	1.06 MHz
Exposure duration	6 s , 1 s
Acoustic pressure (MPa)	3.7 – 14.2
Duty cycle	100%

Table 5.1 *– HIFU exposure parameters for preliminary experiments*

Initially, an exposure duration of 6 s was used, although this was later reduced to 1 s in order to reduce the thermal dose delivered to the focal tissue volume in an attempt to minimize any tissue changes as a number of consecutive measurements were made at each thermocouple location.

5.3.3 Exposure Protocol

In order to assess the effects of perfusion on HIFU-induced heating in both the presence and absence of cavitation, studies were performed at two frequencies: 1.06 MHz and 3.18 MHz. Since cavitation is frequency-dependent, the cavitation threshold is higher at 3.18 MHz than at 1.06 MHz, as demonstrated in Chapter 4. Therefore, acoustic pressures were selected to include values below and above the cavitation threshold at 1.06 MHz and only values below the cavitation threshold at 3.18 MHz. The following HIFU parameters were selected for the thermal response studies as a result of the data obtained from the preliminary experiments:

Frequency	1.06 MHz
Exposure duration	1 s
Peak rarefactional pressures (MPa $_{Pk-}$)	1.88, 2.80, 3.73, 4.65, 5.58
Duty cycle	100%

Table 5.2 *– HIFU exposure parameters for experiments performed at 1.06 MHz*

Frequency	3.18 MHz
Exposure duration	1 s
Peak rarefactional pressures (MPa $_{Pk-}$)	0.90, 1.75, 2.60, 3.46, 4.31, 5.16, 6.86
Duty cycle	100%

Table 5.3 *– HIFU exposure parameters for experiments performed at 3.18 MHz*

Following alignment of the HIFU and thermocouple foci, a series of experiments were performed at each thermocouple location. Experiments were only performed at either 1.06 MHz or 3.18 MHz at a single thermocouple location. In the first experiment, temperature at the HIFU focus was measured during HIFU therapy at increasing peak rarefactional pressures in the presence of blood flow, with the liver perfusion device switched on. The data acquisition system was programmed to commence recording thermocouple data 0.25 s prior to the start of each 1 s HIFU exposure. Focal temperature was monitored for a total of 10 s. A 45 s time interval was left between each 1 s HIFU exposure to allow the focal tissue to cool to its starting temperature prior to commencing the next set of measurements. In total, 5 sets of thermometry

measurements were made at 5 different acoustic pressures at 1.06 MHz in the presence of perfusion at 1.06 MHz and 7 sets of measurements at 7 different acoustic pressures were made at 3.18 MHz. Following each pressure ramp, the thermocouple was retargeted to ensure that the position of the thermocouple had not changed relative to the HIFU focus.

The second experiment at each thermocouple location investigated thermal response during HIFU therapy in the absence of blood flow. The same parameters and protocol applied in the experiment investigating thermal response in the presence of perfusion were used. Prior to commencing the pressure ramp, the liver perfusion device was switched off and the inflow / outflow tracts supplying blood to and draining blood from the liver were clamped with Robinson clamps attached to the arterial, portal venous and IVC cannulae. This process completely stopped blood flow to the liver temporarily, whilst also ensuring that the liver volume remained constant. Following cessation of perfusion, the HIFU focus relative to the thermocouple was checked to ensure accurate alignment and then the same pressure ramp was performed as in the experiment performed in the presence of blood flow. Similarly, a 45 s gap was left in between HIFU exposures to allow the tissue to cool to the baseline temperature before performing the next measurement. Therefore, 5 paired sets of data (perfusion on and perfusion off) for each acoustic pressure tested at 1.06 MHz, or 7 paired sets of data for experiments at 3.18 MHz, were obtained for each thermocouple location.

Throughout each HIFU exposure, passive acoustic data was captured and recorded in order to enable monitoring and quantification of cavitation activity (see Chapter 2,

Section 2.5.2). These data were post-processed and passive acoustic maps spatiotemporally mapping broadband and harmonic emissions throughout each HIFU exposure were constructed, allowing thermal response to be correlated with cavitation energy.

5.4 Results – Real Time Heating During HIFU Therapy

In this section, real-time thermometry data acquired during HIFU therapy are presented, demonstrating the effect of physiological large vessel blood flow and microvascular perfusion on ultrasound-induced heating. In total, 8 isolated, perfused porcine livers were used for the studies described in this chapter.

As described above, in these studies two distinct regions of tissue within the porcine liver were targeted in order to assess the effects of both large vessel blood flow and microvascular perfusion on HIFU-induced heating. Areas of hepatic parenchyma directly adjacent to a large (≥ 5 mm) vessel areas away (> 1 cm) from a large vessel were selected in order to compare the effects of large vessel and microvascular perfusion on real time heating. Measurements were made at each location in the presence of perfusion and in the absence of perfusion, with the liver perfusion device stopped and the inflow/outflow tracts clamped.

4.4.1 Preliminary Studies to Determine Optimal Exposure Protocol

Preliminary experiments to determine the optimal exposure duration and acoustic pressures to achieve clinically relevant temperature rises in perfused liver tissue were conducted in three perfused liver models.

Initially, a 6-second exposure duration was used and the liver was sonicated with increasing acoustic pressures ranging from 3.7 to 14.7 MPa $_{PPK}$. Representative

thermometry curves for these studies are shown below in *Figure 4.3* and *b*. For thermal ablation, a temperature of approximately > 55 ˚C needs to be attained within the target tissue for > 1 s for coagulative necrosis to occur.

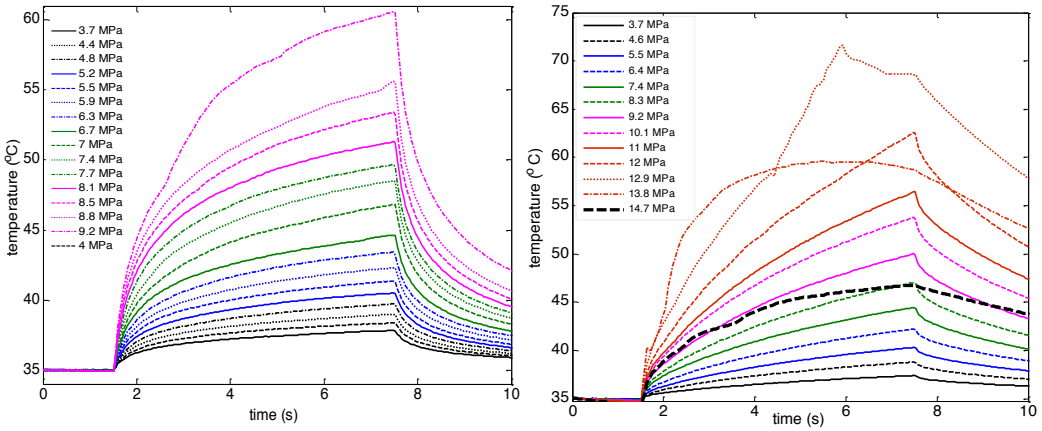


Figure 5.3 a and b *– Representative thermometry curves in a microvascular region (a) and in tissue adjacent to a large (> 5 mm) blood vessel (b) showing temperature changes during 6 s HIFU exposures at acoustic pressures ranging from 3.7 to 14.7 MPa* $_{PPk}$*. An acoustic pressure of 9.2 to 11 MPa induced a temperature of ≥55 ˚C in the target tissue.*

In Figure 5b, the peak temperature rises attained with acoustic pressures of 13.6 and 14.7 MPa is lower than expected and the thermometry curves are of a different shape to those at lower acoustic pressures. At the preceding acoustic pressure of 12.9 MPa $_{PPk}$*, a peak temperature in excess of 70 ˚C was reached and the temperature remained over 60 ˚C for more than 4 s. It is highly likely that this led to ablation in the target tissue, with changes to the tissue properties, including cell necrosis, thermal coagulation and microvascular thrombosis. Consequentially, subsequent measurements at this tissue location would have been affected by the changes to the tissue properties.*

An acoustic pressure of approximately 9.2 to 11 MPa $_{PPK}$ induced a temperature > 55 ˚C within the target liver tissue. However, when higher acoustic pressures beyond the threshold pressure at which thermal ablation would be expected to occur, thermometry data and B-mode diagnostic ultrasound images suggested that thermal damage had occurred within the target tissue had occurred. Therefore, data obtained from subsequent exposures after the thermal ablative temperature threshold had been attained were deemed to be unreliable, as the tissue properties had changed. An example of this can be seen in *Figure 5.3 b*, where the thermometry curves for the two highest acoustic pressures tested (13.6 and 14.7 MPa) are of a significantly different shape to those at other acoustic pressures with a lower peak temperature rise than expected. Therefore, in order to minimize the effect of previous HIFU exposures on subsequent thermometry and cavitation measurements, the exposure duration was decreased to 1 second in order to reduce the amount of tissue damage when a tissue volume was exposed to thermal rise above the ablative threshold.

5.4.2 Effects of Perfusion on Heating at 1.06 MHz

Following preliminary studies, the HIFU exposure parameters were refined to the following protocol for subsequent experiments:

Frequency	1.067 MHz
Exposure duration	1 s
Peak rarefactional pressures (MPa $_{Pk-}$)	1.88, 2.80, 3.73, 4.65, 5.58

Duty cycle	100%

Representative thermometry curves displaying temperature change at the HIFU focus during 1 s exposures over the range of pressure amplitudes at 1.06 MHz in areas adjacent to a large blood vessel and in microperfused areas, away from large vasculature, are shown in *Figure 5.4*. These plots represent measurements made at 2 thermocouple locations: one microperfused region (top row) and one adjacent to a large vessel (bottom row), in the presence of perfusion (left) and in the absence of blood flow (right). Few differences between the measurements made at each location in the presence or absence of perfusion are apparent. Additionally, the peak temperatures attained at a single pressure in the microperfused region are similar to those attained in a tissue area directly adjacent to a large blood vessel.

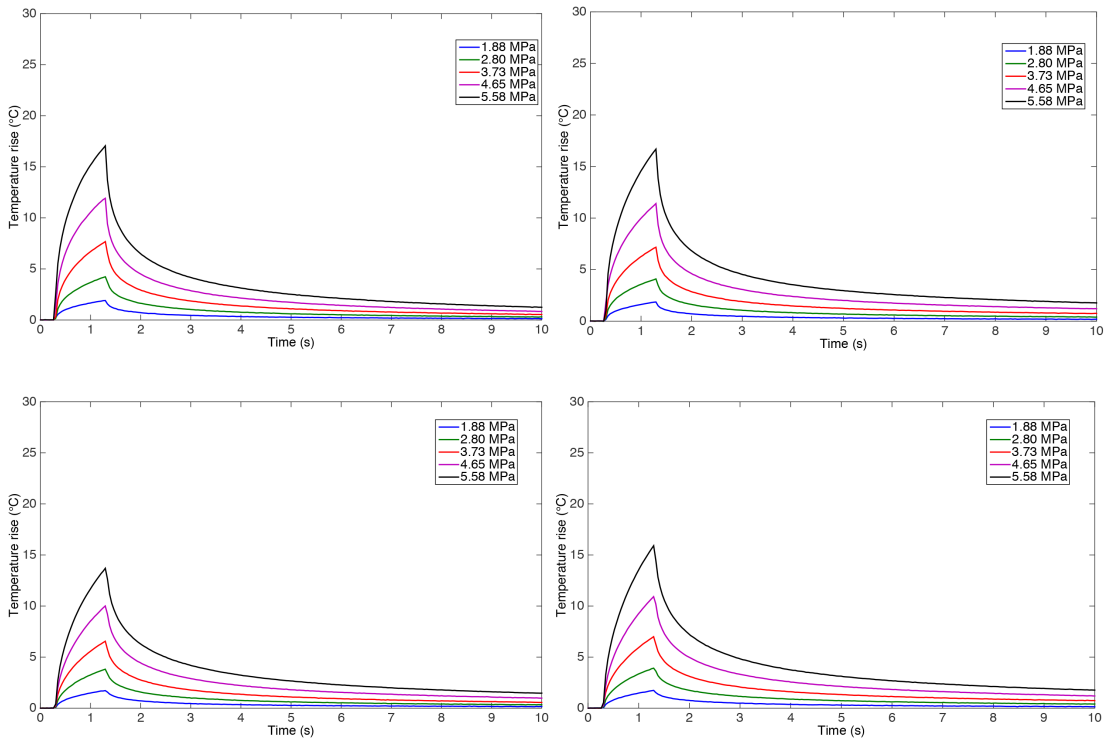


Figure 5.4. *- Representative temperature curves for 1 s 1.06 MHz HIFU exposures at range of peak rarefactional pressures (1.88 MPa $_{pk-}$ to 5.58 MPa $_{pk-}$). HIFU exposures were performed in microvascular areas (top row) and adjacent to a larger (> 5mm) blood vessel (bottom row), both in the presence of blood flow (left) and the absence of blood flow (right).*

In total, 4 paired sets of thermometry data were obtained in microvascular regions in the presence and absence of perfusion. Similarly, 4 paired thermometry data sets were obtained in tissue adjacent to a large (≥ 5 mm) blood vessel, again in the presence and absence of blood flow. The mean peak temperature rises attained during 1s HIFU insonations for each location type, peak rarefactional pressure and perfusion on/off status are shown in *Figures 5.5 a* and *b* below. For the large vessel regions, the large vessel diameter measured on B-mode ultrasound images was 6 mm (range 5 to 7 mm) and mean flow velocity, measured by Doppler, was 5.2 cm/s (4.0 to 6.4 cm/s).

At the lowest peak rarefactional pressure tested (1.88 MPa), a 1 s 1.06 MHz HIFU exposure induced approximately a 1.5 ˚C mean temperature rise at the focus in both microvascular (MV) and large vessel (LV) regions, both in the presence and absence of blood flow, with no significant difference between any of the 4 conditions (MV perfusion on, MV perfusion off, LV perfusion on, LV perfusion off). At higher peak rarefactional pressures, a 1 s HIFU exposure at 4.65 MPa induced a mean peak temperature rise of 11.9 ˚C in microvascular areas in the presence of blood flow compared to 12.6 ˚C in the absence of perfusion. In regions adjacent to a large blood vessel, a 10.6 ˚C mean temperature rise was induced in the presence of blood flow

compared to 11.8 ˚C with the perfusion device switched off. None of these differences were statistically significant (p = 0.38).

The largest differences in mean peak temperature rise were observed at the highest peak rarefactional pressure tested (5.58 MPa), where a 1 s HIFU exposure induced a temperature rise of 22.9 ˚C in MV areas in the presence of perfusion (range 11.7 – 46.0) compared to 20.7 ˚C in the absence of blood flow (range 16.7 – 19.1). For LV areas, the respective values were 15.7 ˚C (perfusion on, range 13.7 – 17.0), compared to 21.2 ˚C (perfusion off, range 15.3 – 32.3). However, compared to lower peak rarefactional pressures, there was a much greater range of peak temperature values at 5.58 MPa, as demonstrated by the wide standard error bars in *Figures 5.5 a* and *b*. The wide variations in peak temperature rise at 5.58 MPa are probably due to inertial cavitation activity. In Chapter 1, the relationship between linear heating in HIFU therapy and acoustic pressure is discussed. The relationship is non-linear, with heating increasing in a parabolic manner with rising acoustic pressure. In the presence of inertial cavitation heating rates are increased further still from those predicted by the linear model. This is discussed further in Section 5.5 below. Given that an approximate temperature rise of 20 ˚C is needed for coagulative necrosis of target tissue, these data demonstrate that temperatures in excess of the ablative threshold could be achieved both in microvascular areas and in tissue directly adjacent to a large (≥ 5 mm) blood vessel in the presence of normal hepatic blood flow using 1.06 MHz HIFU therapy at relatively modest, clinically relevant peak rarefactional pressures.

Figure 5.5 a

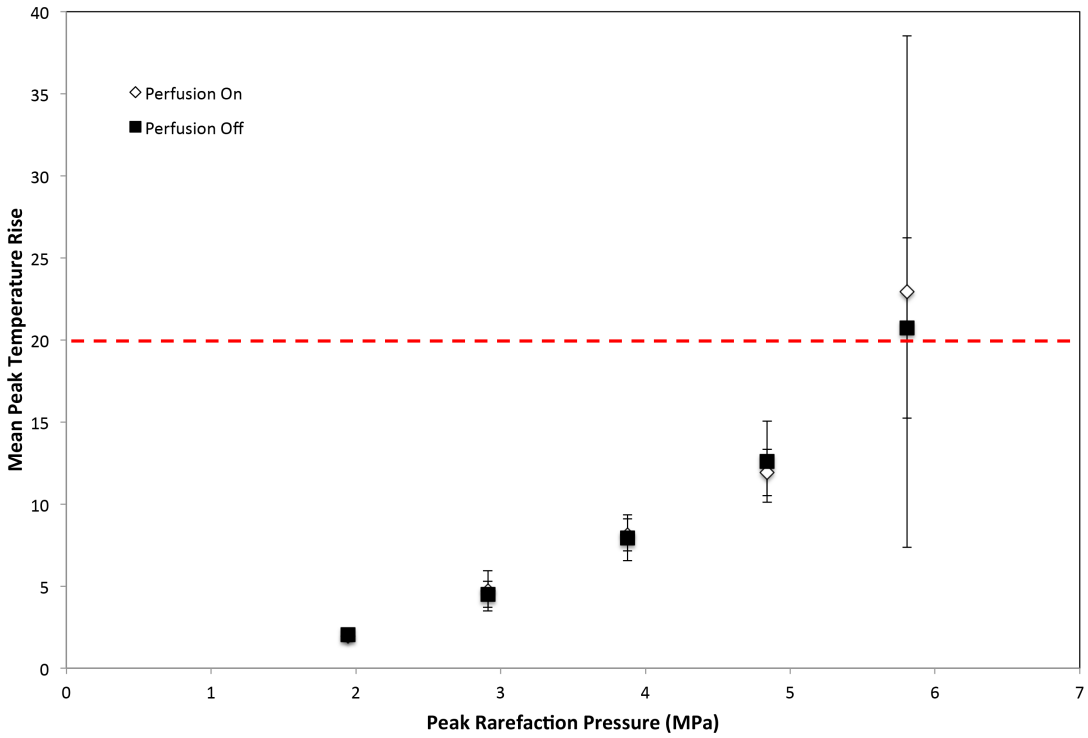


Figure 5.5 b

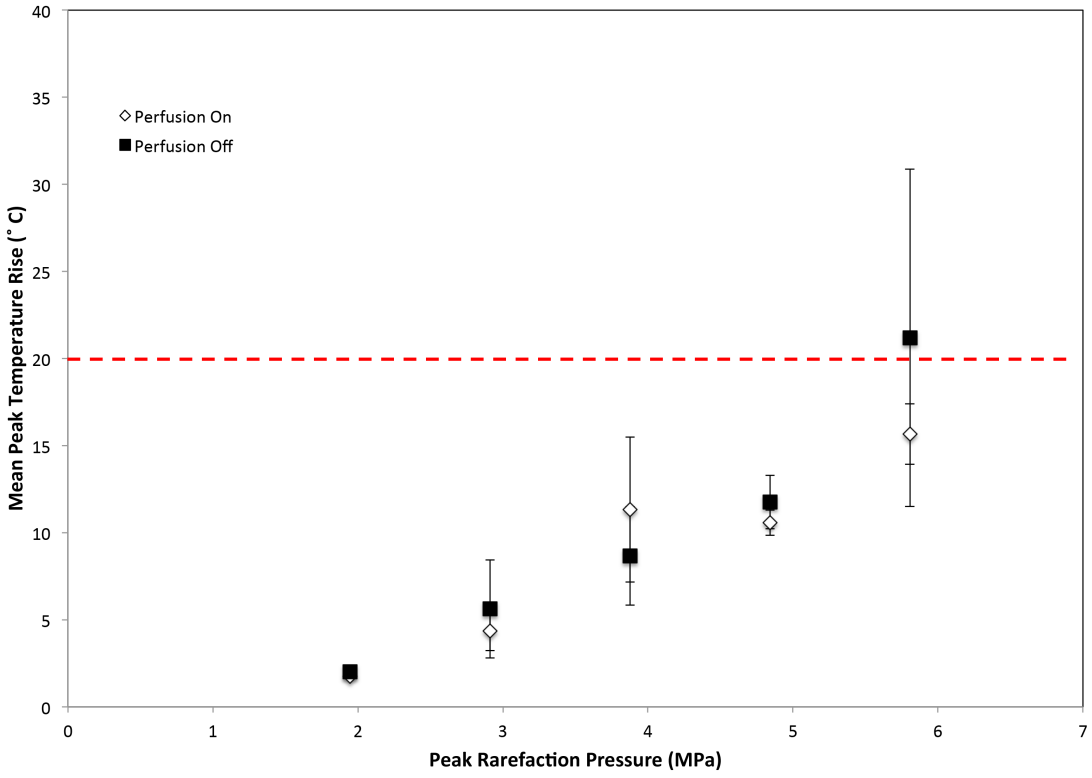


Figure 5.5a and b – *Mean peak temperature rise measured by direct real time thermometry as a function of peak rarefactional pressure in microperfused tissue regions (Figure 4.5 a, n = 4) and in tissue regions adjacent to a large (≥ 5 mm) blood vessel (Figure 4.5 b, n = 4). The diamond markers plot data obtained in the presence of perfusion, whilst the square markers indicate measurements made in the absence of blood flow, with the perfusion device switched off and the inflow / outflow tracts clamped. The wide standard error bars at the highest pressure are probably due to the effects of cavitation activity. There are no statistically significant differences in peak temperature rise between those measured in the presence and in the absence of perfusion at any peak rarefactional pressure ($p > 0.35$).*

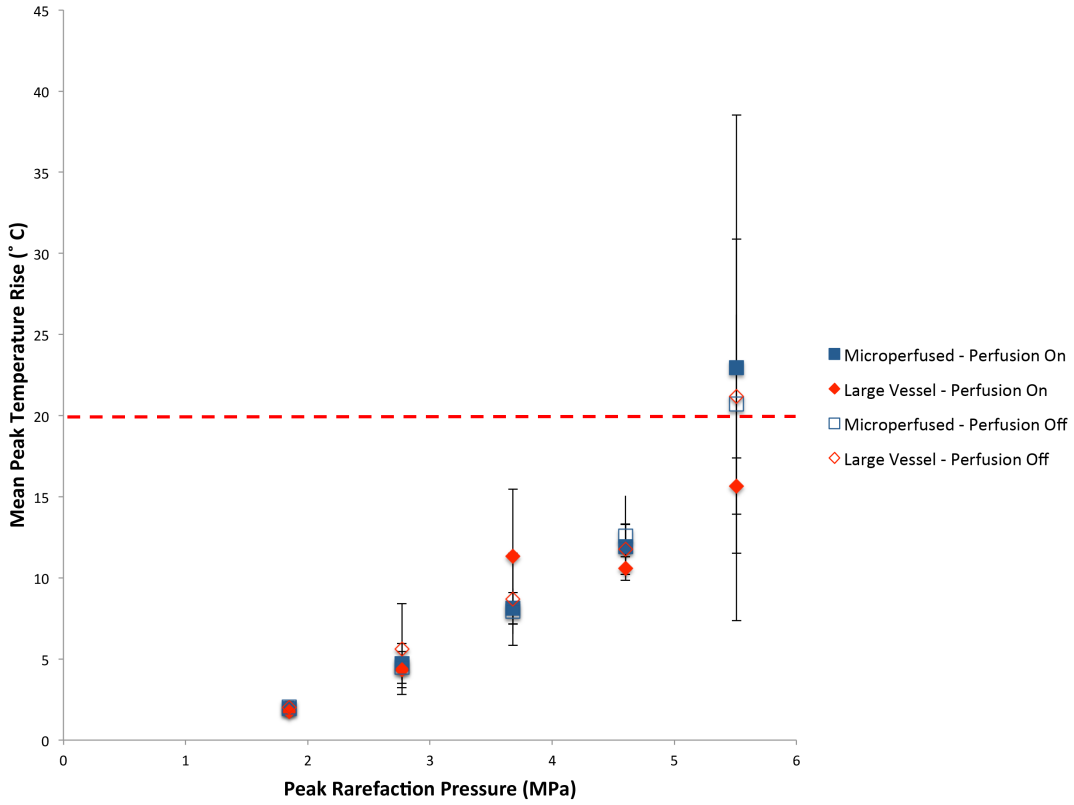


Figure 5.6 – *Mean peak temperature rises during 1 s 1.06 MHz HIFU exposures in both microperfused areas (blue markers) and regions adjacent to a large (≥ 5 mm) blood vessel (red markers) in both the presence of blood flow (solid markers) and the absence of perfusion*

(hollow markers). The red dashed lines approximately represent the temperature rise required to achieve tissue ablation.

As paired thermometry measurements were made at each location, in the presence and absence of perfusion, the difference between the two peak temperature rises at a given acoustic pressure under both of these flow conditions was plotted. These data are displayed in *Figure 5.7* below. This calculation should minimise the impact of other confounding variables between exposure locations, such as small differences in the position of the HIFU focus relative to the thermocouple junction, variations in the proximity of the thermocouple to vascular or biliary structures and differences in tissue properties, more accurately assessing the perfusion effect. These data demonstrate that there appears to be very little perfusion effect on the peak temperature attained during HIFU therapy. At 1.88 – 4.65 MPa $_{Pk-}$, there is a < 3 ˚C difference in mean peak temperature measured in the presence of blood flow compared to the absence of perfusion. At 5.58 MPa $_{Pk-}$ the mean peak temperature rise in areas adjacent to a large blood vessel is ≈ 6 ˚C lower in the presence of blood flow compared to in the absence of perfusion, although a much wider range of peak temperature rises were recorded at this acoustic pressure, probably due to the effects of inertial cavitation, and this difference was not statistically significant. In microvascular areas, a slightly higher mean peak temperature rise (< 2 ˚C) was recorded in the presence of perfusion compared to the absence of perfusion, although again there was a wide range of values and this difference was not statistically significant.

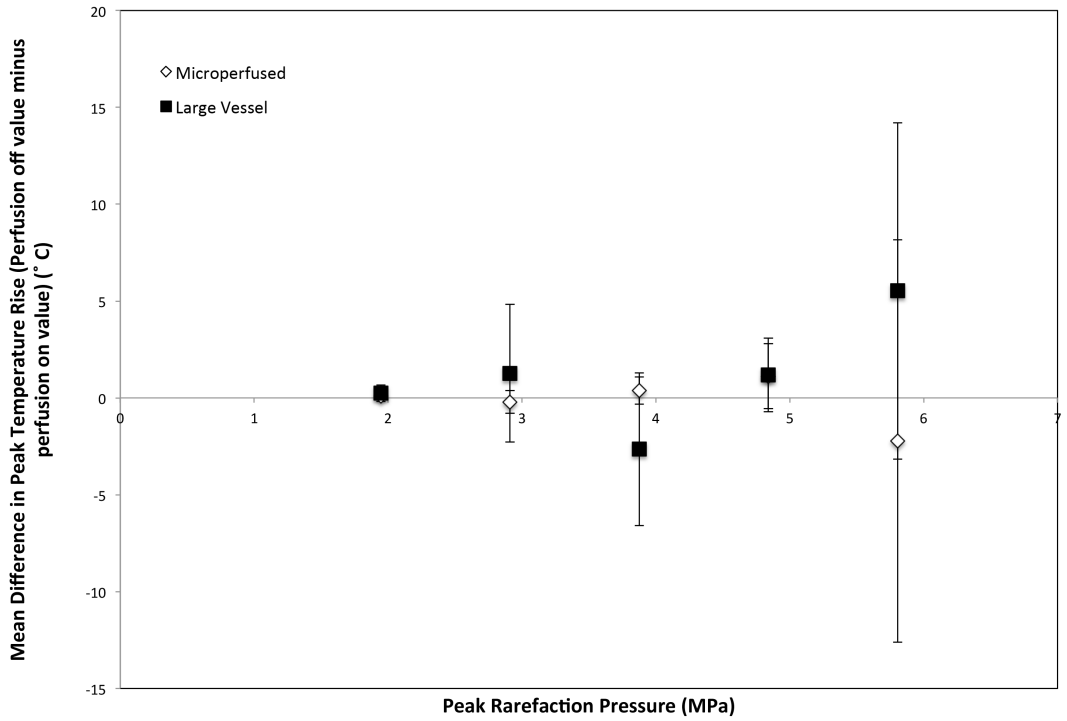


Figure 5.7 – *Paired mean differences in peak temperature rise during 1 s 1.06 MHz HIFU exposures in microperfused tissue (n = 4) and areas immediately adjacent to a large (≥ 5 mm) blood vessel (n = 4). At each thermocouple location at each peak rarefactional pressure, the temperature rise measured in the presence of blood flow was substracted from the paired measurement made in the same location in the absence of blood flow, with the perfusion device turned off. No significantly significant differences exist between the two groups at any peak rarefactional pressure ($p > 0.35$).*

5.4.3 The Relationship Between Cavitation and Heating at 1.06 MHz

Real time passive acoustic mapping (PAM) permitted spatio-temporal mapping of acoustic emissions during HIFU therapy. As discussed in Chapter 4, the cavitation

threshold at 1.06 MHz, i.e. the lowest peak rarefactional pressure at which acoustic cavitation, lies at around 2-3 MPa and both the probability and magnitude of acoustic cavitation increases as a function of acoustic pressure. For the HIFU exposures described above in Section 5.3.2, the maximum broadband energy at the focus was calculated from PAMs of real time acoustic emissions detected during treatment and this is displayed in *Figure 5.8* below. Although there is a wide range in the level of broadband emissions detected at each peak rarefactional pressure tested, it can be seen that cavitation energy increases as a function of acoustic pressure. It can also be seen that slightly higher levels of broadband energy were detected in both microvascular areas and regions adjacent to a large vessel in the presence of perfusion compared to in the absence of blood flow, although these are not statistically significant.

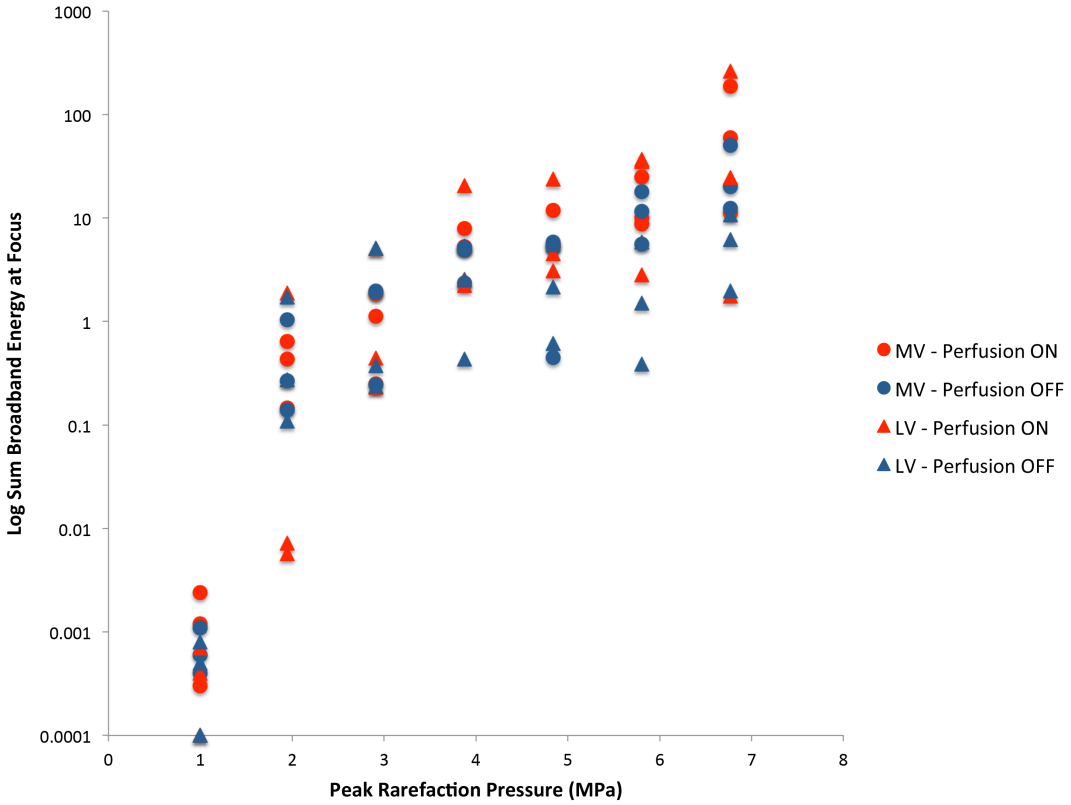


Figure 5.8 *– Maximum broadband energy at the HIFU focus for each of the exposures detailed in 4.3.2, calculated from PAMs, as a function of peak rarefactional pressure. MV =*

microvascular areas (circles, n = 4) and LV = tissue regions adjacent to a large (≥ 5 mm) blood vessel (triangles, n = 4). Measurements were made in each location both in the presence of blood flow (red) and in the absence of perfusion (blue).

It is widely reported that inertial cavitation enhances HIFU-induced heating in excess of that predicted by a linear heating model. Examples of PAMs acquired during the thermometry studies described in Section 5.3.2 are shown below in *Figure 5.9* and *5.10*. In a single microvascular location, a 1 s HIFU exposure at 4.65 MPa $_{Pk-}$ induced a temperature rise of 11.9 ˚C in the presence of blood flow compared to 11.4 ˚C in the absence of perfusion. In the corresponding PAMs (*Figure 5.9 top*), a small amount of off-focus inertial cavitation, shown by the broadband emissions (left hand PAM of each pair) is observed during the HIFU exposure in the presence of blood flow. However, very little broadband activity is observed within the focal volume, with the junction of the thermocouple approximately located at the centre of the oval circle, representing the HIFU focus. Virtually no broadband emissions are seen in the absence of perfusion at 4.65 MPa $_{Pk-}$ (*Figure 5.9 top right*). At 5.58 MPa $_{Pk-}$ a peak temperature rise of 46 ˚C was observed in the presence of blood flow compared to 17.2 ˚C in the absence of perfusion. In the respective PAMs, a significant amount of focal inertial cavitation is seen during the HIFU exposure that induced a 46 ˚C peak temperature rise (*Figure 5.9 bottom left*), whilst minimal focal inertial cavitation is observed in the PAM in the absence of perfusion, corresponding to the 17.2 ˚C temperature rise (*Figure 5.9 bottom right*).

Similarly, in a single location adjacent to a large vessel, there was little inertial cavitation activity at 4.65 MPa $_{Pk-}$, although some prefocal broadband emissions were observed

under flow conditions (*Figure 5.10, top left*) and similar temperature rises were seen in the presence and absence of perfusion. At 5.85 MPa $_{Pk-}$, significant focal inertial cavitation was observed during HIFU therapy in the absence of perfusion (*Figure 5.10 bottom right*), although little was seen during the exposure in the presence of blood flow (*Figure 5.10 bottom left*). A peak temperature rise of 32.4 ˚C was recorded at 5.58 MPa $_{Pk-}$ in the absence of perfusion, corresponding with the higher levels of cavitation activity seen compared to the exposure performed in the presence of blood flow, with minimal cavitation seen on PAM, where a lower peak temperature rise of 17 ˚C was recorded. From these PAMs, it appears that higher levels of focal broadband emissions, representing inertial cavitation, are associated with higher peak temperature rise compared to HIFU exposures with minimal levels of cavitation activity. This observation supports published work that inertial cavitation enhances HIFU-induced heating.

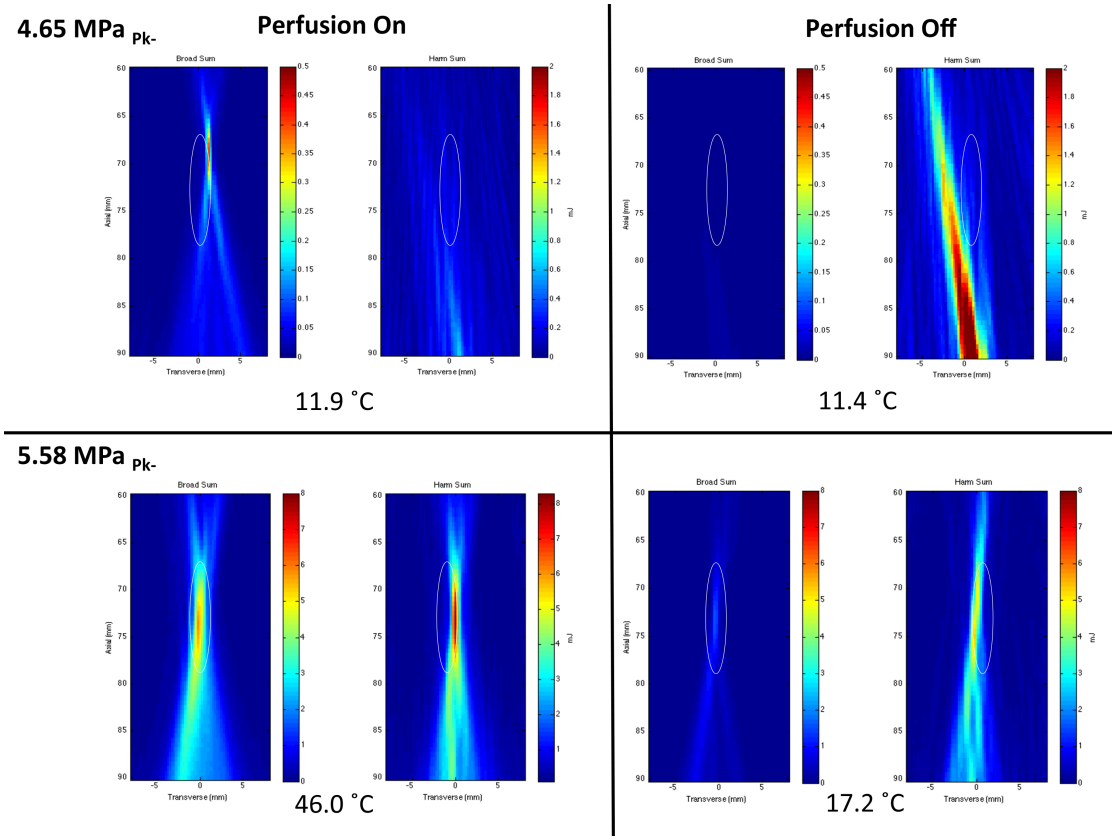


Figure 5.9 *– PAMs mapping both summative broadband emissions and harmonic emissions during 1 s, 1.06 MHz exposures at 4.65 MPa $_{Pk-}$ (top) and 5.58 MPa $_{Pk-}$ (bottom) in a single microvascular-perfused area in the presence of blood flow (left) and in the absence of perfusion (right). The white oval represents the HIFU focus. The thermocouple junction is located approximately in the centre of the HIFU focus.*

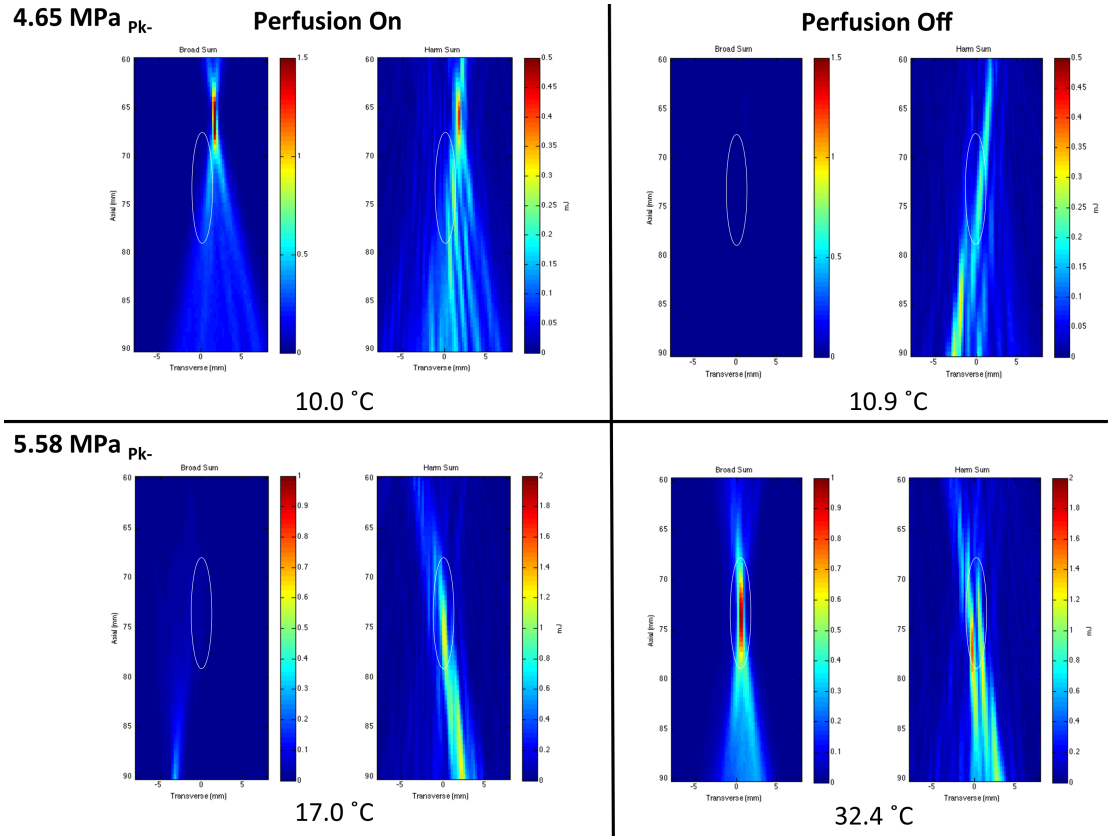


Figure 5.10 – *PAMs mapping both summative broadband emissions and harmonic emissions during 1 s, 1.06 MHz exposures at 4.65 MPa $_{Pk-}$ (top) and 5.58 MPa $_{Pk-}$ (bottom) in a single tissue region adjacent to a large (≥ 5 mm) vessel in the presence of blood flow (left) and in the absence of perfusion (right). The white oval represents the HIFU focus.*

In *Figure 5.11* below, summative broadband energy, representative of inertial cavitation, detected at the focus through PAM is plotted as a function of peak temperature rise for each of the HIFU exposures described in section 5.3.2. Although there is not an absolute correlation between broadband energy levels observed at the HIFU focus and peak temperature rise, there is a trend towards greater levels of inertial cavitation being associated with higher temperatures rises.

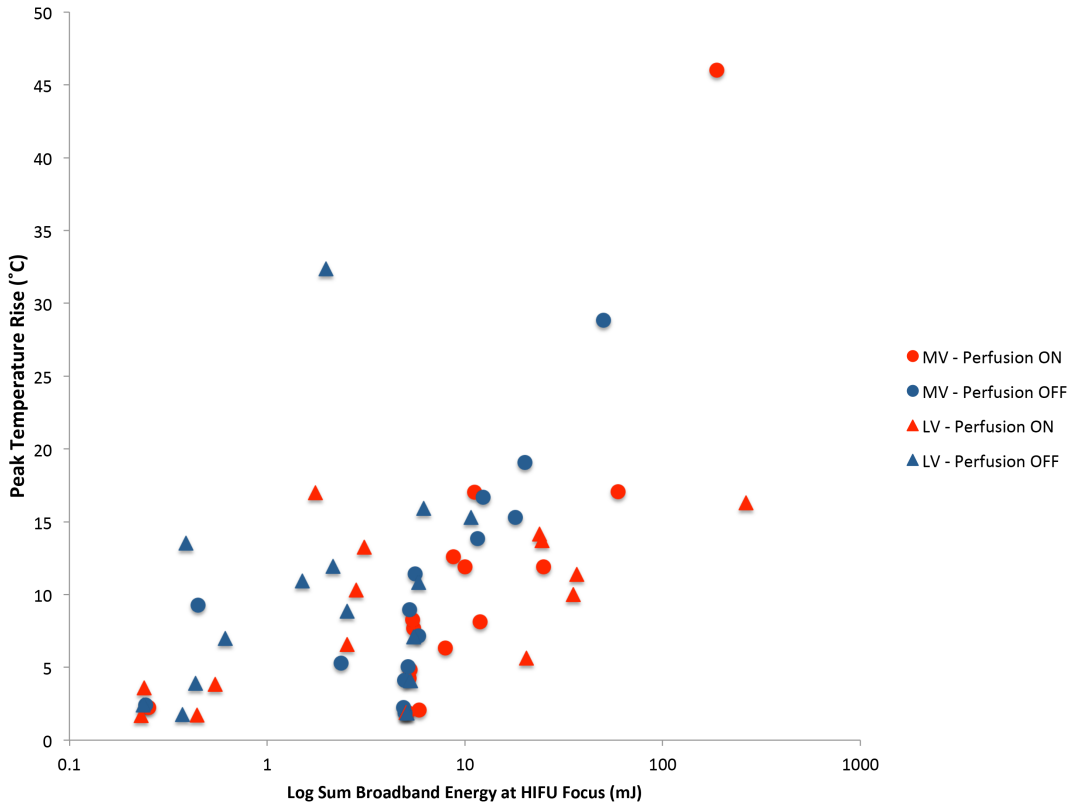


Figure 5.11 *– Peak temperature rise as a function of broadband energy for 1s 1.06 MHz HIFU exposures at 5 peak rarefactional pressures ranging from 1.88 – 5.58 MPa. Data were obtained from microvascular areas (circles) and regions adjacent to a large (≥ 5 mm) vessel, both in the presence of blood flow (red) and the absence of perfusion (blue).*

With regards to the type of tissue targeted, there does not appear to be a difference between microperfused and large vessel regions or whether the perfusion device was running or switched off in terms of either peak focal temperature rise or summative focal broadband energy.

5.4.4 Effects of Perfusion on Heating at 3.18 MHz

The lowest peak rarefactional pressure at which HIFU-induced cavitation occurs: the "cavitation threshold", is frequency and tissue dependent. In a given tissue, as frequency increases, the cavitation threshold also increases. The effects of blood flow on HIFU-induced cavitation in the perfused liver model are described in detail in Chapter 4. At 1.06 MHz the cavitation threshold lies in the region of 3 – 4 MPa $_{Pk-}$ in the isolated, perfused liver and at 3.18 MHz, it appears to lie above 12 MPa $_{Pk-}$. Therefore, further thermometry studies were performed at the driving the 1.06 MHz transducer at the 3rd harmonic (3.18 MHz), in order to investigate the effects of perfusion on HIFU induced tissue heating in the absence of cavitation. The studies were performed using the following HIFU protocol, with the same exposure duration, location characteristics and flow conditions as the 1.06 MHz thermometry studies:

Frequency	3.18 MHz
Exposure duration	1 s
Peak rarefactional pressures (MPa $_{Pk-}$)	0.90, 1.75, 2.60, 3.46, 4.31, 5.16, 6.86
Duty cycle	100%

Representative thermometry curves for a single region adjacent to a large ≥ 5mm blood vessel and for a single microvascular-perfused site, both in the presence and absence of blood flow, are shown below in *Figure 5.12*. At a peak rarefactional pressure of 0.90, a temperature rise of approximately 1 ˚C is induced in both types of tissue region and in both flow conditions

There appears there may be a perfusion effect at higher peak rarefactional pressures, with peak temperatures at 5.15 MPa $_{Pk-}$ between 5 and 10 ˚C lower in the presence of blood flow compared to in the absence of perfusion. However, the perfusion effect is most noticeable in the microvascular region. It is possible that capillary (microvascular) perfusion is the more dominant cooling mechanism and this effect is more pronounced at 3.18 MHz due to the small focus compared to at 1.06 MHz.

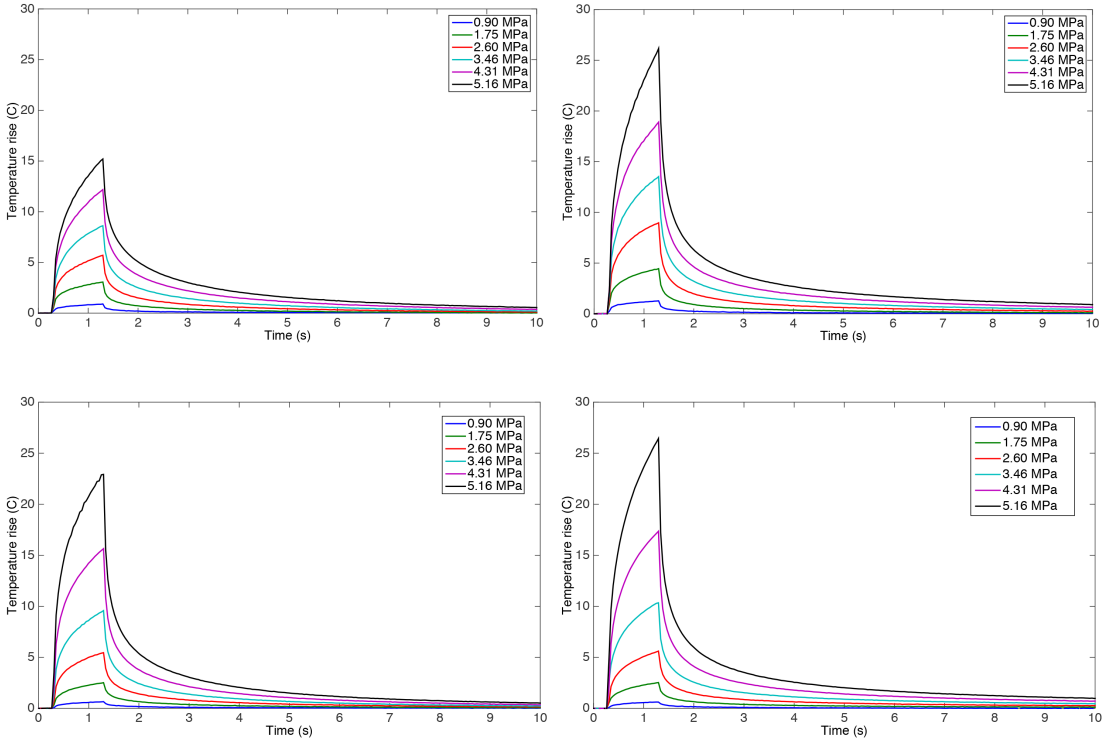


Figure 5.12. *- Representative temperature curves for 1 s 3.18 MHz HIFU exposures at a range of peak rarefactional pressures (0.90 MPa $_{pk-}$ to 5.16 MPa $_{pk-}$). HIFU exposures were performed in microvascular areas (top row) and adjacent to a larger (≥ 5mm) blood vessel (bottom row), both in the presence of blood flow (left) and the absence of blood flow (right).*

However, when data from multiple microvascular (*Figure 5.13 a*) and large vessel regions (*Figure 5.13 b*) are analysed, there is no apparent difference in the mean peak temperature rise either in the presence of blood flow, or in the absence of perfusion, with the perfusion device turned off. Although the sample size is small (n = 3 perfusion on, n = 3 perfusion off) for both microperfused and large vessel regions and the error bars at the highest peak rarefactional pressures are wide, the differences in mean peak temperature rise between measurements made in the presence of perfusion compared to the absence of perfusion are statistically non-significant ($p > 0.15$).

When microvascular and large vessel regions are compared, there again does not appear to be a difference in peak temperature rise between microvascular and large vessel regions, either in the presence or absence of perfusion ($p > 0.10$). However, a larger number of repeats are needed to confirm this with more rigorous statistical analysis. Similar to the studies at 1.06 MHz, a temperature rise in excess of the ablative threshold temperature required to induce coagulative necrosis in the target tissue, indicated by the red dashed line, could be attained at relatively low peak rarefactional pressures of 5.16 MPa in both microvascular areas and tissue immediately adjacent to a large (≥ 5 mm) blood vessel.

Figure 5.13 a

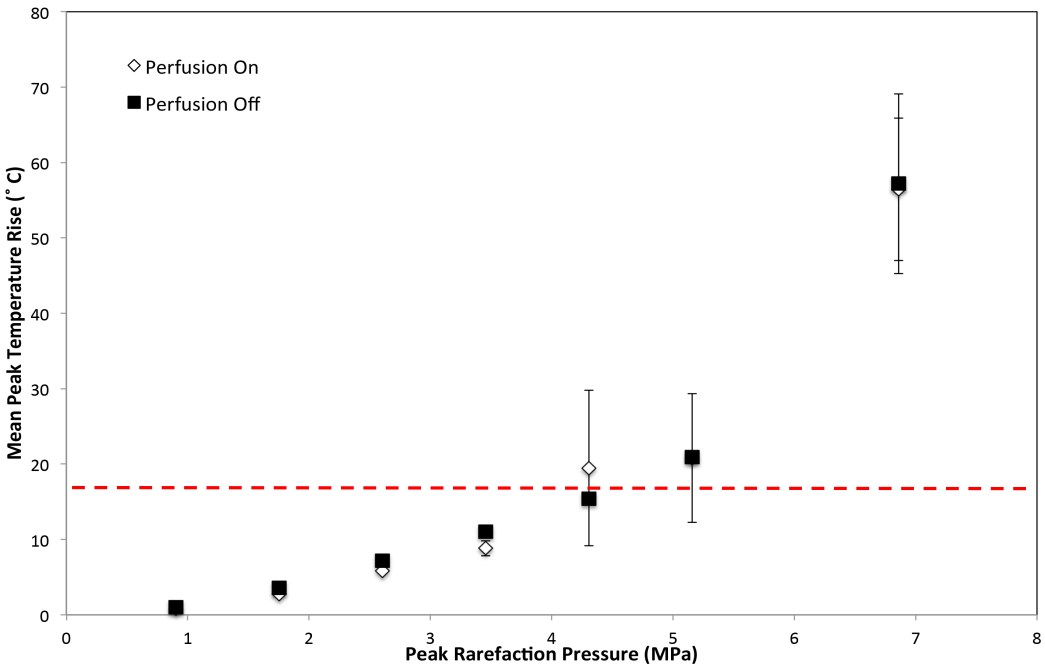


Figure 5.13 b

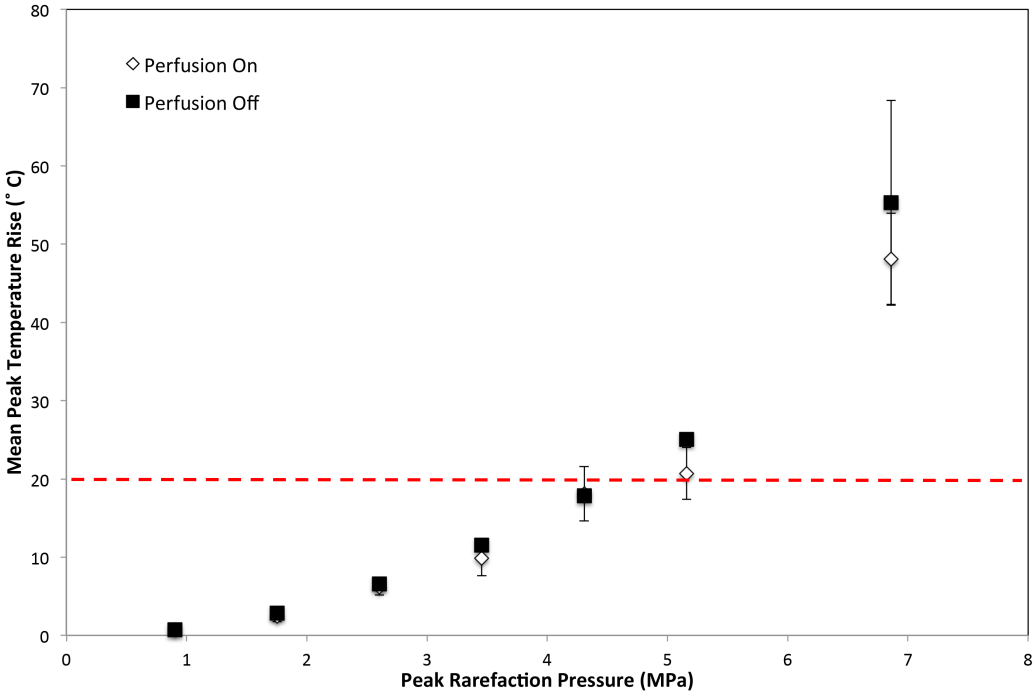


Figure 5.13 a and b – *Mean peak temperature rise as a function of peak rarefactional pressure (MPa) during 1 s continuous wave 3.18 MHz HIFU exposures in microvascular tissue regions (Figure 5.13 a, n = 3) and areas adjacent to a large (≥ 5 mm) blood vessel (Figure 5.13 b, n = 3). The red dashed lines approximately represent the temperature rise required to achieve tissue ablation. No statistically significant differences existed between peak temperatures attained in the presence of blood flow compared to in the absence of perfusion, either in microperfused areas or tissue regions directly adjacent to a large blood vessel (p > 0.15).*

The mean difference in peak temperature rise between the paired thermometry measurements at each thermocouple location (peak temperature rise in the presence of blood flow minus peak temperature rise in the absence of perfusion) was calculated and is displayed in *Figure 5.14*. Similar to the studies performed at 1.06 MHz, there is little difference in mean peak temperature at the lower acoustic pressures tested (0.90 – 4.31 MPa $_{Pk-}$). At 5.15 and 6.86 MPa $_{Pk-}$, in tissue regions adjacent to a large vessel, there appears to be an increasing perfusion effect, with the mean peak temperature rises 2.5 ˚C and 7.2 ˚C lower in the presence of blood flow compared to the absence of perfusion at 5.15 and 6.86 MPa $_{Pk-}$ respectively. This trend was not observed in microvascular regions at the same acoustic pressures, with very similar mean peak temperature rises recorded in both flow conditions. However, no statistically significant differences were detected between measurements made in the presence and absence of blood flow in either large vessel or microperfused regions ($p > 0.15$). Similarly, no statistically significant differences were present between peak temperature rises made in microvascular areas compared to large vessel regions ($p > 0.10$).

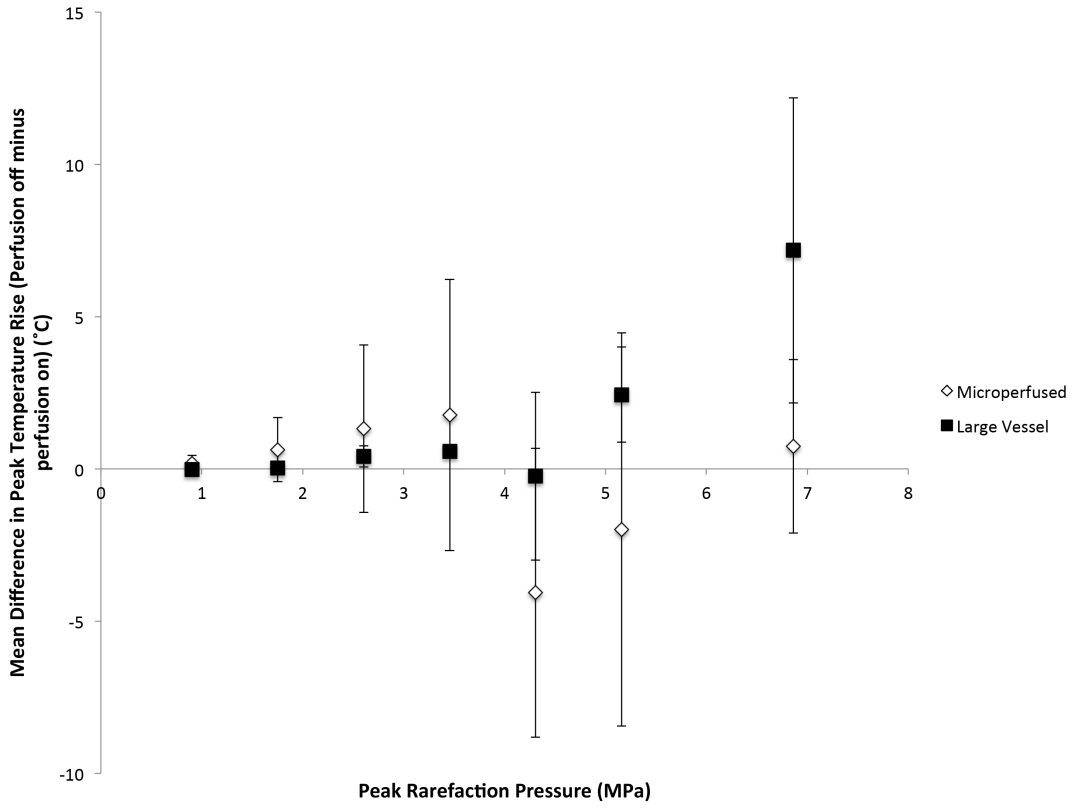


Figure 5.14 – *Mean difference in peak temperature rise during 1 s 3.18 MHz HIFU exposures in microperfused tissue (n = 3) and areas immediately adjacent to a large (≥ 5 mm) blood vessel (n = 3) between values obtained at a given acoustic pressure in the presence and in the absence of blood flow, with the perfusion device turned off.*

5.5 Discussion

In this chapter, real time data assessing the effects of perfusion on HIFU-induced heating and cavitation within a clinically relevant isolated, perfused porcine liver model are presented. These are the first real time thermometry measurements made during HIFU therapy reported that have been performed in perfused tissue, at a physiological temperatures, with blood flow rates and vascular anatomy comparable to the human liver. The unique normothermic liver perfusion preservation device used in this study accounts for physiological arterial, portal venous and hepatic venous pressures and flow rates, although hepatic arterial flow is constant rather than pulsatile. Previous experimental models of isolated liver perfusion used to investigate HIFU therapy have typically either been hypothermic or at room temperature, using an acellular perfusion solution, limiting the physiological applicability of resulting observations in terms of cavitational and thermal tissue characteristics (Bu et al., 2013, Izamis et al., 2014).

5.5.1 The Effects of Perfusion on HIFU-Induced Heating

The relationship between perfusion, particularly large vessel flow, and tissue heating in ablative therapy has been studied fairly extensively, mainly in the context of RFA and MWA, which are the two therapeutic modalities in widespread clinical use. However, the effects of perfusion on HIFU therapy have been studied little in an experimental context, with few *in vivo* studies in the literature. Zhou *et al.* (Zhou et al., 2012) observed that both the cooling phase and lesion size, following HIFU-induced heating of

a rabbit VX2 hepatic tumour, were related to the extent of the tumoural blood supply. However, the temperature-increase phase was not significantly affected by blood supply characteristics. Chen *et al.* also observed a decreased lesion size following *in vivo* HIFU ablation of rat liver tissue, compared to reduced blood flow with the hepatic artery and portal vein ligated (Chen et al., 1993).

Mathematical modeling of heating during HIFU therapy is complicated by the presence and effects of cavitation, non-linear propagation of ultrasound and boiling, all of which differ between different types of tissue and also within the same organ, due to tissue heterogeneity (Khokhlova et al., 2006, Holt and Roy, 2001). The varying cavitation thresholds and levels of cavitation during HIFU exposures of different tissues, potentially leads to highly variable rates of heating due to cavitation enhancement. Various studies, using a variety of different mathematical models, have reported a range of predicted effects of perfusion on heating during HIFU therapy. Hariharan *et al.* modeled the effects of large vessel perfusion on HIFU-induced heating at moderate exposure intensities (Hariharan et al., 2007) and concluded that in most circumstances large vessel blood flow has a minimal effect on heating during HIFU therapy. However, when the treatment volume is placed at a location within one beam width (≈ 2 – 3 mm) of a large vessel, then lesion volume may be reduced by up to 40 %. Using both a numerical and an *in vitro* gel phantom model, Huang *et al*. determined that convective cooling by large vessel perfusion can significantly affect HIFU therapy. They demonstrated that in these models, blood vessels with a flow rate of 2 cm s^{-1} (6.4 ml/min) through a 2.3 mm vessel can reduce the peak temperature rise in the vessel wall by approximately 25 % (Huang et al., 2004a). Solovchuk *et al.* (2013) proposed a mathematical model, accounting for the

effects of both large vessel and microvascular blood flow and also convective cooling from vascular acoustic streaming resulting from HIFU therapy. They demonstrated that velocities due to acoustic streaming could be up to a magnitude higher than physiological blood flow velocities and have a significant effect on HIFU-induced heating, although ablative temperatures could still be attained (Solovchuk et al., 2013).

The results from the current study suggest that no significant heat sink effect on HIFU-induced heating of hepatic tissue is imparted by blood flow through an adjacent large (≥ 5 mm) blood vessel or through microvascular perfusion of the hepatic parenchyma, in terms of the peak focal temperature rise attained during HIFU therapy. No significant differences in peak focal temperature were detected between measurements made in the presence of blood flow compared to the absence of perfusion. Similarly, no differences were seen between peak temperature rises measured in microvascular tissue areas compared to areas directly adjacent to a large (≥ 5 mm) blood vessel. Therefore, the effects of variable tissue perfusion characteristics, due to anatomical location and tissue heterogeneity, on tissue heating during HIFU therapy therefore appear to be minimal and similar peak focal temperatures can be attained irrespective of the anatomical position of the HIFU focus with respect to vascular anatomy.

The results presented in this chapter do not appear to concur with Huang *et al.'s* (2004) prediction of a > 25% reduction in peak temperature at a large vessel wall. However, only the temperature at the HIFU focus was measured and the impact of perfusion on heating towards the peripheries of the HIFU focal volume was not assessed. Therefore, it was not possible to assess the applicability of Hariharan *et al.*'s (2007) model as

temperature changes 2-3 mm away from the focus, indicating the temperature towards the edge of the predicted HIFU lesion, hence influencing lesion size, were not obtained.

4.5.2 Comparison with Perfusion Effects in RFA and MWA

Experimental and clinical studies have demonstrated that a significant heat sink effect is created by large (> 3 mm) vessels in RFA therapy (Lu et al., 2003, Lu et al., 2002, Mulier et al., 2005, Patterson et al., 1998, Tamaki et al., 2004, Welp et al., 2006, Washburn et al., 2003) and, to a lesser degree, in MWA therapy (Liu et al., 2006, Lu et al., 2010, Yu et al., 2008, Wright et al., 2005, Bhardwaj et al., 2011). These effects have significant clinical implications in that tissue adjacent to a large vessel may not reach a temperature sufficient to induce coagulative necrosis, potentially leaving viable malignant cells and therefore increasing the risk of tumoural recurrence. This is particularly evident in RFA of perivascular tumours, particularly those abutting the main, left or right portal veins or hepatic veins (Lu et al., 2002, Tamaki et al., 2004, Metcalfe et al., 2007). In addition, vascular perfusion has been shown to decrease RFA lesion size, increase ablation time and lead to higher energy deposition requirements (Bitsch et al., 2006, Bangard et al., 2006, Chinn et al., 2001, Tamaki et al., 2004, Patterson et al., 1998). Experimental studies have shown that MWA can achieve necrosis up to large vessel walls, but large vessel proximity and also overall tissue perfusion may decrease the lesion size and increase energy requirements (Yu et al., 2008, Sommer et al., 2011).

In contrast, the results presented in this chapter suggest that the effects of perfusion on tissue heating rates during HIFU therapy are minimal, with similar peak focal temperature rises attained in tissue regions adjacent to, and away from large vasculature.

Likewise, the presence or absence of perfusion did not have a significant effect on peak focal temperature rise within a specific focal volume, either in regions adjacent to, or away from a large vessel. These data would support the previous findings of Zhou *et al* in that perfusion does not seem to affect the HIFU-induced heating phase (Zhou et al., 2012). However, unpublished work by Jensen *et al.*, investigating the cooling rate following HIFU therapy, using the same thermometry curves presented in 5.3.2 suggest that, although the rate of heating and peak temperature do not appear to be significantly affected by the presence of blood flow or the proximity of a large blood vessel to the HIFU focal volume, the rate of cooling significantly increases in the presence of these factors. One explanation for these observations is that the heat-increase phase in HIFU therapy is short and rapid, particularly as the exposure duration in the series of experiments performed in this current work was only 1 s. In clinical HIFU therapy, exposure durations are typically under 30 seconds, depending on the specific application. Therefore, in this study, there was a relatively short period of time during which heat advection away from the source at the HIFU focus could occur in order to affect heating, leading to minimal perfusion effects on peak temperature rise. Even with longer exposure durations of up to 30 s, the heating phase in HIFU therapy is still short, in contrast to the much longer heating times encountered in RFA and MWA of up to 30 minutes. The temperature-decrease phase in HIFU therapy is substantially longer than the temperature-increase phase, with slower cooling rates than heating rates. This provides a longer opportunity for heat advection due to blood flow to occur, potentially increasing the cooling rate in tissue with higher perfusion rates, such as those adjacent to large vasculature, compared to those in less-well perfused areas.

5.5.3 The Relationship Between Cavitation and Heating

A number of studies have demonstrated that inertial cavitation can enhance heating rates during HIFU therapy (Coussios et al., 2007, Hynynen, 1991, Miller and Gies, 1998, Holt and Roy, 2001). In this current work, passive acoustic mapping was used to spatiotemporally quantify broadband emissions, representing inertial cavitation activity. The peak focal broadband emissions and the summative focal broadband emissions were both calculated for each HIFU exposure performed and these data are reported in Chapter 4. In Section 5.3.3, peak focal temperature rise is plotted against the total focal cavitation energy. Whilst there does not appear to be a definite correlation between the two parameters, the highest temperature rises are seen with the highest levels of total focal broadband energy, suggesting significant cavitation-induced enhancement of heating rates, which concurs with the findings of previous published studies.

5.5.4 Further Work

Further studies using a variety of HIFU exposure durations are required in order to evaluate perfusion effects on longer treatment durations. Longer exposure durations were not used in this study as thermal tissue damage occurs as a function of both temperature and time and, in order to minimize focal tissue changes for subsequent measurements made in the same thermocouple location, using a short (1 s) exposure duration was necessary. If similar studies to the ones presented in this chapter were to be performed using longer exposure durations (e.g. 5 – 10 s), only single measurements at each thermocouple location could be made as thermal necrosis would occur at lower peak

rarefaction pressures than with 1 s HIFU exposures, thus altering the focal tissue properties for subsequent measurements. A considerable degree of variability is likely to be introduced by changing thermocouple locations between measurements due to anatomical and local perfusion differences and slight variation in the alignment of the thermocouple and HIFU foci.

Histological assessment of the effects of large vessel proximity on HIFU ablation needs to be conducted, in order to correlate heating data with tissue necrosis and these data are presented in the following section. Given that the peak temperature rise measured in this study was that which was achieved at the intersection of the HIFU focus and the thermocouple junction, the thermal effects through the whole HIFU focal volume need to be assessed. The thermal effects of heat advection from perfusion are most pronounced in the tissue immediately encircling a major blood vessel. Therefore, it is these cells that are most likely to remain viable if incomplete thermal ablation occurs through heat advection from major vessel blood flow. In addition, thermometry measurements requiring insertion of a needle thermocouple are prone to several types of error, including thermocouple artifact due to viscous heating, the potential introduction of cavitation nuclei and the provision of a surface for cavitation nucleation to occur. Therefore, validation of thermometry data with histological evidence of successful thermal ablation is needed. A further limitation of this study to date is due to experimental error resulting from the distance of the thermocouple junction from the end of the needle (≈ 2 mm) and in the accuracy of B-mode imaging in that, although the thermocouple needle tip was seen to be immediately adjacent to the vessel wall, the location of the focal point measured could have been several millimetres away from the

vessel itself. If indeed there is little or no "heat sink" effect on HIFU ablation and thermal necrosis can be achieved right up to the wall of major vessels, then HIFU could represent an effective, non-invasive modality for ablative treatment of solid organ tumours in such anatomical locations.

5.6 Conclusions

In a physiologically relevant, isolated perfused liver model, heating induced by 1.06 MHz and 3.18 MHz HIFU over the PRFP range 1.95 – 5.81 MPa at 1.06 MHz and 0.90 – 6.85 MPa at 3.18 MHz is neither significantly affected by the proximity of large (≥ 5 mm) blood vessels, nor by the presence or absence of perfusion. It appears as if the rate of tissue heating observed during HIFU therapy can overcome any heat sink effect from large vessel blood flow and that the presence or absence of cavitation activity impacts the rate of heating more significantly than local differences in tissue perfusion.

CHAPTER 6

THE EFFECT OF PERFUSION ON HISTOLOGICAL ASSESSMENT OF TISSUE ABLATION IN HIFU THERAPY

Blood vessels > 3 - 4 mm in diameter running through, or adjacent to a treatment volume can impart a significant heat sink effect during radiofrequency ablation and, to lesser extent, microwave ablation. Studies have demonstrated that viable tissue can remain immediately adjacent to a ≥ 4 mm vessel wall following RFA, potentially leading to treatment failure. The thermometry data presented in Chapter 4 suggests that HIFU therapy is minimally affected by the vascular heat sink effect in terms of peak focal temperature rise. The aim of the work in this chapter is to elucidate the effects of large vessel perfusion on lesion formation and cell death following HIFU therapy.

6.1 Introduction

Heat advection due to blood flowing through a large vessel or vessels lying adjacent to, or running through an ablative treatment volume can reduce tissue heating to such an extent that the peak temperature throughout the focus does not reach the threshold required to achieve thermal necrosis. Tissue and vascular homogeneity means that there may be a varying degree of heat sink effect at different points within the ablative focal volume, potentially allowing areas of tissue to remain untreated during ablative therapy, whilst successfully destroying cells within other areas. Under these circumstances,

especially when a patient is undergoing ablative therapy for the treatment of cancer, areas of viable malignant tissue may remain post-intervention and treatment failure may ensue.

The tissue regions most susceptible to any heat sink effect are the cells directly adjacent to vessel walls, as the cooling effect of blood flow will be maximal at this point, decreasing as a function of distance from the blood vessel.

The heat sink effect is particularly dominant in radiofrequency ablation and several experimental and clinical studies have demonstrated that vessels > 3 - 4 mm in diameter significantly reduce peak tissue temperatures attained, reduce lesion size, increase treatment times and increase the total energy required (Bitsch et al., 2006, Chang et al., 2002, Chinn et al., 2001, Dodd et al., 2013, Frich et al., 2006, Goldberg et al., 1998, Lu et al., 2002, Metcalfe et al., 2007, Mulier et al., 2005, Patterson et al., 1998, Scott et al., 2002, Shen et al., 2003, Tamaki et al., 2004, Thanos et al., 2008, Welp et al., 2006, Wu et al., 2009). Histologically, viable tissue may remain at the vessel wall – tissue interface, which is the region most affected by any heat sink effect (Lu et al., 2003, Lu et al., 2002). Microwave ablation is affected by large vessel perfusion to a lesser extent than RFA (Dodd et al., 2013, Garrean et al., 2009, Schramm et al., 2007, Bhardwaj et al., 2011), although Yu *et al.* demonstrated that, in a porcine experimental model, viable tissue remained adjacent to vessels ≥ 6 mm in diameter following MWA in approximately 25% of cases.

Although there are minimal experimental data available assessing the histological effects of large vessel blood flow on ablative HIFU therapy, modeling studies have suggested

that temperatures in excess of the ablative threshold can be achieved adjacent to major vasculature (Hariharan et al., 2007, Solovchuk et al., 2013). Similarly, the small amounts of clinical data that are available also suggest that HIFU ablation of tumours adjacent to large blood vessels, including 1st order portal veins, hepatic veins and the retrohepatic IVC is both safe and effective, being minimally affected by perfusion.

6.2 Study Aims

The aim of the studies discussed in this chapter was to elucidate the effects of physiological perfusion on lesion formation and, specifically, cell death following HIFU ablation. The thermal data presented in Chapter 5 suggests that HIFU is minimally affected by large vessel blood flow in terms of the peak focal temperature rise attained during therapy. However, the critical clinical endpoint in terms of immediate treatment success / failure is whether or not complete tissue ablation can be achieved irrespective of vascular anatomy and blood flow at a histopathological level. Therefore, the specific objectives of the work were:

4) To assess whether macroscopic complete tissue ablation (cell death) can be achieved up to the wall of a large (≥ 5 mm) blood vessel adjacent to a HIFU treatment volume
5) To correlate macroscopic findings with histological assessment of cell death / viability in perivascular tissue regions

6.3 Methods

6.3.1 Perfused Liver Model Set Up

An identical normothermically perfused liver model to the set up described in the previous two chapters was used. In total, seven perfused liver studies were undertaken for the studies in this phase of work. Porcine livers were surgically explanted, cold preserved, transported and connected to the extracorporeal normothermic liver perfusion device (ECLPD) according to the standard technique described in Chapter 2, Section 2.3. Once reperfused on the liver perfusion device, each organ was left for 60 minutes to permit recovery from the cold ischaemic phase prior to starting HIFU studies. Following this period of resuscitation, the perfused liver was placed in an acoustically transparent isolation bag (3M, USA) filled with approximately 3 L of isotonic colloid solution (Gelofusine ®; B Braun, UK) that had been degassed in a vacuum flask for 2 hrs prior to use and pre-warmed to 37 ˚C.

6.3.2 HIFU Set Up

The HIFU set up used for this series of studies was identical to that used for the cavitation and thermal response experiments described in Chapters 4 and 5. A transducer with a centre frequency of 1.067 MHz and a rectangular cutout was used to generate HIFU pulses. A 5 - 10 MHz linear diagnostic array (L10-5; Zonare, USA) was mounted to the HIFU transducer through the rectangular cutout in order to allow B-mode imaging of the liver and acquisition of passive acoustic data for cavitation mapping during HIFU exposure. In addition to the 5-10 MHz linear array mounted to the HIFU

transducer, a handheld linear 5 – 14 MHz diagnostic array (L14-5w; Zonare, USA) was also used to facilitate delineation of the vascular anatomy through B-mode imaging and colour Doppler and to aid identification and targeting of suitable vessels.

6.3.3 Lesion Threshold Studies

A preliminary set of studies in 2 isolated perfused livers were performed in order to ascertain the HIFU parameters required in order to achieve visible thermal lesion formation within the perfused liver tissue.

A volume of liver parenchyma was identified within the perfused liver that would allow a linear series of 7 – 8 single HIFU exposures at 1.5 cm intervals at a depth of 1.5 cm from the liver surface avoiding vascular and biliary structures visible on B-mode ultrasound i.e. > 9 cm in either the *x* or *y*-axis, with a depth of ≥ 2 cm (*z*-axis) – see *Figure 6.1*. The liver was repositioned in the bowl so that the HIFU focus could be moved along the > 9 cm length of liver parenchyma through adjustment of a single axis (*x* or *y*) of the manual positioning system. If a vascular / biliary structure was encountered < 1 cm from an intended exposure location, then the spacing between sites was increased from 1.5 cm to a point when the vascular/biliary structure was ≥ 1 cm away from it. The *z*-axis of the manual positioning system was adjusted so that the HIFU focus remained at a depth of 1.5 cm within the liver parenchyma from the surface of the liver.

Two surface marks 1.5 cm proximal to the start and 1.5 cm distal to the end of the linear series of HIFU exposures were placed in order to facilitate identification of the HIFU exposure locations for post-perfusion sectioning. This was achieved by placing the HIFU

focus at the liver surface and then performing a 10 s 7.74 MPa $_{Pk-}$ HIFU exposure to create a surface lesion. It was checked that hyperecho on B-mode ultrasound post HIFU exposure was visualized in order to ensure that a marker lesion had been formed.

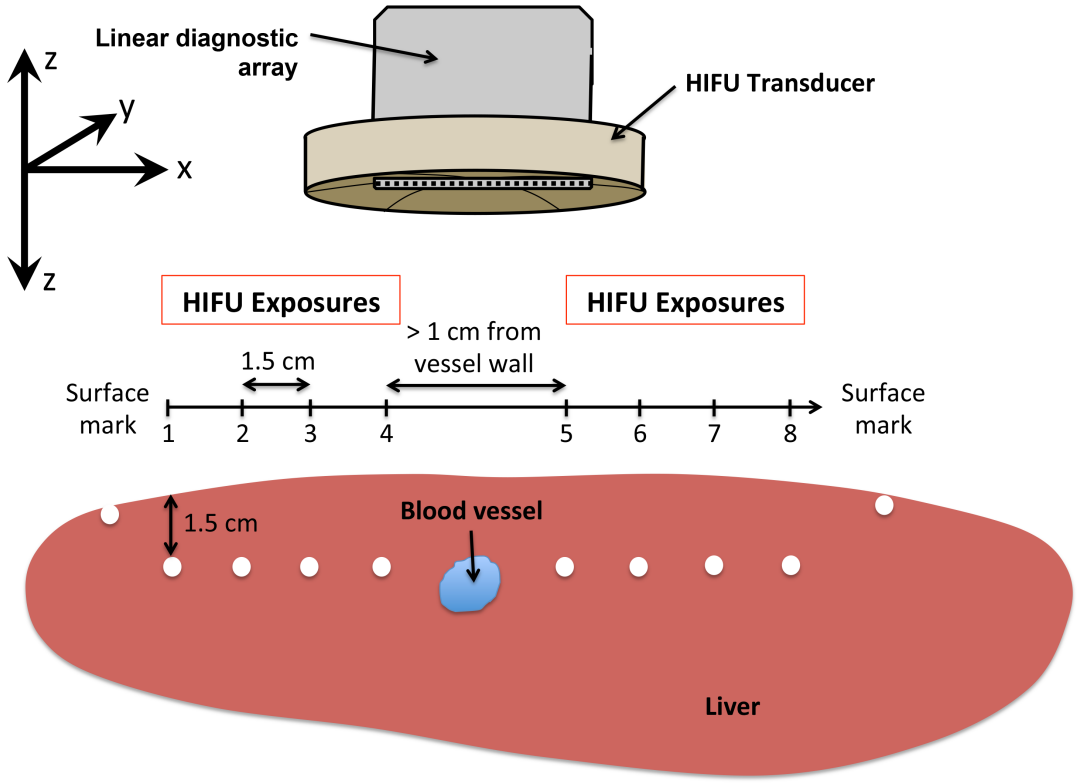


Figure 6.1 *– Schematic diagram showing protocol for lesion threshold studies. The liver was orientated so that 7-8 HIFU exposures could be performed at 1.5 cm intervals along a single axis at a depth of 1.5 cm. Major blood vessels and biliary structures were avoided.*

Following completion of the perfused liver study, the inflow / outflow tracts were clamped and the liver was taken off the perfusion device. The surface marks were used to guide sectioning of the liver with the aim of bisecting the centre of each HIFU exposure location / lesion. Each section was examined for the presence of ablative lesions at each HIFU exposure location.

6.3.4 Volume Ablation Studies

The aim of the volume ablation studies was to determine whether large vasculature (≥ 5 mm) imparts a significant heat sink effect on HIFU ablation at a histological level and if complete tissue ablation can be achieved up to a large vessel wall. In total, 5 isolated perfused livers were used for the studies in this section of work.

Each liver was examined using a hand held linear 5 – 14 MHz diagnostic ultrasound probe in order to delineate and characterize the vascular anatomy, in particular identifying blood vessels ≥ 5 mm. Additionally, the type of vessel (HPV, HV or HA) was checked by sequential brief occlusion of each inflow /outflow tract, with monitoring of vessel flow by colour Doppler. In contrast to the thermal response studies in Chapter 4, only tissue regions adjacent to large (≥ 5 mm) blood vessels were targeted for the studies described in this phase.

The HIFU transducer was aligned with the vessel identified using the handheld ultrasound probe, so that the vessel lay in cross section relative to the mounted linear diagnostic array. Vascular confluences and bifurcations were avoided. The vessel diameter was calculated using B-mode ultrasound and flow velocities were measured and recorded using colour Doppler.

Following the preliminary lesion threshold studies that determined the peak rarefactional pressure and exposure duration require for ablative lesion formation, the HIFU parameters selected for the volume ablation Raster scans were as follows:

Frequency	1.06 MHz
Exposure duration	5 s
Peak rarefactional pressures (MPa $_{Pk-}$)	6.77 MPa
Duty cycle	100%

Table 6.1 – HIFU parameters for volume ablation studies. The peak rarefaction pressure used is within the range of peak rarefaction pressures used for clinical HIFU ablation currently (Dubinsky et al., 2008, Ritchie et al., 2013)

A 5 x 3 Raster scan composed of 15 individual HIFU exposures, with a lateral spacing of 3 mm (*x*-axis) and vertical spacing of 7 mm (*z*-axis) was performed (see *Figure 5.2*), so that approximately half of the vessel in cross section was included within the treatment volume.

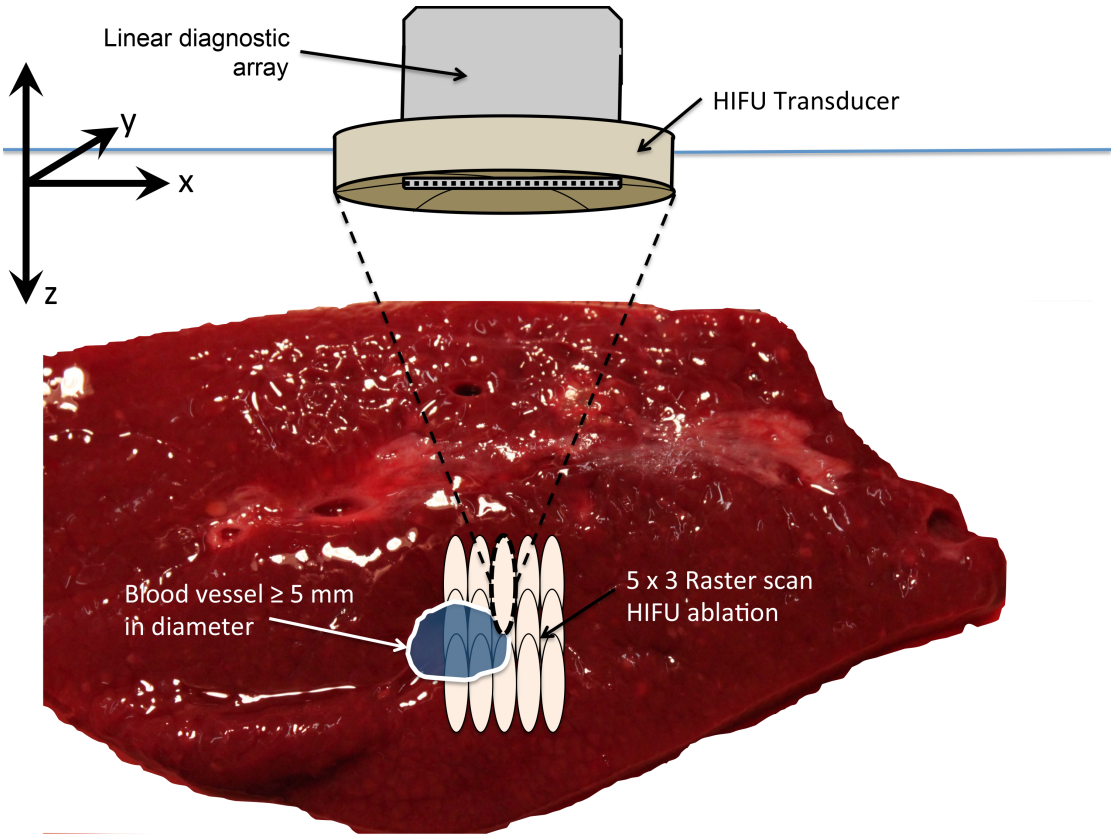


Figure 6.2 *– Diagram showing 5 x 3 Raster scan ablation of a perivascular volume of hepatic parenchyma. The liver was orientated so that the vessel was seen in cross section relative to the ultrasound image from the mounted linear diagnostic array. Each cream coloured oval represents a 5 s, 6.77 MPa $_{Pk-}$ HIFU exposure at 1.06 MHz. The scan was performed so that approximately half of the vessel was included within the targeted volume.*

During each HIFU exposure, real time B-mode imaging acquired using the coaxially aligned L10-5 diagnostic array permitted visualisation of hyperecho appearance, which is being used in current ultrasound-guided HIFU systems as a positive indicator of lesioning(Wu et al., 2004). After each attempted volume ablation, surface markers were placed 1 cm proximal and distal to the transverse axis of the Raster scan in order to identify the targeted location for post-perfusion sectioning. Marker lesions were formed by placing the HIFU focus at the liver surface and then performing a 10 s 7.74 MPa $_{Pk-}$ HIFU exposure to create a surface lesion. It was checked that hyperecho on B-mode ultrasound post HIFU exposure was visualized in order to ensure that a marker lesion had been formed.

Multiple volume ablations were performed in each perfused liver (up to 3 in total). A distance of ≥ 3 cm was left in between each target location to avoid interference and to allow for subsequent sectioning of the liver.

6.3.5 Gross Histopathology

Following completion of all HIFU exposures, the perfusion device was turned off after a period of at least 2 hours, the inflow / outflow tracts to and from the liver were clamped

and the liver was removed from the perfusion circuit. The surface markings identifying the position of the HIFU ablations were located and the liver was sectioned at 5 mm intervals so that the plane of sectioning ran parallel to the long x-axis of each volume ablation. Photographs of each section were taken and slices were tagged and labeled for future identification and reference. When an ablative lesion was located, the dimensions of the lesion were measured and particular attention was given to the area directly adjacent to any vasculature in close proximity to assess whether any potentially viable tissue remained adjacent to the vessel wall.

Snap freezing of living cells or tissue rapidly halts all metabolic processes within the specimen, preventing further degradation of the sample of interest. Given that the aim of subsequent histological studies was to assess cell viability / death within the expected HIFU lesion, tissue samples were therefore snap frozen as quickly as possible following the termination of perfusion preservation. In order to snap freeze tissue samples they were immersed in liquid nitrogen for 2 minutes, removed, wrapped in cling film and were stored at - 70 ˚C until required for cryosectioning.

6.3.6 Frozen Sectioning Technique

Snap frozen tissue samples were removed from the – 70 ˚C freezer and kept on dry ice at all times during the embedding procedure. Tissue samples were placed in optimal cutting temperature compound (OCT; Fisher Scientific, Loughborough, UK) on metallic cryotome chucks precooled to – 70 ˚C. Once the OCT had solidified and the tissue sample was fully embedded, the chuck and mounted specimen were transferred to

the cyrotome cutting chamber, which was maintained at a temperature – 21 ˚C. A Bright Instruments cryotome (OTF 5000; Bright Instruments, Cambridge, UK) was used to section the OTC-embedded specimens at 20 μm intervals. Sections were mounted on glass microscope slides (Ultrafrost; Thermo Scientific, Loughborough, UK) and stored at -70 ˚C until ready for staining.

6.3.7 Histological Assessment of Tissue Viability Following Ablation

Thermally mediated tissue ablation occurs when a temperature in excess of 55 ˚C is reached and maintained for > 1 second. However, in practice, the temperature attained at the focus of the target tissue volume during thermal ablation is often significantly higher than this and are maintained for longer periods of time. In RFA therapy, boiling frequently occurs, followed by tissue desiccation in the region adjacent to the RFA probe. However, the rate of tissue heating and the peak tissue temperature decreases rapidly as a function of distance from the probe, particularly when a heat sink exists e.g. from a large blood vessel.

In the desiccated areas, architectural tissue changes may be seen on haematoxylin and eosin (H&E) staining. However, in tissue regions where the temperature does not exceed boiling point, yet is in excess of the threshold required for thermally mediated cell death, histological changes are frequently absent on H&E staining as the temperature reached is not sufficiently high to cause architectural changes, yet high enough for cellular death to occur. Additionally, architectural changes associated with tissue necrosis usually take at least 24 – 48 hours to develop following thermal ablation. Therefore, early H&E

histological examination of ablative lesion specimens obtained immediately post-procedure may not demonstrate any differences between normal, viable tissue and thermally ablated tissue, with the ablated tissue failing to show any characteristic changes associated with necrosis.

6.3.8 NADH Staining

Nicotinamide adenine dinucleotide (NADH) is a coenzyme that is present in the cellular mitochondria and cytoplasm and is critical to a number of oxidation-reduction (redox) reactions within cellular metabolic cascades. In particular, it is an integral coenzyme in the Kreb's cycle, glycolysis pathway and in aerobic / anaerobic respiration. The intracellular enzyme, NADH diaphorase, catalyses the reduction of various substrates through the transfer of electrons from NADH. The products of this redox reaction are NAD^+ and the reduced substrate. However, NADH diaphorase activity only occurs in viable cells and it has been demonstrated that it becomes inactive within 2 hours following cell death (Anderson et al., 2007). Staining for NADH diaphorase activity, therefore, may avoid the problems associated with routine histological H&E staining of acutely ablated tissue.

Nitro blue tetrazolium (NBT) can be used as a substrate for the NADH redox reaction. In its oxidized form, NBT is a colourless compound but forms a blue coloured diformazan on reduction and can therefore be used as a semiquantitative, colourimetric assay to assess a redox reaction. When used as a histological stain or as an assay of cellular viability, reduction of NBT, catalyzed by NADH, only occurs in metabolically active

cells. Therefore, cells staining dark blue following NADH staining with NBT indicate viability, whereas non-viable, dead cells remain unstained and colourless in appearance. The characteristic appearances of dead / live cells after thermal ablation, when stained for NADH activity are shown below in *Figure 6.3*.

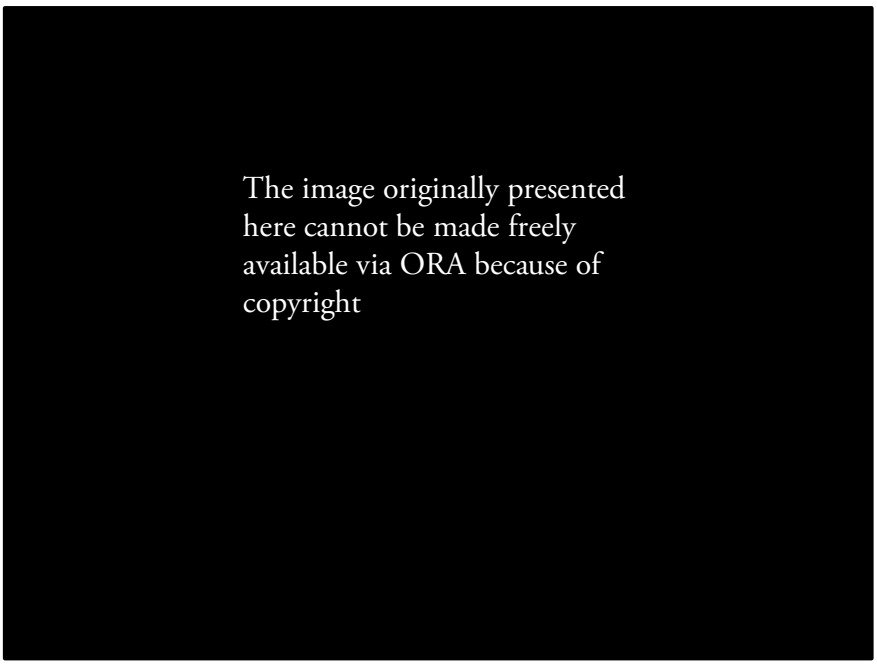


Figure 6.3 – *NADH staining following HIFU ablation. The ablative zone (A) remains pale and does not exhibit any blue staining, whilst the transition zone demonstrates positive staining for NADH activity, appearing dark blue in colour (Luo et al., 2009).*

NADH staining was performed on snap-frozen tissue specimens that had been sectioned and mounted on microscope slides according to the following protocol:

Materials

β-nicotinamide adenine dinucleotide disodium salt (NADH; Sigma, UK)

Saline (see *Appendix*)

Phosphate buffer (see *Appendix*)

Nitro blue tetrazolium (NBT) solution (see *Appendix*)

Aqueous mounting medium (Sigma, UK)

1) The incubation medium was prepared by combining 5 mg of NADH, 2 ml of distilled water, 1 ml of saline, 1 ml phosphate buffer and 4 ml NBT solution.
2) The frozen sections, mounted on glass microscope slides, were removed from the – 70 ˚C freezer and placed in a humidity chamber. Approximately 0.5 - 1 ml of incubation medium was carefully pipetted onto each section so that it completely covered the tissue. The sections were incubated for 30 minutes at 37 ˚C, following which they were rinsed gently with distilled water.
3) A drop of aqueous mounting medium was placed onto each tissue section and a glass coverslip was applied, carefully excluding air bubbles.

Sections were examined using an inverted bright light microscope (Eclipse Ti-E; Nikon, Japan) at 4 x, 10 x and 20 x magnification, which could also be used to acquire still digital images.

6.3.9 Ethidium Homodimer-1 Staining

Ethidium homodimer-1 (Ethd-1) is a high affinity, nucleic acid stain, which binds to cellular DNA. It is only weakly fluorescent until bound to DNA, at which point it produces a bright red fluorescence, with excitation / emission wavelengths of 528 nm / 617 nm. Ethidium homodimer-1 is membrane-impermeable and is unable to cross the intact plasma membrane boundary of healthy, live cells, and is hence unable to bind to

the intracellular DNA. Therefore, healthy cells do not exhibit fluorescent ethidium homodimer-1 staining. However, following cellular death, the plasma membrane becomes disrupted, allowing membrane-impermeable molecules to cross into the intracellular compartment. Ethidium homodimer-1 is able to bind to intracellular DNA contained within dead cells and these cells exhibit positive fluorescence within the excitation/emission range for ethidium homodimer-1. Unlike TUNEL staining, which only marks cells that have undergone apoptosis, ethidium homodimer-1 stains all dead cells, whether they have died through apoptosis or necrosis.

6.3.10 Immunofluorochemistry

Immunofluorescence staining uses antibodies labeled with fluorescent markers to detect specific antigens within a tissue or cell sample. Either a direct method, where a fluorophore is conjugated to a primary antibody specific to the antigen of interest, or an indirect method, where the fluorophore is instead conjugated to a secondary antibody specific to the species of the primary antibody, can be used (*Figure 6.4*). A number of fluorophores are available, which have different excitation and absorption frequencies, thus enabling multiple fluorophores to be used on the same sample at one time.



Figure 6.4 – *Indirect immunofluorescence using a primary IgG antibody to the specific antigen target e.g. mouse anti-Caspase-3, and a fluorophore-conjugated secondary antibody to the species of the primary antibody, e.g. FITC-conjugated donkey anti-mouse. (Odell and Cook, 2013)*

6.3.11 Assessment of Apoptotic Activity

Whereas necrosis occurs due to an acute cellular injury, leading to traumatic and rapid cellular death, apoptosis is the process of programmed cell death, which occurs as part of the normal cell life cycle, but can also be induced as a result of sublethal cellular stress. Apoptosis provides an innate protective mechanism by effecting controlled death in cells that have unrepaired damage to cellular DNA, thus reducing the risk of potential tumourigenesis. Approximately 50 to 70 billion cells within the human body undergo apoptosis each day.



Figure 6.5 *– Apoptotic cell signaling pathways (Xu and Shi, 2007). Caspase-3, once of the "effector caspases", is activated by both the intrinsic (mitochondrial) and extrinsic (death ligand) apoptotic pathways.*

A number of markers can be used to detect cells undergoing apoptosis. Caspase-3 is activated in cells undergoing apoptosis by both the extrinsic (death ligand-receptor) and intrinsic (mitochondrial) pathways (*Figure 6.5*). Death ligand-receptor binding, initiating the extrinsic pathway, triggers the caspase cascade, initially through activation of caspase-8. Initiation of the intrinsic pathway activates caspase-3 via cytochrome-c, Apaf-1 and caspase-9. In healthy cells, phosphatidylserine is predominantly located on the cytosolic surface of the plasma membrane. However, on initiation of the apoptotic pathway, phosphatidylserine translocates to the extracellular membrane. Annexins are calcium-dependent phospholipid binding proteins that bind to phosphatidylserine but

do not cross the cell membrane. As such, they can be used to mark cells undergoing apoptosis expressing extracellular phosphatidylserine.

In order to assess apoptotic activity within and outwith the HIFU ablative lesions, immunofluorochemistry was performed on snap frozen tissue samples, which had been sectioned using a cryostat, according to the protocol described in Section 6.3.6 and stored at – 70 ˚C.

Immumofluorochemistry was performed according to the following protocol:

Materials

Acetone (Sigma, Gillingham, UK), stored at – 20˚C

20X PBS (see *Appendix 2*)

1X PBS (see *Appendix 2*)

Blocking buffer in PBS (see *Appendix 2*)

Primary antibody – rabbit polyclonal anti-pig caspase-3 (Abcam, Cambridge, UK)

Secondary antibody – goat anti-rabbit IgG, FITC conjugated (Abcam, Cambridge, UK)

Slide rack

Wash container x 3

Humidifying chamber

Cover slips (Fisher, UK)

Hydrophobic pen (ImmEdge; Vector Laboratories, Peterborough, UK)

Mounting medium containing DAPI (VectaShield; Vector Laboratories, Peterborough, UK)

1) Tissue was initially fixed and permeabilised using acetone. Slides were removed from the – 70 ˚C freezer, inserted into a slide rack, placed in a bath containing acetone cooled to – 20 ˚C and left for 10 minutes.
2) After 10 minutes, the slides were removed, placed on paper towels and were allowed to air dry for 15 minutes. When dry, a hydrophobic barrier was drawn around the tissue sections using an ImmEdge pen
3) Slides were washed in PBS for 5 minutes and repeated three times. Following this, the slides were removed from the rack, blotted dry using paper towel and placed in a humidifying slide chamber.
4) Tissue sections were covered in blocking buffer and incubated in the humidified chamber at room temperature for 1 hour. After this period, the slides were washed in PBS for 5 minutes, three times, using fresh PBS for each rinse.
5) Slides were dried on tissue paper, placed back in the humidifying chamber, primary antibody was pipetted onto the tissue section and then incubated overnight at 4 ˚C. The slides were then washed again in fresh PBS for 5 minutes, three times, using fresh PBS for each rinse.
6) Secondary antibody was added to each section and the slides were incubated in the humidifying chamber, which had been wrapped in aluminum foil to shield the tissue sections from light, for 1 hour at room temperature.
7) Slides were washed in PBS for 5 minutes, three times, using fresh PBS on each occasion and then blotted dry on tissue paper
8) Three drops of DAPI-containing mounting medium was pipetted onto each tissue section and a coverslip was placed on top, attempting to exclude all air bubbles.

9) Slides were left to dry for 30 minutes in the dark and then the tissue specimens were examined using a fluorescent microscope (Eclipse Ti-E; Nikon, Japan) with a FITC/TRITC filter at 4 x, 10 x and 20 x magnification, which could also be used to acquire still digital images. FITC has an excitation and emission spectrum peak wavelength of approximately 495 nm / 519 nm.

Negative controls were performed, where the primary antibody was omitted and the tissue sample was incubated in 1 x PBS instead. Lymphoid porcine tonsillar tissue was used for positive controls.

6.4 Results

In total, 7 isolated, perfused porcine livers were used for the work described in this chapter.

6.4.1 Preliminary Lesion Threshold Studies

Preliminary studies were performed in order to assess the acoustic power threshold needed to achieve visible lesion formation and to determine the HIFU exposure parameters for the subsequent volume ablation studies. Although cell death may occur without a visible lesion forming at the HIFU focus, macroscopic lesion formation was sought in order to identify the HIFU focus on sectioning for subsequent histological studies.

Liver parenchyma away (> 1 cm) from major vascular or biliary structures, at a depth of 1.5 cm below the liver surface was targeted following identification using B-mode ultrasonography and colour Doppler. A series of single HIFU exposures at various peak rarefactional pressures and exposure durations was performed in order to assess the HIFU parameters required for visible lesion formation. A visible ablative lesion was seen following 6 s HIFU exposures with a PRFP of 4.84 MPa and above (*Figure 6.6*). No lesions were seen at 2.91 and 3.88 MPa, despite longer exposure durations of 10 s. Lesion dimensions increased as a function of PRFP, with lesions formed at 6.77, 7.74 and 8.70 MPa measuring approximately 3 mm x 7 mm in the sectioned liver tissue. However, these dimensions are likely to be significantly greater in the perfused liver tissue as the parenchyma collapses and the liver volume decreases following sectioning.

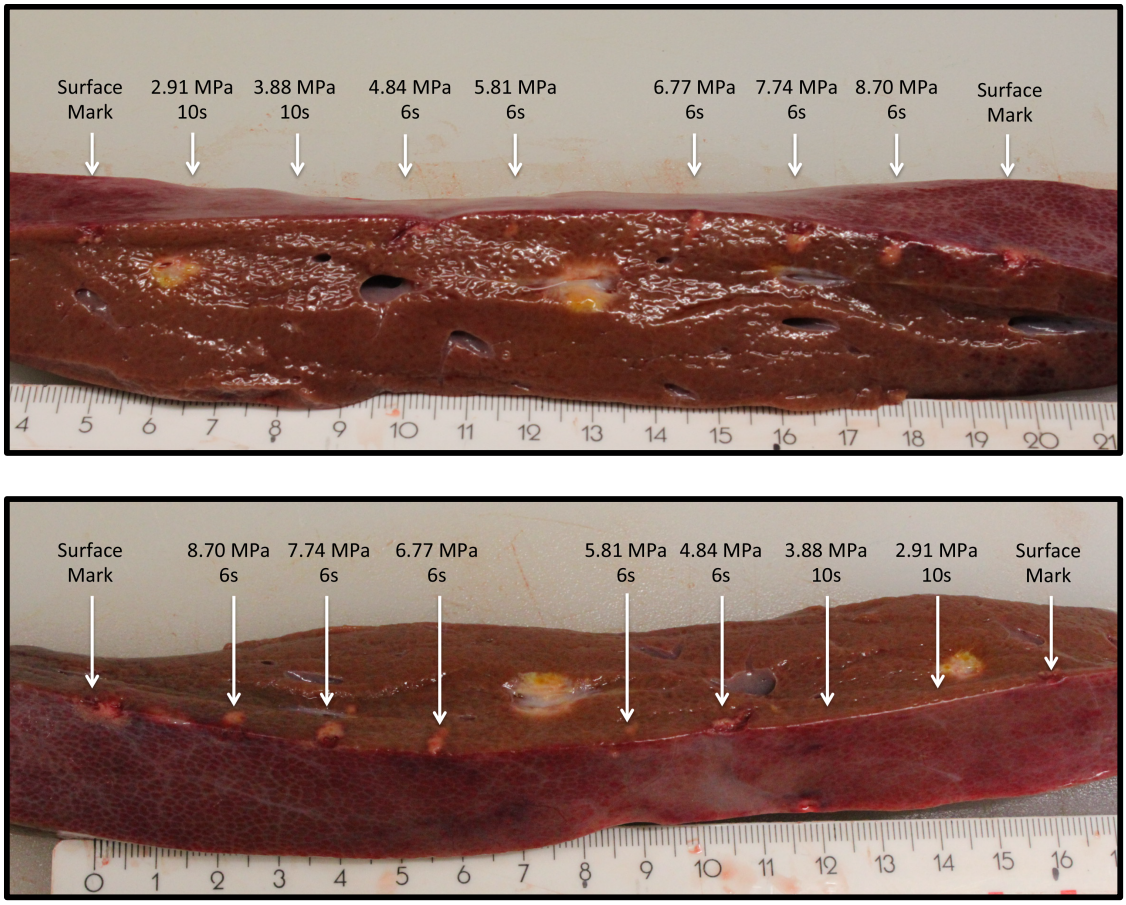


Figure 6.6 *– Gross histology following lesion threshold studies. Single HIFU exposures at a range of PRFPs and exposure durations were performed at a number of locations away from large vasculature. The HIFU focus was placed within the liver parenchyma at a depth of 1.5 cm below the surface of the liver. Visible ablative lesions appear at 4.84 MPa and beyond. A consistently-sized lesion was seen at 6.77 MPa and above.*

Therefore, a peak rarefactional focal pressure of 6.77 MPa, coupled with an exposure duration of 6 seconds, was selected for the subsequent HIFU ablation studies at 1.06 MHz, as these parameters created an ablative lesion consistently, with approximate lesion dimensions corresponding to the expected HIFU focus size after, accounting for hepatic volume loss due to blood loss.

6.4.2 Volume Ablation Studies

In total, 9 large (≥ 5 mm) blood vessels were identified in 5 isolated, perfused livers. Vessel diameters and flow velocities were calculated using B-mode ultrasound and colour Doppler (see *Figures 5.7 and 5.8*). The mean vessel diameter was 7 mm (range 5 to 10), mean flow velocity was 5.3 cm/s^{-1} (range 4 to 7.5 cm/s^{-1}) and of the 9 blood vessels, 7 were portal venous in nature, with the remaining 2 vessels identified as being hepatic venous branches. Tissue locations for subsequent volume ablations were selected away from vascular confluences / bifurcations.

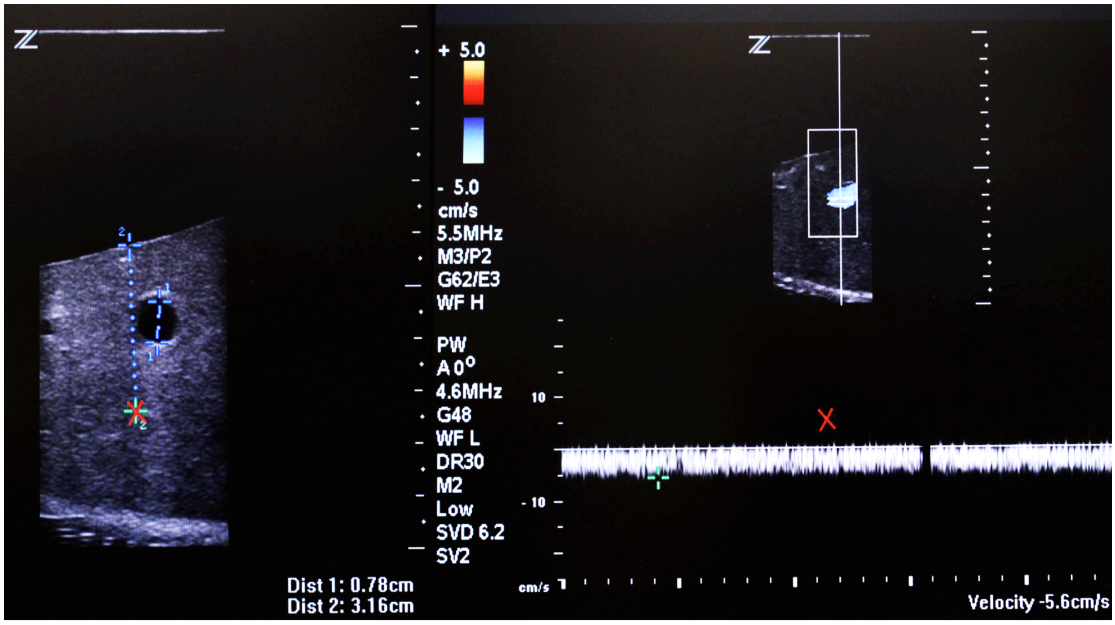


Figure 6.7 *– Measurement of vessel diameter using B-mode ultrasound (L) and subsequent quantification of flow velocity using colour Doppler (R).*

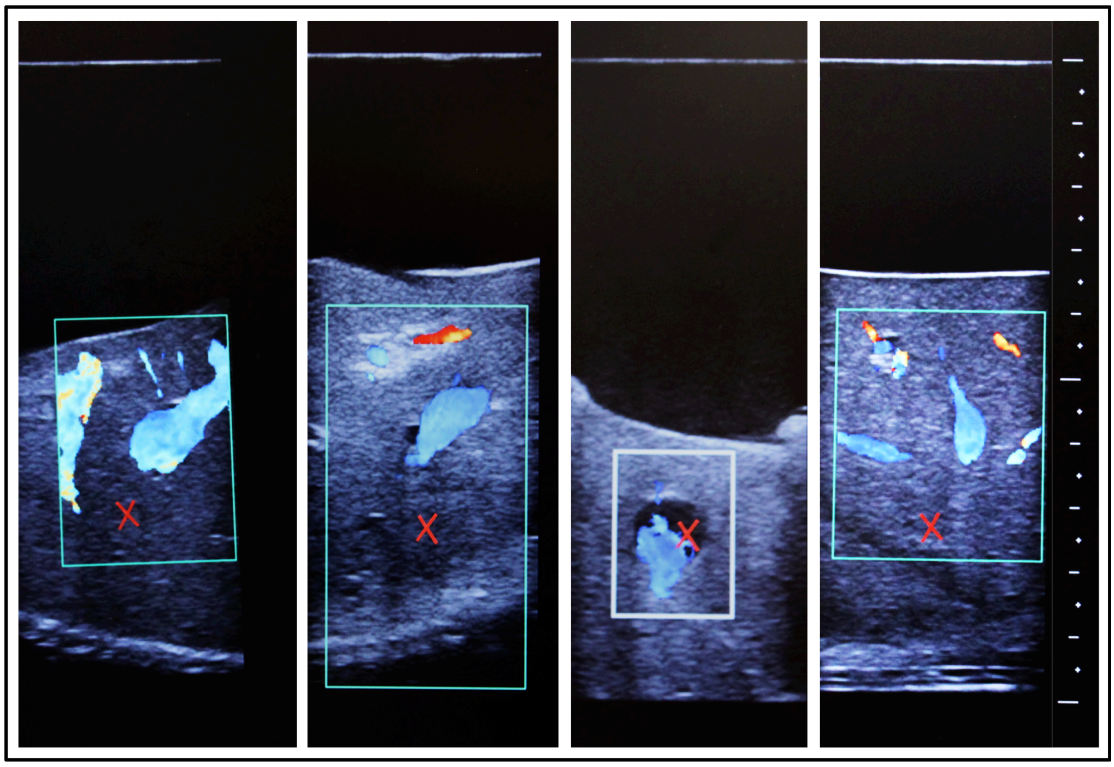


Figure 6.8 *– B-mode images of 4 individual large vessels locations with colour Doppler, assessing vessel flow rates.*

Once the vessel adjacent to the planned HIFU treatment volume had been characterised, a raster scan of 5 x 3 HIFU exposures was performed as described in section xx, in order to ablate a volume of approximate dimensions of 17 x 25 x 3 mm. Real time B-mode imaging during HIFU ablation allowed visualisation of lesion formation through the appearance of hyperecho (see *Figure 6.9*).

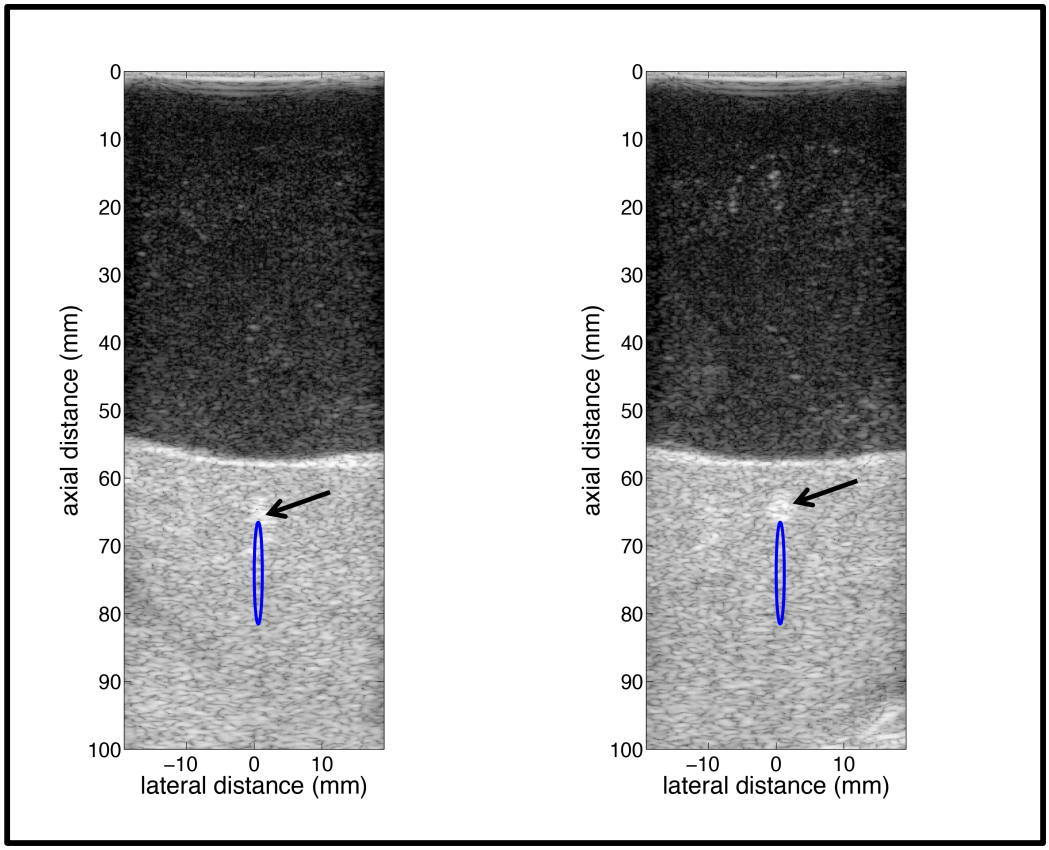


Figure 6.9 *– Hyperecho formation during HIFU exposure. The blue ellipse represents the expected HIFU focus and the black arrow points to the area of hyperecho (white) on real time B-mode imaging during HIFU exposure.*

Following termination of perfusion preservation, each liver was sectioned immediately using the surface markers to identify lesion position. The livers were dissected so that the blood vessels and long-axis of the ablative lesion appeared in cross section, using the previously placed surface marker lesions as a guide. Each lesion was examined macroscopically and then snap-frozen for subsequent histological studies. Photographs displaying the macroscopic appearance of 4 representative ablative lesions are shown below in *Figures 6.10 and 6.11*.

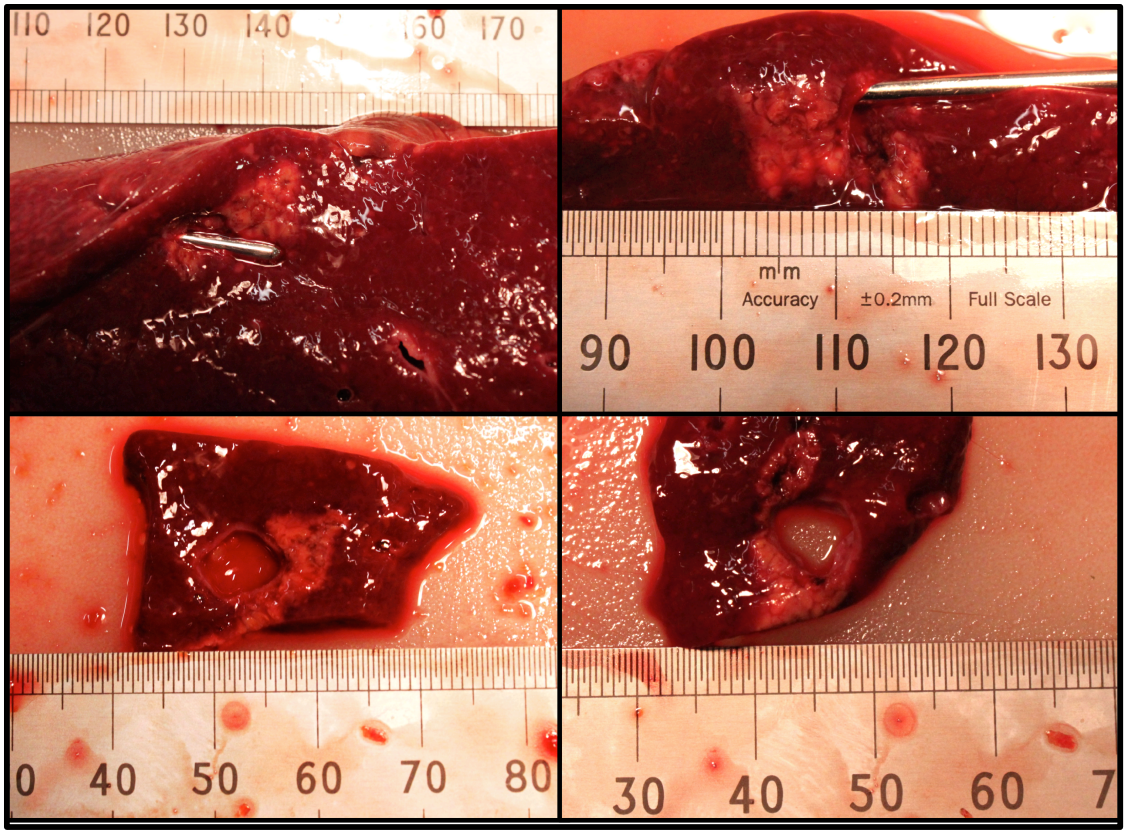


Figure 6.10 *– Macroscopic appearance of 4 perivascular HIFU lesions. In all cases (n=8) the ablative lesion appeared to extend right up to the vessel wall, with no sparing of tissue at the vessel wall – tissue interface.*

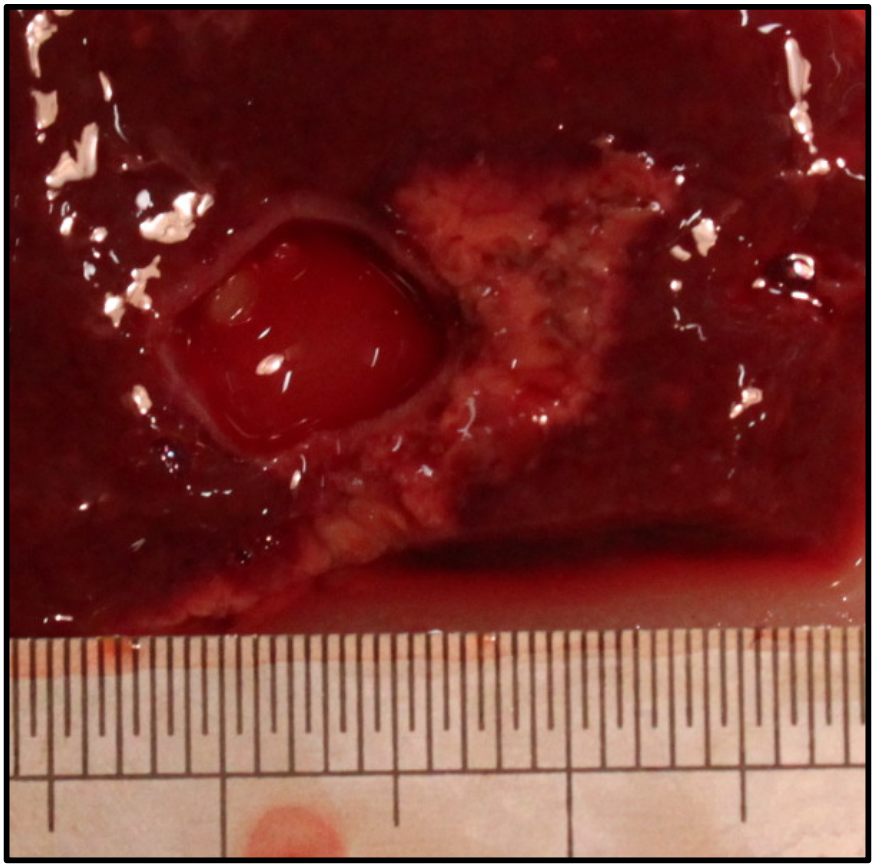


Figure 6.11 *– Close up appearance of a perivascular HIFU lesion. There does not appear to be viable tissue remaining between the ablative lesion and the vessel wall, with the cream coloured ablative lesion seemingly extending up to the vessel wall.*

In all cases, the cream coloured ablative lesion appeared to extend up to the vessel, with no spared tissue at the vessel wall – tissue interface (*Figure 6.11*). The measured dimensions of each lesion were smaller than those predicted by the HIFU transducer co-ordinates and those calculated from the B-mode images acquired during liver perfusion. However, lesion geometry in the sectioned liver was greatly affected by the ≈ 50 – 75% reduction in liver volume resulting from blood loss during sectioning, leading to collapse of the hepatic parenchyma. Mean lesion dimension was 9 mm x 15 mm (range 8 – 11 mm x 10 – 17 mm) compared with the expected dimensions of approximately 17 mm x 25 mm.

6.4.3 Assessment of Cell Viability

Frozen sectioning and staining for NADH activity was performed on the same tissue samples containing the HIFU lesions as displayed in *Figure 6.10* and *6.11* showing the macroscopic appearance, together with the vessel and surrounding tissue. These tissue samples had been snap frozen immediately following sectioning and macroscopic examination. Positive control tissue was taken from normothermically perfused porcine livers not exposed to HIFU therapy. Negative control tissue was obtained from porcine liver heated to 60 ˚C for 10 minutes in a water bath.

Results of NADH staining of control tissues are shown in *Figures 6.12* and *6.13*. Positive control tissue demonstrated strong purple NADH staining, signifying the presence of metabolically active, viable cells, throughout the liver parenchyma. The NADH stain also demonstrated the lobular and sinusoidal hepatic structure of the liver well. Fibrotic connective tissue remained unstained within these specimens due to the lack of metabolically active cells within this tissue component. Conversely, in the negative control samples, no staining was observed throughout the hepatic tissue, indicating complete tissue death (*Figure 6.14*).

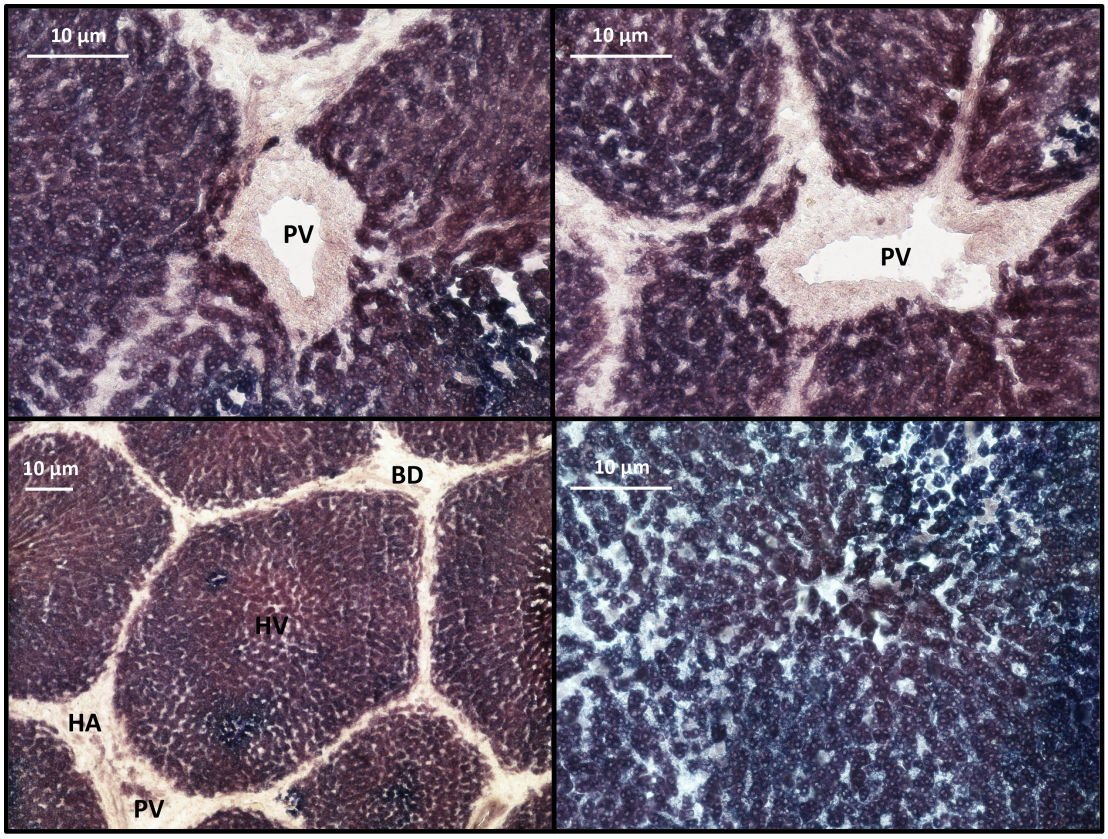


Figure 6.12 *– Positive NADH stain controls. Normothermically preserved liver tissue that had not been subjected to HIFU therapy was snap frozen, sectioned and stained for NADH activity. Metabolically active cells stain dark purple in colour, whilst connective tissue and dead cells remain pale / cream in colour. The hexagonal lobule structure of the liver can be seen in the bottom left section and a fibrotic connective tissue layer surrounds each lobule. An end portal venule (PV), hepatic arteriole (HA) and bile ductile (BD) are present at the apex of each side of the hexagonal lobule and a hepatic venule (HV) is present in the centre of the lobule.*

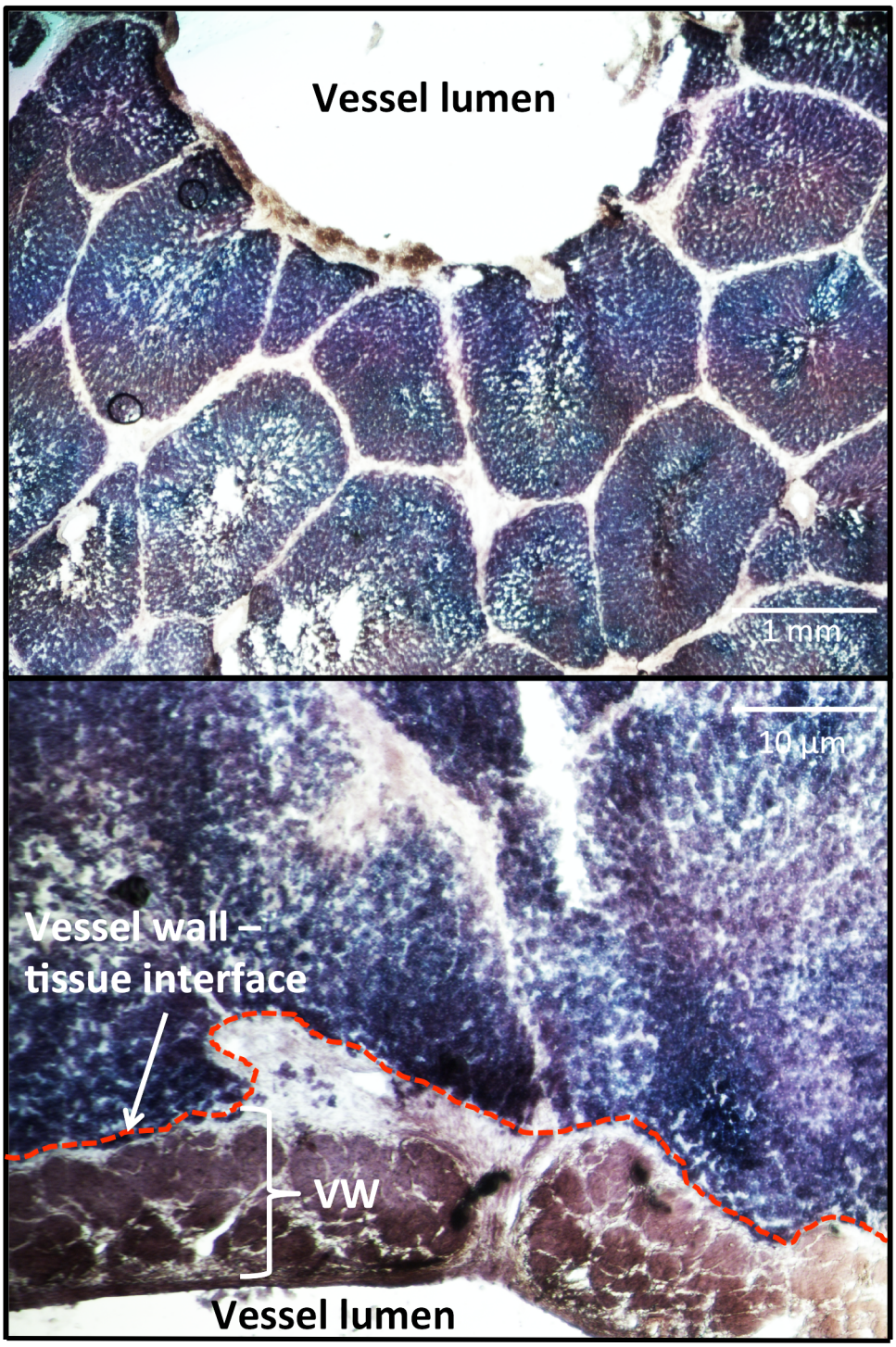


Figure 6.13 *– NADH staining of control liver parenchyma (4 x magnification (top) and 10 x magnification (bottom)), showing metabolically active cells staining dark purple as a result of reduced diformazan production from the NADH-catalysed redox reaction. The dark purple stain extends right up to the connective tissue surrounding the vessel wall (VW).*

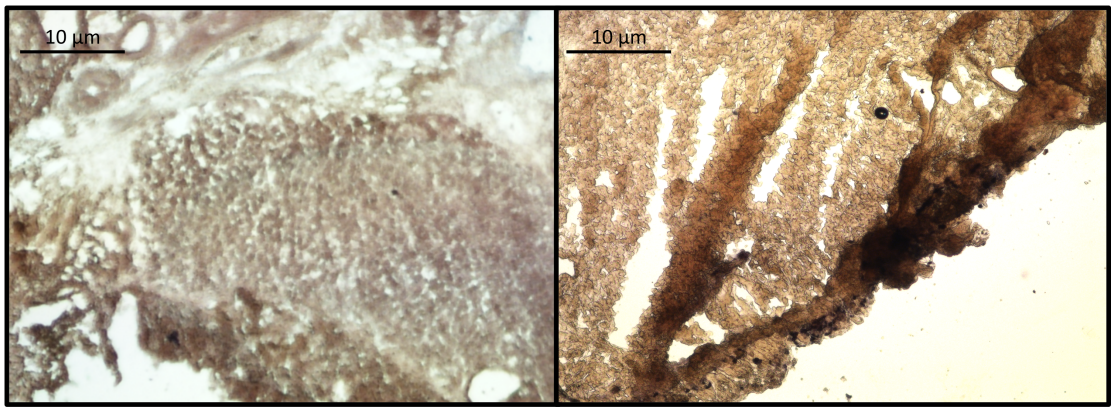


Figure 6.14 – *Negative NADH stain controls. Liver tissue was heated to 60 ˚C for 10 minutes in a water bath and subsequently snap frozen, sectioned and stained for NADH activity. Non-viable or metabolically inactive cells remain pale / cream in colour. No positive NADH staining, indicating the presence of metabolically active cells, were identified in these samples.*

Examination of HIFU lesions (n=9) and surrounding tissue following NADH staining demonstrated strong staining outwith the HIFU ablation zone, similar to that seen in the positive controls. The lesion boundaries were very well defined and demarcated, with a transition from completely viable liver parenchyma to complete necrosis, signified by the lack of any NADH staining, over a distance of 5 – 10 µm (*Figure 6.15*). Within the HIFU lesion, no NADH staining was observed in any of the 8 lesions examined, signifying complete cellular death due to coagulative necrosis.

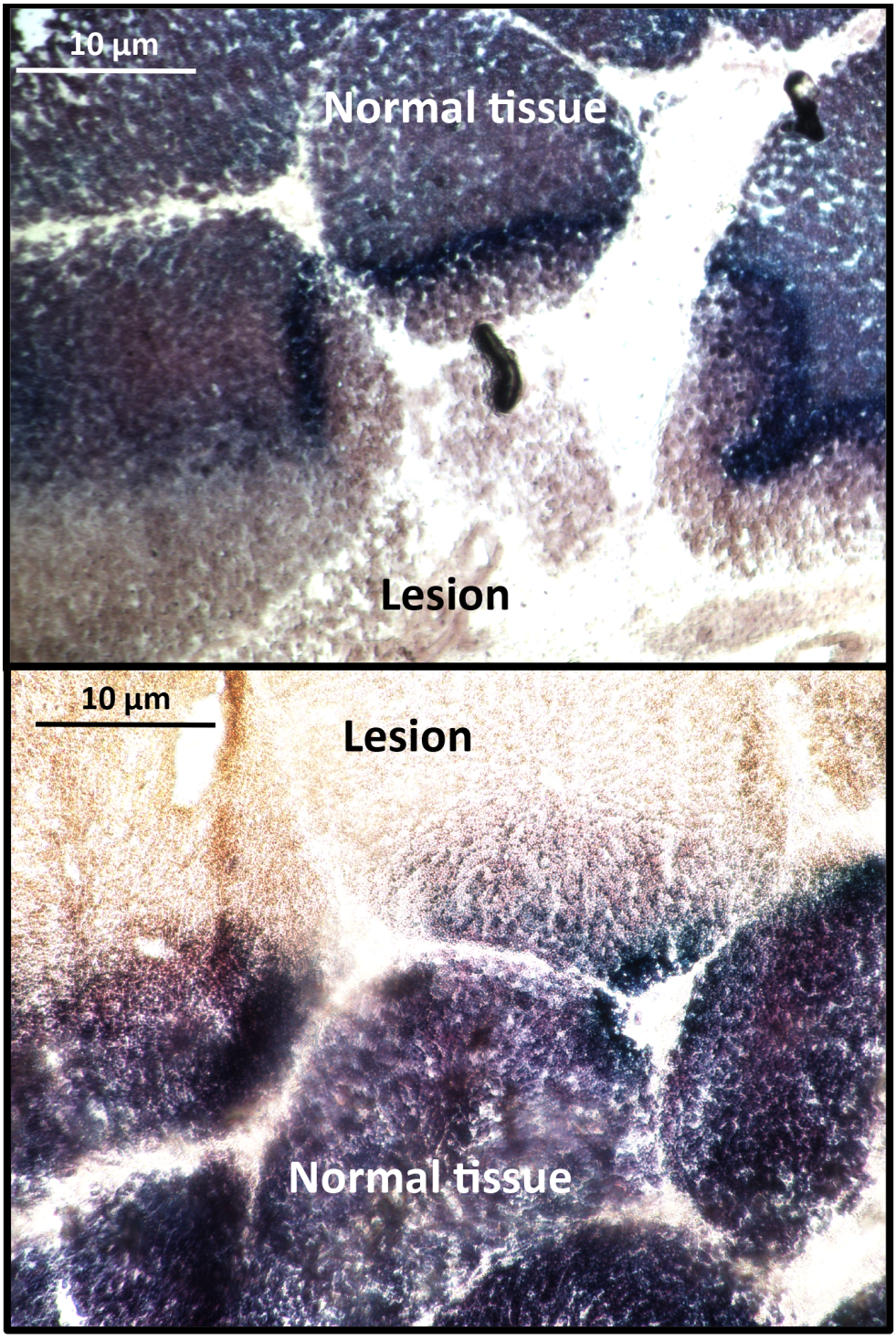


Figure 6.15 *– Micrographs (10 x magnification) showing NADH staining at the HIFU lesion periphery. There is a clearly demarcated transition between ablated tissue, containing necrotic cells (cream) and viable liver parenchyma (purple), demonstrating the accuracy of HIFU ablation.*

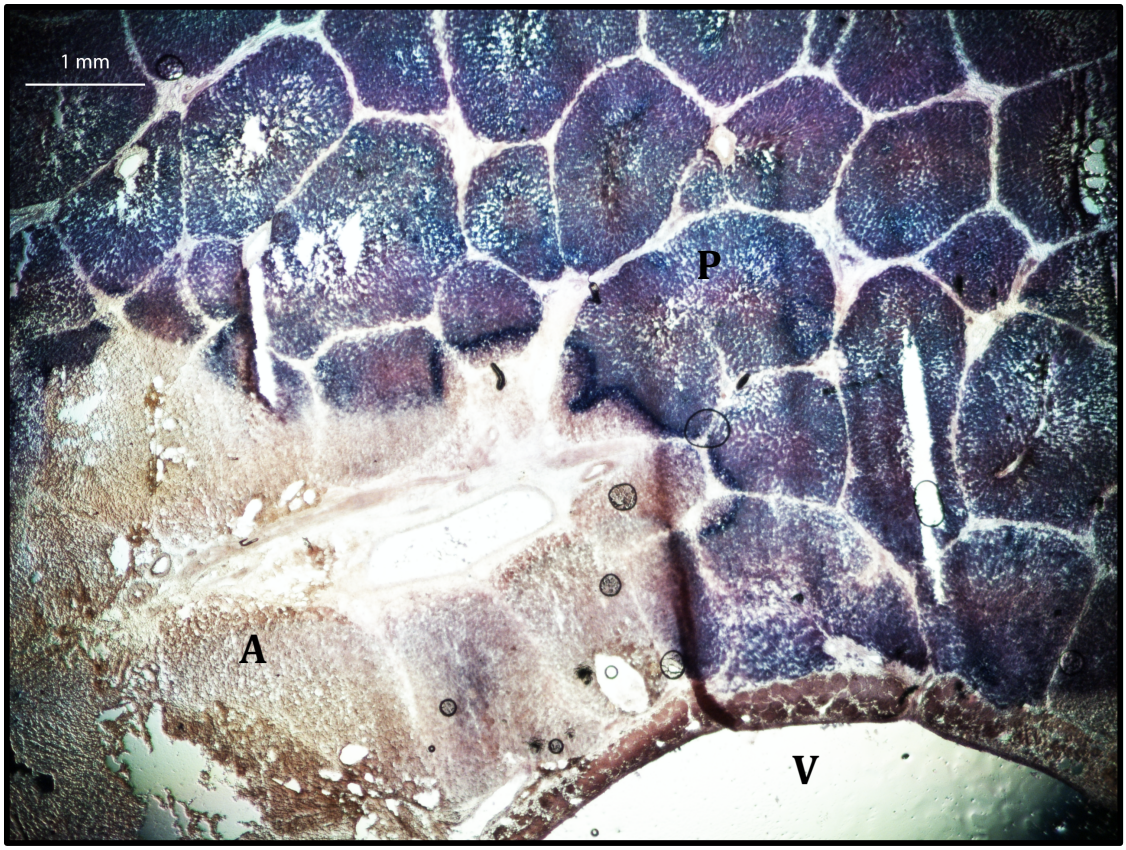


Figure 6.16 – *Image of a NADH stained frozen section of a HIFU lesion adjacent to a large blood vessel (V - bottom right). Viable tissue (P) stains dark purple in colour, whilst non-viable ablated tissue (A) remains unstained and appears cream coloured (4 x magnification).*

Given that cooling due to heat advection from blood flow decreases as a function of distance from the vessel, the cells most susceptible to any heat sink effect are within the tissue present adjacent to the vessel wall interface. Particular attention was therefore paid to this tissue region in all of the sections examined to assess whether there was any microscopic evidence of a significant heat sink effect, in particular if any viable, metabolically active cells remained within this zone. In all specimens, the HIFU lesion extended right up to the vessel wall. No metabolically active cells staining positive for NADH activity were observed at the vessel wall – parenchymal interface in any of the

HIFU lesions. These data are shown below in *Figures 6.17 a* and *b, 6.18, 6.19* and *6.20*.

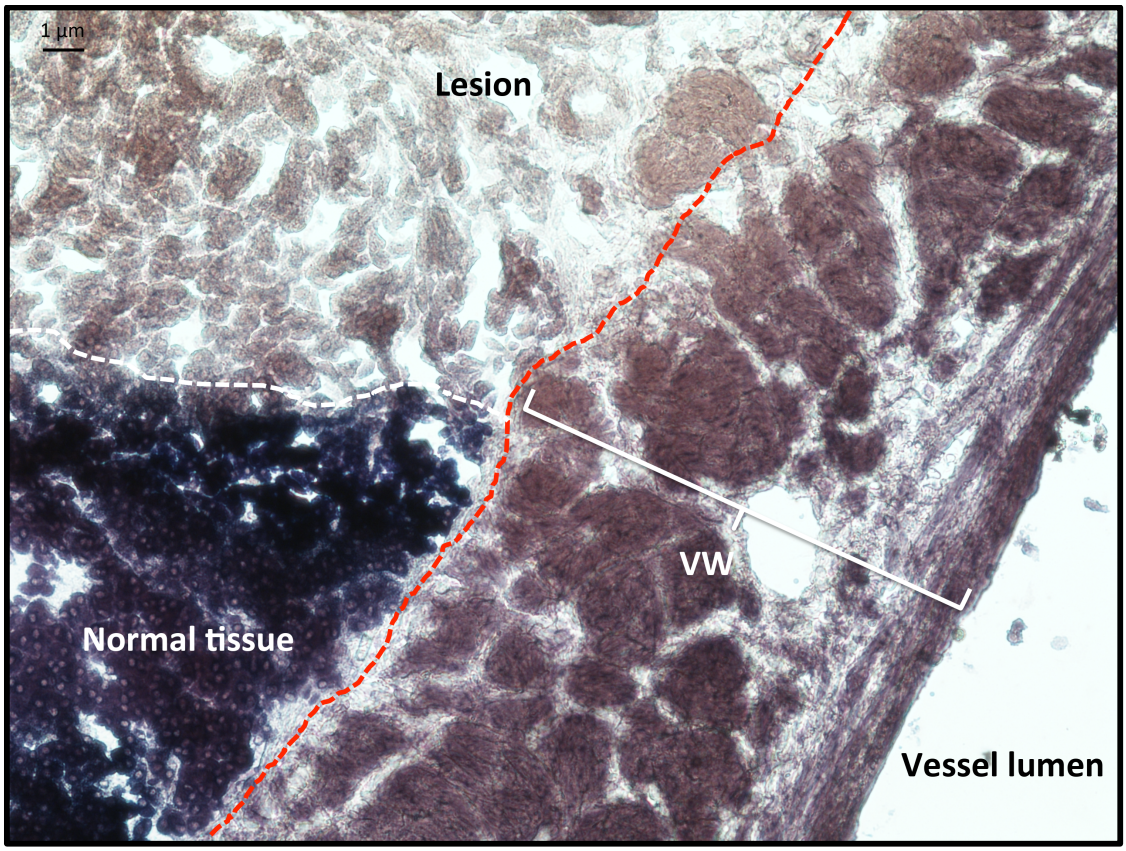


Figure 6.17 a – *NADH staining of tissue adjacent to the vessel wall (VW) at the edge of the HIFU lesion.*

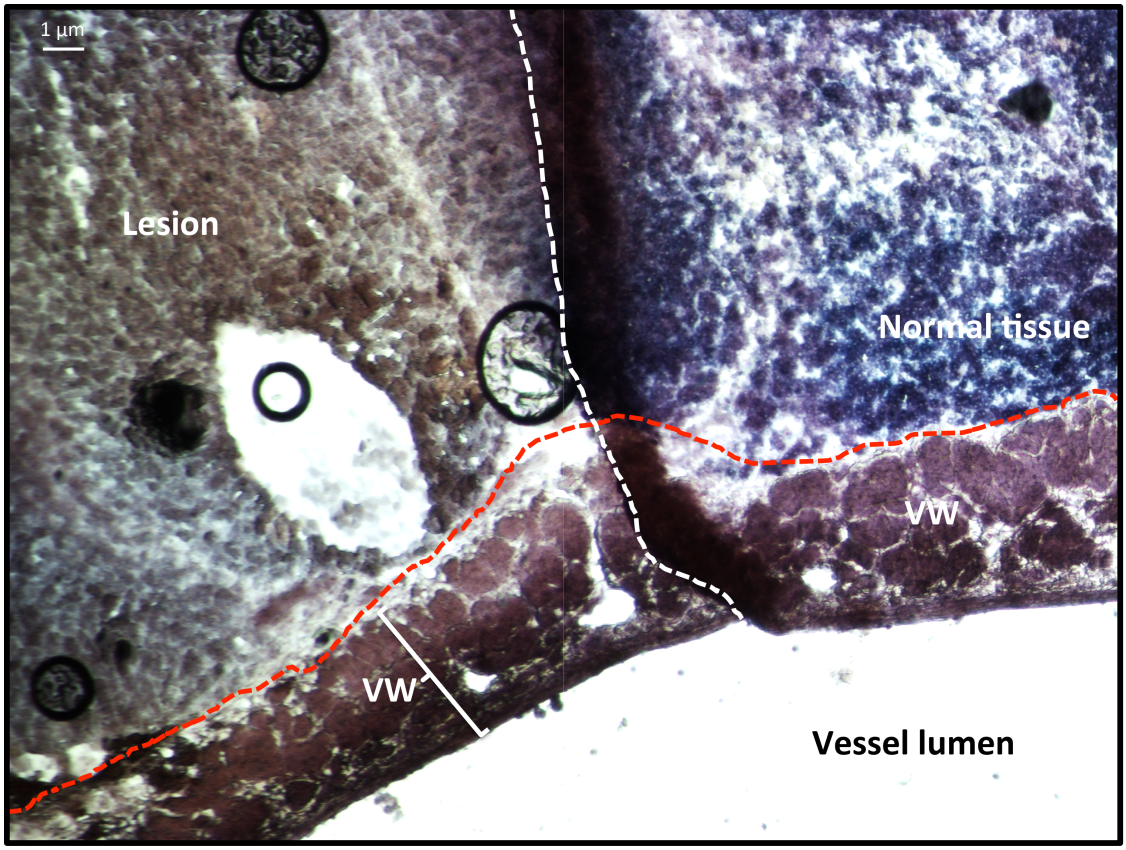


Figure 6.17 b – *NADH staining of tissue adjacent to the vessel wall (VW) at the edge of the HIFU lesion. The red dotted line marks the interface between the vessel wall and the liver parenchyma whilst the white dotted line represents the edge of the HIFU ablative lesion. No viable (purple) cells are seen within the ablated liver parenchyma at the vessel wall interface, compared to the dark purple, viable cells next to the vessel wall outwith the ablation zone. This indicates that complete ablation has occurred right up to the large vessel wall.*

Figures 6.17 a and *b* show the edges of two HIFU lesions at the vessel wall interface. Purple staining extends up to the vessel wall within the region of unablated tissue, similar to that seen in the positive control tissues (*Figure 6.13*). However, no purple stained cells are visible within the ablated region. Examination of the entire vessel wall – HIFU lesion interface did not reveal any purple staining in each of the studies performed (*Figure 6.18 b and d* below).

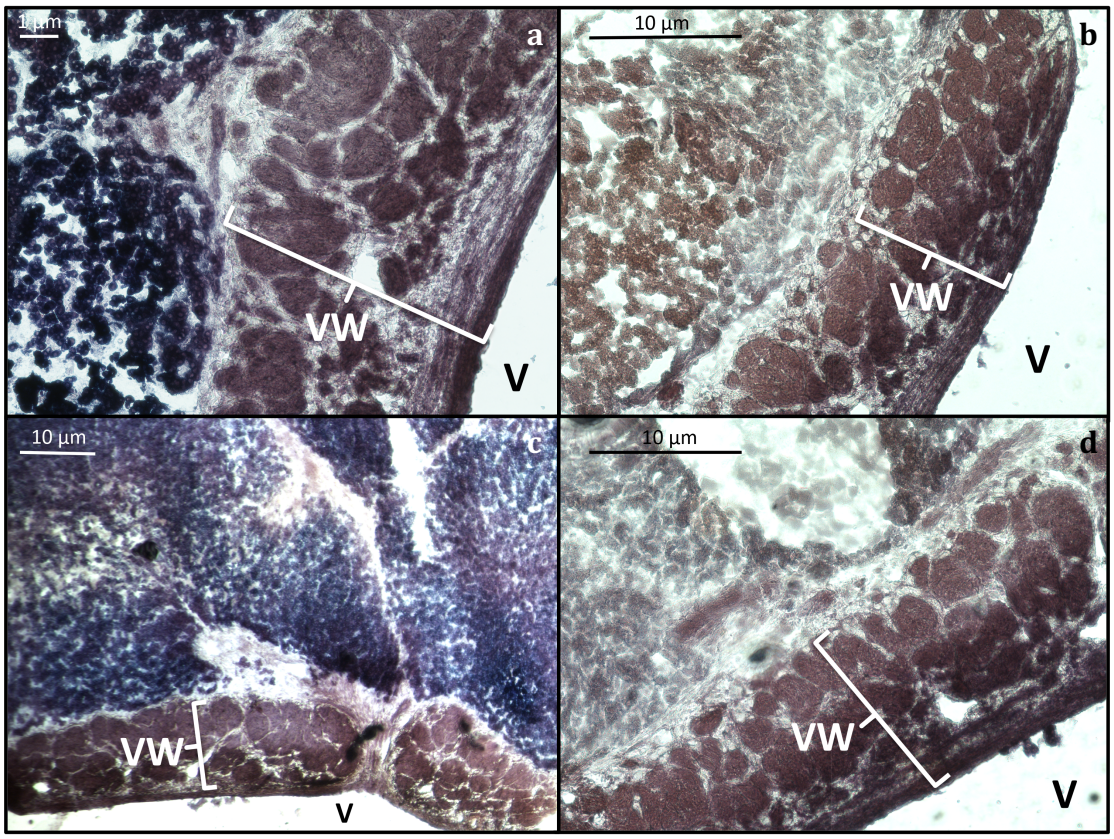


Figure 6.18 *– NADH staining of vessel wall (VW) and perivascular tissue away from the HIFU lesion (a and c) and within 2 separate HIFU lesions (b and d). No metabolically active cells are present at the vessel wall – parenchymal interface within the HIFU lesion and this is signified by the absence of NADH staining in b and d. V = vessel lumen.*

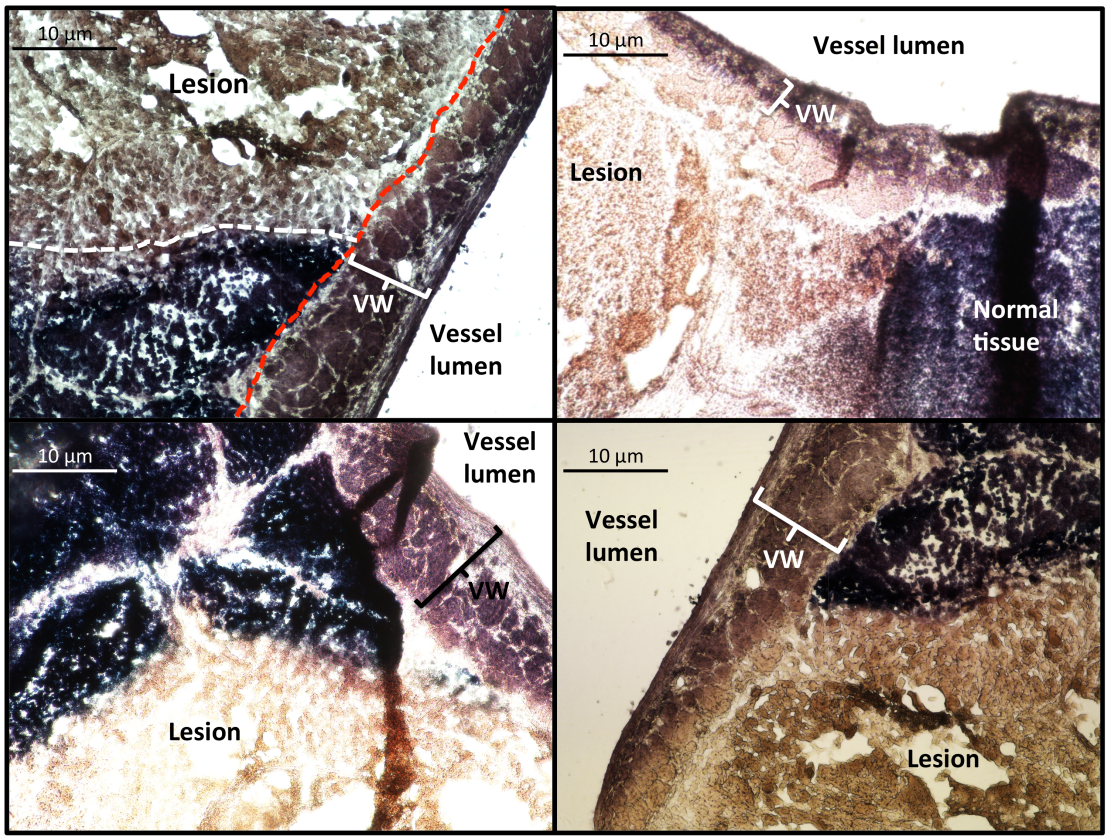


Figure 6.19 *– NADH staining of tissue at the vessel wall interface at the periphery of 4 HIFU lesions. Similar to the lesions in Figure 6.18 b and d, no viable cells were seen within the ablation zone, with tissue necrosis extending right up to the blood vessel wall.*

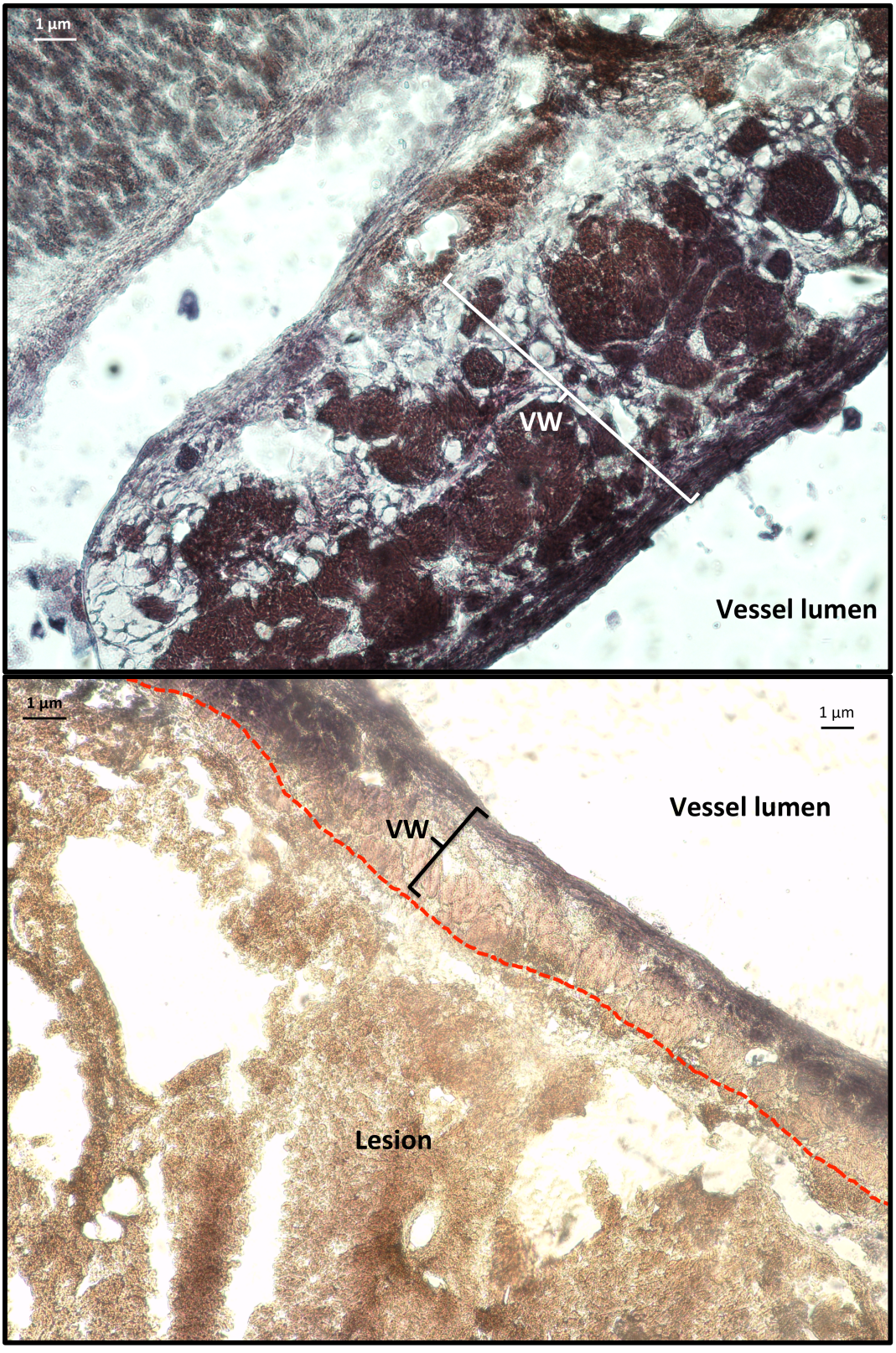


Figure 6.20 *– NADH staining of tissue within the HIFU ablation volume from 2 different lesions, adjacent to a large vessel. Tissue necrosis extends up to the vessel wall (VW) and no viable cells remain.*

In summary, these data demonstrate that complete tissue necrosis due to HIFU ablation can be attained right up to the wall of vessels 5 – 10 mm in diameter and that no viable cells remain within the treated region, particularly at the vessel wall interface, where the heat sink effect is maximal

6.4.4 Assessment of Cell Death

Assessment of cell death using ethidium homodimer-1 (Ethd-1) staining was performed, although cell viability following HIFU ablation is a more useful, relevant metric in terms of the clinical endpoint of these studies. Additionally, NADH staining was performed in order to correlate cell death and cell viability. Ethd-1 fluoresces bright red with excitation / emission wavelengths of 518 / 627 nm. In the negative control tissues (*Figure 6.21*), some background fluorescence was visible within the hepatic parenchyma and some hepatocytes within each liver lobule demonstrated positive Ethd-1 staining.

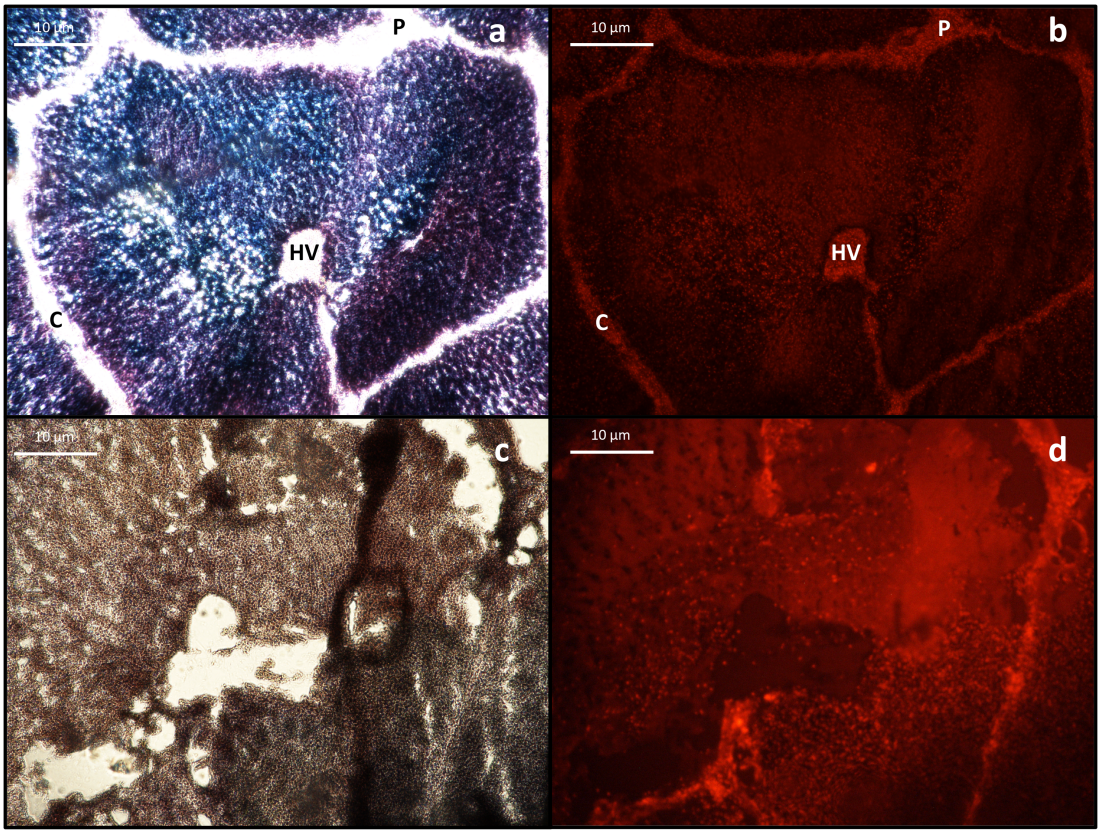


Figure 6.21 *– NADH staining (a and c) and ethidium homodimer-1 fluorescent staining (b and d) of negative control liver parenchyma from untreated normothermically perfused porcine livers (top) and positive control tissue from liver samples heated to 60 °C for 10 minutes in a water bath (bottom). Some background fluorescence is present in the negative controls, particularly within the central hepatic vein (HV), portal triad (P) and connective tissue (C). However, this tissue stains positively for NADH activity, indicating cell viability. The positive control tissue (bottom) displays strong red fluorescence, indicating dead cells, whilst no positive NADH staining is demonstrated.*

Within the negative control tissue, the central hepatic veins, perilobular connective tissue and hepatic triad structures also appeared to fluoresce more strongly than the lobular parenchyma. This may be due to the trapping of dead blood cells within these structures as they are either hollow (central hepatic vein lumen and portal triad structure), or

composed of fibrous connective tissue. Positive control staining exhibited a much higher level of fluorescence within the heated liver parenchyma compared to the negative control tissue (*Figure 6.21 b and d*).

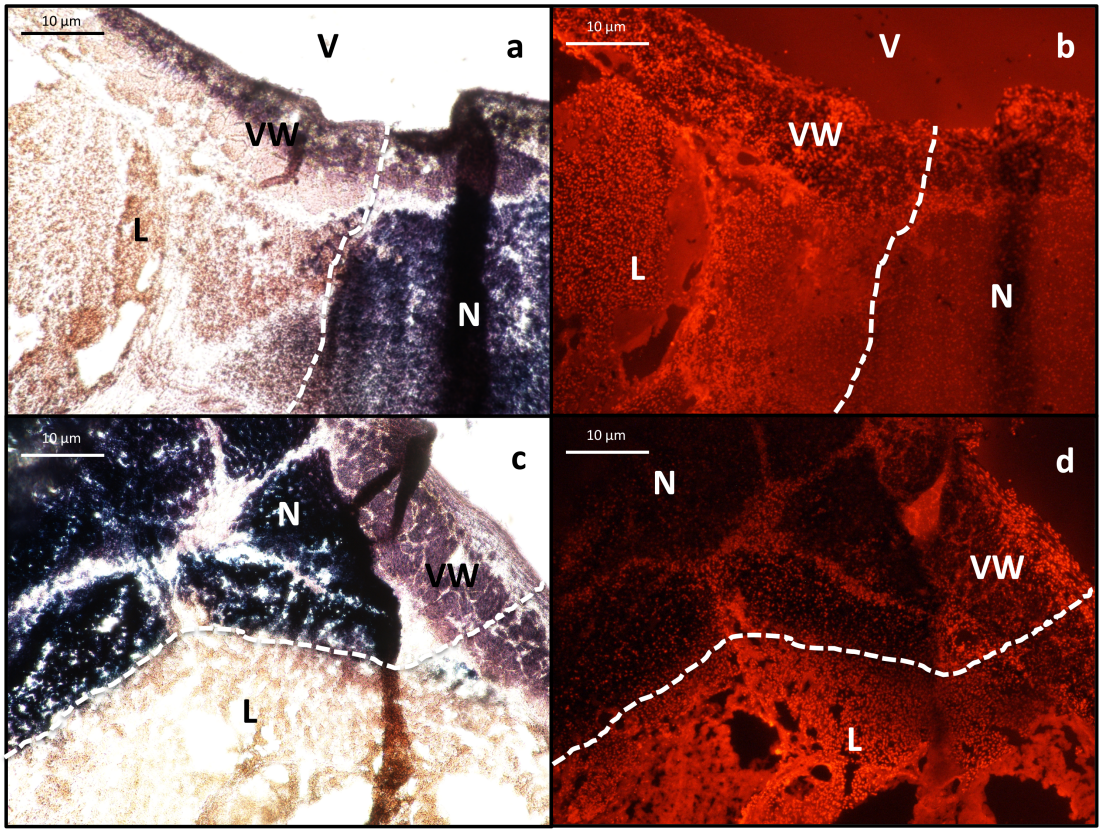


Figure 6.22 *– NADH staining (a and c) and ethidium homodimer-1 (b and d) staining of the edge of a HIFU lesion positioned at the vessel wall (VW) – vessel (V) interface. There is strong red Ethd-1 fluorescence, within the ablated regions (L) but much lower levels within the unablated normal liver parenchyma (N). The dotted white line marks the boundary of the ablative zone.*

Ethidium homodimer-1 staining of the HIFU lesions adjacent to large blood vessels, demonstrated high levels of fluorescence within the ablated region of hepatic tissue, corresponding with the unstained regions following NADH staining of the same tissues

(*Figures 6.22, 6.23* and *6.24*).

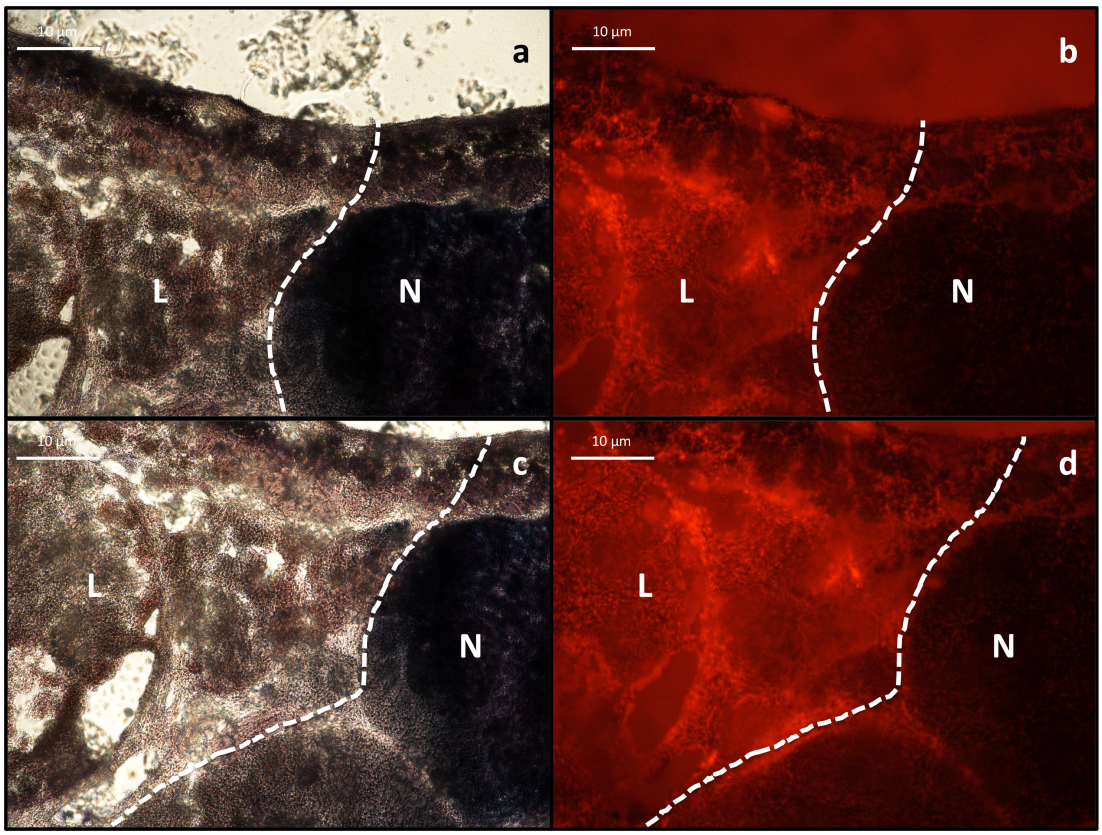


Figure 6.23 – *NADH staining (a and c) and corresponding ethidium homodimer-1 staining (b and d) of the same tissue from the edge of two HIFU lesions adjacent to large vessels. The ablated regions, which appear colourless on NADH staining, exhibit strong Ethd-1 fluorescence, whereas the unablated tissue has comparable background fluorescence to the negative control tissue.*

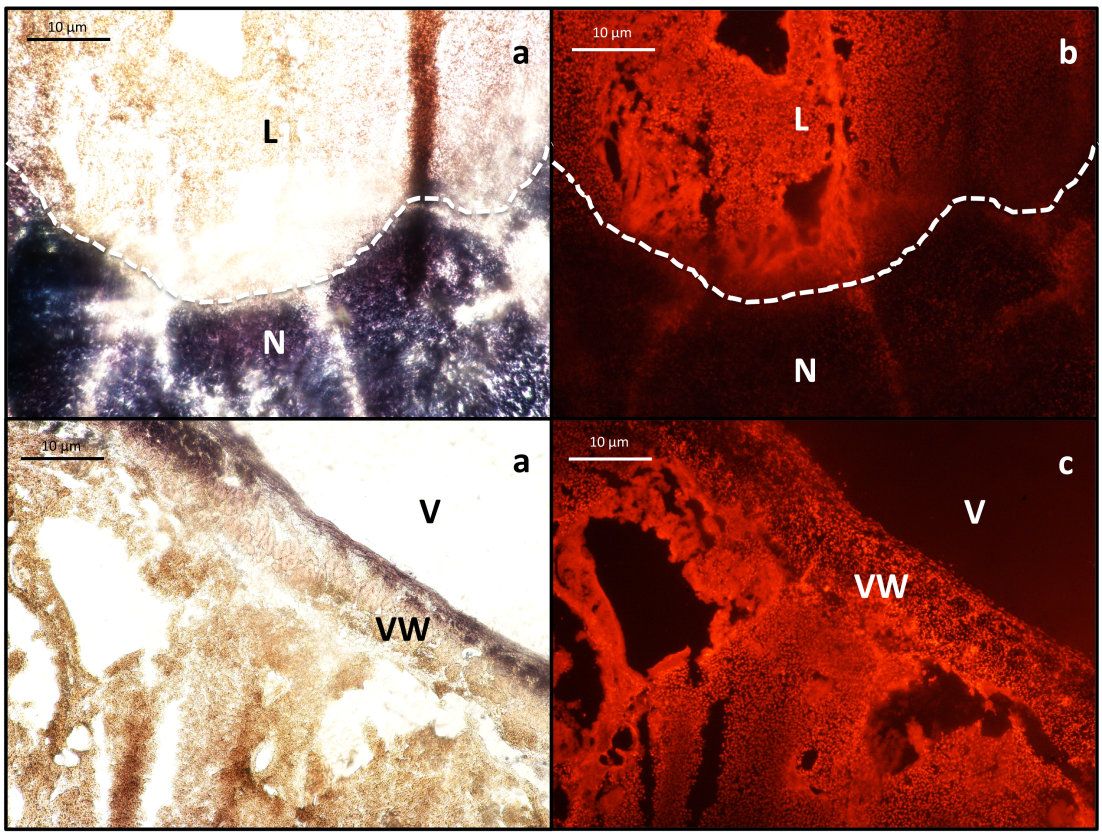


Figure 6.24 *– NADH staining (a and c) and ethidium homodimer-1 (b and d) staining of the edge of a HIFU lesion. The top row is from the lesion edge away from the vessel and the bottom row shows staining of the tissue at the vessel wall (VW) and blood vessel (V) interface. There is strong red Ethd-1 fluorescence, within the ablated regions (L) but much lower levels within the unablated normal liver parenchyma (N). The dotted white line marks the boundary of the ablative zone.*

Histological assessment of cell death is less relevant than assessment of cell viability, as treatment success is predominantly determined by whether complete ablation is attained adjacent to vasculature, or if untreated cells remain. It is not possible to tell from Ethd-1 staining whether or not complete tissue necrosis has occurred within ablated area, only that there is a larger number of dead cells within the treated tissue region compared to the unablated liver parenchyma.

6.4.5 Assessment of Apoptotic Activity

Immunofluorochemistry was performed on frozen sections in order to assess apoptotic activity in relation to the HIFU ablative lesions. Cells expressing cleaved caspase-3, a protein that is activated in the apoptotic cell, were marked with a rabbit anti-pig caspase-3 monoclonal primary antibody and subsequently a goat anti-rabbit secondary antibody, tagged with a FITC fluorophore. Negative controls did not exhibit any fluorescent staining, whilst positive controls demonstrated strong fluorescence and cleaved caspase-3 activity.

Tissue within the HIFU lesion and viable, unablated parenchyma well outwith the ablated zone demonstrated similar levels of fluorescence, suggesting similar levels of cleaved caspase-3 expression and apoptotic activity (*Figure 6.25*).

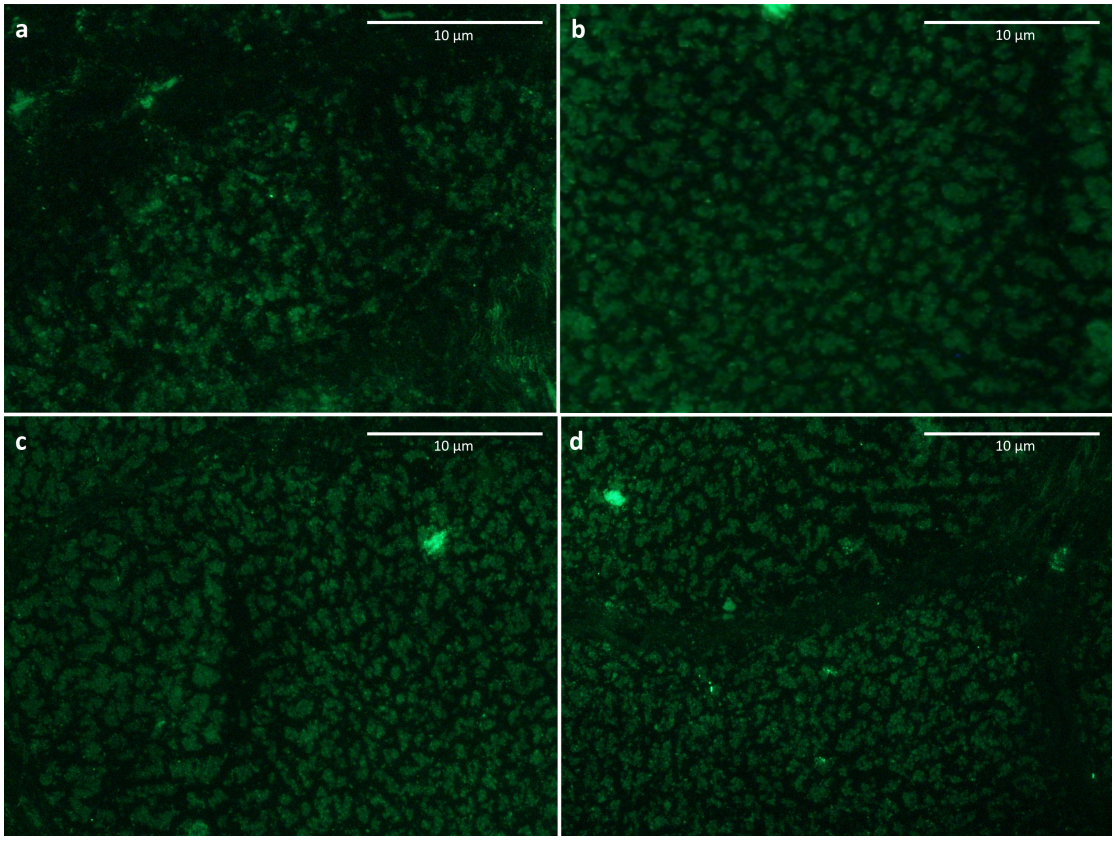


Figure 6.25 *– Cleaved caspase-3 expression within ablated areas of liver parenchyma (a and b) and untreated tissue (c and d).*

Examination of the lesion peripheries revealed slightly higher levels of fluorescence in a region corresponding to the area of tissue just outwith the ablative lesion (*Figure 6.26*). The region of higher fluorescence was approximately 5 – 10 µm in width. This suggests that there is a zone bordering the HIFU ablative lesion containing a higher number of cells undergoing apoptosis compared to the lesion itself and the liver parenchyma well away from the treated tissue.

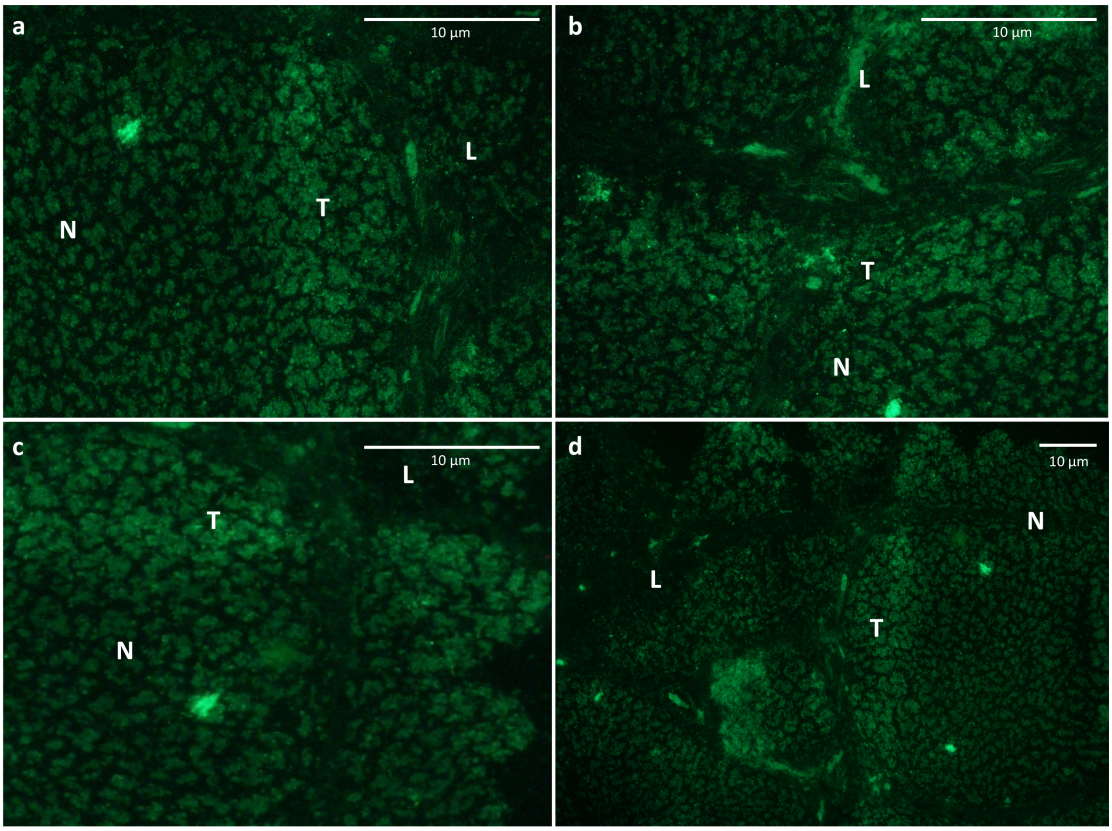


Figure 6.26 *– Cleaved caspase-3 immunofluorescence at the HIFU lesion periphery. There is a slightly higher level of fluorescence within the transition zone (T) compared with the ablated region (L) and the normal liver parenchyma (N), well outwith the ablative focus.*

6.5 Discussion

In this chapter, data assessing tissue necrosis and cell viability following HIFU ablation in regions of hepatic parenchyma immediately adjacent to large (≥ 5 mm) vasculature are presented. One of the major limitations affecting the efficacy of thermal ablative therapies, particularly radiofrequency ablation (RFA) and microwave ablation to a lesser extent, is the "heat sink" effect caused by heat advection away from the ablative focus from large (≥ 4 mm) peritumoural blood vessels. This can lead to incomplete ablation of tumoural tissue immediately adjacent to the vessel wall and treatment failure. A number of studies have demonstrated that a cuff of viable tissue may remain immediately surrounding a ≥ 4 mm vessel following RFA of a perivascular tissue volume.

In Chapter 4, thermometry data is presented suggesting that large vessel perfusion does not significantly affect peak focal temperature during HIFU-induced heating. However, the experimental design of the thermometry studies intentionally attempted to limit the peak focal temperature rise to below the ablative threshold in order to minimise changes to the focal tissue properties. Clinically, whilst knowledge of any perfusion effect on peak temperature rise is important in terms of treatment planning in predicting the required energy necessary to achieve ablation at different anatomical locations, the critical endpoint in terms of a thermal ablative therapy is whether or not a peak focal temperature in excess of the threshold required to achieve coagulative necrosis can be attained for any given tissue region. If thermal ablation can be achieved irrespective of vascular anatomy, it would indicate that any heat sink effect imparted by blood flow can be overcome, attaining the critical clinical endpoint that primarily determines treatment

success or failure.

The aim of the studies described in this chapter, was to assess whether complete ablation could be achieved right up to the wall of large vessels, i.e. determining whether HIFU-induced heating can overcome any heat sink effect present due to large vessel perfusion. Vessels were selected with a diameter in excess of the threshold diameter at which a significant heat sink effect is seen in RFA therapy, where viable tissue can remain post-treatment. Histological evidence of complete hepatic tissue ablation following HIFU therapy in areas immediately adjacent to large (≥ 5 mm) vessel walls is demonstrated.

Lu *et al.* (2002 and 2003) demonstrated that a viable cuff of tissue adjacent to a ≥ 4 mm vessel wall could remain following RFA therapy. Similarly, studies by Yu *et al.* (2008) suggested that incomplete ablation could occur following MWA, when tissue surrounding a 6 mm hepatic vein was targeted. Assessment of cell viability through NADH staining demonstrated a rim of positively stained tissue interpositioned between the MWA lesion and the vessel wall, indicating incomplete ablation of perivascular tissue. The data acquired from NADH cell viability staining demonstrate that complete ablation following HIFU therapy can be achieved surrounding blood vessels up to 10 mm in diameter. Even when blood vessels significantly larger than the threshold diameter of 3 – 4 mm, at which the heat sink effect becomes significant in RF ablation, complete cellular necrosis, extending right up to the vessel wall, was observed following HIFU therapy, with no evidence of tissue sparing.

The largest blood vessel targeted in this series of studies was 10 mm in diameter,

approximately equivalent to the upper boundary of the normal adult diameter of the right or left portal vein or 1st order hepatic vein branches (Trigaux et al., 1991). However, the maximum vessel diameter was significantly lower than the reported mean normal retrohepatic IVC diameter of 23.5 +/- 3.4 mm (Kitamura and Kobayashi, 2005). Due to the anatomical features of the porcine liver and physical constraints of the liver perfusion device, it was not possible to target the pericaval tissue in the studies described in this chapter, which is the largest diameter blood vessel, with the highest blood flow velocities encountered during clinical liver ablation. *In vivo* studies using a large animal model would need to be performed in order to assess thus further.

6.5.1 Assessment of Cell Death

As discussed previously, there are two distinct mechanisms of cell death: necrosis and apoptosis. The dominant mechanism investigated in the series of studies presented in this chapter was cellular necrosis. Thermal necrosis is a near-instant process, causing irreversible damage to critical mitochondrial and cytosolic enzyme complexes and protein coagulation. Degradation of products of cellular metabolism, such as NADH, occurs within a period of approximately 2 hours following cellular necrosis. However, the second mechanism of programmed cellular death, apoptosis, may also play a role in cell death following thermal ablation. Whilst necrosis generally occurs in the tissue regions where the thermal dose, a product of temperature and exposure duration, exceeds the threshold required for cell death, apoptosis may occur in the peripheral regions surrounding the ablative lesion, or in areas where the tissue temperature has not exceeded the threshold. There is a temperature gradient at the periphery of the ablative focus whereby some tissue outwith the region that is heated to a temperature sufficient to

induce coagulative necrosis, undergoes exposure to sublethal hyperthermic temperatures. Hyperthermia is known to induce apoptosis through cellular stress mechanisms, including formation of reactive oxygen species and through the cytokine cascade (Bhardwaj et al., 2012, Rai et al., 2005, Chen et al., 2008). Following RFA therapy, a transitional zone of around 8 – 10 mm in depth outwith the necrotic zone has been shown to exist, in which apoptosis is induced in most cells, further expanding the volume of ablated tissue (Bhardwaj et al., 2012, Vanagas et al., 2009). However, induction of apoptotic pathways can take up to 24 hours following the initial cellular stress exposure and therefore assessment of apoptosis following ablation is limited by time constraints using the isolated, perfused liver model. In all the studies performed in this chapter, the livers were removed, sectioned and specimens were snap frozen after 2 hours following the final ablation. Therefore, an insufficient period of time may have been left for up-regulation and expression of cellular markers associated with apoptosis to have occurred following HIFU ablation in the perfused liver model. However, it appears likely that a that a region of tissue bordering the HIFU focus exists, where tissue heating occurs through a combination of direct pre/post focal energy deposition and heat diffusion away from the focus. As a result, tissue heating occurs but to a lesser extent than within the focal tissue and to a degree insufficient for tissue temperatures to reach the threshold required for ablation. The cells within this "transition" zone are subjected to a degree of hyperthermia, activating cellular stress responses and potentially inducing apoptosis.

Additionally, a high background level of cleaved caspase-3 expression was detected in the non-ablated perfused liver tissue. Whilst the isolated, perfused porcine liver accurately models *in vivo* anatomy, there are a number of physiological influences that may affect

assessment of cellular stress and cell death, particularly apoptotic mechanisms. During organ procurement, there is an inherent period of cold ischaemia, which places hepatic tissue in a stress environment for a period of time. A degree of ischaemic injury may occur and induction of apoptosis may arise through ischaemic stress.

A number of published studies modeling the effects of blood flow on HIFU-induced heating observed that the heat sink effect is more pronounced when the longitudinal axis of the HIFU focus is placed parallel to the vessel wall (Hariharan et al., 2007, Solovchuk et al., 2013). Although the orientation of the focus relative to the vessel wall was not tested intentionally, due to the configuration of the raster scan for the volume ablation studies, there were different locations within the overall treatment volume at which the short axis and long axis were parallel to the blood vessel. No viable tissue was observed adjacent to the vessel wall at any point in each of the ablated volumes, so if a difference in the heat sink effect exists depending on whether the longitudinal or transverse axis of the HIFU focus is placed parallel to the blood vessel wall, then it appears as if it is a subclinical one and complete ablation can be achieved irrespective of the orientation of the focus.

6.5.2 Limitations

A further limitation of the porcine liver model is that only normal hepatic parenchyma was available for ablation studies, as no porcine oncological model exists. Variation in thermal sensitivity exists between different species, tissues and cell types. Neoplastic cells may behave differently to normal hepatocytes and may be more resistant to thermal

injury, requiring higher thermal doses in order to induce cell death. There may also be significant variation and heterogeneity in the thermal dose threshold within tumours of the same cell type, e.g. adeneocarcinoma, hepatocellularcarcinoma. However, no optimal preclinical model exists as the tumour models available are in smaller species with significant vascular and anatomical differences compared to humans. Therefore, clinical *in vivo* studies need to be performed in order to assess the efficacy of HIFU ablation to allow testing in a situation both with accurate disease pathology, cell characteristics and clinically relevant anatomical features.

6.6 Conclusions

In this chapter, histopathogical evidence of complete tissue ablation adjacent to large (5 - 10 mm) vasculature with physiological flow rates, following HIFU ablation is presented. In all cases, no tissue sparing was observed at the vessel wall interface and complete tissue necrosis throughout the ablative region was attained. The histopathological data suggest that HIFU is not affected by the heat sink effect of large blood vessel perfusion and that successful clinical ablation of perivascular tumours should be achievable. The studies presented in this chapter back up the thermometry data presented in Chapter 5, which also suggested that no significant heat sink effect is present in terms of peak temperature attained during HIFU treatment.

Compared to RFA and MWA, which are the two thermal ablative modalities in mainstream clinical use, HIFU appears to be superior to RFA and at least equivalent to MWA in its potential to ablate hepatic tissue adjacent to blood vessels of ≥ 4 mm in diameter. Clinical studies need to be performed in order to assess this further, combining real life disease pathology and vascular anatomy.

CHAPTER 7

CONCLUSIONS AND FURTHER WORK

7.1 Summary of Achievements

The primary aim of the present work was to elucidate the effects of perfusion, in particular large vessel blood flow, on HIFU ablative therapy. A unique *ex vivo,* normothermically perfused porcine liver model was used in order to provide a physiologically and anatomically relevant test bed. Previous work has demonstrated that the normothermically perfused liver model can remain in a functional state, with physiological blood flow rates and vascular pressures for in excess of 72 hours (Brockmann et al., 2009, Butler et al., 2002, Reddy et al., 2004).

In Chapter 4, the cavitation threshold of functional, perfused *ex vivo* liver tissue was determined, both at frequencies of 1.06 MHz and at 3.18 MHz. It was determined that the cavitation threshold at 1.06 MHz lay between 3 – 4 MPa $_{Pk-}$, which is comparable to the cavitation threshold of *in vivo* pancreatic tumours, but higher than that demonstrated in *ex vivo* unperfused liver tissue. At 3.18 MHz, the cavitation threshold was not reached by the maximum PRFP tested in the current study and was determined to be in excess of 12 MPa. These frequencies were therefore used for subsequent thermal studies in order to investigate HIFU-induced heating i) in the presence of cavitation and ii) in the

absence of cavitation, as it is known that cavitation can significantly enhance heating rates during HIFU therapy (Holt and Roy, 2001).

In Chapter 5, thermometry data measuring real time temperature changes during HIFU treatment were presented, comparing peak focal temperature rise in areas of hepatic parenchyma immediately adjacent to large (≥ 5 mm) vasculature to microperfused regions of liver tissue, both in the presence and complete absence of perfusion. Measurements were made at 1.06 MHz, in the presence of cavitation and at 3.18 MHz, in the absence of cavitation. Acoustic pressures inducing temperature rises below the ablative threshold were chosen in order to minimise the tissue bio-effects and any alteration to the focal tissue / perfusion characteristics as multiple measurements were made at each thermocouple location. It was found that there was no significant difference in HIFU-induced peak focal temperature rise in areas of hepatic tissue adjacent to large vasculature compared with microperfused regions at any acoustic pressure tested at either 1.06 MHz or 3.18 MHz. Similarly, no apparent differences in peak focal temperature were observed at any location between measurements made in the presence of perfusion, compared to measurements made in the complete absence of blood flow, with the liver perfusion device switched off. These data suggest that there is no significant heat sink effect from large or small vessel perfusion in HIFU therapy, either in the presence or absence of cavitation-enhanced heating.

Limitations of the thermometry studies included the fact that only single point temperature measurements at the HIFU focus were obtained, rather than across the whole focal volume and also that, whilst placement of the thermocouple as close to the

vessel wall as possible was attempted, experimental error and variability meant that the thermocouple junction was within approximately 2 mm of the vessel wall. Although the thermal data presented in Chapter 5 strongly suggested that HIFU is not affected by any vascular heat sink effect, histological assessment of complete tissue ablation needed to be performed in order to evaluate this hypothesis further. Given that any heat sink effect is maximal in the cell layers immediately in contact with the vascular wall and the effects of heat advection decrease as a function of distance from the blood vessel, it was important to assess this tissue region closely through histological analysis of cell viability / cell death.

In Chapter 6, histological studies evaluating the effects of large (5 – 10 mm) vessel perfusion on HIFU ablation were presented. Assessment of cell viability through NADH staining demonstrated that no viable cells remained throughout the HIFU lesion. In particular, no viable cells were identified at the lesion – vessel wall interface, which is the tissue region where any potential heat sink effect is maximal. Viable cells can remain following RFA of tissue adjacent to ≥ 3 mm blood vessels (Lu et al., 2002) and following MWA of tissue adjacent to ≥ 6 mm vessels (Yu et al., 2008). Vessels with diameters of 5 – 10 mm were used for the histological studies, which are comparable to human 1st order portal vein and hepatic vein diameters, although smaller than the retrohepatic IVC diameter. Evaluation of any heat sink effect in pericaval tissue ablation would need to be conducted *in vivo* due to the physical constraints of the isolated, perfused liver model. Similarly, the isolated, perfused liver is a suboptimal model for investigating apoptosis as tissue changes and characteristics associated with this process of programmed cell death can take up to 24 to evolve following the period of cellular stress. Even allowing for this, immunofluorescent staining for cleaved caspase-3 expression, a cell surface protein

associated with apoptosis, demonstrated an apparent zone of increased expression in a region of tissue at the HIFU lesion periphery, just outwith the area of ablated tissue. Therefore, it is likely that there is a region of tissue bordering the HIFU focus, where tissue heating occurs, but to a degree insufficient for tissue temperatures to reach the threshold required for ablation. Hyperthermia activates cellular stress responses, induces apoptosis and, subsequently, there is a "transition zone" bordering the necrotic ablative focus where further programmed cell death may result.

Most previous work investigating perfusion effects on HIFU therapy has been performed using computer and *ex vivo* phantom modeling, lacking real life cavitation and tissue characteristics, or small animal models that do not accurately reflect human vascular anatomy and blood flow. Several studies have suggested that blood flow through vessels greater than approximately 3 mm in diameter can reduce lesion size by 24 – 40 %, when the HIFU focus is within 2 – 3 mm of the vessel wall (Hariharan et al., 2007, Huang et al., 2004b) and that approximately 10 – 20 % more energy was required to ablate hepatic tissue immediately adjacent to a portal vein compared to 10 mm away from the portal vein. In terms of the effects of perfusion on temperature rise, Huang *et al.* (2004) demonstrated in an *ex vivo* tissue phantom that peak temperature rise in a 2.3 mm vessel wall was approximately 25 % lower than away from the vessel, whilst Zhou *et al.* (2012) concluded that only the temperature-decrease phase following HIFU therapy and not the heating phase during HIFU treatment was affected by tumoural perfusion rates. The data presented in this current work appears to concur with Zhou *et al.* (2012) in that the temperature-increase phase during HIFU therapy was neither affected by the presence of an adjacent large (≥ 5 mm) vessel, nor by the presence or complete absence of whole

organ perfusion, with similar peak temperature rises being attained under all blood flow conditions. This work also agrees with the conclusions of Solovchuk *et al.* (2013), Melodelima *et al.* (2009) and Parmentier *et al.* (2009) that, even if a heat sink effect is imparted from physiological blood flow and vasculature up to 5 mm in diameter, this can be overcome during HIFU therapy; ablative temperatures can still be attained and complete tissue ablation can be achieved.

The rapid heating encountered during HIFU ablation, compared to the slower rates present in MWA and, in particular RFA, may provide an explanation for the lack of a clinically relevant heat sink effect in HIFU therapy compared to other ablative modalities. As heating occurs and peak tissue temperatures are attained over a period of a few seconds, there is very little opportunity for heat diffusion and advection to occur. In RFA and MWA, heating occurs over a period of several minutes, which provides a much greater opportunity for advection of heat to occur away from the ablative focus by perfusion, thus lowering the focal heating rate and peak temperature.

In summary, the real time thermometry and histological studies presented in this current work suggest that hepatic HIFU ablative therapy is not significantly affected by any heat sink effect imparted by large vessel, or microvascular perfusion. It is suggested that the rapid heating rates observed during HIFU ablation and the effects of cavitation-enhanced heating are able to overcome the effects of varying degrees of heat advection due to local differences in tissue perfusion. The ability of HIFU to achieve complete tissue ablation independent of local perfusion characteristics and irrespective of the anatomical location of the focal volume, could offer a major advantage over alternative ablative modalities

such as RFA and MWA.

One of the main limitations affecting clinical HIFU therapy for solid organ tumours is the treatment time required in order to ablate an entire tumour, or multiple tumours in the case of multifocal disease, due to the small focal volume. However its small focus means that small tissue volumes can be targeted and treatment is accurate and precise. A further advantage is that, as HIFU is completely non-invasive, it can be used potentially to treat tumours anatomically inaccessible via the percutaneous route used by RFA and MWA.

One of the main factors limiting clinical ablation of tumours, particularly those ≥ 4 cm in diameter, and the observed discrepancy in outcomes between ablation and surgical resection of tumours, is treatment variability due to perfusion effects. Therefore, an ablative modality that is minimally affected by variability in perfusion could confer a significant advantage over current modalities in terms of long-term clinical outcomes, both in the treatment of liver and in the treatment of other solid organ cancers in close proximity to significant vasculature.

7.2 Suggestions for Future Work

7.2.1 Validation of the Isolated, Perfused Porcine Liver Model

In this current work, a novel isolated, perfused liver model was used to investigate HIFU-induced cavitation, heating and tissue ablation in an anatomically and physiologically relevant test bed. However, although it has been demonstrated that hepatic tissue within the normothermically perfused liver is maintained in a functional state *ex vivo*, with near physiological partial pressures of O_2 / CO_2, acid-base balance and vascular pressures / flow rates, it is not known whether this model accurately represents the cavitation characteristics of *in vivo* tissue. In order to assess whether liver tissue maintained *ex vivo* using normothermic machine preservation has the same cavitation and thermal characteristics as *in vivo* tissue, validating this current work, the studies should be repeated in an *in vivo* porcine model.

Whilst the isolated, perfused liver has been demonstrated to maintain normal physiological parameters *ex vivo* in preclinical transplant studies, providing a functional test bed and allowing complex studies to be performed that would be difficult to undertake *in vivo*, a degree of deterioration in the quality and function of the livers used in these studies was observed. It is unclear as to whether changes in the liver parenchyma over the duration of the experiments affected the cavitational, thermal or histological studies performed, so *in vivo* validation of the data obtained from the studies performed in the isolated, perfused porcine liver model is required.

Whilst the effects of blood vessels up to 10 mm in diameter were evaluated in the current work, as discussed previously, assessment of the effects of IVC blood flow, which is the largest of the hepatic blood vessels and has the greatest potential heat sink effect, on ablation of a pericaval tissue volume could not be undertaken in the isolated, perfused liver model due to physical constraints. Assessment of pericaval ablation and any significant caval heat sink effect therefore needs to be assessed *in vivo*.

Whilst the isolated, perfused porcine liver fairly accurately models the large vessel and biliary anatomy found in humans, no pathological porcine liver tumour model is available. The studies performed in this current work were performed in normal hepatic parenchyma rather than malignant tissue and, therefore, an assumption is made that these all types of tissue will behave similarly in terms of cavitation, heating and cell damage / death. It is known that different cell types have varying degrees of thermal sensitivity, reflected by different CEM_{43} values (Sapareto and Dewey, 1984) and that different tissues have different ablation thresholds (Hynynen, 1991). Validation of the results performed in normal hepatic parenchyma therefore needs to be undertaken within the confines of a clinical trial, which is the only method of combining accurate disease pathology, anatomy and physiology within a single test bed.

7.2.2 Real Time Treatment Monitoring During HIFU Ablation

A further factor limiting ablative therapies in current clinical use is the lack of real time monitoring that can accurately and consistently predict successful / incomplete treatment. In HIFU therapy, hyperecho on B-mode ultrasound during treatment and

MRI are the two modalities in current clinical use. A novel passive acoustic mapping technique, first described by Gyongy and Coussios (2010), was employed in the present work to quantify and map acoustic emissions, hence cavitation activity during HIFU exposure.

The same passive acoustic mapping technique has been shown to accurately predict lesion formation in *ex vivo*, unperfused liver tissue (Jensen et al., 2012). However, this treatment monitoring modality has not been tested in perfused liver tissue or *in vivo*. The cavitation dynamics present in the present of blood flow and *in vivo* are likely to differ substantially to those found in degassed *ex vivo* tissue due to differences in tissue characteristic and availability / replenishment of cavitation nuclei. This current study demonstrated a substantially different cavitation threshold (3 - 4 MPa $_{Pk-}$) in perfused liver tissue, compared to reported values measured in unperfused liver tissue of 8 – 9 MPa $_{Pk-}$ (Li et al., 2014). Therefore, further studies need to be performed in order to investigate the highly promising technique further, in tissue with characteristics more representative of the clinical situation than unperfused *ex vivo* tissue. Similar to the work by Jensen *et al.* (2012), a study encompassing a range of HIFU parameters comparing lesion prediction by B-mode ultrasound and PAM with histological evidence of tissue necrosis needs to be performed either in the perfused liver model or *in vivo.*

7.2.3 Clinical Trials

Radiofrequency and microwave are the main thermal ablative modalities in routine clinical use currently. RFA, in particular, is particularly susceptible to local variation in

perfusion characteristics and is affected by the heat sink effect imparted by ≥ 3 mm blood vessels. MWA is affected to a lesser extent by tissue perfusion. It is thought that treatment variability due to local perfusion differences and the heat sink effect are partially responsible for poorer treatment outcomes following thermal ablative therapy compared to surgical resection. One problem of clinical ablation trials is that it is difficult and uncommon to obtain tissue in order to assess histological outcome post procedure. The majority of clinical trials use radiological assessment of disease recurrence and survival as treatment outcome endpoints. In order to clarify the histological results reported in Chapter 6 within a clinical trial, an ablation-resection study could be performed in patients with small volume disease who are suitable for surgical resection, whereby HIFU ablation would be performed prior to conventional resection, thus allowing post-procedure histological examination. A subsequent clinical trial could then be performed assessing mid- to long-term treatment outcomes in terms of disease free survival and overall survival.

There is a paucity of evidence; particularly high quality randomised controlled studies comparing treatment modalities to each other and also to surgical resection. A 3-armed randomised controlled trial comparing HIFU ablation to RFA and MWA for e.g. the treatment of early stage HCC in patients unsuitable for or who do not meet the criteria for liver transplantation could be performed to assess short-, mid- and long-term oncological outcomes following the various modalities of thermal ablation.

7.2.4 Applicability of the Current Work to Other Uses of HIFU

HIFU ablation can be used to treat a range of other solid organ tumours in addition to hepatic malignancies. The current work is most applicable to treatment foci in anatomical locations with high perfusion rates, such as renal tumours, with normal renal blood flow being approximately 1.0 – 1.2 L/min.

The effects of perfusion on cavitation and heating that are detailed in this current work are not only applicable to ablative therapy, but also to other uses of HIFU, including targeted drug delivery. For example, clinical trials investigating HIFU-mediated release of chemotherapeutic agents encapsulated in thermosensitive shells are currently in progress. HIFU-induced heating in the mild hyperthermia range within the target tissue triggers release of doxorubicin, allowing high concentrations of the chemotherapeutic drug to be delivered to the desired tissue, minimising exposure other tissues within the body to the agent, reducing systemic side effects (de Smet et al., 2013, Dromi et al., 2007, Staruch et al., 2015). Similarly, any local variability in heating rates due to heterogeneous tissue perfusion on heating may affect treatment efficacy and outcome. Cavitation-enhanced drug delivery, in addition to hyperthermia-mediated drug delivery, is also a promising use of HIFU (Chen et al., 2013, Fowler et al., 2013, Graham et al., 2014). In this, various agents are combined with a drug and ultrasound exposure in order to promote cavitation, increasing the delivery of the drug to the target tissue through mechanical bio-effects. However, the inherent cavitational characteristics of tissues need to be known in order to determine treatment protocols, maximise safety and minimise unwanted effects.

APPENDIX

Saline buffer

0.85 g sodium chloride (Sigma, UK)

100 ml distilled water

Phosphate buffer

0.343 g sodium dihydrogenphosphate (Sigma, UK)

100 ml distilled water

pH adjusted to 7.4 with 1 M hydrochloric acid

Phosphate buffered saline

7.52 g dipotassium phosphate (Sigma, UK)

13.2 g sodium dihydrogen phosphate (Sigma, UK)

7.2 g sodium chloride (Sigma, UK)

1000 ml distilled water

pH adjusted to 7.4 with 1 M hydrochloric acid

Nitro blue tetrazolium solution

250 mg nitro blue tetrazolium (Sigma, UK)

100 ml distilled water

REFERENCES

ABDALLA, E. K., ADAM, R., BILCHIK, A. J., JAECK, D., VAUTHEY, J. N. & MAHVI, D. 2006. Improving resectability of hepatic colorectal metastases: expert consensus statement. *Ann Surg Oncol,* 13**,** 1271-80.

ABDALLA, E. K., VAUTHEY, J. N., ELLIS, L. M., ELLIS, V., POLLOCK, R., BROGLIO, K. R., HESS, K. & CURLEY, S. A. 2004. Recurrence and outcomes following hepatic resection, radiofrequency ablation, and combined resection/ablation for colorectal liver metastases. *Ann Surg,* 239**,** 818-25; discussion 825-7.

AHMED, M., BRACE, C. L., LEE, F. T., JR. & GOLDBERG, S. N. 2011. Principles of and advances in percutaneous ablation. *Radiology,* 258**,** 351-69.

AL-ASFOOR, A., FEDOROWICZ, Z. & LODGE, M. 2008. Resection versus no intervention or other surgical interventions for colorectal cancer liver metastases. *Cochrane database of systematic reviews***,** CD006039.

ALOIA, T. A., VAUTHEY, J. N., LOYER, E. M., RIBERO, D., PAWLIK, T. M., WEI, S. H., CURLEY, S. A., ZORZI, D. & ABDALLA, E. K. 2006. Solitary colorectal liver metastasis: resection determines outcome. *Arch Surg,* 141**,** 460-6; discussion 466-7.

ANDERSON, J. K., BAKER, M., JAFFERS, O., PEARLE, M. S., LINDBERG, G. L. & CADEDDU, J. A. 2007. Time course of nicotinamide adenine dinucleotide

diaphorase staining after renal radiofrequency ablation influences viability assessment. *J Endourol,* 21**,** 223-7.

BAGEACU, S., KACZMAREK, D., LACROIX, M., DUBOIS, J., FOREST, J. & PORCHERON, J. 2007. Cryosurgery for resectable and unresectable hepatic metastases from colorectal cancer. *Eur J Surg Oncol,* 33**,** 590-6.

BAILEY, M. R., COURET, L. N., SAPOZHNIKOV, O. A., KHOKHLOVA, V. A., TER HAAR, G., VAEZY, S., SHI, X., MARTIN, R. & CRUM, L. A. 2001. Use of overpressure to assess the role of bubbles in focused ultrasound lesion shape in vitro. *Ultrasound Med Biol,* 27**,** 695-708.

BAKER, M. E. & PELLEY, R. 1995. Hepatic metastases: basic principles and implications for radiologists. *Radiology,* 197**,** 329-37.

BALA, M. M., RIEMSMA, R. P., WOLFF, R. & KLEIJNEN, J. 2013. Microwave coagulation for liver metastases. *Cochrane Database Syst Rev,* 10**,** CD010163.

BANGARD, C., GOSSMANN, A., KASPER, H. U., HELLMICH, M., FISCHER, J. H., HOLSCHER, A., LACKNER, K. & STIPPEL, D. L. 2006. Experimental radiofrequency ablation near the portal and the hepatic veins in pigs: differences in efficacy of a monopolar ablation system. *The Journal of surgical research,* 135**,** 113-9.

BAZAN-PEREGRINO, M., RIFAI, B., CARLISLE, R. C., CHOI, J., ARVANITIS, C. D., SEYMOUR, L. W. & COUSSIOS, C. C. 2013. Cavitation-enhanced delivery of a replicating oncolytic adenovirus to tumors using focused ultrasound. *J Control Release,* 169**,** 40-7.

BHARDWAJ, N., DORMER, J., AHMAD, F., STRICKLAND, A. D., GRAVANTE, G., BECKINGHAM, I., WEST, K., DENNISON, A. R. & LLOYD, D. M. 2012. Heat shock protein 70 expression following hepatic radiofrequency ablation is affected by adjacent vasculature. *J Surg Res,* 173**,** 249-57.

BHARDWAJ, N., DORMER, J., AHMAD, F., STRICKLAND, A. D., GRAVANTE, G., WEST, K., DENNISON, A. R. & LLOYD, D. M. 2011. Microwave ablation of the liver: a description of lesion evolution over time and an investigation of the heat sink effect. *Pathology,* 43**,** 725-31.

BITSCH, R. G., DUX, M., HELMBERGER, T. & LUBIENSKI, A. 2006. Effects of vascular perfusion on coagulation size in radiofrequency ablation of ex vivo perfused bovine livers. *Investigative radiology,* 41**,** 422-7.

BOKEMEYER, C., BONDARENKO, I., HARTMANN, J. T., DE BRAUD, F., SCHUCH, G., ZUBEL, A., CELIK, I., SCHLICHTING, M. & KORALEWSKI, P. 2011. Efficacy according to biomarker status of cetuximab plus FOLFOX-4 as first-line treatment for metastatic colorectal cancer: the OPUS study. *Ann Oncol,* 22**,** 1535-46.

BOWLES, B. J., MACHI, J., LIMM, W. M., SEVERINO, R., OISHI, A. J., FURUMOTO, N. L., WONG, L. L. & OISHI, R. H. 2001. Safety and efficacy of radiofrequency thermal ablation in advanced liver tumors. *Arch Surg,* 136**,** 864-9.

BROCKMANN, J., REDDY, S., COUSSIOS, C., PIGOTT, D., GUIRRIERO, D., HUGHES, D., MOROVAT, A., ROY, D., WINTER, L. & FRIEND, P. J. 2009. Normothermic perfusion: a new paradigm for organ preservation. *Ann Surg,* 250**,** 1-6.

BRUIX, J., LLOVET, J. M., CASTELLS, A., MONTANA, X., BRU, C., AYUSO, M. C., VILANA, R. & RODES, J. 1998. Transarterial embolization versus symptomatic treatment in patients with advanced hepatocellular carcinoma: results of a randomized, controlled trial in a single institution. *Hepatology,* 27**,** 1578-83.

BU, R., YIN, L., YANG, H., WANG, Q., WU, F. & ZOU, J. Z. 2013. Tissue ablation accelerated by peripheral scanning mode with high-intensity focused ultrasound: a study on isolated porcine liver perfusion. *Ultrasound Med Biol,* 39**,** 1410-9.

BUTLER, A. J., REES, M. A., WIGHT, D. G., CASEY, N. D., ALEXANDER, G., WHITE, D. J. & FRIEND, P. J. 2002. Successful extracorporeal porcine liver perfusion for 72 hr. *Transplantation,* 73**,** 1212-8.

CARLISLE, K. M., HALLIWELL, M., READ, A. E. & WELLS, P. N. 1992. Estimation of total hepatic blood flow by duplex ultrasound. *Gut,* 33**,** 92-7.

CHANG, C. K., HENDY, M. P., SMITH, J. M., RECHT, M. H. & WELLING, R. E. 2002. Radiofrequency ablation of the porcine liver with complete hepatic vascular occlusion. *Annals of surgical oncology,* 9**,** 594-8.

CHEN, C. C., SHEERAN, P. S., WU, S. Y., OLUMOLADE, O. O., DAYTON, P. A. & KONOFAGOU, E. E. 2013. Targeted drug delivery with focused ultrasound-induced blood-brain barrier opening using acoustically-activated nanodroplets. *J Control Release,* 172**,** 795-804.

CHEN, F., WANG, C. C., KIM, E. & HARRISON, L. E. 2008. Hyperthermia in combination with oxidative stress induces autophagic cell death in HT-29 colon cancer cells. *Cell Biol Int,* 32**,** 715-23.

CHEN, L., TER HAAR, G., HILL, C. R., DWORKIN, M., CARNOCHAN, P., YOUNG, H. & BENSTED, J. P. 1993. Effect of blood perfusion on the ablation of liver parenchyma with high-intensity focused ultrasound. *Physics in medicine and biology,* 38**,** 1661-73.

CHEN, M. S., LI, J. Q., ZHENG, Y., GUO, R. P., LIANG, H. H., ZHANG, Y. Q., LIN, X. J. & LAU, W. Y. 2006. A prospective randomized trial comparing percutaneous local ablative therapy and partial hepatectomy for small hepatocellular carcinoma. *Ann Surg,* 243**,** 321-8.

CHEUNG, T. T., POON, R. T., YAU, T., TSANG, D. S., LO, C. M. & FAN, S. T. 2011. High-intensity focused ultrasound as a treatment for colorectal liver metastasis in difficult position. *International journal of colorectal disease*.

CHINN, S. B., LEE, F. T., JR., KENNEDY, G. D., CHINN, C., JOHNSON, C. D., WINTER, T. C., 3RD, WARNER, T. F. & MAHVI, D. M. 2001. Effect of vascular occlusion on radiofrequency ablation of the liver: results in a porcine model. *AJR. American journal of roentgenology,* 176**,** 789-95.

CHU, K. F. & DUPUY, D. E. 2014. Thermal ablation of tumours: biological mechanisms and advances in therapy. *Nat Rev Cancer,* 14**,** 199-208.

CLAVIEN, P. A., LESURTEL, M., BOSSUYT, P. M., GORES, G. J., LANGER, B. & PERRIER, A. 2012. Recommendations for liver transplantation for hepatocellular carcinoma: an international consensus conference report. *The lancet oncology,* 13**,** e11-22.

COURT, F. G., WEMYSS-HOLDEN, S. A., MORRISON, C. P., TEAGUE, B. D., LAWS, P. E., KEW, J., DENNISON, A. R. & MADDERN, G. J. 2003. Segmental

nature of the porcine liver and its potential as a model for experimental partial hepatectomy. *The British journal of surgery,* 90**,** 440-4.

COUSSIOS, C. C., FARNY, C. H., HAAR, G. T. & ROY, R. A. 2007. Role of acoustic cavitation in the delivery and monitoring of cancer treatment by high-intensity focused ultrasound (HIFU). *Int J Hyperthermia,* 23**,** 105-20.

CROUZET, S., REBILLARD, X., CHEVALLIER, D., RISCHMANN, P., PASTICIER, G., GARCIA, G., ROUVIERE, O., CHAPELON, J. Y. & GELET, A. 2010. Multicentric oncologic outcomes of high-intensity focused ultrasound for localized prostate cancer in 803 patients. *European urology,* 58**,** 559-66.

CROUZET, S., ROUVIERE, O., MARTIN, X. & GELET, A. 2014. High-intensity focused ultrasound as focal therapy of prostate cancer. *Curr Opin Urol,* 24**,** 225-30.

DAMIANOU, C. & HYNYNEN, K. 1993. Focal spacing and near-field heating during pulsed high temperature ultrasound therapy. *Ultrasound Med Biol,* 19**,** 777-87.

DASGUPTA, S., BANERJEE, R. K., HARIHARAN, P. & MYERS, M. R. 2011. Beam localization in HIFU temperature measurements using thermocouples, with application to cooling by large blood vessels. *Ultrasonics,* 51**,** 171-80.

DE SENNEVILLE, B. D., MOUGENOT, C., QUESSON, B., DRAGONU, I., GRENIER, N. & MOONEN, C. T. 2007. MR thermometry for monitoring tumor ablation. *European radiology,* 17**,** 2401-10.

DE SMET, M., HEIJMAN, E., LANGEREIS, S., HIJNEN, N. M. & GRULL, H. 2010. Magnetic resonance imaging of high intensity focused ultrasound mediated drug

delivery from temperature-sensitive liposomes: An in vivo proof-of-concept study. *J Control Release,* 150**,** 102-110.

DE SMET, M., HIJNEN, N. M., LANGEREIS, S., ELEVELT, A., HEIJMAN, E., DUBOIS, L., LAMBIN, P. & GRULL, H. 2013. Magnetic resonance guided high-intensity focused ultrasound mediated hyperthermia improves the intratumoral distribution of temperature-sensitive liposomal doxorubicin. *Invest Radiol,* 48**,** 395-405.

DOBSON, E. L., WARNER, G. F., FINNEY, C. R. & JOHNSTON, M. E. 1953. The measurement of liver circulation by means of the colloid disappearance rate. I. Liver blood flow in normal young men. *Circulation,* 7**,** 690-5.

DODD, G. D., 3RD, DODD, N. A., LANCTOT, A. C. & GLUECK, D. A. 2013. Effect of Variation of Portal Venous Blood Flow on Radiofrequency and Microwave Ablations in a Blood-perfused Bovine Liver Model. *Radiology,* 267**,** 129-36.

DROMI, S., FRENKEL, V., LUK, A., TRAUGHBER, B., ANGSTADT, M., BUR, M., POFF, J., XIE, J., LIBUTTI, S. K., LI, K. C. & WOOD, B. J. 2007. Pulsed-high intensity focused ultrasound and low temperature-sensitive liposomes for enhanced targeted drug delivery and antitumor effect. *Clin Cancer Res,* 13**,** 2722-7.

DROUGAS, J. G., BARNARD, S. E., WRIGHT, J. K., SIKA, M., LOPEZ, R. R., STOKES, K. A., WILLIAMS, P. E. & PINSON, C. W. 1996. A model for the extended studies of hepatic hemodynamics and metabolism in swine. *Lab Anim Sci,* 46**,** 648-55.

DUAN, C., LIU, M., ZHANG, Z., MA, K. & BIE, P. 2013. Radiofrequency ablation versus hepatic resection for the treatment of early-stage hepatocellular carcinoma meeting Milan criteria: a systematic review and meta-analysis. *World J Surg Oncol,* 11**,** 190.

DUBINSKY, T. J., CUEVAS, C., DIGHE, M. K., KOLOKYTHAS, O. & HWANG, J. H. 2008. High-intensity focused ultrasound: current potential and oncologic applications. *AJR Am J Roentgenol,* 190**,** 191-9.

FARNY, C. H., HOLT, R. G. & ROY, R. A. 2009. Temporal and spatial detection of HIFU-induced inertial and hot-vapor cavitation with a diagnostic ultrasound system. *Ultrasound in medicine & biology,* 35**,** 603-15.

FENG, K., YAN, J., LI, X., XIA, F., MA, K., WANG, S., BIE, P. & DONG, J. 2012. A randomized controlled trial of radiofrequency ablation and surgical resection in the treatment of small hepatocellular carcinoma. *J Hepatol,* 57**,** 794-802.

FERLAY, J., SHIN, H. R., BRAY, F., FORMAN, D., MATHERS, C. & PARKIN, D. M. 2010. Estimates of worldwide burden of cancer in 2008: GLOBOCAN 2008. *Int J Cancer,* 127**,** 2893-917.

FONDEVILA, C., HESSHEIMER, A. J., FLORES, E., VENDRELL, M., MUNOZ, J., ESCOBAR, B., CALATAYUD, D., TAURA, P., FUSTER, J. & GARCIA-VALDECASAS, J. C. 2011. Step-by-Step Guide for a Simplified Model of Porcine Orthotopic Liver Transplant. *The Journal of surgical research,* 167**,** e39-45.

FONG, Y., COHEN, A. M., FORTNER, J. G., ENKER, W. E., TURNBULL, A. D., COIT, D. G., MARRERO, A. M., PRASAD, M., BLUMGART, L. H. & BRENNAN, M. F. 1997. Liver resection for colorectal metastases. *Journal of clinical oncology : official journal of the American Society of Clinical Oncology,* 15**,** 938-46.

FORNER, A., LLOVET, J. M. & BRUIX, J. 2012. Hepatocellular carcinoma. *Lancet.*

FOWLER, R. A., FOSSHEIM, S. L., MESTAS, J. L., NGO, J., CANET-SOULAS, E. & LAFON, C. 2013. Non-invasive magnetic resonance imaging follow-up of sono-sensitive liposome tumor delivery and controlled release after high-intensity focused ultrasound. *Ultrasound Med Biol,* 39**,** 2342-50.

FRENKEL, V., ETHERINGTON, A., GREENE, M., QUIJANO, J., XIE, J., HUNTER, F., DROMI, S. & LI, K. C. 2006. Delivery of liposomal doxorubicin (Doxil) in a breast cancer tumor model: investigation of potential enhancement by pulsed-high intensity focused ultrasound exposure. *Acad Radiol,* 13**,** 469-79.

FREVERT, U., ENGELMANN, S., ZOUGBEDE, S., STANGE, J., NG, B., MATUSCHEWSKI, K., LIEBES, L. & YEE, H. 2005. Intravital observation of Plasmodium berghei sporozoite infection of the liver. *PLoS Biol,* 3**,** e192.

FRICH, L., MALA, T. & GLADHAUG, I. P. 2006. Hepatic radiofrequency ablation using perfusion electrodes in a pig model: effect of the Pringle manoeuvre. *European journal of surgical oncology : the journal of the European Society of Surgical Oncology and the British Association of Surgical Oncology,* 32**,** 527-32.

FRY, W. J., MOSBERG, W. H., JR., BARNARD, J. W. & FRY, F. J. 1954. Production of focal destructive lesions in the central nervous system with ultrasound. *J Neurosurg,* 11**,** 471-8.

FUKUDA, H., ITO, R., OHTO, M., SAKAMOTO, A., KARASAWA, E., YAMAGUCHI, T., SHINOZUKA, N., ZHU, H. & WANGA, Z. B. 2011. Treatment of Small Hepatocellular Carcinomas with US-Guided High-Intensity Focused Ultrasound. *Ultrasound in medicine & biology,* 37**,** 1222-9.

GANZER, R., FRITSCHE, H. M., BRANDTNER, A., BRUNDL, J., KOCH, D., WIELAND, W. F. & BLANA, A. 2013. Fourteen-year oncological and functional outcomes of high-intensity focused ultrasound in localized prostate cancer. *BJU Int,* 112**,** 322-9.

GAO, H. F., WANG, K., MENG, Z. Q., CHEN, Z., LIN, J. H., ZHOU, Z. H., WANG, P., SHI, W. D. & SHENG, Y. H. 2013. High intensity focused ultrasound treatment for patients with local advanced pancreatic cancer. *Hepatogastroenterology,* 60**,** 1906-10.

GARREAN, S., HERING, J., SAIED, A., HOOPES, P. J., HELTON, W. S., RYAN, T. P. & ESPAT, N. J. 2009. Ultrasound monitoring of a novel microwave ablation (MWA) device in porcine liver: lessons learned and phenomena observed on ablative effects near major intrahepatic vessels. *J Gastrointest Surg,* 13**,** 334-40.

GATEAU, J., AUBRY, J. F., CHAUVET, D., BOCH, A. L., FINK, M. & TANTER, M. 2011. In vivo bubble nucleation probability in sheep brain tissue. *Phys Med Biol,* 56**,** 7001-15.

GATTA, G., CAPOCACCIA, R., SANT, M., BELL, C. M., COEBERGH, J. W., DAMHUIS, R. A., FAIVRE, J., MARTINEZ-GARCIA, C., PAWLEGA, J., PONZ DE LEON, M., POTTIER, D., RAVERDY, N., WILLIAMS, E. M. & BERRINO, F. 2000. Understanding variations in survival for colorectal cancer in Europe: a EUROCARE high resolution study. *Gut,* 47**,** 533-8.

GOLDBERG, S. N., HAHN, P. F., TANABE, K. K., MUELLER, P. R., SCHIMA, W., ATHANASOULIS, C. A., COMPTON, C. C., SOLBIATI, L. & GAZELLE, G. S.

1998. Percutaneous radiofrequency tissue ablation: does perfusion-mediated tissue cooling limit coagulation necrosis? *Journal of vascular and interventional radiology : JVIR,* 9**,** 101-11.

GRAHAM, S. M., CARLISLE, R., CHOI, J. J., STEVENSON, M., SHAH, A. R., MYERS, R. S., FISHER, K., PEREGRINO, M. B., SEYMOUR, L. & COUSSIOS, C. C. 2014. Inertial cavitation to non-invasively trigger and monitor intratumoral release of drug from intravenously delivered liposomes. *J Control Release,* 178**,** 101-7.

GRAVANTE, G., ONG, S. L., METCALFE, M. S., LLOYD, D. M. & DENNISON, A. R. 2011. The Porcine Hepatic Arterial Supply, Its Variations and Their Influence on the Extracorporeal Perfusion of the Liver. *The Journal of surgical research,* 168**,** 56-61.

GYONGY, M. & COUSSIOS, C. C. 2010. Passive spatial mapping of inertial cavitation during HIFU exposure. *IEEE transactions on bio-medical engineering,* 57**,** 48-56.

HADDAD, A. J., BANI HANI, M., PAWLIK, T. M. & CUNNINGHAM, S. C. 2011. Colorectal liver metastases. *International journal of surgical oncology,* 2011**,** 285840.

HARIHARAN, P., MYERS, M. R. & BANERJEE, R. K. 2007. HIFU procedures at moderate intensities--effect of large blood vessels. *Physics in medicine and biology,* 52**,** 3493-513.

HESS, K. R., VARADHACHARY, G. R., TAYLOR, S. H., WEI, W., RABER, M. N., LENZI, R. & ABBRUZZESE, J. L. 2006. Metastatic patterns in adenocarcinoma. *Cancer,* 106**,** 1624-33.

HOLT, R. G. & ROY, R. A. 2001. Measurements of bubble-enhanced heating from focused, MHz-frequency ultrasound in a tissue-mimicking material. *Ultrasound Med Biol,* 27**,** 1399-412.

HUANG, J., HOLT, R. G., CLEVELAND, R. O. & ROY, R. A. 2004a. Experimental validation of a tractable numerical model for focused ultrasound heating in flow-through tissue phantoms. *J Acoust Soc Am,* 116**,** 2451-8.

HUANG, J., HOLT, R. G., CLEVELAND, R. O. & ROY, R. A. 2004b. Experimental validation of a tractable numerical model for focused ultrasound heating in flow-through tissue phantoms. *The Journal of the Acoustical Society of America,* 116**,** 2451-8.

HUANG, J., YAN, L., CHENG, Z., WU, H., DU, L., WANG, J., XU, Y. & ZENG, Y. 2010. A randomized trial comparing radiofrequency ablation and surgical resection for HCC conforming to the Milan criteria. *Ann Surg,* 252**,** 903-12.

HUANG, L., DODD, G. D., 3RD & LANCTOT, A. C. 2012. Radiofrequency ablation of the liver: effect of variation of portal venous blood flow on lesion size in an in-vitro perfused bovine liver. *Acad Radiol,* 19**,** 1018-22.

HYNYNEN, K. 1991. The threshold for thermally significant cavitation in dog's thigh muscle in vivo. *Ultrasound Med Biol,* 17**,** 157-69.

HYNYNEN, K., MCDANNOLD, N., SHEIKOV, N. A., JOLESZ, F. A. & VYKHODTSEVA, N. 2005. Local and reversible blood-brain barrier disruption by noninvasive focused ultrasound at frequencies suitable for trans-skull sonications. *Neuroimage,* 24**,** 12-20.

HYNYNEN, K., MCDANNOLD, N., VYKHODTSEVA, N. & JOLESZ, F. A. 2001. Noninvasive MR imaging-guided focal opening of the blood-brain barrier in rabbits. *Radiology,* 220**,** 640-6.

ILLING, R. O., KENNEDY, J. E., WU, F., TER HAAR, G. R., PROTHEROE, A. S., FRIEND, P. J., GLEESON, F. V., CRANSTON, D. W., PHILLIPS, R. R. & MIDDLETON, M. R. 2005. The safety and feasibility of extracorporeal high-intensity focused ultrasound (HIFU) for the treatment of liver and kidney tumours in a Western population. *British journal of cancer,* 93**,** 890-5.

IMBER, C. J., ST PETER, S. D., LOPEZ DE CENARRUZABEITIA, I., PIGOTT, D., JAMES, T., TAYLOR, R., MCGUIRE, J., HUGHES, D., BUTLER, A., REES, M. & FRIEND, P. J. 2002. Advantages of normothermic perfusion over cold storage in liver preservation. *Transplantation,* 73**,** 701-9.

ISHIZAKI, Y., YOSHIMOTO, J., MIWA, K., SUGO, H. & KAWASAKI, S. 2006. Safety of prolonged intermittent pringle maneuver during hepatic resection. *Archives of surgery,* 141**,** 649-53; discussion 654.

IWANAGA, K., TOMINAGA, K., YAMAMOTO, K., HABU, M., MAEDA, H., AKIFUSA, S., TSUJISAWA, T., OKINAGA, T., FUKUDA, J. & NISHIHARA, T. 2007. Local delivery system of cytotoxic agents to tumors by focused sonoporation. *Cancer Gene Ther,* 14**,** 354-63.

IZAMIS, M. L., EFSTATHIADES, A., KERAVNOU, C., LEEN, E. L. & AVERKIOU, M. A. 2014. Dynamic contrast-enhanced ultrasound of slaughterhouse porcine livers in machine perfusion. *Ultrasound Med Biol,* 40**,** 2217-30.

JAKAB, F., RATH, Z., SCHMAL, F., NAGY, P. & FALLER, J. 1995. The interaction between hepatic arterial and portal venous blood flows; simultaneous measurement by transit time ultrasonic volume flowmetry. *Hepatogastroenterology,* 42**,** 18-21.

JAMIESON, R. W., ZILVETTI, M., ROY, D., HUGHES, D., MOROVAT, A., COUSSIOS, C. C. & FRIEND, P. J. 2011. Hepatic Steatosis and Normothermic Perfusion-Preliminary Experiments in a Porcine Model. *Transplantation,* 92**,** 289-95.

JEMAL, A., BRAY, F., CENTER, M. M., FERLAY, J., WARD, E. & FORMAN, D. 2011. Global cancer statistics. *CA Cancer J Clin,* 61**,** 69-90.

JENSEN, C. R., RITCHIE, R. W., GYONGY, M., COLLIN, J. R., LESLIE, T. & COUSSIOS, C. C. 2012. Spatiotemporal monitoring of high-intensity focused ultrasound therapy with passive acoustic mapping. *Radiology,* 262**,** 252-61.

JIANG, F., HE, M., LIU, Y. J., WANG, Z. B., ZHANG, L. & BAI, J. 2013. High intensity focused ultrasound ablation of goat liver in vivo: Pathologic changes of portal vein and the "heat-sink" effect. *Ultrasonics,* 53**,** 77-83.

JIN, C., ZHU, H., WANG, Z., WU, F., CHEN, W., LI, K., SU, H., ZHOU, K. & GONG, W. 2010. High-intensity focused ultrasound combined with transarterial chemoembolization for unresectable hepatocellular carcinoma: Long-term follow-up and clinical analysis. *European journal of radiology*.

JONES, R. P., JACKSON, R., DUNNE, D. F., MALIK, H. Z., FENWICK, S. W., POSTON, G. J. & GHANEH, P. 2012. Systematic review and meta-analysis of follow-up after hepatectomy for colorectal liver metastases. *Br J Surg,* 99**,** 477-86.

JOOSTEN, J., JAGER, G., OYEN, W., WOBBES, T. & RUERS, T. 2005. Cryosurgery and radiofrequency ablation for unresectable colorectal liver metastases. *Eur J Surg Oncol,* 31**,** 1152-9.

KENNEDY, J. E., WU, F., TER HAAR, G. R., GLEESON, F. V., PHILLIPS, R. R., MIDDLETON, M. R. & CRANSTON, D. 2004. High-intensity focused ultrasound for the treatment of liver tumours. *Ultrasonics,* 42**,** 931-5.

KHOKHLOVA, V. A., BAILEY, M. R., REED, J. A., CUNITZ, B. W., KACZKOWSKI, P. J. & CRUM, L. A. 2006. Effects of nonlinear propagation, cavitation, and boiling in lesion formation by high intensity focused ultrasound in a gel phantom. *J Acoust Soc Am,* 119**,** 1834-48.

KIM, K. H., YOON, Y. S., YU, C. S., KIM, T. W., KIM, H. J., KIM, P. N., HA, H. K. & KIM, J. C. 2011. Comparative analysis of radiofrequency ablation and surgical resection for colorectal liver metastases. *J Korean Surg Soc,* 81**,** 25-34.

KIM, S. K., LIM, H. K., RYU, J. A., CHOI, D., LEE, W. J., LEE, J. Y., LEE, J. H., SUNG, Y. M., CHO, E. Y., HONG, S. M. & KIM, J. S. 2004. Radiofrequency ablation of rabbit liver in vivo: effect of the pringle maneuver on pathologic changes in liver surrounding the ablation zone. *Korean journal of radiology : official journal of the Korean Radiological Society,* 5**,** 240-9.

KIM, Y. S., RHIM, H., CHO, O. K., KOH, B. H. & KIM, Y. 2006. Intrahepatic recurrence after percutaneous radiofrequency ablation of hepatocellular carcinoma: analysis of the pattern and risk factors. *European journal of radiology,* 59**,** 432-41.

KITAMURA, H. & KOBAYASHI, C. 2005. Impairment of change in diameter of the hepatic portion of the inferior vena cava: a sonographic sign of liver fibrosis or cirrhosis. *J Ultrasound Med,* 24**,** 355-9; quiz 360-1.

KYRIAKOU, Z., CORRAL-BAQUES, M. I., AMAT, A. & COUSSIOS, C. C. 2011. HIFU-induced cavitation and heating in ex vivo porcine subcutaneous fat. *Ultrasound in medicine & biology,* 37**,** 568-79.

LEHMANN, K. S., RITZ, J. P., VALDEIG, S., KNAPPE, V., SCHENK, A., WEIHUSEN, A., RIEDER, C., HOLMER, C., ZURBUCHEN, U., HOFFMANN, P., PEITGEN, H. O., BUHR, H. J. & FRERICKS, B. B. 2009. Ex situ quantification of the cooling effect of liver vessels on radiofrequency ablation. *Langenbeck's archives of surgery / Deutsche Gesellschaft fur Chirurgie,* 394**,** 475-81.

LEUNG, J. H., YU, S. C., CHEUNG, E. C., WONG, A. S., TONG, M. M., HO, S. S., LEUNG, V. Y. & AHUJA, A. T. 2014a. Safety and efficacy of sonographically guided high-intensity focused ultrasound for symptomatic uterine fibroids: preliminary study of a modified protocol. *J Ultrasound Med,* 33**,** 1811-8.

LEUNG, U., KUK, D., D'ANGELICA, M. I., KINGHAM, T. P., ALLEN, P. J., DEMATTEO, R. P., JARNAGIN, W. R. & FONG, Y. 2014b. Long-term outcomes following microwave ablation for liver malignancies. *Br J Surg*.

LI, P. Z., ZHU, S. H., HE, W., ZHU, L. Y., LIU, S. P., LIU, Y., WANG, G. H. & YE, F. 2012. High-intensity focused ultrasound treatment for patients with unresectable pancreatic cancer. *Hepatobiliary Pancreat Dis Int,* 11**,** 655-60.

LI, T., CHEN, H., KHOKHLOVA, T., WANG, Y. N., KREIDER, W., HE, X. & HWANG, J. H. 2014. Passive cavitation detection during pulsed HIFU exposures of ex vivo tissues and in vivo mouse pancreatic tumors. *Ultrasound Med Biol,* 40**,** 1523-34.

LI, Y. Y., SHA, W. H., ZHOU, Y. J. & NIE, Y. Q. 2007. Short and long term efficacy of high intensity focused ultrasound therapy for advanced hepatocellular carcinoma. *Journal of gastroenterology and hepatology,* 22**,** 2148-54.

LIU, Y. J., QIAO, A. K., NAN, Q. & YANG, X. Y. 2006. Thermal characteristics of microwave ablation in the vicinity of an arterial bifurcation. *International journal of hyperthermia : the official journal of European Society for Hyperthermic Oncology, North American Hyperthermia Group,* 22**,** 491-506.

LU, D. S., RAMAN, S. S., LIMANOND, P., AZIZ, D., ECONOMOU, J., BUSUTTIL, R. & SAYRE, J. 2003. Influence of large peritumoral vessels on outcome of radiofrequency ablation of liver tumors. *Journal of vascular and interventional radiology : JVIR,* 14**,** 1267-74.

LU, D. S., RAMAN, S. S., VODOPICH, D. J., WANG, M., SAYRE, J. & LASSMAN, C. 2002. Effect of vessel size on creation of hepatic radiofrequency lesions in pigs: assessment of the "heat sink" effect. *AJR. American journal of roentgenology,* 178**,** 47-51.

LU, D. S., YU, N. C., RAMAN, S. S., LIMANOND, P., LASSMAN, C., MURRAY, K., TONG, M. J., AMADO, R. G. & BUSUTTIL, R. W. 2005. Radiofrequency ablation of hepatocellular carcinoma: treatment success as defined by histologic examination of the explanted liver. *Radiology,* 234**,** 954-60.

LU, Y., NAN, Q., DU, J., LI, L., QIAO, A. & LIU, Y. 2010. Experimental study on thermal field in the vicinity of arterial bifurcation in microwave ablation therapy. *International journal of hyperthermia : the official journal of European Society for Hyperthermic Oncology, North American Hyperthermia Group,* 26**,** 316-26.

LUKKA, H., WALDRON, T., CHIN, J., MAYHEW, L., WARDE, P., WINQUIST, E., RODRIGUES, G. & SHAYEGAN, B. 2011. High-intensity focused ultrasound for prostate cancer: a systematic review. *Clinical oncology,* 23**,** 117-27.

LUO, W., ZHOU, X., YU, M., HE, G., ZHENG, X., LI, Q., LIU, Q., HAN, Z., ZHANG, J. & QIAN, Y. 2009. Ablation of high-intensity focused ultrasound assisted with SonoVue on Rabbit VX2 liver tumors: sequential findings with histopathology, immunohistochemistry, and enzyme histochemistry. *Annals of surgical oncology,* 16**,** 2359-68.

LYNN, J. G., ZWEMER, R. L., CHICK, A. J. & MILLER, A. E. 1942. A New Method for the Generation and Use of Focused Ultrasound in Experimental Biology. *J Gen Physiol,* 26**,** 179-93.

MACHI, J., UCHIDA, S., SUMIDA, K., LIMM, W. M., HUNDAHL, S. A., OISHI, A. J., FURUMOTO, N. L. & OISHI, R. H. 2001. Ultrasound-guided radiofrequency thermal ablation of liver tumors: percutaneous, laparoscopic, and open surgical approaches. *J Gastrointest Surg,* 5**,** 477-89.

MANFREDI, S., LEPAGE, C., HATEM, C., COATMEUR, O., FAIVRE, J. & BOUVIER, A. M. 2006. Epidemiology and management of liver metastases from colorectal cancer. *Ann Surg,* 244**,** 254-9.

MARMOTTANT, P. & HILGENFELDT, S. 2003. Controlled vesicle deformation and lysis by single oscillating bubbles. *Nature,* 423**,** 153-6.

MAUGHAN, T. S., ADAMS, R. A., SMITH, C. G., MEADE, A. M., SEYMOUR, M. T., WILSON, R. H., IDZIASZCZYK, S., HARRIS, R., FISHER, D., KENNY, S. L., KAY, E., MITCHELL, J. K., MADI, A., JASANI, B., JAMES, M. D., BRIDGEWATER, J., KENNEDY, M. J., CLAES, B., LAMBRECHTS, D., KAPLAN, R., CHEADLE, J. P. & INVESTIGATORS, M. C. T. 2011. Addition of cetuximab to oxaliplatin-based first-line combination chemotherapy for treatment of advanced colorectal cancer: results of the randomised phase 3 MRC COIN trial. *Lancet,* 377**,** 2103-14.

MAUGHAN, T. S., MEADE, A. M., ADAMS, R. A., RICHMAN, S. D., BUTLER, R., FISHER, D., WILSON, R. H., JASANI, B., TAYLOR, G. R., WILLIAMS, G. T., SAMPSON, J. R., SEYMOUR, M. T., NICHOLS, L. L., KENNY, S. L., NELSON, A., SAMPSON, C. M., HODGKINSON, E., BRIDGEWATER, J. A., FURNISS, D. L., ROY, R., POPE, M. J., POPE, J. K., PARMAR, M., QUIRKE, P. & KAPLAN, R. 2014. A feasibility study testing four hypotheses with phase II outcomes in advanced colorectal cancer (MRC FOCUS3): a model for randomised controlled trials in the era of personalised medicine? *Br J Cancer,* 110**,** 2178-86.

MCLAUGHLAN, J., RIVENS, I., LEIGHTON, T. & TER HAAR, G. 2010. A study of bubble activity generated in ex vivo tissue by high intensity focused ultrasound. *Ultrasound Med Biol,* 36**,** 1327-44.

MELODELIMA, D., N'DJIN, W. A., FAVRE-CABRERA, J., PARMENTIER, H., RIVOIRE, M. & CHAPELON, J. Y. 2009. Thermal ablation produced using a surgical

toroidal high-intensity focused ultrasound device is independent from hepatic inflow occlusion. *Physics in medicine and biology,* 54**,** 6353-68.

MEMON, M. A. & BECKINGHAM, I. J. 2001. Surgical resection of colorectal liver metastases. *Colorectal Dis,* 3**,** 361-73.

METCALFE, M. S., MULLIN, E. J., TEXLER, M., BERRY, D. P., DENNISON, A. R. & MADDERN, G. J. 2007. The safety and efficacy of radiofrequency and electrolytic ablation created adjacent to large hepatic veins in a porcine model. *European journal of surgical oncology : the journal of the European Society of Surgical Oncology and the British Association of Surgical Oncology,* 33**,** 662-7.

MILLER, D. L. & GIES, R. A. 1998. The interaction of ultrasonic heating and cavitation in vascular bioeffects on mouse intestine. *Ultrasound Med Biol,* 24**,** 123-8.

MOLINA, C. A., RIBO, M., RUBIERA, M., MONTANER, J., SANTAMARINA, E., DELGADO-MEDEROS, R., ARENILLAS, J. F., HUERTAS, R., PURROY, F., DELGADO, P. & ALVAREZ-SABIN, J. 2006. Microbubble administration accelerates clot lysis during continuous 2-MHz ultrasound monitoring in stroke patients treated with intravenous tissue plasminogen activator. *Stroke,* 37**,** 425-9.

MULIER, S., MULIER, P., NI, Y., MIAO, Y., DUPAS, B., MARCHAL, G., DE WEVER, I. & MICHEL, L. 2002. Complications of radiofrequency coagulation of liver tumours. *The British journal of surgery,* 89**,** 1206-22.

MULIER, S., NI, Y., JAMART, J., MICHEL, L., MARCHAL, G. & RUERS, T. 2008a. Radiofrequency ablation versus resection for resectable colorectal liver metastases: time for a randomized trial? *Ann Surg Oncol,* 15**,** 144-57.

MULIER, S., NI, Y., JAMART, J., RUERS, T., MARCHAL, G. & MICHEL, L. 2005. Local recurrence after hepatic radiofrequency coagulation: multivariate meta-analysis and review of contributing factors. *Annals of surgery,* 242**,** 158-71.

MULIER, S., RUERS, T., JAMART, J., MICHEL, L., MARCHAL, G. & NI, Y. 2008b. Radiofrequency ablation versus resection for resectable colorectal liver metastases: time for a randomized trial? An update. *Dig Surg,* 25**,** 445-60.

NG, K. K., POON, R. T., CHAN, S. C., CHOK, K. S., CHEUNG, T. T., TUNG, H., CHU, F., TSO, W. K., YU, W. C., LO, C. M. & FAN, S. T. 2011. High-Intensity Focused Ultrasound for Hepatocellular Carcinoma: A Single-Center Experience. *Annals of surgery*.

NG, K. K., POON, R. T., LAM, C. M., YUEN, J., TSO, W. K. & FAN, S. T. 2006. Efficacy and safety of radiofrequency ablation for perivascular hepatocellular carcinoma without hepatic inflow occlusion. *The British journal of surgery,* 93**,** 440-7.

NI, J. Y., XU, L. F., SUN, H. L., ZHOU, J. X., CHEN, Y. T. & LUO, J. H. 2013. Percutaneous ablation therapy versus surgical resection in the treatment for early-stage hepatocellular carcinoma: a meta-analysis of 21,494 patients. *J Cancer Res Clin Oncol,* 139**,** 2021-33.

NIU, R., YAN, T. D., ZHU, J. C., BLACK, D., CHU, F. & MORRIS, D. L. 2007. Recurrence and survival outcomes after hepatic resection with or without cryotherapy for liver metastases from colorectal carcinoma. *Ann Surg Oncol,* 14**,** 2078-87.

NORDENSTEDT, H., WHITE, D. L. & EL-SERAG, H. B. 2010. The changing pattern of epidemiology in hepatocellular carcinoma. *Dig Liver Dis,* 42 Suppl 3**,** S206-14.

NORDLINGER, B., SORBYE, H., GLIMELIUS, B., POSTON, G. J., SCHLAG, P. M., ROUGIER, P., BECHSTEIN, W. O., PRIMROSE, J. N., WALPOLE, E. T., FINCH-JONES, M., JAECK, D., MIRZA, D., PARKS, R. W., COLLETTE, L., PRAET, M., BETHE, U., VAN CUTSEM, E., SCHEITHAUER, W. & GRUENBERGER, T. 2008. Perioperative chemotherapy with FOLFOX4 and surgery versus surgery alone for resectable liver metastases from colorectal cancer (EORTC Intergroup trial 40983): a randomised controlled trial. *Lancet,* 371**,** 1007-16.

OBERLI, M. A., SCHOELLHAMMER, C. M., LANGER, R. & BLANKSCHTEIN, D. 2014. Ultrasound-enhanced transdermal delivery: recent advances and future challenges. *Ther Deliv,* 5**,** 843-57.

ODELL, I. D. & COOK, D. 2013. Immunofluorescence techniques. *J Invest Dermatol,* 133**,** e4.

OLSEN, A. H., PARKIN, D. M. & SASIENI, P. 2008. Cancer mortality in the United Kingdom: projections to the year 2025. *British journal of cancer,* 99**,** 1549-54.

OSHOWO, A., GILLAMS, A., HARRISON, E., LEES, W. R. & TAYLOR, I. 2003. Comparison of resection and radiofrequency ablation for treatment of solitary colorectal liver metastases. *Br J Surg,* 90**,** 1240-3.

PARK, D., RYU, H., KIM, H. S., KIM, Y. S., CHOI, K. S., PARK, H. & SEO, J. 2012. Sonophoresis using ultrasound contrast agents for transdermal drug delivery: an in vivo experimental study. *Ultrasound Med Biol,* 38**,** 642-50.

PARK, I. J., KIM, H. C., YU, C. S., KIM, P. N., WON, H. J. & KIM, J. C. 2008. Radiofrequency ablation for metachronous liver metastasis from colorectal cancer after curative surgery. *Ann Surg Oncol,* 15**,** 227-32.

PARK, M. J., KIM, Y. S., RHIM, H. & LIM, H. K. 2014. Safety and therapeutic efficacy of complete or near-complete ablation of symptomatic uterine fibroid tumors by MR imaging-guided high-intensity focused US therapy. *J Vasc Interv Radiol,* 25**,** 231-9.

PARMENTIER, H., MELODELIMA, D., N'DJIN, A., CHESNAIS, S., CHAPELON, J. Y. & RIVOIRE, M. 2009. High-intensity focused ultrasound ablation for the treatment of colorectal liver metastases during an open procedure: study on the pig. *Annals of surgery,* 249**,** 129-36.

PATHAK, S., JONES, R., TANG, J. M., PARMAR, C., FENWICK, S., MALIK, H. & POSTON, G. 2011. Ablative therapies for colorectal liver metastases: a systematic review. *Colorectal disease : the official journal of the Association of Coloproctology of Great Britain and Ireland,* 13**,** e252-65.

PATTERSON, E. J., SCUDAMORE, C. H., OWEN, D. A., NAGY, A. G. & BUCZKOWSKI, A. K. 1998. Radiofrequency ablation of porcine liver in vivo: effects of blood flow and treatment time on lesion size. *Annals of surgery,* 227**,** 559-65.

PAYNE, S. J., PENG, T. & O'NEILL, D. P. 2010. Mathematical modeling of thermal ablation. *Crit Rev Biomed Eng,* 38**,** 21-30.

PELLETIER, G., DUCREUX, M., GAY, F., LUBOINSKI, M., HAGEGE, H., DAO, T., VAN STEENBERGEN, W., BUFFET, C., ROUGIER, P., ADLER, M., PIGNON, J. P. & ROCHE, A. 1998. Treatment of unresectable hepatocellular carcinoma with lipiodol chemoembolization: a multicenter randomized trial. Groupe CHC. *J Hepatol,* 29**,** 129-34.

PENNES, H. H. 1948. Analysis of tissue and arterial blood temperatures in the resting human forearm. *J Appl Physiol,* 1**,** 93-122.

QI, X., TANG, Y., AN, D., BAI, M., SHI, X., WANG, J., HAN, G. & FAN, D. 2014. Radiofrequency ablation versus hepatic resection for small hepatocellular carcinoma: a meta-analysis of randomized controlled trials. *J Clin Gastroenterol,* 48**,** 450-7.

RAI, R., RICHARDSON, C., FLECKNELL, P., ROBERTSON, H., BURT, A. & MANAS, D. M. 2005. Study of apoptosis and heat shock protein (HSP) expression in hepatocytes following radiofrequency ablation (RFA). *J Surg Res,* 129**,** 147-51.

REDDY, S. P., BHATTACHARJYA, S., MANIAKIN, N., GREENWOOD, J., GUERREIRO, D., HUGHES, D., IMBER, C. J., PIGOTT, D. W., FUGGLE, S., TAYLOR, R. & FRIEND, P. J. 2004. Preservation of porcine non-heart-beating donor livers by sequential cold storage and warm perfusion. *Transplantation,* 77**,** 1328-32.

RICCI, S., DINIA, L., DEL SETTE, M., ANZOLA, P., MAZZOLI, T., CENCIARELLI, S. & GANDOLFO, C. 2012. Sonothrombolysis for acute ischaemic stroke. *Cochrane database of systematic reviews,* 6**,** CD008348.

RITCHIE, R., COLLIN, J., COUSSIOS, C. & LESLIE, T. 2013. Attenuation and de-focusing during high-intensity focused ultrasound therapy through peri-nephric fat. *Ultrasound Med Biol,* 39**,** 1785-93.

RITCHIE, R. W., LESLIE, T., PHILLIPS, R., WU, F., ILLING, R., TER HAAR, G., PROTHEROE, A. & CRANSTON, D. 2010. Extracorporeal high intensity focused ultrasound for renal tumours: a 3-year follow-up. *BJU international,* 106**,** 1004-9.

RYDER, S. D. 2003. Guidelines for the diagnosis and treatment of hepatocellular carcinoma (HCC) in adults. *Gut,* 52 Suppl 3**,** iii1-8.

SAPARETO, S. A. & DEWEY, W. C. 1984. Thermal dose determination in cancer therapy. *Int J Radiat Oncol Biol Phys,* 10**,** 787-800.

SCHRAMM, W., YANG, D., WOOD, B. J., RATTAY, F. & HAEMMERICH, D. 2007. Contribution of direct heating, thermal conduction and perfusion during radiofrequency and microwave ablation. *The open biomedical engineering journal,* 1**,** 47-52.

SCOTT, D. J., FLEMING, J. B., WATUMULL, L. M., LINDBERG, G., TESFAY, S. T. & JONES, D. B. 2002. The effect of hepatic inflow occlusion on laparoscopic radiofrequency ablation using simulated tumors. *Surgical endoscopy,* 16**,** 1286-91.

SEIFERT, J. K., SPRINGER, A., BAIER, P. & JUNGINGER, T. 2005. Liver resection or cryotherapy for colorectal liver metastases: a prospective case control study. *Int J Colorectal Dis,* 20**,** 507-20.

SHEN, P., FLEMING, S., WESTCOTT, C. & CHALLA, V. 2003. Laparoscopic radiofrequency ablation of the liver in proximity to major vasculature: effect of the Pringle maneuver. *Journal of surgical oncology,* 83**,** 36-41.

SHIBATA, T., NIINOBU, T., OGATA, N. & TAKAMI, M. 2000. Microwave coagulation therapy for multiple hepatic metastases from colorectal carcinoma. *Cancer,* 89**,** 276-84.

SIRIWARDENA, A. K., MASON, J. M., MULLAMITHA, S., HANCOCK, H. C. & JEGATHEESWARAN, S. 2014. Management of colorectal cancer presenting with synchronous liver metastases. *Nat Rev Clin Oncol,* 11**,** 446-59.

SOLOVCHUK, M., SHEU, T. W. & THIRIET, M. 2013. Simulation of nonlinear Westervelt equation for the investigation of acoustic streaming and nonlinear propagation effects. *J Acoust Soc Am,* 134**,** 3931-42.

SOMMER, C. M., KOCH, V., PAP, B., BELLEMANN, N., HOLZSCHUH, M., GEHRIG, T., SHEVCHENKO, M., ARNEGGER, F. U., NICKEL, F., MOGLER, C., ZELZER, S., MEINZER, H. P., STAMPFL, U., KAUCZOR, H. U. & RADELEFF, B. A. 2011. Effect of tissue perfusion on microwave ablation: experimental in vivo study in porcine kidneys. *J Vasc Interv Radiol,* 22**,** 1751-7.

ST PETER, S. D., IMBER, C. J. & FRIEND, P. J. 2002a. Liver and kidney preservation by perfusion. *Lancet,* 359**,** 604-13.

ST PETER, S. D., IMBER, C. J., KAY, J., JAMES, T. & FRIEND, P. J. 2003. Hepatic control of perfusate homeostasis during normothermic extrocorporeal preservation. *Transplant Proc,* 35**,** 1587-90.

ST PETER, S. D., IMBER, C. J., LOPEZ, I., HUGHES, D. & FRIEND, P. J. 2002b. Extended preservation of non-heart-beating donor livers with normothermic machine perfusion. *Br J Surg,* 89**,** 609-16.

STARUCH, R. M., HYNYNEN, K. & CHOPRA, R. 2015. Hyperthermia-mediated doxorubicin release from thermosensitive liposomes using MR-HIFU: Therapeutic effect in rabbit Vx2 tumours. *Int J Hyperthermia,* 31**,** 118-33.

STEELE, G., JR. & RAVIKUMAR, T. S. 1989. Resection of hepatic metastases from colorectal cancer. Biologic perspective. *Ann Surg,* 210**,** 127-38.

SUN, R. R., NOBLE, M. L., SUN, S. S., SONG, S. & MIAO, C. H. 2014. Development of therapeutic microbubbles for enhancing ultrasound-mediated gene delivery. *J Control Release,* 182**,** 111-20.

SUNG, H. Y., JUNG, S. E., CHO, S. H., ZHOU, K., HAN, J. Y., HAN, S. T., KIM, J. I., KIM, J. K., CHOI, J. Y., YOON, S. K., YANG, J. M., HAN, C. W. & LEE, Y. S. 2011. Long-term outcome of high-intensity focused ultrasound in advanced pancreatic cancer. *Pancreas,* 40**,** 1080-6.

SWANSON, K. S., MAZUR, M. J., VASHISHT, K., RUND, L. A., BEEVER, J. E., COUNTER, C. M. & SCHOOK, L. B. 2004. Genomics and clinical medicine: rationale for creating and effectively evaluating animal models. *Exp Biol Med (Maywood),* 229**,** 866-75.

TAMAKI, K., SHIMIZU, I., OSHIO, A., FUKUNO, H., INOUE, H., TSUTSUI, A., SHIBATA, H., SANO, N. & ITO, S. 2004. Influence of large intrahepatic blood vessels on the gross and histological characteristics of lesions produced by radiofrequency

ablation in a pig liver model. *Liver international : official journal of the International Association for the Study of the Liver,* 24**,** 696-701.

TANIGUCHI, H., OGURO, A., TAKEUCHI, K., MIYATA, K., TAKAHASHI, T., INABA, T. & NAKAHASHI, H. 1993. Difference in regional hepatic blood flow in liver segments--non-invasive measurement of regional hepatic arterial and portal blood flow in human by positron emission tomography with H2(15)O. *Ann Nucl Med,* 7**,** 141-5.

TERATANI, T., YOSHIDA, H., SHIINA, S., OBI, S., SATO, S., TATEISHI, R., MINE, N., KONDO, Y., KAWABE, T. & OMATA, M. 2006. Radiofrequency ablation for hepatocellular carcinoma in so-called high-risk locations. *Hepatology,* 43**,** 1101-8.

THANOS, L., MYLONA, S., GALANI, P., POMONI, M., POMONI, A. & KOSKINAS, I. 2008. Overcoming the heat-sink phenomenon: successful radiofrequency thermal ablation of liver tumors in contact with blood vessels. *Diagnostic and interventional radiology,* 14**,** 51-6.

THUROFF, S., CHAUSSY, C., VALLANCIEN, G., WIELAND, W., KIEL, H. J., LE DUC, A., DESGRANDCHAMPS, F., DE LA ROSETTE, J. J. & GELET, A. 2003. High-intensity focused ultrasound and localized prostate cancer: efficacy results from the European multicentric study. *J Endourol,* 17**,** 673-7.

TORZILLI, G., PROCOPIO, F., DONADON, M., DEL FABBRO, D., CIMINO, M. & MONTORSI, M. 2012. Safety of intermittent Pringle maneuver cumulative time

exceeding 120 minutes in liver resection: a further step in favor of the "radical but conservative" policy. *Ann Surg,* 255**,** 270-80.

TRIGAUX, J. P., VAN BEERS, B., MELANGE, M. & BUYSSCHAERT, M. 1991. Alcoholic liver disease: value of the left-to-right portal vein ratio in its sonographic diagnosis. *Gastrointest Radiol,* 16**,** 215-20.

TUNG, Y. S., LIU, H. L., WU, C. C., JU, K. C., CHEN, W. S. & LIN, W. L. 2006. Contrast-agent-enhanced ultrasound thermal ablation. *Ultrasound Med Biol,* 32**,** 1103-10.

VAN CUTSEM, E., KOHNE, C. H., LANG, I., FOLPRECHT, G., NOWACKI, M. P., CASCINU, S., SHCHEPOTIN, I., MAUREL, J., CUNNINGHAM, D., TEJPAR, S., SCHLICHTING, M., ZUBEL, A., CELIK, I., ROUGIER, P. & CIARDIELLO, F. 2011. Cetuximab plus irinotecan, fluorouracil, and leucovorin as first-line treatment for metastatic colorectal cancer: updated analysis of overall survival according to tumor KRAS and BRAF mutation status. *J Clin Oncol,* 29**,** 2011-9.

VAN CUTSEM, E., NORDLINGER, B., CERVANTES, A. & GROUP, E. G. W. 2010. Advanced colorectal cancer: ESMO Clinical Practice Guidelines for treatment. *Ann Oncol,* 21 Suppl 5**,** v93-7.

VANAGAS, T., GULBINAS, A., SADAUSKIENE, I., DAMBRAUSKAS, Z., PUNDZIUS, J. & BARAUSKAS, G. 2009. Apoptosis is activated in an early period after radiofrequency ablation of liver tissue. *Hepatogastroenterology,* 56**,** 1095-9.

VIADANA, E. & AU, K. L. 1975. Patterns of metastases in adenocarcinomas of man. An autopsy study of 4,728 cases. *J Med,* 6**,** 1-14.

WALL, P. D., FRY, W. J., STEPHENS, R., TUCKER, D. & LETTVIN, J. Y. 1951. Changes produced in the central nervous system by ultrasound. *Science,* 114**,** 686-7.

WASHBURN, W. K., DODD, G. D., 3RD, KOHLMEIER, R. E., MCCOY, V. A., NAPIER, D. H., HUBBARD, L. G., HALFF, G. A., ESTERL, R. M., CIGARROA, F. G. & SHARKEY, F. E. 2003. Radiofrequency tissue ablation: effect of hepatic blood flow occlusion on thermal injuries produced in cirrhotic livers. *Annals of surgical oncology,* 10**,** 773-7.

WEIS, S., FRANKE, A., MOSSNER, J., JAKOBSEN, J. C. & SCHOPPMEYER, K. 2013. Radiofrequency (thermal) ablation versus no intervention or other interventions for hepatocellular carcinoma. *Cochrane Database Syst Rev,* 12**,** CD003046.

WEISS, L., GRUNDMANN, E., TORHORST, J., HARTVEIT, F., MOBERG, I., EDER, M., FENOGLIO-PREISER, C. M., NAPIER, J., HORNE, C. H., LOPEZ, M. J. & ET AL. 1986. Haematogenous metastatic patterns in colonic carcinoma: an analysis of 1541 necropsies. *J Pathol,* 150**,** 195-203.

WEISS, L., HAYDOCK, K., PICKREN, J. W. & LANE, W. W. 1980. Organ vascularity and metastatic frequency. *The American journal of pathology,* 101**,** 101-13.

WELP, C., SIEBERS, S., ERMERT, H. & WERNER, J. 2006. Investigation of the influence of blood flow rate on large vessel cooling in hepatic radiofrequency ablation. *Biomedizinische Technik. Biomedical engineering,* 51**,** 337-46.

WIART, M., CURIEL, L., GELET, A., LYONNET, D., CHAPELON, J. Y. & ROUVIERE, O. 2007. Influence of perfusion on high-intensity focused ultrasound prostate ablation: a first-pass MRI study. *Magnetic resonance in medicine : official journal*

of the Society of Magnetic Resonance in Medicine / Society of Magnetic Resonance in Medicine, 58**,** 119-27.

WRIGHT, A. S., SAMPSON, L. A., WARNER, T. F., MAHVI, D. M. & LEE, F. T., JR. 2005. Radiofrequency versus microwave ablation in a hepatic porcine model. *Radiology,* 236**,** 132-9.

WU, F., CHEN, W. Z., BAI, J., ZOU, J. Z., WANG, Z. L., ZHU, H. & WANG, Z. B. 2002. Tumor vessel destruction resulting from high-intensity focused ultrasound in patients with solid malignancies. *Ultrasound in medicine & biology,* 28**,** 535-42.

WU, F., WANG, Z. B., CAO, Y. D., CHEN, W. Z., BAI, J., ZOU, J. Z. & ZHU, H. 2003. A randomised clinical trial of high-intensity focused ultrasound ablation for the treatment of patients with localised breast cancer. *Br J Cancer,* 89**,** 2227-33.

WU, F., WANG, Z. B., CHEN, W. Z., ZHU, H., BAI, J., ZOU, J. Z., LI, K. Q., JIN, C. B., XIE, F. L. & SU, H. B. 2004. Extracorporeal high intensity focused ultrasound ablation in the treatment of patients with large hepatocellular carcinoma. *Annals of surgical oncology,* 11**,** 1061-9.

WU, F., WANG, Z. B., CHEN, W. Z., ZOU, J. Z., BAI, J., ZHU, H., LI, K. Q., JIN, C. B., XIE, F. L. & SU, H. B. 2005. Advanced hepatocellular carcinoma: treatment with high-intensity focused ultrasound ablation combined with transcatheter arterial embolization. *Radiology,* 235**,** 659-67.

WU, H., EXNER, A. A., KRUPKA, T. M., WEINBERG, B. D. & HAAGA, J. R. 2009. Vasomodulation of tumor blood flow: effect on perfusion and thermal ablation size. *Annals of biomedical engineering,* 37**,** 552-64.

WU, T., FELMLEE, J. P., GREENLEAF, J. F., RIEDERER, S. J. & EHMAN, R. L. 2001. Assessment of thermal tissue ablation with MR elastography. *Magnetic resonance in medicine : official journal of the Society of Magnetic Resonance in Medicine / Society of Magnetic Resonance in Medicine,* 45**,** 80-7.

XU, G. & SHI, Y. 2007. Apoptosis signaling pathways and lymphocyte homeostasis. *Cell Res,* 17**,** 759-71.

YAN, D. B., CLINGAN, P. & MORRIS, D. L. 2003. Hepatic cryotherapy and regional chemotherapy with or without resection for liver metastases from colorectal carcinoma: how many are too many? *Cancer,* 98**,** 320-30.

YARMOLENKO, P. S., MOON, E. J., LANDON, C., MANZOOR, A., HOCHMAN, D. W., VIGLIANTI, B. L. & DEWHIRST, M. W. 2011. Thresholds for thermal damage to normal tissues: an update. *Int J Hyperthermia,* 27**,** 320-43.

YU, N. C., RAMAN, S. S., KIM, Y. J., LASSMAN, C., CHANG, X. & LU, D. S. 2008. Microwave liver ablation: influence of hepatic vein size on heat-sink effect in a porcine model. *Journal of vascular and interventional radiology : JVIR,* 19**,** 1087-92.

ZARDI, E. M., PICARDI, A., AMBROSINO, G., FAZIO, V. M., DOBRINA, A., AFELTRA, A. & FREGO, M. 2003. Enhanced portal flow velocity and volume following Iloprost treatment. *Acta Biomed,* 74 Suppl 2**,** 108-10.

ZHANG, L., ZHU, H., JIN, C., ZHOU, K., LI, K., SU, H., CHEN, W., BAI, J. & WANG, Z. 2009. High-intensity focused ultrasound (HIFU): effective and safe therapy for hepatocellular carcinoma adjacent to major hepatic veins. *European radiology,* 19**,** 437-45.

ZHANG, P. & PORTER, T. 2010. An in vitro study of a phase-shift nanoemulsion: a potential nucleation agent for bubble-enhanced HIFU tumor ablation. *Ultrasound Med Biol,* 36**,** 1856-66.

ZHOU, P., HE, W., WANG, L. H., LI, X. H., TIAN, S. M., QIAN, Y. & CHEN, L. R. 2012. The influence of blood supply on high intensity focused ultrasound a preliminary study on rabbit hepatic VX2 tumors of different ages. *Academic radiology,* 19**,** 40-7.